

FZR - 123
February 1996

Annual Report 1995

Institute of Radiochemistry

Editor: Prof. Dr. H. Nitsche

Editorial staff: Dr. H.-J. Engelmann
Dr. G. Bernhard

Preface

During 1995, we have made considerable progress in meeting the Institute's scientific profile. Most of the essential research equipment is now installed and operating, and many projects are underway. The transition was successfully made from the initial start-up and consolidation phase to a now fully operational institute. There were several highlights in 1995 that deserve mentioning.

The European Radiation Facility (ESRF) at Grenoble, France, accepted our proposal to establish a Rossendorf Beam Line (ROBL) for hard X-ray Absorption Spectroscopy (XAS) to carry out research on radioactive samples and new materials. The hard work of the ROBL project group, which is jointly staffed by members of the Institute of Ion-Beam Physics and Materials Research, the Institute of Radiochemistry and the Department of Experimental Facilities and Information Technology, was rewarded by the signing of the contract. The beam line is projected to be fully operational by the end of 1998.

Meanwhile, our efforts have substantially increased to apply synchrotron radiation for studying radionuclide-substrate interaction, as well as structure and bonding, on a variety of environmentally relevant systems. Several measuring campaigns were conducted at the Stanford Synchrotron Radiation Laboratory (SSRL), Stanford, California, U.S.A. and at the Deutsches Elektronen-Synchrotron (DESY, HASYLAB), Hamburg, Germany. I would like to especially thank the Actinide Group of the Lawrence Berkeley National Laboratory and the Glenn T. Seaborg Institute for Transactinium Science at the Lawrence Livermore National Laboratory for the successful collaboration. But also at home, the number of collaborating research groups for synchrotron-based Extended X-ray Absorption Fine Structure (EXAFS) is steadily increasing. Joint projects were initiated with FZR's Institute of Bioinorganic and Radiopharmaceutical Chemistry and with the Institute of Inorganic Chemistry of the Technical University Dresden (TUD), and first results were obtained. Colleagues from Switzerland, France, Sweden, Finland and Russia have expressed interest to work with us on applying XAS to scientific tasks in the fields of environmental chemistry and nuclear waste disposal.

The construction of the new Radiochemistry Building was completed, and the inauguration will take place this month. We sincerely hope to obtain the license to handle radioactive materials by early summer and then be fully operational for handling actinides beyond uranium.

We would like to thank the many visitors, German and international, for their interest in our research and for their participation in the institute's seminars. We would like to also thank the visiting scientists for coming to Rossendorf during 1995 to share their knowledge and experience with us. We strongly encourage the continuation of visits by scientists in the future.

Rossendorf, February 1996

Prof. Dr. Heino Nitsche

CONTENTS

I. SCIENTIFIC CONTRIBUTIONS

1. SPECIATION AND MIGRATION OF RADIONUCLIDES

| | |
|---|----|
| SPECIATION OF URANIUM IN SEEPAGE WATERS OF A MINE TAILING PILE G. Bernhard, G. Geipel, V. Brendler, H. Nitsche | 1 |
| URANIUM-(VI)SULFATE COMPLEXATION STUDIED BY TIME-RESOLVED LASER-INDUCED FLUORESCENCE SPECTROSCOPY (TRLFS) G. Geipel, A. Brachmann, V. Brendler, G. Bernhard, H. Nitsche | 5 |
| DETERMINATION OF STABILITY CONSTANTS FOR AQUEOUS URANYL PHOSPHATE COMPLEXES AT LOW IONIC STRENGTHS WITH TIME- RESOLVED LASER-INDUCED FLUORESCENCE SPECTROSCOPY (TRLFS) AND POTENTIOMETRY V. Brendler, G. Geipel, A. Brachmann | 8 |
| INFLUENCE OF PHOSPHATE ON URANIUM SPECIATION AND MIGRATION IN SEEPAGE WATERS V. Brendler, G. Bernhard, H. Nitsche | 11 |
| SOLUBILITY AND SPECIATION OF $(\text{UO}_2)_2\text{SiO}_4 \cdot 2\text{H}_2\text{O}$ IN AQUEOUS SYSTEMS H. Moll, G. Geipel, W. Matz, G. Bernhard, H. Nitsche | 15 |
| USING A SURFACE COMPLEXATION MODEL TO SIMULATE THE ADSORP- TION OF U(VI) ON FERRIHYDRITE T. Arnold, M. Kohler, G. Bernhard, H. Nitsche | 18 |
| SORPTION OF URANIUM-(VI) ON ROCK MATERIAL OF A MINE TAILING PILE: SOLUTION SPECIATION BY FLUORESCENCE SPECTROSCOPY G. Geipel, G. Bernhard, V. Brendler, H. Nitsche | 20 |
| X-RAY PHOTOELECTRON STUDY OF THE INTERACTION OF $\text{UO}_2(\text{ClO}_4)_2$ WITH CALCITE Y.A. Teterin, V.I. Nefedov, K.E. Ivanov, A.S. Baev, G. Grambole, G. Geipel, G. Bernhard, T. Reich, H. Nitsche | 23 |
| RADIUM SORPTION ON SANDY AND CLAYEY SEDIMENTS OF THE UPPER SAXON ELBE RIVER VALLEY L. Baraniak, M. Thieme, G. Bernhard, K. Nindel, J. Schreyer, H. Nitsche | 25 |
| RADIUM SPECIATION STUDIES IN GROUNDWATERS AND LEACHING SOLUTION OF THE KÖNIGSTEIN URANIUM MINE M. Thieme, L. Baraniak, V. Brendler, G. Hüttig, H. Zänker, H. Nitsche, K. Nindel, J. Schreyer | 27 |
| DENSITY, SPECIFIC SURFACE AREA AND POROSITY OF THE ELBE VALLEY SEDIMENTS G. Schuster, L. Baraniak, M. Thieme, G. Bernhard, H. Nitsche, K. Nindel, J. Schreyer | 31 |

| | |
|---|----|
| SEQUENTIAL EXTRACTION ON RADIOACTIVITY-CONTAINING SEDIMENTARY ROCKS OF THE KÖNIGSTEIN REGION, SAXONY M. Thieme, L. Baraniak, G. Bernhard, K. Nindel, J. Schreyer, H. Nitsche | 34 |
| MODELLING OF RADIUM MIGRATION PROCESSES IN THE UPPER ELBE-VALLEY SANDSTONE SEDIMENTS H. Funke, L. Baraniak, M. Thieme, K. Nindel, J. Schreyer | 39 |
| DIRECT ALPHA-SPECTROSCOPIC MEASUREMENT OF THIN-LAYER CONCRETE SOURCES C. Nebelung, S. Hübener, G. Bernhard | 42 |
| 2. BEHAVIOR OF COLLOIDS AND AEROSOLS | |
| DEPENDENCE OF SCATTERED LIGHT INTENSITIES ON THE PARTICLE CONCENTRATION OF LOW-CONCENTRATED COLLOIDS G. Hüttig, W. Richter, H. Zänker | 45 |
| TESTING OF A PHOTON CORRELATION SPECTROSCOPE WITH LOW-CONCENTRATION COLLOIDS W. Richter, H. Zänker, G. Hüttig | 47 |
| FIRST RESULTS OF SEQUENTIAL FILTRATION OF GROUNDWATER FROM AN AQUIFER IN THE UPPER ELBE VALLEY SANDSTONE H. Zänker, G. Hüttig, E. Christalle, W. Richter | 50 |
| PRODUCTION OF NH_4Cl AND $(\text{NH}_4)_2\text{SO}_4$ AEROSOLS AND INTERACTION WITH IODINE M. Kalberer, B. Eichler, R. Dressler, U. Baltensperger, H.W. Gäggeler, S. Hübener | 53 |
| GENERATION AND CHARACTERIZATION OF SODIUM CHLORIDE AEROSOLS D. Rettig, P. Merker | 55 |
| 3. ORGANIC MATTER AND THEIR INTERACTION WITH RADIONUCLIDES | |
| SYNTHETIC HUMIC ACIDS: SYNTHESIS AND CHARACTERIZATION IN COMPARISON TO NATURAL MATERIALS S. Pompe, M. Meyer, M. Bubner, A. Brachmann, R. Nicolai, K.H. Heise, H. Nitsche | 57 |
| CHARACTERIZATION OF CARBOXYLIC GROUPS IN SYNTHETIC HUMIC SUBSTANCES BY PYROLYSIS GAS CHROMATOGRAPHY R. Jander, S. Pompe, M. Bubner, K.H. Heise | 60 |
| THERMOANALYSIS OF METHYLATION REACTIONS OF SYNTHETIC HUMIC ACIDS G. Schuster, S. Pompe, M. Bubner, K.H. Heise | 62 |
| COMPLEXATION OF U(VI) WITH MODEL SUBSTANCES FOR SIMULATING HUMIC ACID FUNCTIONALITY A. Brachmann, G. Geipel, V. Brendler, G. Bernhard, H. Nitsche | 66 |
| INVESTIGATIONS ON THE HYDROTHERMAL DEGRADATION OF WOOD IN FLOODED MINES K. Jelen, R. Schiene, K. Fischer, L. Baraniak, H. Nitsche | 69 |

| | |
|---|----|
| SIZE EXCLUSION CHROMATOGRAPHY (SEC) OF LIGNIN AND HUMIC ACIDS M. Schmidt, L. Baraniak, G. Bernhard, H. Nitsche | 71 |
| COMPLEXATION OF U(VI) WITH LIGNIN DEGRADATION PRODUCTS: DETERMINATION OF COMPLEX STABILITY BY ION-EXCHANGE AND TIME-RESOLVED LASER FLUORESCENCE SPECTROSCOPY M. Schmidt, L. Baraniak, G. Geipel, G. Bernhard, H. Nitsche | 73 |
| INVESTIGATION OF MICROBIAL DEGRADATION OF [¹⁴ C]PCB NO.77 IN SOIL M. Bubner, K.H. Heise, M. Matucha, V. Sasek | 75 |
| TiO ₂ -PHOTOCATALYZED OXIDATION OF ORGANIC COMPOUNDS E. Förster, K.H. Heise, K. Wolf, H. Nitsche | 77 |
| MINERALIZATION OF ORGANIC COMPOUNDS WITH SILVER CONTAINING SULFURIC-CHROMIC ACID E. Förster, K.H. Heise, K. Wolf, H. Nitsche | 80 |
| 4. APPLICATION OF X-RAY ABSORPTION SPECTROSCOPY | |
| A PREPARATION METHOD OF SOLID SAMPLES FOR EXAFS MEASURE- MENTS R. Nicolai, K.H. Heise, T. Reich | 83 |
| INVESTIGATION OF THE INTERACTION OF HUMIC ACIDS WITH URANYL IONS BY EXTENDED X-RAY ABSORPTION FINE STRUCTURE SPECTROS- COPY S. Pompe, M.A. Denecke, H. Moll, M. Bubner, H. Funke, T. Reich, K.H. Heise, G. Bernhard, H. Nitsche | 85 |
| EXAFS STUDIES ON ANHYDROUS COMPLEXES OF URANYL AND ORTHO- SUBSTITUTED BENZOIC ACIDS M.A. Denecke, S. Pompe, H. Moll, K.H. Heise, T. Reich, G. Bernhard, H. Nitsche | 87 |
| EXAFS DETERMINATIONS OF URANIUM STRUCTURES: THE URANYL ION COMPLEXED WITH TARTARIC, CITRIC, AND MALIC ACIDS P.G. Allen, D.K. Shuh, J.J. Bucher, N.M. Edelstein, T. Reich, M.A. Denecke, H. Nitsche | 89 |
| DETERMINATION OF THE ARSENIC OXIDATION STATE IN ENVIRONMEN- TALLY RELEVANT WATERS BY XANES SPECTROSCOPY M.A. Denecke, H. Moll, S. Pompe, D. Rettig, H. Friedrich, G. Bernhard, T. Reich, H. Nitsche | 90 |
| EXAFS STUDY OF URANIUM (VI) SORBED ONTO SILICA T. Reich, H. Moll, M.A. Denecke, G. Geipel, G. Bernhard, H. Nitsche, P.G. Allen, J.J. Bucher, N. Kaltsoyannis, N.M. Edelstein, D.K. Shuh | 92 |
| STRUCTURAL INVESTIGATIONS OF TECHNETIUM AND RHENIUM COMPLEXES BY EXAFS: 1. STUDIES ON "n+1" MIXED-LIGAND RHENIUM COMPLEXES T. Reich, G. Bernhard, H. Nitsche, H. Spies, B. Johannsen | 94 |

| | |
|--|-----|
| 5. CHEMISTRY OF HEAVIEST ELEMENTS | |
| MONTE CARLO SIMULATION OF REACTION GAS CHROMATOGRAPHY OF GROUP 6 ELEMENTS | 99 |
| A. Vahle, S. Hübener, R. Dressler, B. Eichler, A. Türler | |
| THERMOCHROMATOGRAPHY OF HEAVY ACTINIDES ON METAL SURFACES AT HIGH TEMPERATURES | 101 |
| S. Taut, S. Hübener, B. Eichler, H.W. Gäggeler, M. Schädel, E. Jäger, W. Brüchle | |
| STUDIES OF MOLYBDENUM OXICHLORIDES AS HOMOLOGUES OF ELEMENT 106 OXICHLORIDES | 104 |
| A. Thürler, B. Eichler, D.T. Jost, R. Dressler, D. Piguet, S. Hübener, M. Boettger, M. Grantz | |
| MODEL EXPERIMENTS FOR THE SEPARATION OF ELEMENT 106 SORPTION BEHAVIOUR OF SHORT-LIVED MO ISOTOPES ON CATION AND ANION EXCHANGERS | 106 |
| D. Schumann, A. Andrassy, H. Nitsche, S. Hübener, M. Grantz, St. Taut, R. Brückner, H. Guratzsch | |
| CALCULATION OF THE RATE CONSTANTS OF THE BASIC REACTIONS OF REACTION GAS CHROMATOGRAPHY - SOLVING THE DIFFERENTIAL EQUATION SYSTEM | 108 |
| M. Grantz, S. Hübener | |
| FIRST ON-LINE GAS CHEMISTRY OF ELEMENT 106 (SEABORGIUM) | 110 |
| S. Hübener for a collaboration | |
| II. PUBLICATIONS, PATENTS, LECTURES AND POSTERS | 113 |
| III. SEMINARS | 121 |
| IV. PERSONNEL | 125 |
| V. ACKNOWLEDGEMENTS | 127 |

I. SCIENTIFIC CONTRIBUTIONS

Speciation and Migration of Radionuclides

SPECIATION OF URANIUM IN SEEPAGE WATERS OF A MINE TAILING PILE

G. Bernhard, G. Geipel, V. Brendler, H. Nitsche
 Forschungszentrum Rossendorf e.V., Institute of Radiochemistry

Solution chemistry of uranium in natural aquatic systems is mainly influenced by the pH-value, the redox-potential and the presence of different complexing agents. The composition of seepage waters depends on the kind and weathering of the stored rock material. It is influenced by the chemical reactions inside the rock pile such as the solubility of the formed compounds and the interaction of the soluble species with the rock's surface. For the investigations, we used the seepage water coming from the rockpile No. 66 in Schlema, Saxony, Germany. The composition of this seepage water is given in Tab. 1; it is representative for seepage waters coming from other piles within this region.

| Component | Concentration [mM] | Methods |
|-------------------------------|--------------------|-----------------------------------|
| Mg | 16.46 | ICP-MS |
| Ca | 11.45 | AAS |
| U | 0.011 | UV-vis, ICP-MS, γ -Spectr. |
| Na | 0.572 | AAS |
| K | 0.465 | AAS |
| As | 0.012 | ICP-MS |
| Si | 0.064 | ICP-MS |
| CO ₃ ²⁻ | 1.933 | IC |
| Cl ⁻ | 0.121 | IC |
| NO ₃ ⁻ | 0.026 | IC |
| SO ₄ ²⁻ | 25.5 | IC |
| pH | 8.14 | Potentiometry |

Tab. 1: Characterization of the seepage water (rockpile No.66, Schlema, Saxony)

Leaching of the rocks is caused by the large amount of rain fall (800 mm per year) and the relative high acidity of the rain (pH-value 4.3) /1/. The high contents of sulfate, carbonate and alkaline earth ions indicate an ongoing weathering process. Chemical reactions inside the rockpile cause the change of the pH-value from 4.3 for the rain to 8.1 in the seepage water.

According to the quantitative composition of this seepage water, the distribution of U(VI) species was calculated with the speciation modeling software EQ3/6 /2/ using the NEA data base /3/. The ionic strength of the seepage water was determined to be 0.073 M. Preliminary computations showed that the speciation is rather sensitive to changes of the ionic strength. The uranium speciation, however, is not altered significantly if one simplifies the model by omitting minor components like Cl⁻, NO₃⁻, AsO₃³⁻, K⁺ and Na⁺. The calculations indicate that seepage water with a pH of 8.14 is supersaturated with respect to various minerals: dolomite, CaCO₃·MgCO₃, soddyite, (UO₂)₂SiO₄·2H₂O, calcite, CaCO₃, aragonite CaCO₃, calcium uranate, CaU₄O₁₀, magnesite, MgCO₃, talc [Mg₃(OH)₂][Si₄O₁₀] and other somewhat more exotic minerals. The sample solution, however, was clear and homogeneous and did not show any precipitate even after a storage of more than one year. The uranium speciation was computed assuming that the above supersaturation would not lead to precipitation of any minerals. The modeling results are shown in Fig.1.

At pH 8.14, the measured pH of the seepage water, the uranium speciation is dominated by carbonato complexes, mainly UO₂(CO₃)₃⁴⁻ (84%) and UO₂(CO₃)₂²⁻ (14%). At a pH above 10 the formation of higher hydroxide complexes dominates.

One could expect from the computation that the uranium in seepage water is mainly present as carbonato complexes. Time-resolved laser-induced fluorescence spectroscopy (TRLFS) is a suitable tool for determination of uranium speciation. Uranium speciation can be detected by the

characteristic lifetimes (τ) and the main fluorescence wavelengths (λ) of the different complexes.

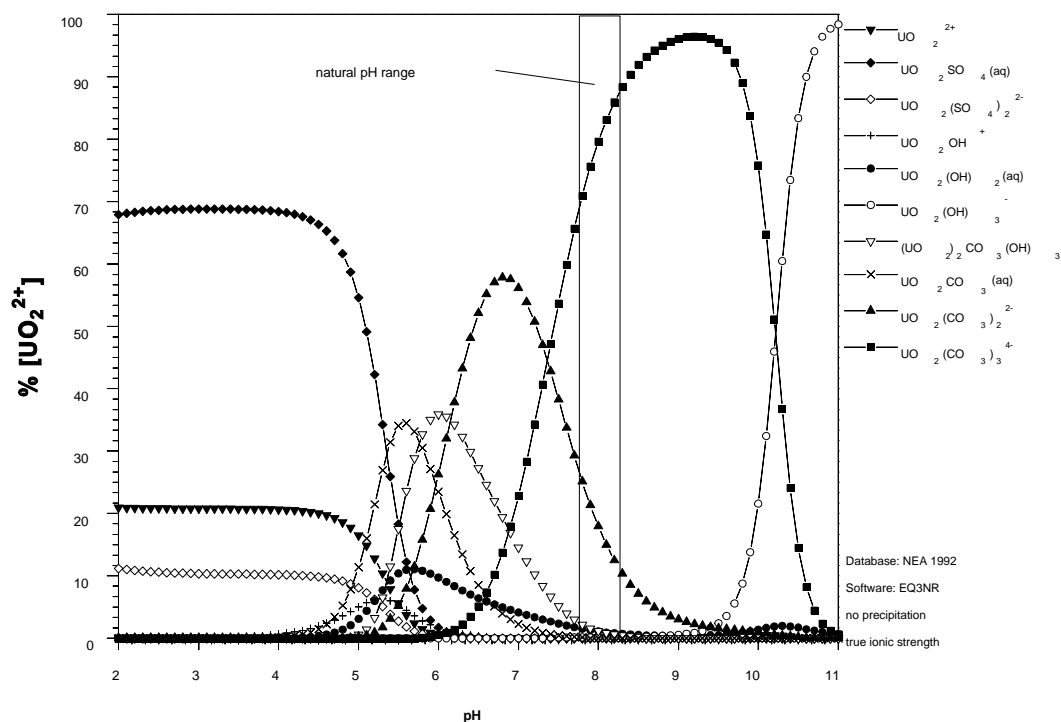


Fig. 1: Uranium speciation in seepage water (EQ3/6 software with NEA data base, all precipitation suppressed, true ionic strength 0.073 M, $1.1 \cdot 10^{-5}$ M U).

As it reported in reference /4/ and was also observed in our TRFLFS measurements of solutions containing $1 \cdot 10^{-5}$ mol U/L and a relevant carbonate content at pH 8.1, the total fluorescence emission is strongly decreased. Therefore, fluorescence components like dimeric and trimeric uranium carbonato complexes cannot be found at the concentration ratio of seepage water Fig. 2.

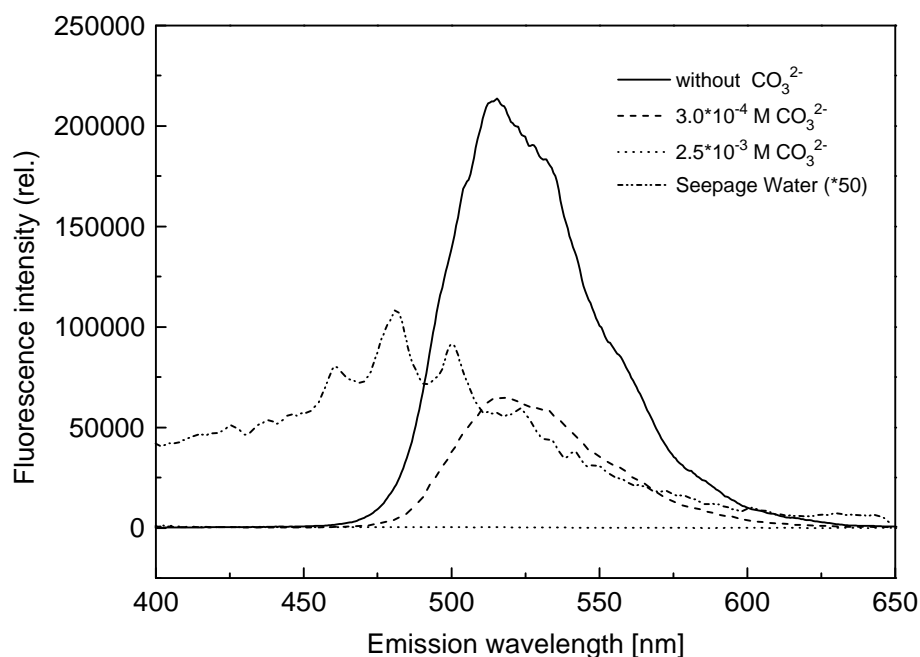


Fig. 2: Uranium fluorescence spectra in carbonate medium. ($1 \cdot 10^{-5}$ M UO_2^{2+} , $1 \cdot 10^{-1}$ M ClO_4^- , pH 8.0, $I = 10^{-1}$ M, gate 1 μ s, delay time 10^{-1} μ s)

Given this observation and the uranium speciation obtained by EQ3/6 calculation, it was surprising to obtain a pronounced fluorescence spectra from the original seepage water. Fig. 3 shows such a 3-D uranium fluorescence spectrum. The five characteristic peaks are located at 463.9, 483.6, 502.8, 524.3, and 555.4 nm. The lifetime was determined to be 64 ± 17 ns.

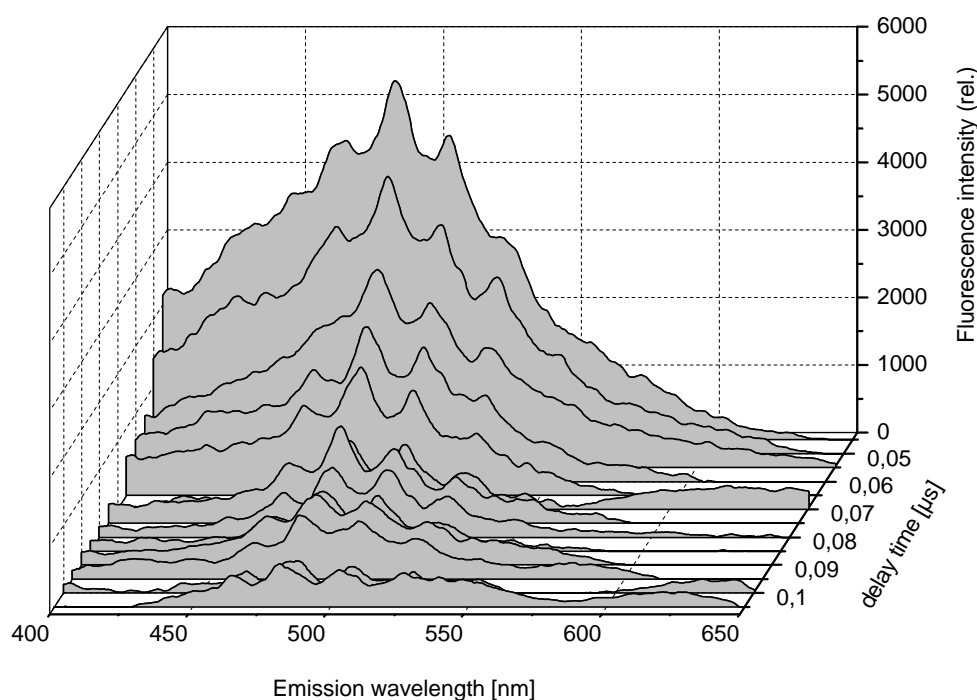


Fig. 3: Time-resolved fluorescence spectrum of seepage water. (rockpile No. 66, MP 017, Schlema)

Similar spectra, like the ones that were obtained from seepage water, were also recorded from modeling solutions containing uranium, carbonate and calcium concentrations that are comparable to the seepage water. From the speciation calculations and the experimental results (ion exchange, comparison of recorded relevant spectra - spectrum of liebigite, $\text{Ca}_2\text{UO}_2(\text{CO}_3)_3 \cdot 10 \text{H}_2\text{O}$ e.g. -, we postulate that the main uranium species in the investigated seepage water is a soluble aquo complex of di-calcium uranyl carbonate $[\text{Ca}_2[\text{UO}_2(\text{CO}_3)_3]]_{(\text{aq})}$. An equilibrium constant, $\log K = 5.0 \pm 0.7$ of this species is calculated from the typical titration curves (fluorescence signal versus calcium, carbonate and uranium concentration at ionic strength, $I = 0.1$, $\text{pH} = 8.1$ and $T = 25^\circ\text{C}$). Considering the overall stability constant for $\text{UO}_2(\text{CO}_3)_3^{4-}$ [5], the overall stability constant of the complex $[\text{Ca}_2[\text{UO}_2(\text{CO}_3)_3]]_{(\text{aq})}$ was determined to be $\log \beta = 26.8 \pm 0.7$. Existing thermodynamic data bases do not contain this species and therefore modeling calculation must lead to erroneous results. Due to the high fluorescence-quenching of the free carbonate complexes, additional measurements by laser-induced photoacoustic spectroscopy (LIPAS) are being planned.

Acknowledgements

The authors would like to thank the Department of Analytics, Forschungszentrum Rossendorf e.V., for the ICP-MS and AAS measurements.

References

- /1/ Geipel, G., Thieme, M., Bernhard, G., Nitsche, H.: Distribution of Uranium and Radionuclides in a Uranium-Mining Rockpile in Schlema, Saxony, Germany. *Radiochim. Acta* **66/67**, 305 (1994).

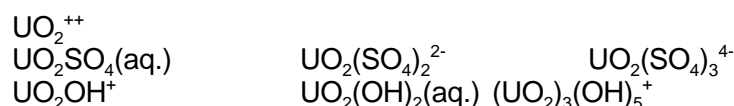
- /2/ Wolery, T.J.: EQ3/6, A software package for the geochemical modeling of aqueous systems. UCRL-MA-110662 Part I, Lawrence Livermore National Laboratory, California, USA 1992.
- /3/ Grenthe, I., Fuger, J., Lemire, R.J., Mueller, A.B., Nguyen-Trung, C., Wanner, H.: *Chemical Thermodynamics of Uranium*, 1st ed., Elsevier Science Publishers, Amsterdam 1992
- /4/ Kato, Y., Meinrath, G., Kimura, T., Yoshida, Z.: A Study of U(VI) Hydrolysis and Carbonate Complexation by Time-Resolved Laser-Induced Fluorescence Spectroscopy (TRLFS). *Radiochim. Acta* **64**, 107 (1994)
- /5/ Maya, L. : Detection of Hydroxo and Carbonato Species of Dioxouranium(VI) in Aqueous Media by Differential Pulse Polarography, *Inorg. Chim. Acta*, **65**, 13 (1982)

URANIUM-(VI) SULFATE COMPLEXATION STUDIED BY TIME-RESOLVED LASER-INDUCED FLUORESCENCE SPECTROSCOPY (TRLFS)

G. Geipel, A. Brachmann, V. Brendler, G. Bernhard, H. Nitsche
Forschungszentrum Rossendorf e.V., Institute of Radiochemistry

Seepage waters from the mill piles of the Saxonian uranium mining area have uranium and sulfate concentrations of about $1 \cdot 10^{-5}$ M, and $3 \cdot 10^2$ M respectively. As a first step to study speciation in seepage waters, we determined the speciation of uranium in the pure uranyl sulfate system, using time-resolved laser-induced fluorescence spectroscopy.

The spectra were measured with delay times ranging from 0.1 μ s to 20.1 μ s with increments of 0.5 μ s. The gate of the diode array was opened for 5 μ s to achieve a signal to noise ratio better than 5. The use of a delay step width that is smaller than the gate time only influences the measured fluorescence amplitude, but not the experimentally determined fluorescence life times. At a constant sulfate concentration of 0.05 M, a series of spectra were measured at several different pH values. In the investigated pH range from 2 to 6 and with a total uranium concentration of $1 \cdot 10^{-5}$ M the following seven main uranium-(VI)-species must be taken into account [1/:



To calculate the lifetimes and fractions of the different species from the pH-dependent spectra, the integrated fluorescence signal from 450 nm to 600 nm was fitted with a sum of experimental decay functions. Through the lifetime fitting process the fraction of each species was determined, and a speciation diagram was established for the uranyl ion in sulfate solution (Fig. 1).

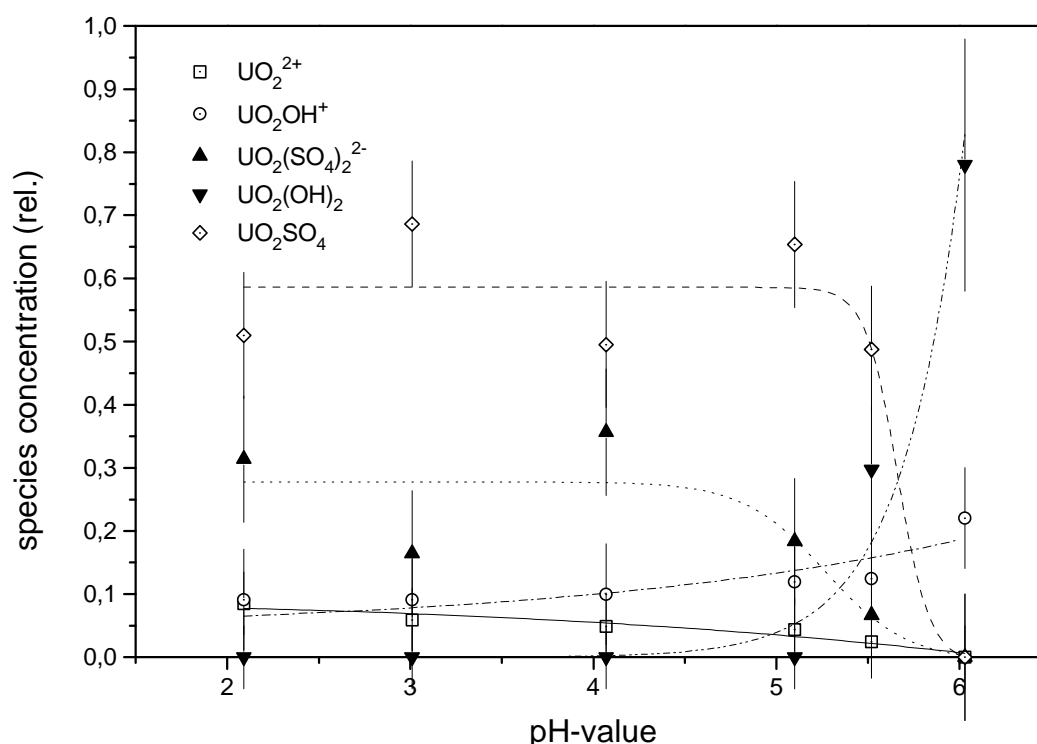


Fig.1: Relative uranium species concentration as function of pH
($c_{\text{uranium, total}} = 10^{-5}$ M ; $c_{\text{sulfate, total}} = 0.05$ M)

The diagram shows that mainly uranyl sulfate complexes (UO_2SO_4 and $\text{UO}_2(\text{SO}_4)_2^{2-}$) exist between pH 2 and pH 5. At higher pH values, the hydrolysis of the uranyl ion becomes increas-

ingly important. The iteration calculations carried out on the measurements showed the presence of only five species. It appears that the product of the fluorescence signal at t_0 and the fraction of the species $\text{UO}_2(\text{SO}_4)_3^{4-}$ and $(\text{UO}_2)_2(\text{OH})_5^+$, respectively, was too low for detection of these species by this method.

Tab.1: Lifetimes and fluorescence signals relative to UO_2^{2+} at an ionic strength of 0.2 M and a total sulfate concentration of 0.05 M

| Species | Lifetime [μs] | Fluorescence signal (rel. to UO_2^{2+}) |
|---|----------------------------|---|
| UO_2^{2+} | < 3.0 | 1 |
| $\text{UO}_2\text{SO}_{4(\text{aq})}$ | 4.7 +/- 0.3 | 4.9 |
| $\text{UO}_2(\text{SO}_4)_2^{2-}$ | 11.5 +/- 0.3 | 23 |
| $\text{UO}_2(\text{SO}_4)_3^{4-}$ | 18.3 +/- 1.0 | 49 |
| UO_2OH^+ | 8.3 +/- 0.3 | 370 |
| $\text{UO}_2(\text{OH})_{2(\text{aq})}$ | 18.1 +/- 0.3 | 1430 |

Tab. 1 shows the calculated intensity of the fluorescence signals relative to the uncomplexed uranyl ion, and the respective lifetimes at an ionic strength of 0.2 M.

To investigate the speciation of uranyl ions in sulfate media, a series of solutions with varying sulfate concentrations were measured. Each spectrum was measured three times. The sulfate concentration ranged from $1 \cdot 10^{-4}$ M to $2.5 \cdot 10^1$ M. The ionic strength of 1 M was maintained by addition of NaClO_4 . The pH of these solutions was 2.0 ± 0.05 . Lifetime curves were fitted in the same manner as described earlier. From the calculated fractions of the different uranyl species, the speciation diagram in Fig. 2 was constructed.

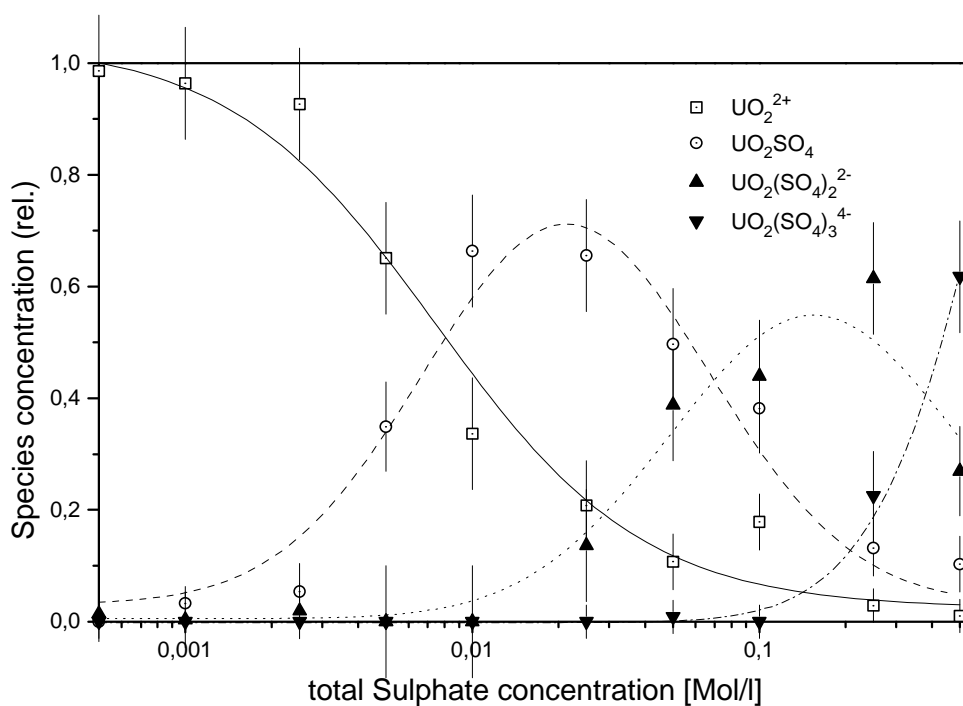
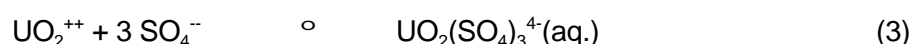
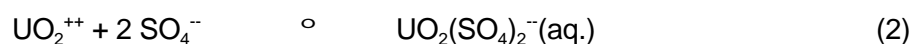


Fig.2: Relative uranium species concentration as function of total sulfate concentration at pH = 2; $c_{\text{uranium, total}} = 10^{-5}$ M

Starting at low sulfate concentrations, the concentration of non-complexed uranyl ions decreases with increasing sulfate concentration.

The concentrations of the two uranyl sulfate complexes UO_2SO_4 and $\text{UO}_2(\text{SO}_4)_2^{2-}$ increase and show maxima at sulfate concentrations of 0.02 M and 0.18 M, respectively. At higher sulfate concentrations the $\text{UO}_2(\text{SO}_4)_3^{4-}$ complex becomes the dominant solution species.

From the dependence of the distribution of the uranyl species with the total sulfate concentration it was possible to calculate the complex formation constants for the three reactions:



The results and a comparison with literature values are given in Tab. 2.

Tab.2: Complex formation constants between uranyl and sulfate ions

| Reaction | This Work, log K (I = 1 M, 25°C) | NEA data basis /1,2/, log K (1 M NaClO ₄ ; 20° C) |
|----------|-------------------------------------|---|
| (1) | 2.1 +/- 0.5 | 1.75 +/- 0.2 |
| (2) | 3.4 +/- 0.5 | 2.5 +/- 0.2 |
| (3) | 3.6 +/- 0.7 | 3.4 |

References

- /1/ I. Grenthe, J. Fuger, R.J.M. Konings, R.J. Lemire, A.B. Muller, Ch. Nguyen-Trung, Cregu H. Wanner, *Chemical Thermodynamics of Uranium*, NEA OECD, 1992, p. 241.
- /2/ S. Ahrland, On the complex chemistry of the uranyl ion: V. The complexity of uranyl sulfate, *Acta Chem. Scand.* **5**, 1151-1167 (1951)
- /3/ Ch. Moulin, P. Decambox, V. Moulin, J.G. Decaillon, Uranium Speciation in Solution by time resolved Laser-Induced Fluorescence, *Anal. Chem.* **67**, 348 (1995)
- /4/ V. Eliet, G. Bidoglio, N. Omenetto, L.Parma, I. Grenthe; Characterization of Hydroxide Complexes of Uranium(VI) by Time Resolved Fluorescence Spectroscopy, *J. Chem. Soc. Far. Transactions*, **91**, 2275-2285 (1995)

DETERMINATION OF STABILITY CONSTANTS FOR AQUEOUS URANYL PHOSPHATE COMPLEXES AT LOW IONIC STRENGTHS WITH TIME-RESOLVED LASER-INDUCED FLUORESCENCE SPECTROSCOPY (TRLFS) AND POTENTIOMETRY

V. Brendler, G. Geipel, A. Brachmann
 Forschungszentrum Rossendorf e.V., Institute of Radiochemistry

The impact of phosphate on uranium speciation in seepage waters was investigated. Available complexation data are not fully consistent and based only on few experiments. Stability constants were determined for the complexes $\text{UO}_2(\text{H}_2\text{PO}_4)_2(\text{aq})$, $\text{UO}_2(\text{H}_2\text{PO}_4)^+$ and $\text{UO}_2\text{HPO}_4(\text{aq})$ over a pH range from 2 to 5 and for uranyl and phosphate concentrations down to 10^{-6} molar. The results are compared with values recommended by NEA /1/ and with some recent publications. They will be applied on the characterization of water samples from mill tailings in former uranium mining areas in Saxony and Thuringia. This shall aid the development of remediation strategies.

Experimental

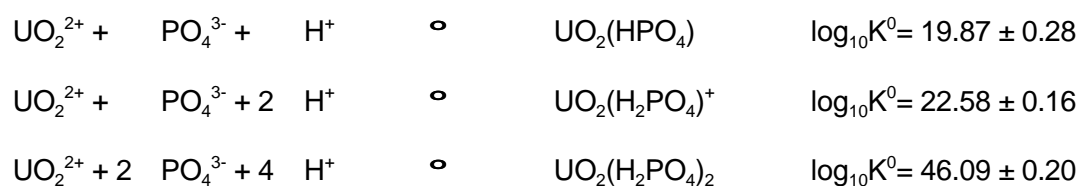
Potentiometric titrations were performed with an automatic titrator (TPC 2000, Schott/Germany) using the accompanying TR 600 software (version 5.02). Modelling with the NEA data base /1/ and RAMESSES speciation software /2/ showed the expected pH effect to be always smaller than 0.1 units. To allow for high precision measurements, a variety of pH glass electrodes were tested to find the best compromise between reproducibility, linear response, short equilibration time, long term stability of the signal and low sensitivity to stirring effects. The chosen electrodes (EGA 151, Meinsberg/Germany and U402-M6-S7, Ingold/Germany) were used simultaneously during the titration for comparison of the pH readings. Both electrodes were calibrated before each run with NBS buffers at pH 6.86, 4.01 and 1.68 and additional buffers at pH 3.00, 2.00 and 1.00. The calibration data were corrected to 22.0 °C and fitted to a quadratic equation. For the titrations nominally 0.01 M H_3PO_4 was added to different starting concentrations of $\text{UO}_2(\text{NO}_3)_2$ - solution. After an initialization period of 300 seconds, the following titration loop procedure was applied: adding of 0.1 mL acid, stirring for 20 seconds, waiting for 40 seconds, measuring of the pH until the signal was stable, temperature recording, next titration step.

For *Time-Resolved Laser-Induced Fluorescence Spectroscopy* (TRLFS) a Nd-YAG laser (GCR-190, Spectra Physics, USA) was applied to the samples. The true laser power was monitored with an optical energymeter (model 1835, Newport, USA) to correct energy oscillations. The measuring time controlled by a gated diode array (M 1475, EG&G) could be varied from 5 ns to 2 ms. A delay generator allows to start the signal recording in a range from 5 ns to 95 ms relative to the laser pulse. A more detailed description of our laser equipment can be found in /3/. The excitation wavelength was 355 nm; spectra were recorded in the range from 304.3 to 722.8 nm with a resolution of 0.6 nm. The temperatures of sample and detector were held at 20 ± 0.5 °C and -30 °C, respectively. The actual laser energy was 2.2 - 2.4 mJ.

All spectra were analyzed for fluorescence lifetimes with the C-program POLYLIFE, developed in our group. It fits lifetimes and fluorescence yields for each wavelength separately, thus giving much better statistic for the lifetime determination than in previous investigations.

Results

20 potentiometric titrations were performed with a total of 338 points in a pH range from 2.5 to 4.8. The data were corrected to 22 °C and processed with the evaluation software C-Letagrop /4/. The following brutto stability constants were calculated (errors represent 3F, the DAVIES equation was used to correct to zero ionic strength):



For the TRLFS lifetime determinations two sets of solutions were prepared:

$$[\text{UO}_2^{2+}]_{\text{total}} = 10^{-5} \text{ mol/L, phosphate to uranyl ratio } R_{\text{P:U}} \text{ varying from 0 to 100,}$$

$$[\text{UO}_2^{2+}]_{\text{total}} = 5 \cdot 10^{-6} \text{ mol/L, } R_{\text{P:U}} \text{ fixed at 200, pH varying.}$$

Fig. 1 shows the 2-D TRLFS spectrum of one sample. A red shift with increasing time is detectable. The spectrum in Fig. 1 was analyzed with the program POLYLIFE for two distinct species; the results are combined in Fig. 2. Assuming existence of three species did not give satisfying results: the lifetimes for $\text{UO}_2(\text{H}_2\text{PO}_4)^+$ and $\text{UO}_2(\text{HPO}_4)$ were strongly correlated. The lifetimes selected as the best parameter set are:

$$J_1 = 1.1 \pm 0.1 \mu\text{s for } \text{UO}_2^{2+} \text{ and } J_2 = 14.0 \pm 1.3 \mu\text{s for } \text{UO}_2(\text{H}_2\text{PO}_4)^+ / \text{UO}_2(\text{HPO}_4).$$

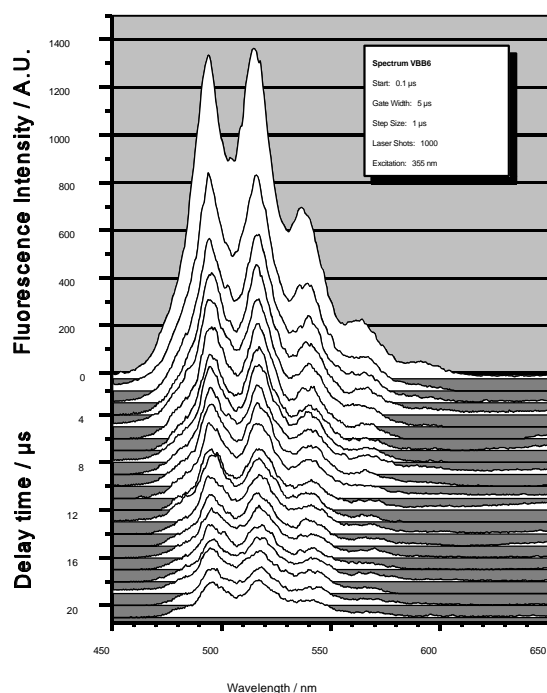


Fig. 1: 2-D TRLFS spectrum for a solution of $10^{-5} \text{ M UO}_2(\text{NO}_3)_2 + 10^{-3} \text{ M H}_3\text{PO}_4$

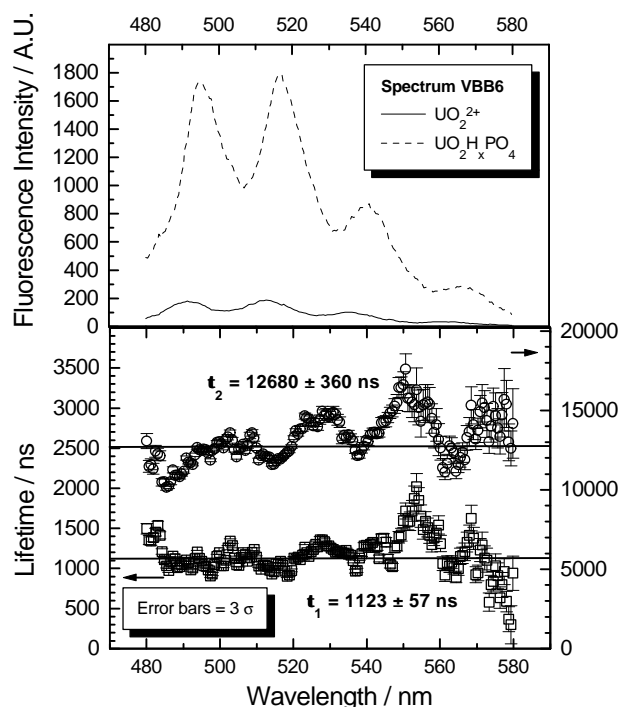


Fig. 2: Fluorescence lifetimes and single species spectra for a solution of $10^{-5} \text{ M UO}_2(\text{NO}_3)_2 + 10^{-3} \text{ M H}_3\text{PO}_4$

After determining the lifetimes, experimental conditions were adjusted to better isolate the fluorescence spectra of the different uranyl species in solution from each other:

Series A) delay time $0.5 \mu\text{s}$, gate width $2 \mu\text{s}$, 500 laser shots

Series B) delay time $5 \mu\text{s}$, gate width $10 \mu\text{s}$, 1000 laser shots

The recorded spectra were analyzed with the SQUAD program /5/ to obtain the stability constants (corrected to $I = 0$, errors = $3F$):



Discussion

The assignment of the fluorescence lifetime $J_1 = 1.1 \pm 0.1 \mu\text{s}$ to $\text{UO}_2^{2+}(\text{aq})$ is in good agreement with literature data: $J_1 = 1.0 \mu\text{s}$ /6/ and $J_1 = 0.83 \mu\text{s}$ /7/. For the system $\text{UO}_2^{2+}/\text{PO}_4^{3-}/\text{H}_2\text{O}$ the only available lifetimes are for $[\text{H}_3\text{PO}_4] > 0.75 \text{ molar}$ are: $J_2 = 232.1 \pm 0.5 \mu\text{s}$ /6/, $J_2 = 187 \mu\text{s}$ /8/ and $J_2 = 200 \mu\text{s}$ /9/. No species were assigned to the spectra. We report the first fluorescence

lifetimes for uranyl phosphate complexes. The $\text{UO}_2(\text{HPO}_4)$ stability constant agrees well with Sandino and Bruno's value /10/. Our value for $\text{UO}_2(\text{H}_2\text{PO}_4)^+$ is slightly lower than their value, whereas the value for $\text{UO}_2(\text{H}_2\text{PO}_4)_2$ is larger. These differences may be due to the rather high ionic strengths (usually either 0.5 or 1.0 mol/L) used in most of the previous investigations. Extrapolations to infinite dilution of data at such relatively high ionic strengths may be hampered by inaccuracies of the thermodynamic model. In this work the ionic strength never exceeded 10^{-2} mol/L, which simplifies the extrapolation to standard conditions.

References

- /1/ Grenthe, I., Fuger, J., Lemire, R. J., Muller, A. B., Nguyen-Trung, C., Wanner, H.: *Chemical Thermodynamics of Uranium*, 1st ed., Elsevier Science, Amsterdam, 1992
- /2/ Leung, V. W.-H., Darvell, B. W., Chan, P.-C., *Talanta* **35**, 713 (1988)
- /3/ Bernhard, G., Geipel, G., Brendler, V., Nitsche, H., submitted to publication in *Radiochim. Acta*
- /4/ Östhols, E., Royal Inst. Technology Report, TRITA-OOK-2051, Stockholm, 1984
- /5/ Leggett, D. J. In: *Computational methods for the determination of formation constants* (Leggett, D. J. ed.), Plenum Press, New York, 1985, p.159
- /6/ Kato, Y., Meinrath, G., Kimura, T., Yoshida, Z., *Radiochim. Acta* **64**, 107 (1994)
- /7/ Meinrath, G., Kato, Y., Yoshida, Z., *J. Radioanal. Nucl. Chem. (Art.)* **174**, 299 (1993)
- /8/ Moriyasu, M., Yokoyama, Y., Ikeda, S., *J. Inorg. Nucl. Chem.* **39**, 2199 (1977)
- /9/ Moulin, C., Decambox, P., Moulin, V., Decaillon, J. G., *Anal. Chem.* **67**, 348 (1995)
- /10/ Sandino, A., Bruno, J., *Geochim. Cosmochim. Acta* **56**, 4135 (1992)

INFLUENCE OF PHOSPHATE ON URANIUM SPECIATION AND MIGRATION IN SEEPAGE WATERS

V. Brendler, G. Bernhard, H. Nitsche
Forschungszentrum Rossendorf e.V., Institute of Radiochemistry

New and more precise stability constants for uranyl phosphate complexes were used for geochemical modeling to compute the speciation of uranium in several waters that are relevant for former mining areas in Saxony and Thuringia. Scenarios are shown where it could be profitable to *add phosphates* to rock piles and mine tailings in order to inhibit impacts on aquifers, especially in acidic and neutral environments.

Experimental

Comprehensive investigations of the stability constants of uranium phosphate complexes were carried out to better understand the impacts of phosphates on the uranium speciation in natural waters. The at present most comprehensive data compilation of uranium thermodynamics /1/ shows, that most of the published uranyl phosphate stability constants are based on experiments at rather high concentrations of either uranium or phosphate. The concentration at which these data were gathered are significantly above the levels found in natural systems, even when they are heavily affected by the uranium mining. Therefore we conducted experiments with concentrations of uranyl and phosphate, not exceeding 10^{-4} and 10^{-3} mol/L, respectively, to verify and to correct (if necessary) the available literature for uranyl phosphate complexes. These potentiometric titrations and time-resolved laser-induced fluorescence spectroscopy (TRLFS) investigations are described in detail elsewhere /2/. The following results were obtained (mean of all investigations, corrected to zero ionic strength, errors represent three standard deviations):



A comparison of our results from potentiometry and TRLFS with the literature data /1/ is given in Tab. 1. Our experiments give slightly lower values for the brutto stability constants of $\text{UO}_2(\text{H}_2\text{PO}_4)^+$ and $\text{UO}_2(\text{HPO}_4)$, but a larger value for $\text{UO}_2(\text{H}_2\text{PO}_4)_2$. The main reason for these differences may lie in the relatively high ionic strengths used in most of the previous investigations. Usually they are either 0.5 or 1.0 mol/L, which requires extrapolation of the stability constants to zero ionic strength by means of thermodynamic models. Because of assumptions made and the underlying simplified theories the models may not be very reliable at such high ionic strengths. But in this work the ionic strength never exceeded 10^{-3} mol/L making it straightforward to transform to infinite dilution.

Tab.1: Brutto stability constants $\log_{10} K^0$ for uranyl phosphate complexes at zero ionic strength

| | GRENTHE et al. /1/ (NEA data base) | present work /2/ (Potentiometry) | present work /2/ (TRLFS) |
|--|---------------------------------------|-------------------------------------|-----------------------------|
| $\text{UO}_2(\text{HPO}_4)$ | 19.59 ± 0.26 | 19.87 ± 0.27 | 19.53 ± 0.12 |
| $\text{UO}_2(\text{H}_2\text{PO}_4)^+$ | 22.82 ± 0.06 | 22.58 ± 0.15 | 22.31 ± 0.14 |
| $\text{UO}_2(\text{H}_2\text{PO}_4)_2$ | 44.04 ± 0.11 | 46.09 ± 0.19 | - |

Modelling

To estimate the impact of phosphate on the uranium speciation in waters affected by uranium mining, the following representative examples were chosen:

- Sample A: acidic flood water from a uranium mine (Königstein / Saxony)
- Sample B: water from aquifer IV (Königstein / Saxony)
- Sample C: seepage water from a mill tailing pile, later used as waste dump site (Freital / Saxony)

The concentration of the main components are listed in Tab. 2. The samples are described by THIEME (samples A & B) /3/ and REICHERT (sample C) /4/.

Tab.2: Composition of model waters

| Component | Concentration [mmol / L] | | | Method |
|-------------------------------|--------------------------|----------|----------|---------------|
| | Sample A | Sample B | Sample C | |
| Na | 5.48 | 0.24 | 47.85 | AAS |
| K | 0.033 | 0.21 | 0.16 | AAS |
| Mg | 1.00 | 0.027 | 1.85 | ICP-MS |
| Ca | 6.74 | 0.23 | 2.25 | AAS |
| U | 0.09 | 0.003 | 0.004 | ICP-MS |
| Al | 2.32 | - | - | ICP-MS |
| CO ₃ ²⁻ | 0.17 | 1.13 | 11.47 | IC |
| Cl ⁻ | 4.49 | 0.12 | 3.39 | IC |
| NO ₃ ⁻ | 0.10 | 0.016 | - | IC |
| SO ₄ ²⁻ | 26.01 | 0.40 | 29.15 | IC |
| pH | 2.28 | 5.80 | 7.08 | Potentiometry |

The speciation program RAMESES /5/ and the geochemical software package EQ3/6 /6/ were used for the computer simulations. The NEA recommended data base /1/ was used except the phosphate complexes that we determined as it is discussed above. In the modeling of the unaltered solution (pH-scan) the sulfate concentration was allowed to float to adjust the solution's electrical imbalance with changing pH. Then the original solution with added phosphate was modeled. The pH-scan was simulated by addition of small amounts of aqueous NaOH solution.

Results and Discussion

The uranium speciation modeling of all the unaltered waters indicated no precipitation of any minerals. The simulated addition of phosphate changes the speciation dramatically. In the figures graph I gives the speciation for the original field sample, whereas graphs II to IV correspond to the same water, but with an addition of various amounts of phosphate.

Fig. 1 shows the uranium speciation in the strongly acidic flood water of the Königstein mine.

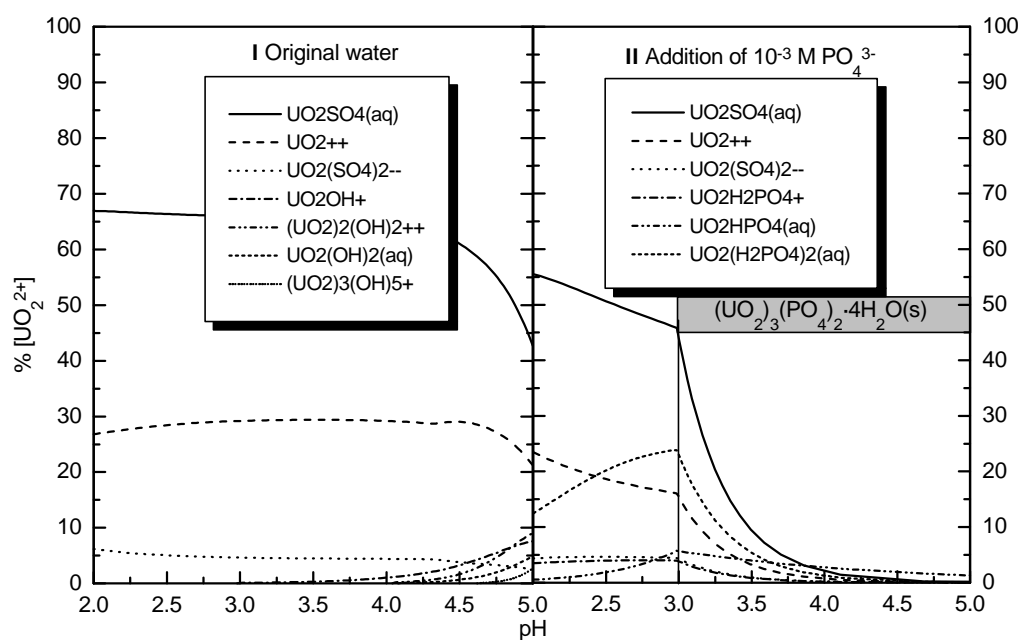


Fig. 1: Uranium speciation for sample A
left: original water, right: with 10⁻³ mol/L additional phosphate

When 10^{-3} M phosphate is added to this water, the aqueous $\text{UO}_2(\text{H}_2\text{PO}_4)_2$ complex forms between pH 2 and 3. At pH 3.0, solid $(\text{UO}_2)_3(\text{PO}_4)_2 \cdot 4\text{H}_2\text{O}$ precipitates. This causes a dramatic decrease of the dissolved uranium.

Fig. 2 depicts another situation. The water from aquifer IV at the Königstein area is much less acidic and has a lower ionic strength and sulfate concentration. Here modeling was performed at three different phosphate concentrations. With increasing PO_4^{3-} - content, the existence region for solid $(\text{UO}_2)_3(\text{PO}_4)_2 \cdot 4\text{H}_2\text{O}$ extends to higher pH, thus binding most (up to 70 %) of the uranyl cations. At the highest phosphate level (10^{-3} M), however, the precipitate is partially dissolved due to the formation of soluble uranium phosphate complexes.

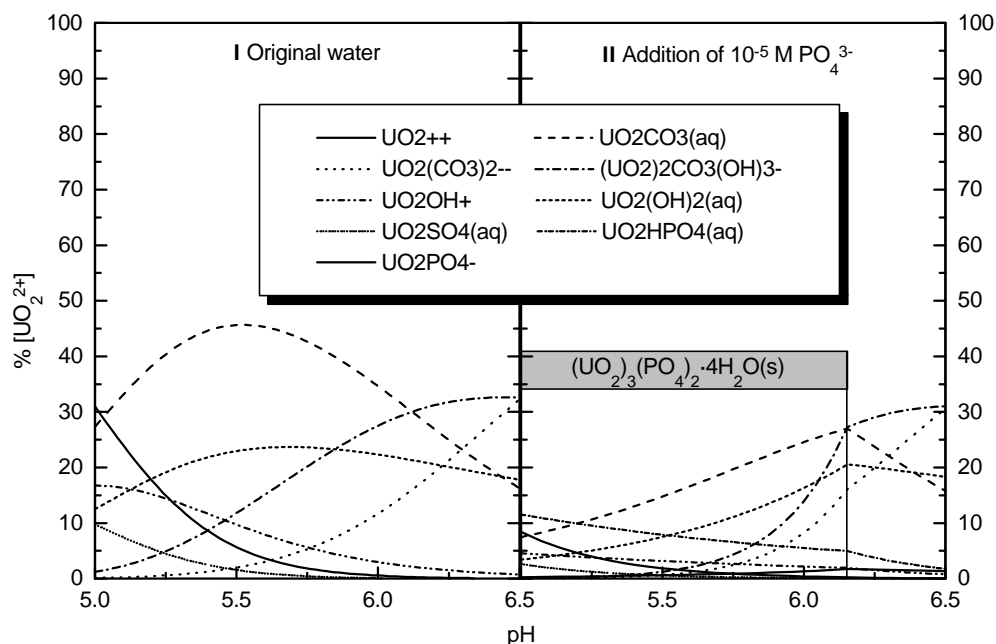


Fig.2a: Uranium speciation for sample B
left: original water, right: with 10^{-5} mol/L additional phosphate

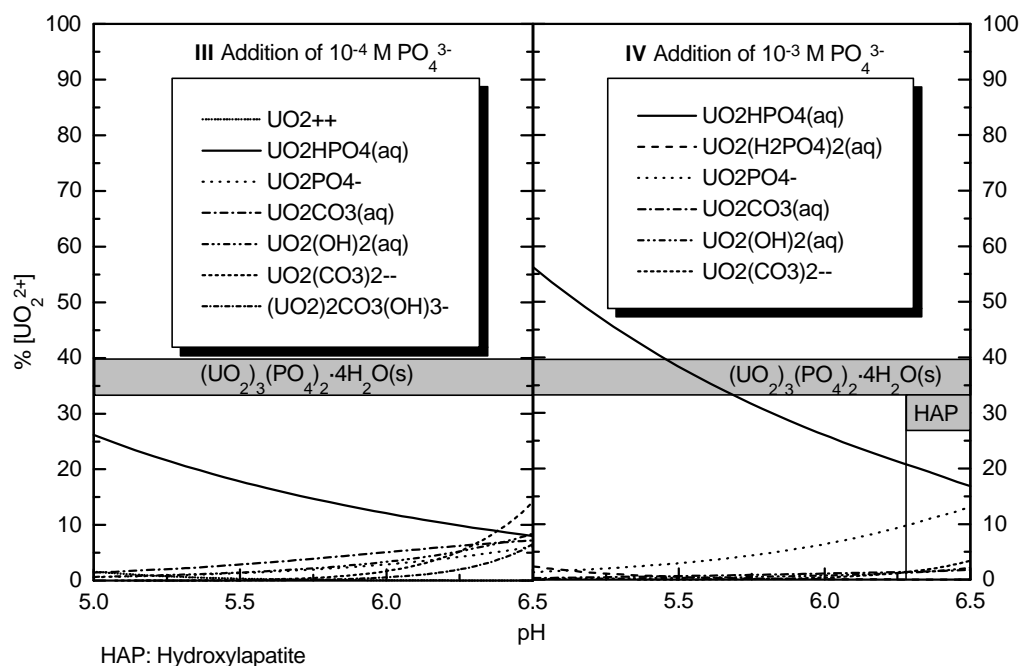


Fig.2b: Uranium speciation for sample B
left: with 10^{-4} mol/L, right: with 10^{-3} mol/L additional phosphate

Fig. 3 shows the results for a neutral water from the mill tailings at Freital. The addition of 10^{-4} M phosphate to the original water changes the uranium speciation. At a pH of 6.3 the solid $\text{Mg}(\text{UO}_2)_2(\text{PO}_4)_2$ (Saleeite) is re-dissolved, Saleeite binds a large fraction of the uranium. Furthermore, at pH 6.35 hydroxylapatite begins to precipitate. For this solution the uranium speciation is independent of phosphate above pH 6.35.

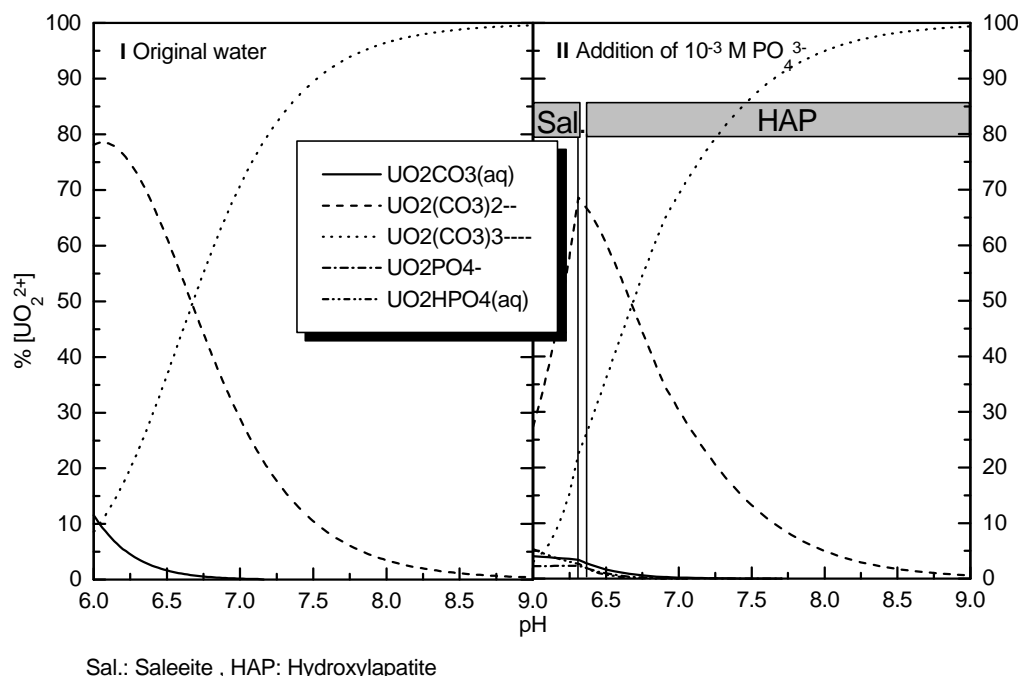


Fig. 3: Uranium speciation for sample C
left: original water, right: with 10^{-3} mol/L additional phosphate

Adding phosphate to acid or neutral waters can immobilize uranium by precipitation of solid uranyl phosphates.

We plan to further evaluate the thermodynamic database for the $\text{UO}_2^{2+}/\text{PO}_4^{3-}/\text{OH}^-$ (aq) system at higher pH values including solid phases.

References

- /1/ Grenthe, I., Fuger, J., Lemire, R. J., Muller, A. B., Nguyen-Trung, C., Wanner, H.: *Chemical Thermodynamics of Uranium*, 1st ed., Elsevier Science, Amsterdam, 1992
- /2/ Brendler, V., Geipel, G., Bernhard, G., Nitsche, H.: Complexation in the system $\text{UO}_2^{2+}/\text{PO}_4^{3-}/\text{OH}^-$ (aq): Investigations at very low ionic strengths. Poster at MIGRATION 95, St.Malo, 1995
- /3/ Thieme, M.: Forschungszentrum Rossendorf, Institute of Radiochemistry, private communication, 1994
- /4/ Reichert: Projekt Deponie Freital (7.Bericht), Vertiefende Erkundung der Sickerwasserhorizonte im Liegenden der Tailings Teich II und Teich III, Landratamt Weißeritzkreis, 1994
- /5/ Leung, V. W.-H., Darvell, B. W., Chan, P.-C.: A rapid algorithm for the solution of the equations of multiple equilibrium systems - RAMESSES, *Talanta* **35**, 713 (1988)
- /6/ Wolery, T. J.: EQ3/6, A software package for the geochemical modeling of aqueous systems. UCRL-MA-110662 Part I, Lawrence Livermore National Laboratory, 1992

SOLUBILITY AND SPECIATION OF $(\text{UO}_2)_2\text{SiO}_4 \cdot 2\text{H}_2\text{O}$ IN AQUEOUS SYSTEMS

H. Moll, G. Geipel, W. Matz¹, G. Bernhard, H. Nitsche
Forschungszentrum Rossendorf e.V., Institute of Radiochemistry,
¹ Institute of Ion Beam Physics and Materials Research

We studied the solubility of uranyl orthosilicate $[(\text{UO}_2)_2\text{SiO}_4 \cdot 2\text{H}_2\text{O}]$ from undersaturation in aqueous solution in air and in N_2 -atmosphere at 25 °C and in a pH range from 3 to 9. The results of such experiments will aid in the evaluation of the source term for migration behavior of uranyl orthosilicate.

We conducted our solubility experiments according to the guidelines given by Nitsche /1/. $(\text{UO}_2)_2\text{SiO}_4 \cdot 2\text{H}_2\text{O}$ was synthesized following a newly developed preparation method /2/. For each run, a known mass of uranyl orthosilicate was transferred to a Teflon cell containing 0.1 M NaClO_4 (p.A., Merck) of known pH ranging from 3 to 9. The pH was adjusted with 0.1 M NaOH (p.A., CO_2 -free, Merck) and 0.1 M HClO_4 (Suprapur, Merck). The pH values obtained for the final solutions were within ± 0.08 of the desired pH. The ratio between the solid phase and the liquid phase was 11 g/L for all experiments. The cells were thermostated at 25 °C and shaken at 100 rpm with an automatic agitator. The approach of steady-state conditions was determined by taking periodically 500 μL samples and analysing them for U and Si content using ICP-MS. The samples were ultrafiltered through Minisart cellulose nitrate membrane filters of 25 nm pore size (Schleicher&Schuell, Dassel, Germany). The X-ray diffraction diagrams of the solid residues at steady-state were recorded in the 2θ range from 8° to 50° (URD 6, Freiburger Präzisionsmechanik, Freiberg, Germany). The Time Resolved Laser-induced Fluorescence Spectroscopy (TRLFS) measurements were performed with a Nd: YAG-MOPO system (SPECTRA PHYSICS, Mountain View, CA, U.S.A.). The excitation wavelength was 355 nm /3/.

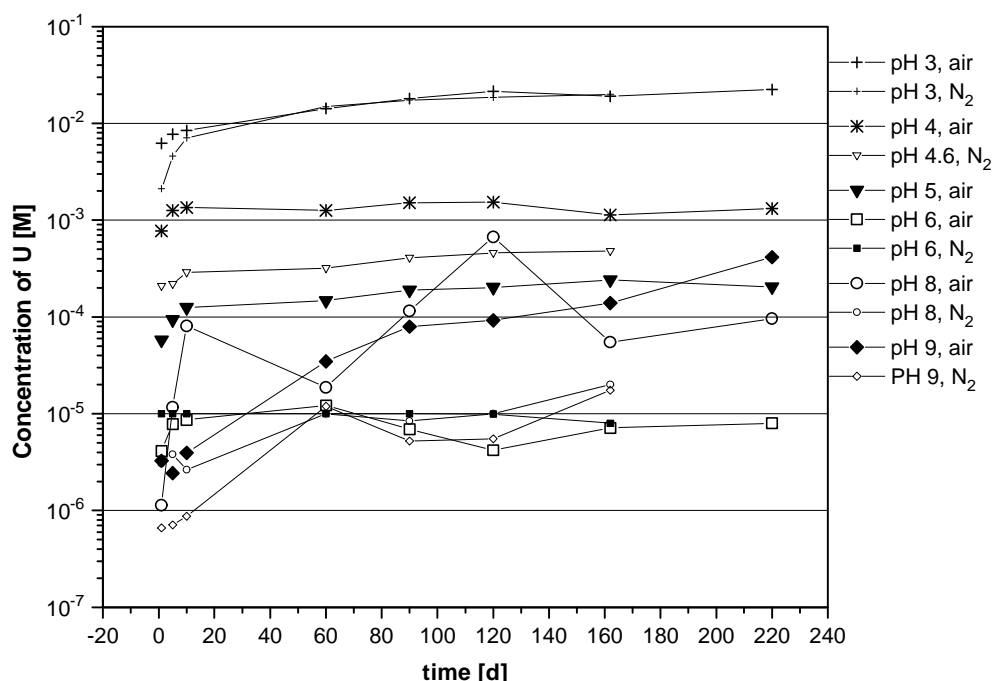


Fig. 1: Concentration of U in 0.1 M NaClO_4 [starting solid phase: $(\text{UO}_2)_2\text{SiO}_4 \cdot 2\text{H}_2\text{O}$] at 25 °C under air and N_2 -atmosphere as a function of time (undersaturation, error is within the size of the symbols)

Fig. 1 depicts the uranium solubility at a given pH as a function of time. Most solutions reached steady-state after about 40 days. The solubility behavior at pH 8 and 9, especially for the systems under air, shows an irregular course. The observed decrease followed by an increase

in uranyl concentration may be due to changes of the uranyl silicate phases. The formation of sodium uranyl silicate phases /4/ and/or uranyl carbonate silicate may occur. XRD measurements of the solid residues at steady-state were performed and showed that the starting compound $(\text{UO}_2)_2\text{SiO}_4 \cdot 2\text{H}_2\text{O}$ was the solubility-controlling solid phase. Nguyen et al. /4/ reported the same result after their solubility test at pH 3. However, the formation of a second solid phase could not be excluded. To investigate the limitations of XRD for detecting a second crystalline phase a mixture of 92.5 wt % $(\text{UO}_2)_2\text{SiO}_4 \cdot 2\text{H}_2\text{O}$ and 7.5 wt % $\text{Na}_2\text{SiO}_3 \cdot 9\text{H}_2\text{O}$ was subjected to X-ray analysis. The measurement showed that the method could clearly distinguish between the two phases at this concentration ratio. The presence of a second crystalline phase with an abundance below 7.5 wt %, however, may remain undetected. Furthermore, it may be difficult or even impossible to detect possible changes at the solid/solution interface by XRD.

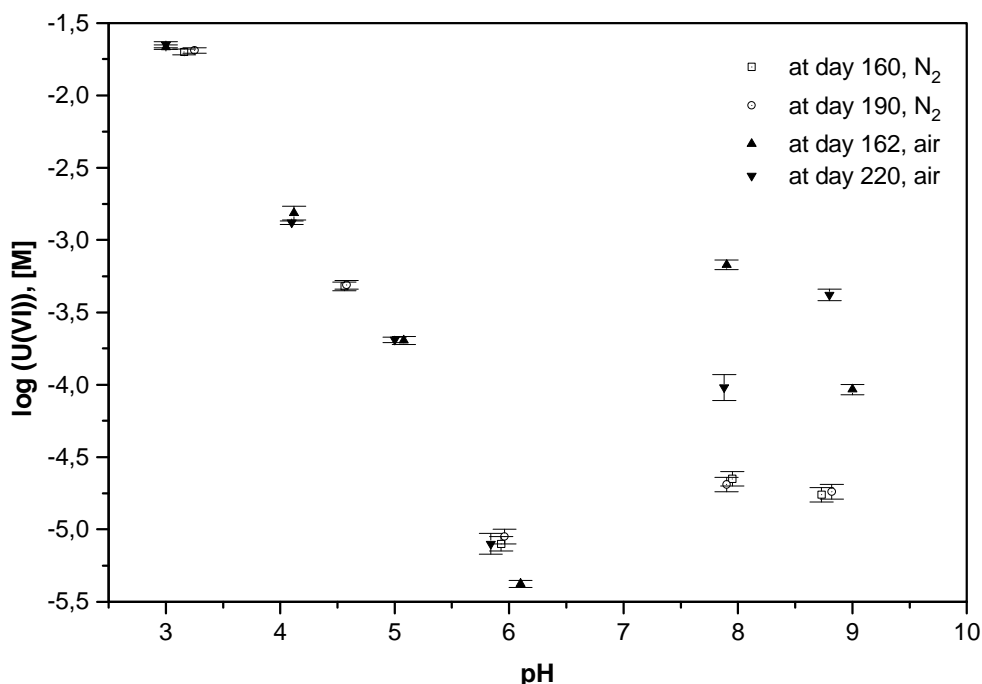


Fig. 2: Solubility of $(\text{UO}_2)_2\text{SiO}_4 \cdot 2\text{H}_2\text{O}$ in 0.1 M NaClO_4 at different times under N_2 -atmosphere and under air as a function of pH.

Fig. 2 shows the pH dependence of the dissolution process of $(\text{UO}_2)_2\text{SiO}_4 \cdot 2\text{H}_2\text{O}$ in 0.1 M NaClO_4 at 25 °C in a nitrogen atmosphere and in air. The solubility of uranyl orthosilicate has a minimum between pH 6 and 7. The observed concentration minimum is more pronounced in the air experiments than in the ones under inert atmosphere. This may be due to the formation of uranyl carbonate complexes in the air-exposed solutions. Calculations are in progress to explain the solubility behavior of $(\text{UO}_2)_2\text{SiO}_4 \cdot 2\text{H}_2\text{O}$ in air and in N_2 -atmosphere using our solubility data and published complexation constants.

Nguyen et al. /4/, studied the solubility of uranyl orthosilicate at pH 3 and described the dissolution with the following reaction:



For reaction (1), the solubility-product constant K_{sp} (I) can be described as :

$$K_{\text{sp}} = \{c(\text{UO}_2^{2+}, \text{aq})\}^2 c(\text{SiO}_2, \text{aq}) / \{c(\text{H}^+, \text{aq})\}^4 \quad (2).$$

The measured solubility products at pH 3, 25 °C and an ionic strength of about 0.1 M are: $\log K(0.1 \text{ M}) = 6.60 \pm 0.53$ and $\log K(0.1 \text{ M}) = 6.46 \pm 0.45$ for air and N_2 -atmosphere, respectively. The values were extrapolated to infinite dilution using the SIT method /5/. The values are $\log K_{\text{air}}^\circ = 6.10 \pm 0.53$ and $\log K_{\text{N}_2}^\circ = 5.98 \pm 0.45$. Our solubility constants agree within the uncertain-

ties with the value of $\log K_{sp}^{\circ} = 5.74 \pm 0.21$ at 30 °C that was reported by Nguyen et al. /4/. The soluble uranium(VI) species at steady-state that were formed in the inert gas-controlled experiments were characterized by TRLFS. Different uranium(VI) species can be distinguished by their different fluorescence life times. Speciation calculations using the program RAMESSES /6/ showed that at each given pH only one uranyl species is present and that the formation of the $UO_2OSi(OH)_3^+$ /7/ complex appears to be negligible. At pH 3 only UO_2^{2+} was detected with a life time of $1.95 \pm 0.1 \mu s$ /8/. Life times of $4.65 \pm 0.1 \mu s$, $18.58 \pm 0.18 \mu s$, $18.80 \pm 1 \mu s$ and $16.80 \pm 3.6 \mu s$ were determined for pH 4.6, 6, 8 and 9, respectively. These life times are typical for hydrolyzed uranyl species. Further measurements are in progress to clarify this issue and to measure the formation of possible uranyl carbonate complexes in the air-controlled experiments by Photoacoustic Spectroscopy.

Acknowledgements

The authors thank Dr. W. Wiesener and Ms. Schäfer for the ICP-MS measurements and Ms. A. Scholz for the XRD measurements.

References

- /1/ Nitsche, H.: *Radiochim. Acta* **52/53**, 3-8 (1991).
- /2/ Moll, H., Matz, W., Schuster, G., Brendler, E., Bernhard, G., Nitsche, H.: *J. Nucl. Mater.* **227**, 40-49 (1995).
- /3/ Bernhard, G., Geipel, G., Brendler, V., Nitsche, H.: *Speciation of Uranium in Seepage Waters of a Mining Tailing Pile Studies by Time-Resolved Laser-Induced Fluorescence Spectroscopy (TRLFS)*, V. Int. Conference on the Chemistry and Migration Behavior of Actinides and Fission Products in the Geosphere, St. Malo, France, Sept. 10-15, 1995.
- /4/ Nguyen, S. N., Silva, J. R., Weed, H. C., Andrews, Jr., J. E.: *J. Chem. Thermodyn.* **24**, 359-376 (1992).
- /5/ Grenthe, I., Fuger, J., Konings, R. J. M., Lemire, R. J., Muller, A. B., Nguyen-Trung C., Wanner, H., in: Wanner, H. and Forrest, I. (eds.): *NEA-TDB Appendix B Ionic strength corrections*.
- /6/ Leung, V. W.-H., Darvell, B. W., Chan, A. P.-C.: *Talanta* **35**(9), 713 (1988).
- /7/ Porter, R.A., Weber, W.J.: *J. Inorg. Nucl. Chem.* **33**, 2443 (1971).
- /8/ Eliet, V., Bidoglio, G., Omenetto, N., Parma, L., Grenthe, I.: *J. Chem. Soc. Faraday Trans.* **91**(15), 2275 (1995).

USING A SURFACE COMPLEXATION MODEL TO SIMULATE THE ADSORPTION OF U(VI) ON FERRIHYDRITE

T. Arnold, M. Kohler¹, G. Bernhard, H. Nitsche
 Forschungszentrum Rossendorf e.V., Institute of Radiochemistry
¹ U.S. Geological Survey, Menlo Park, CA, U.S.A.

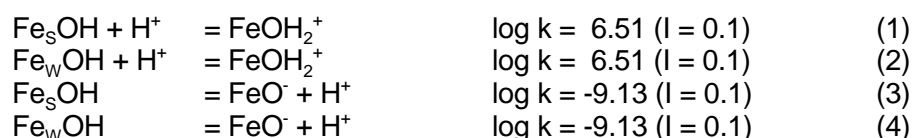
The adsorption of U(VI) onto ferrihydrite was studied in 0.1 M NaNO₃ solution over a wide range of pH in a system open to the atmosphere. The experimental results were modelled in the pH range of 3.5 to 6.0 with the diffuse double layer model and the program FITEQL version 3.1.

Results, discussion and modelling

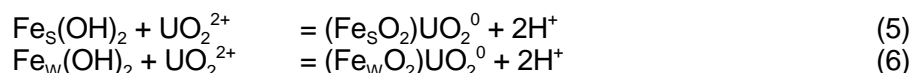
Experimental data derived from batch experiments with various U(VI) concentrations (10⁻⁷ M, 10⁻⁶ M, 10⁻⁵ M, 10⁻⁴ M) were used to model the adsorption of U(VI) onto ferrihydrite in the pH range of 3.5 - 6.0 using the Diffuse Double Layer Model (DDLML). The non-linear least-squares optimization program FITEQL version 3.1 /3/ was applied to the experimental data. FITEQL can adjust the values of one or two unknown surface complex formation constants in a chemical equilibrium model to yield the best fit of the reaction set to experimental data.

The modelling approach considered the simplest stoichiometry and number of reactions possible. The adsorption data were best described using the two-site Langmuir approach with strong and weak coordinative sites to simulate site heterogeneity.

Two types of amphoteric sites are considered, a strong binding site Fe_SOH and a weak binding site Fe_WOH. The acidity constants for both types are identical.



The electrical potential at the surface is assumed to be uniform, that is, of equal value at strong- and weak binding sites. For the model simulations to the U(VI) adsorption, the following bidentate reactions were considered for strong and weak-binding sites.



Calculation with FITEQL, using the above given 6 equations, were performed with experimental adsorption data at pH # 6.0. Site densities were used as recommended by Waite et al./1/, i.e., 1.8 · 10⁻⁶ mol strong sites/mol Fe and 0.875 mol weak sites/mol Fe. A surface area of 600 m²/g of Fe₂O₃ was used, as recommended by Dzombak and Morel /2/. The results of the calculated surface complexation constants of equations (5) and (6) are summarized in Tab. 1 and are graphically displayed in Fig. 1.

Tab. 1: Results of the calculated surface complexation constants

| U _{total} /M | log k (Fe _S O ₂)UO ₂ ⁰ | log k (Fe _W O ₂)UO ₂ ⁰ | WSOS/DF *3 |
|-----------------------|---|---|--------------------|
| 10 ⁻⁴ | - | -6.27 *1 | 14.48 |
| 10 ⁻⁵ | -3.28 | -6.23 | 0.022 |
| 10 ⁻⁶ | -3.37 | -6.19 | 0.004 |
| 10 ⁻⁷ | -2.71 | *2 | 1·10 ⁻⁵ |

*1 Only the weak binding sites were considered, because the number of strong binding sites was very small and therefore could be neglected.

*2 Only the strong binding sites were considered, because their number exceed the number of moles of uranium present in solution and thus the weak binding site could be neglected.

*3 WSOS/DF stands for weighted sum of squares divided by degree of freedom and is an indicator of the goodness-of-fit. The smaller WSOS/DF the better the fit to the experimental data.

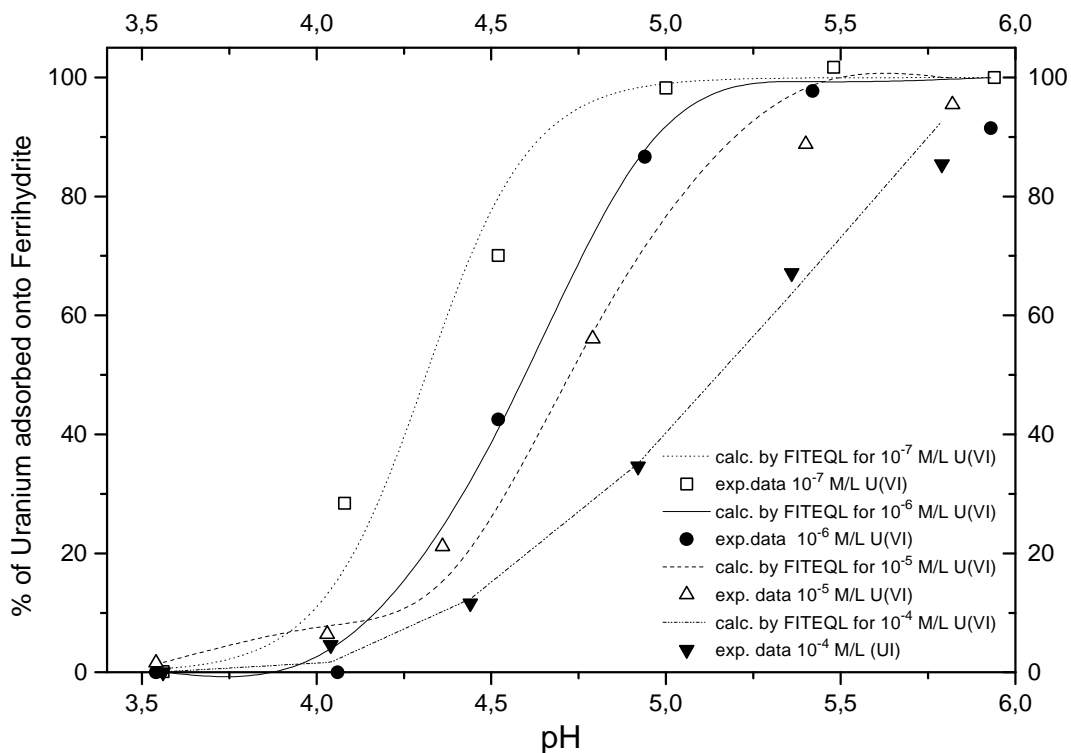


Fig. 1: Experimental sorption data and FITEQL calculations.

Conclusions

A two site diffuse double layer model was able to well describe the adsorption of U(VI) on ferrihydrite over a wide range of pH and U(VI) concentrations, with only one species formed with each site type: an inner-sphere, mononuclear, bidentate complex of the type $\text{Fe}(\text{OH})_2$. Based on these results, it can be concluded that the surface speciation of U(VI) may be far simpler than that observed in aqueous solution. It seems likely that the coordination environment of the ferrihydrite surface may limit the complexity of U(VI) surface speciation. The surface speciation may be significantly less complex than the aqueous solution speciation.

References

- /1/ Waite, T.D., Davis, J.A., Payne, T.E., Waychunas, G.A., Xu, N.: Uranium (VI) adsorption to ferrihydrite: Application of a surface complexation model. *Geochim. Cosmochim. Acta* **58**, 5465 (1994)
- /2/ Dzombak, D.A., Morel, F.M.M. *Surface Complexation Modelling: Hydrous ferric oxide*. Wiley-Interscience. (1990)
- /3/ Herbelin, A., Westall, J. *FITEQL A Computer program for determination of chemical equilibrium constants from experimental data - version 3.1*. Report 94-01 Department of Chemistry, Oregon State University, Corvallis, Oregon 97331. (1994)

SORPTION OF URANIUM-(VI) ON ROCK MATERIAL OF A MINE TAILING PILE : SOLUTION SPECIATION BY FLUORESCENCE SPECTROSCOPY

G. Geipel, G. Bernhard, V. Brendler, H. Nitsche
Forschungszentrum Rossendorf e.V., Institute of Radiochemistry

Sorption experiments of uranium in the concentration range of $1 \cdot 10^{-5}$ - $1 \cdot 10^{-2}$ mol/L were carried out on different rock materials obtained from a mine tailing pile in Schlema, Saxony. The sorption experiments were carried out without external pH control. The experiments were conducted on the bench top. No pH adjustments were made and the pH of the solution was controlled by the properties of the rock material. It reached a characteristic value for each rock material. The initial uranyl perchlorate solution ($1 \cdot 10^{-5}$ M - $1 \cdot 10^{-2}$ M, 0.1 M NaClO₄, pH ~ 3.0) was brought in contact with the rock material for 48 hours /1/, and then the solid and solution were separated by centrifugation (10 min; 3000 rpm). The pH of the contact solution after phase separation was 6.8, 7.9, 8.0, and 9.5 for dark phyllite, mine tailing material, calcite, diabase and dolomite respectively. A solid to solution ratio of 1 to 20 was used for all experiments /2/. The uranium sorbed on the rock material was calculated as the difference between the uranium concentration in solution before and after the sorption process.

Uranium is already present in the rock material from the mine tailing piles. The loosely-bond uranium in the mine tailing rock material was determined by sequential extraction using 0.1 M sodium perchlorate solution /2, 3, 4/, and was later accounted for consideration in the sorption experiments.

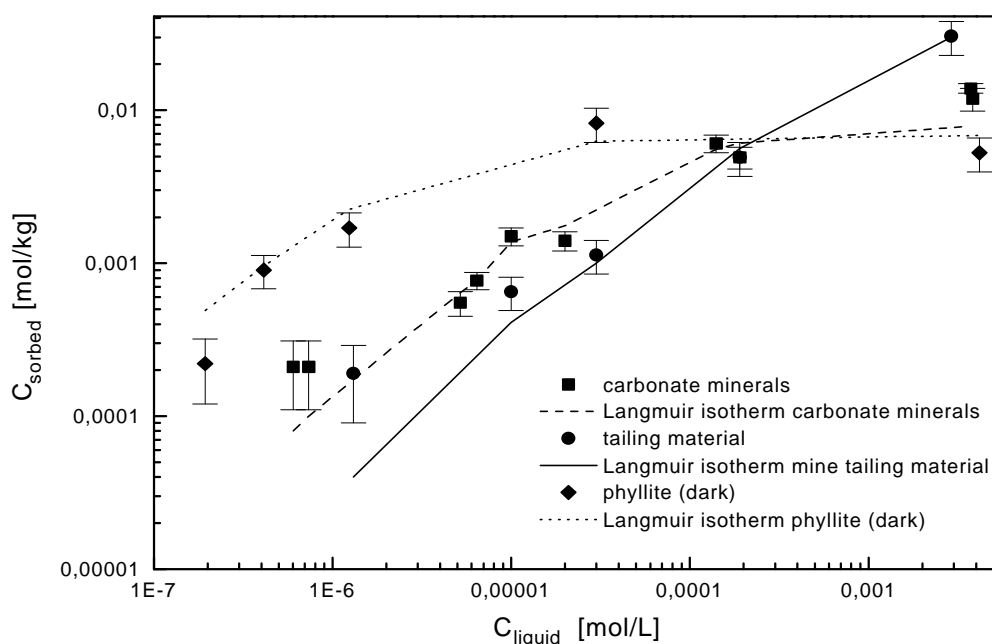


Fig. 1: Sorption data and Langmuir adsorption isotherms for different sorbing materials

Fig. 1 shows the experimentally determined Langmuir isotherms for carbonate minerals, dark phyllite and mine tailing material. The calculated maximum surface concentrations were found to be $8 \cdot 10^{-3}$ mol/kg, $7 \cdot 10^{-3}$ mol/kg and $4 \cdot 10^{-2}$ mol/kg, respectively. Using the specific surface area (BET) the respective surface concentrations were calculated as: $1.2 \cdot 10^{-6}$ mol/m², $1.7 \cdot 10^{-6}$ mol/m² and $2.2 \cdot 10^{-6}$ mol/m². This shows that the maximum surface concentration of uranium for the materials used are closed to each other.

An adsorption constant was derived from the Langmuir isotherms. This constant can be seen as a surface complex formation constant /5/. Tab. 1 shows the calculated values for the different sorbing materials. The adsorption constants increase in the following sequence: mine tailing material < carbonate minerals < dark phyllite.

Tab.1: Specific surface area, maximum surface concentration and adsorption constant of uranium on different sorbing materials

| sorbing material | specific surface area [m ² /g] | maximum surface concentration of uranium [mol/m ²] | adsorption constant [mL/g] |
|-----------------------|---|--|----------------------------|
| mine tailing material | 20.0 +/- 3.0 | (2.2 +/- 0.4)·10 ⁻⁶ | 8·10 ² |
| carbonate minerals | 6.8 +/- 0.5 | (1.2 +/- 0.3)·10 ⁻⁶ | 1.7·10 ⁴ |
| phyllite (dark) | 5.9 +/- 0.5 | (1.2+/- 0.3)·10 ⁻⁶ | 4·10 ⁵ |
| diabase | 4.5 +/- 0.4 | (1.7+/- 0.3) ·10 ⁻⁶ | 5·10 ² |

Compared to the dark phyllite, the carbonate minerals show similar maximum uranium surface concentration (mol/kg). The adsorption constants were smaller for the carbonate minerals than for the phyllite. Non-sorbing uranium(VI) carbonate complexes are formed in the solution. The mine tailing material has a much higher maximum surface concentration than the rest of the investigated materials. It contains multi-layer minerals which can bind uranium via ion exchange processes.

After the sorption process was completed the species in contact solution were studied by time-resolved laser-induced fluorescence spectroscopy (TRLFS). At steady-state conditions, the solution species are in (near-)equilibrium with the sorbing surface and knowledge about their composition should possibly allow conclusions about the sorption reaction mechanism.

The time-resolved fluorescence spectra of the contact solutions show two different types of spectra. In acidic solutions, the spectra show free uranyl ions. In solutions which have pH values between 7 and 8 after the sorption experiments, the spectra indicate the presence of two different uranium species.

Fig. 2 shows the spectra for the calcite contact solution at pH 7.8. The spectra were taken with delay times between 0.03 and 0.17 μs after the applications of the laser pulse. From the spectra, two species were identified with lifetimes of 40 ns and 17 μs.

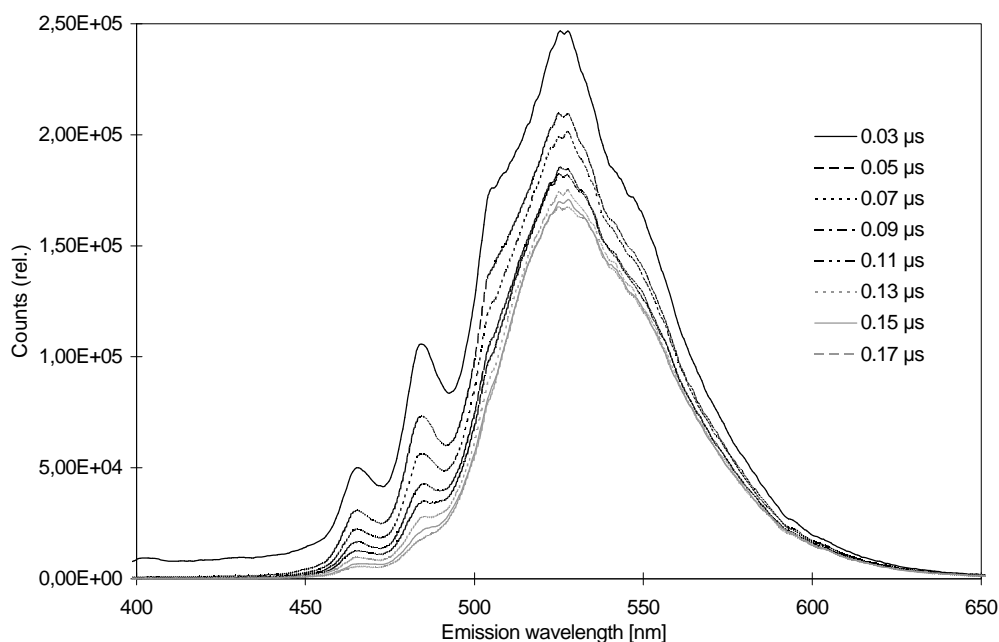


Fig. 2: Time resolved fluorescence spectra of the uranyl solution after contact with calcite

The 17 μs-species could be a hydrolysis product. The emission lines (464 nm, 483 nm, 505 nm and 526 nm) of the 40ns-species are shifted to shorter wavelengths when compared to the lines

of the free uranyl ion. Compared to the fluorescence of the hydroxo species and free uranyl ion, the fluorescence of this species is very small. Other investigations have shown that this species is a calcium-uranyl-carbonate complex.

Both species coexist in the calcite and dolomite solutions. The ratio of these two species depends on the uranium concentration. The concentration of the hydroxo species increases with higher uranium concentrations. Only the uranium hydroxo species exist in sorption experiments with phyllite (Fig.3).

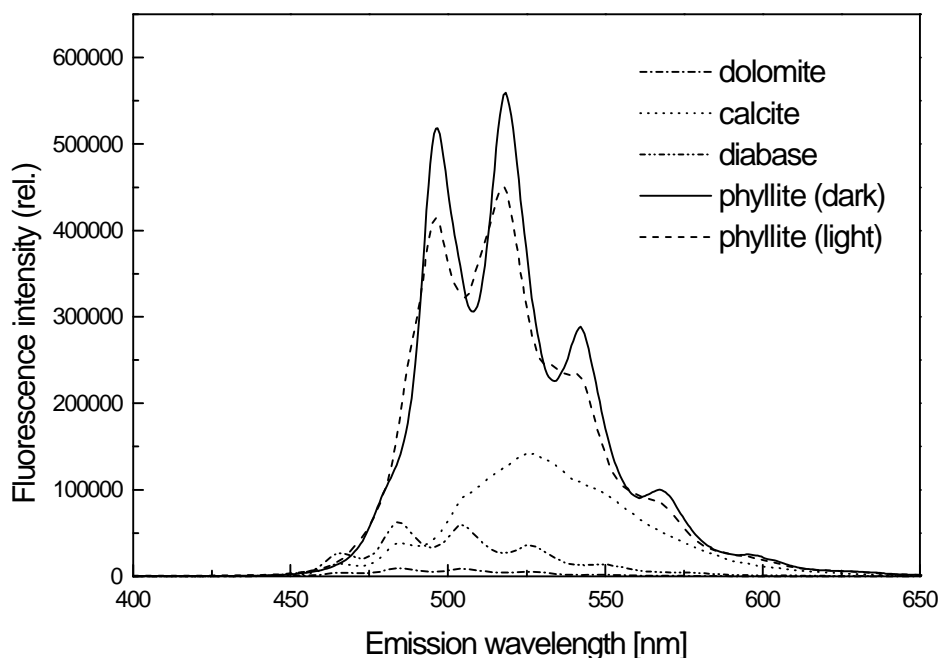


Fig. 3: Fluorescence spectra of U(VI) in different contact solutions (start conc. $1 \cdot 10^{-3}$ M U)

Only the species with the 40 ns-lifetime can be seen in the solution spectrum from sorption experiments with mine tailing material. ESCA measurements of sorbed uranium on diabase, indicate that an exchange of calcium with uranium occurs /6/.

The investigations show that the speciation of uranium in solution can be influenced very strongly by the sorption process. Also an exchange of cations (Ca) from the mineral against uranium can occur. Further studies about the nature of the species in solution and the exchange mechanism are in progress.

References

- /1/ Morris, D. E., Cisholm-Brause, C.J., Barr, M.E., Conradson, S. D., Eller, P.G.: Optical Spectroscopic Studies of the Sorption of UO_2^{++} Species on a Reference Smectite, *Geochim Cosmochim. Acta* **58**, 3613 (1994)
- /2/ Förstner, U.: *Fresenius Zeitschr. Anal. Chem.* **316**, 604-611 (1983)
- /3/ Geipel, G., Thieme, M., Bernhard, G.: Verhalten radiotoxischer Schadstoffe in Hinterlassenschaften des Uranbergbaus als Grundlage für Sanierungskonzepte, Final report 1994, Bundesministerium für Forschung und Technologie, contract no. 02 S 7533
- /4/ Seim, R., Tischendorf, G.: *Grundlagen der Geochemie*, Deutscher Verl. f. Grundstoff-industrie, Leipzig, 1988, S.370
- /5/ Stumm, W.: *Chemistry of the Solid-Water Interface*, J. Wiley & Sons, Inc. New York-Chichester-Brisbane-Toronto-Singapore, 1992, p.91
- /6/ Teterin, Yu. A., Nefedov, V. I., Ivanov, K.E., Baev, A.S., Reich, T., Geipel, G., Nitsche, H.: X-Ray Photoelectron Spectroscopy Study of the Interaction of UO_2ClO_4 with Diabase, publication in preparation

X-RAY PHOTOELECTRON STUDY OF THE INTERACTION OF $\text{UO}_2(\text{ClO}_4)_2$ WITH CALCITE

Yu.A. Teterin¹, V.I. Nefedov², K.E. Ivanov¹, A.S. Baev¹, G. Grambole, G. Geipel, G. Bernhard, T. Reich, H. Nitsche

Forschungszentrum Rossendorf e.V., Institute of Radiochemistry

¹ Russian Research Center "Kurchatov Institute", Moscow, Russia

² Kurnakov Institute, Russian Academy of Sciences, Moscow, Russia

The sorption of uranyl ions from aqueous solutions onto minerals is of great practical interest. In the proximity of uranium deposits, water-soluble uranyl compounds can be formed as a result of various chemical processes. These compounds may migrate through the rock to the source of human water supplies. In particular, this is important in the Erzgebirge, Germany, where uranium may be separated from ground waters by approximately 200 m thick rock formations. Calcite, CaCO_3 , is one of the major components of these rock formations. Therefore, we performed a quantitative surface analysis by X-ray Photoelectron Spectroscopy (XPS) of the calcite before and after treatment with aqueous uranyl perchlorate solution.

Tab. 1: Samples and their preparation.

| Sample | Treatment | Ratio solution/mineral [mL/g] | Final pH | Loading (mg U/g calcite) |
|----------|---|-------------------------------|----------|--------------------------|
| <u>1</u> | untreated | - | - | - |
| <u>2</u> | HClO_4 | 20/1 | 8.18 | - |
| <u>3</u> | de-ionized water | 20/1 | 8.21 | - |
| <u>4</u> | $\text{UO}_2(\text{ClO}_4)_2$ 1 sec rinse with water | 100/1 | 8.65 | 12.8 |
| <u>5</u> | $\text{UO}_2(\text{ClO}_4)_2$ 1 sec rinse with water | 500/1 | 8.93 | 66.3 |
| <u>6</u> | $\text{UO}_2(\text{ClO}_4)_2$ 2 hours rinse with water | 100/1 | 8.75 | 12.5 |
| <u>7</u> | $\text{UO}_2(\text{ClO}_4)_2$ 2 hours rinse with water | 500/1 | 8.58 | 56.8 |

The treatment of samples 1-7 is given in Tab. 1. The mineral CaCO_3 was used in form of a crystalline powder with a particle size smaller than 63 μm and a specific surface area of 6.8 m^2/g . The mineral powder was contacted for 5 hours with 10^{-3} M uranyl solution in a perchlorate medium (0.1 M NaClO_4) with an initial pH of 6. Then, the two phases were separated and the samples were rinsed several times with de-ionized water and dried. The XPS spectra were measured at the Kurchatov Institute, Moscow, with a HP 5950A spectrometer using monochromatized Al $\text{K}_{1,2}$ (1486.6 eV) X-rays. The electron binding energies E_b given in this paper are relative to E_b of C1s electrons (285.0 eV) of the hydrocarbon layer. The uncertainties in the electron binding energy and the relative line intensity are ± 0.1 eV and $\pm 10\%$, respectively. The XPS measurements and their results are described in more detail in /1/.

Based on the results given in Tab. 2, we conclude the following:

1. As one would expect, the atomic ratio U:Ca at the calcite surface increases with the amount of adsorbed uranium (see the results for samples 4 - 7 given in Tab. 1).
2. The absence of ClO_4^- in the interaction product of uranyl perchlorate solution with CaCO_3 shows that there is no physi- or chemisorption of a $\text{UO}_2(\text{ClO}_4)_2$ layer at the calcite surface and no diffusion of ClO_4^- into the calcite grains.
3. The decrease of the $\text{U}4f_{7/2}$ electron binding energy for samples 4 - 7 as compared to E_b for $\text{UO}_2(\text{ClO}_4)_2$ (382.9 eV) and its similarity to E_b in $\text{K}_4\text{UO}_2(\text{CO}_3)_3$ (382.1 eV) indicate the possibility that the uranyl ions enter the calcite lattice and replace calcium ions. In several cases the extent of this exchange at the surface is greater than 20%. However, one has to take into

account that in addition to the CO_3^{2-} groups, the uranyl ions at the calcite surface can be surrounded also by OH^- groups as a result of hydrolysis /2/.

4. As one would expect, the exchange of calcium ions by uranyl ions proceeds more actively in the surface layers of the calcite grains. Therefore, the U:Ca ratio decreases after the grinding of samples 5 - 7.

Tab. 2: Electron binding energies in eV for several elements and the atomic ratio U:Ca.

| Sample | U4f _{7/2} | Ca2p _{3/2} | O1s | C1s (CO_3) ²⁻ | Cl2p _{3/2} | U:Ca |
|----------|--------------------|---------------------|-------|-------------------------------------|---------------------|---------|
| <u>1</u> | | 347.1 | 531.5 | 289.6 | | - |
| <u>2</u> | | 347.2 | 531.5 | 289.6 | 208.4** | - |
| <u>3</u> | | 347.2 | 531.7 | 289.7 | - | - |
| <u>4</u> | 381.9 | 347.3 | 531.7 | 289.7 | - | (0.07)* |
| <u>5</u> | 382.0 | 347.0 | 531.6 | 289.8 | - | 0.45 |
| | 381.9 | 347.0 | 531.5 | 289.7 | - | (0.30)* |
| <u>6</u> | 381.9 | 347.1 | 531.6 | 289.6 | - | 0.08 |
| | 381.9 | 347.0 | 531.6 | 289.6 | - | (0.07)* |
| <u>7</u> | 382.0 | 347.1 | 531.5 | 289.7 | - | 0.21 |
| | 381.9 | 347.1 | 531.5 | 289.7 | - | (0.14)* |

* The atomic ratio U:Ca ratio after sample grinding is given in parenthesis.

** A weak line was observed (content of Cl approx. 2.5 atom percent).

The obtained results agree with the main conclusions of previous studies on the interaction of $\text{UO}_2(\text{ClO}_4)_2$ with CaCO_3 /3,4/. We confirmed that uranyl carbonates are formed mostly at the CaCO_3 grain surface. In addition, the atomic ratio U:Ca at the grain surface was measured also after the sample grinding.

Acknowledgment

We thank Dr. G. Schuster for the determination of the specific calcite surface area.

References

- /1/ Teterin, Yu. A., Nefedov, V. I., Ivanvov, K. E., Baev, A. S., Geipel, G., Reich, T., Nitsche, H.: Doklady Akademii Nauk **344**, 206 (1995) (in Russian).
 /2/ Stipp, S. I., Hochella, M. F.: Geochim. Cosmochim. Acta **55**, 1723 (1991).
 /3/ Carroll, S. A., Bruno, J.,: Radiochim. Acta **52/53**, 187 (1991).
 /4/ Carroll, S. A., Bruno, J., Petit, J. C., Dran, J. C.: Radiochim. Acta **58/59**, 245 (1992).

RADIUM SORPTION ON SANDY AND CLAYEY SEDIMENTS OF THE UPPER SAXON ELBE RIVER VALLEY

L. Baraniak, M. Thieme, G. Bernhard, K. Nindel¹, J. Schreyer¹, H. Nitsche
 Forschungszentrum Rossendorf e.V., Institute of Radiochemistry
¹ WISMUT GmbH, Chemnitz

The interaction of radium with characteristic sediments of the upper Saxon Elbe river valley was investigated with a two-fold aim: to provide key data for transport modelling within the frame of mining site restoration and to study the influence of barium-radium-sulfate coprecipitation on the radium sorption behaviour.

For this purpose sorption measurements were carried out on site-specific sediments (different kinds of sandstone, claystone and lime marl ("Pläner"/)) using (1) original low-mineralized groundwater (Gw) of this area, (2) typical acidic mine water (Mw) coming from sulfuric acid residues of a former in-situ leaching process (~3 g/L SO₄²⁻, pH • 2.5) and (3) groundwater which was contaminated by 2% mine water. The distribution ratios (R_d) were determined by batch technique using 1-10 g crushed and air-dried sediment and 5-50 mL liquid phase. Experiments were performed at least in triplicate. After two-weeks pre-equilibration of the rock with the appropriate water ²²⁶Ra was added with an activity varying from 40 to 2·10³ Bq. The samples were gently agitated for 8 weeks at constant temperature of 14 °C, which is similar to the aquifers' temperature.

Radium sorption from pure and slightly contaminated groundwater onto limonite-rich turonian sandstone (t_{1sLi}), for example, is characterized by relatively low distribution ratios (Tab. 1). When contacted with mine water, the sorption was enhanced by more than 20-fold compared to the pure and contaminated groundwaters. For the typical lime marl ("Pläner"), the strongest sorption occurs from the groundwater and a slightly reduced sorption took place from the acidic mine water.

Tab. 1: Radium distribution ratios of sandstone and lime marl in dependence on the water type (c₀(Ra) = 0.5·10⁻⁹ - 4.86·10⁻⁹ mol/L, R_d [mL/g]), Gw = low-mineralized groundwater, Mw = mine water, Gw/Mw = Gw contaminated with 2% Mw

| water type Y geomaterial \ | Gw (pH•6.2) | Gw/Mw(2%) (pH•4.9) | Mw (pH•2.6) |
|--------------------------------|----------------|-----------------------|----------------|
| sandstone (t _{1sLi}) | 55 - 180 | 100 - 180 | 1280 - 3420 |
| lime marl (t _{1p}) | 390 - 520 | 380 - 760 | 230 - 390 |

The radium sorption was studied as a function of the Ba²⁺ and SO₄²⁻ concentration (Tab. 2 and Tab. 3). At low [Ba²⁺] and [SO₄²⁻] the average R_d of sandstone and lime marl amounts to 54 and 500 mL/g, respectively. For sulfate concentration from 0.01 to 0.1 mol/L, a three-fold increase in R_d was observed for both sediments. Using the ion product of barium and sulfate (I_p), this increase becomes significant above 2.5·10⁻⁹ mol²/L². We found that the solubility product was exceeded for all solutions when compared with the solubility product of BaSO₄, K_{s,0} = 6.34·10⁻¹¹ mol²/L² at 14°C (calculated by linear interpolation of log K_{s,0} = -10.486 and -9.971 for 0 °C and 25 °C, respectively). Beneš et al. /1/ pointed out that the overall barium or radium concentration can be higher than expected if one only considers the solubility product. The concentration of the undissociated dissolved barium sulfate complex is determined by the product of the formation constant of the neutral complex (log K₁ = 2.30) and the solubility product; it is about 2.1·10⁻⁸ mol/L at 25 °C.

The high radium sorption on both sediments from either 0.1 M NaSO₄ solution or the sulfate-rich mine water indicates that surface precipitation is the main sorption mechanism. This is in addition to the ion-exchange on the clayey components. Similar findings are reported by Reichel and Koß /2/ who concluded from the radium distribution ratios for Gorleben sediments /3, 4/ that the main sorption mechanisms are precipitation and surface complexation.

Tab. 2: Radium sorption on sandstone as a function of the Ba^{2+} and SO_4^{2-} concentration of the aqueous phase

| | | | | | | |
|-----------------------------------|-----------------------|----------------------|----------------------|----------------------|---------------------|---------------------|
| $c(\text{Ba}^{2+})$ ¹⁾ | $7.3 \cdot 10^{-7}$ | $4.0 \cdot 10^{-6}$ | $7.3 \cdot 10^{-7}$ | $2.0 \cdot 10^{-5}$ | $7.3 \cdot 10^{-7}$ | $7.3 \cdot 10^{-7}$ |
| $c(\text{SO}_4^{2-})$ | $1.25 \cdot 10^{-4}$ | $1.25 \cdot 10^{-4}$ | $1.0 \cdot 10^{-3}$ | $1.25 \cdot 10^{-4}$ | $1.0 \cdot 10^{-2}$ | $1.0 \cdot 10^{-1}$ |
| I_p/BaSO_4 ²⁾ | $9.13 \cdot 10^{-11}$ | $5.0 \cdot 10^{-10}$ | $7.3 \cdot 10^{-10}$ | $2.5 \cdot 10^{-9}$ | $7.3 \cdot 10^{-9}$ | $7.3 \cdot 10^{-8}$ |
| R_d ³⁾ | 64.7 | 47.4 | 56.5 | 47.7 | 90.4 | 140 |
| $\log R_d$ | 1.81 | 1.68 | 1.75 | 1.68 | 1.96 | 2.15 |

¹⁾ c [mol/L], ²⁾ I_p [mol^2/L^2], ³⁾ R_d [mL/g]

Tab. 3: Radium sorption on lime marl as a function of the Ba^{2+} and SO_4^{2-} concentration of the aqueous phase

| | | | | | | |
|-----------------------------------|-----------------------|----------------------|----------------------|----------------------|---------------------|---------------------|
| $c(\text{Ba}^{2+})$ ¹⁾ | $7.3 \cdot 10^{-7}$ | $4.0 \cdot 10^{-6}$ | $7.3 \cdot 10^{-7}$ | $2.0 \cdot 10^{-5}$ | $7.3 \cdot 10^{-7}$ | $7.3 \cdot 10^{-7}$ |
| $c(\text{SO}_4^{2-})$ | $1.25 \cdot 10^{-4}$ | $1.25 \cdot 10^{-4}$ | $1.0 \cdot 10^{-3}$ | $1.25 \cdot 10^{-4}$ | $1.0 \cdot 10^{-2}$ | $1.0 \cdot 10^{-1}$ |
| I_p/BaSO_4 ²⁾ | $9.13 \cdot 10^{-11}$ | $5.0 \cdot 10^{-10}$ | $7.3 \cdot 10^{-10}$ | $2.5 \cdot 10^{-9}$ | $7.3 \cdot 10^{-9}$ | $7.3 \cdot 10^{-8}$ |
| R_d ³⁾ | 643 | 420 | 463 | 485 | 951 | 1490 |
| $\log R_d$ | 2.81 | 2.62 | 2.67 | 2.69 | 2.98 | 3.17 |

¹⁾ c [mol/L], ²⁾ I_p [mol^2/L^2], ³⁾ R_d [mL/g]

Acknowledgements

The authors would like to thank the WISMUT/Sanierungsbetrieb Königstein for sampling and for supplying the geomaterials, the groundwater and mine water. The laboratory assistance of H. Neubert and A. Otto is gratefully acknowledged.

References

- /1/ Beneš, P., Obdrňálek, M., „ejchanová, M.: The Physicochemical Forms of Traces of Radium in Aqueous Solutions Containing Chlorides, Sulfates and Carbonates. *Radiochem. Radioanal. Letters* **50**, 227 (1982).
- /2/ Reichel, A., Koß, V.: Modelling of Radium Sorption and Speciation in Natural Sediment-Groundwater Systems. In Merkel, B., Hurst, S., Löhnert, E.P., Struckmeier (eds.), *Proc. Internat. Conf. and Workshop on Uranium-Mining and Hydrogeology*, Freiberg, Germany, Oct. 1995.
- /3/ Meier, H., Zimmerhackl, E., Zeitler, G., Menge, P., Albrecht, W.: Experimental Investigation of Radionuclide Diffusion in Site-Specific Sediment/Groundwater Systems. *Radiochim. Acta* **58/59**, 341 (1992).
- /4/ Meier, H., Zimmerhackl, E., Zeitler, G., Menge, P., Hecker, W.: *J. Radioanal. Nucl. Chem., Articles*, **109**, 139 (1987).

RADIUM SPECIATION STUDIES IN GROUNDWATERS AND LEACHING SOLUTION OF THE KÖNIGSTEIN URANIUM MINE

M. Thieme, L. Baraniak, V. Brendler, G. Hüttig, H. Zänker, H. Nitsche, K. Nindel¹, J. Schreyer¹
 Forschungszentrum Rossendorf e.V., Institute of Radiochemistry
¹WISMUT GmbH, Chemnitz

The migration of hazardous elements and radionuclides in ground waters depends on the degree of their interaction with the surrounding rock material. This interaction will be influenced by the speciation of each of the solutes.

We studied the speciation of radium in different solutions that are actual or potential carriers of this contaminant:

- i) ground water of the lowest Aquifer no. 4 at Königstein that contains considerable amounts of radium (GwIV, <100 Bq ²²⁶Ra / dm³).
- ii) drain solution (DFE) which is collected within the mine at the bottom of rock sections ("blocks") that were previously leached with sulphuric acid. Tab. 1 shows, that this solution is still rich in acid, whereas the concentration of Ra isotopes are low. The leached rock is thought to contain the majority of the original Ra inventory and DFE may therefore represent an important source for the output of Ra.
- iii) ground water of Aquifer no. 3 (GwIII) that is located above the mine. This aquifer may become contaminated in the flooding process by ascending waters of Aquifer no. 4 because the two watertables are connected by natural fractures.

Tab. 1: Selected parameters of the fluids tested; sampling March 21/22, 1995

| Parameter | Unit | Draining solution | Ground water GwIV | Ground water GwIII |
|-------------------------------|--------------------|-------------------|-------------------|--------------------|
| pH | | 2.6 | 4.5 | 6.1 |
| Specific Conductance | mS/cm | 5.47 | 0.09 | 0.15 |
| Na (AAS) | mg/dm ³ | 170 | 3.71 | 2.53 |
| Ca | " | 289 | 5.39 | 17.2 |
| Fe (ICP-MS) | " | 3.3 | 0.77 | <0.1 |
| Zn | " | 49 | 0.25 | 0.025 |
| Ba | " | 0.005 | 0.089 | 0.275 |
| Pb | " | 0.147 | 0.004 | 0.007 |
| Th | " | 0.40 | 0.0003 | <0.0001 |
| U | " | 23 | 0.29 | 0.006 |
| U-238(-Spectrometry) | Bq/dm ³ | 285 | <40 | <8 |
| Th-234 | " | 272 | 3.7 | 0.9 |
| Ra-226 | " | 14 | 46 | 2.4 |
| U-235 | " | 13.3 | <1.9 | 0.4 |
| Ra-223 | " | 28 | <1.7 | 0.4 |
| Ra-224 | " | <1.1 | <0.4 | 0.3 |
| Ra-226 (Emanation) | " | 0.9 | 57 | 2.4 |
| TIC (Ion Chromatography) | mg/dm ³ | <2 | 43 | 95 |
| SO ₄ ²⁻ | " | 2820 | 21 | 12 |
| NO ₃ ⁻ | " | 7.5 | <1 | 3 |
| Cl ⁻ | " | 171 | 3.9 | 4.6 |

Radium in ground waters is most frequently reported in the literature to exist in dissolved chemical forms but it has also been found in particulate forms /1,2/.

We examined the groundwater from Aquifer no. 4 (i) with ultrafiltration in order to determine if radium was bound to colloids. The filters had pore sizes of 400 nm (Sartorius), 15 nm (Nuclepore) and 3 kDa (about 4 nm; Amicon). To minimize alteration of the oxidic water due to the transport, we established the ultrafiltration apparatus below ground just in the neighborhood of the collecting site of GwIV. The Ra liquids were analysed by liquid scintillation counting (LSC) after Ra was separated by (Pb,Ba,Ra)SO₄ precipitation, dissolved and re-precipitated as (Ba,Ra)SO₄. The relative standard deviation of this method was 2% at an activity level of 40 Bq.

Tab. 2: ²²⁶Ra activity concentrations of ground water GwIV before and after filtration using filters of different pore sizes.

| Sample | Filtrate volume [dm ³] | ²²⁶ Ra [Bq dm ⁻³] |
|-------------------|------------------------------------|--|
| GwIV, original | | |
| | 0.050 | 50.8 |
| | 0.050 | 44.4 |
| Filtrates, 400 nm | | |
| fraction 1 | 0.051 | 46.5 |
| fraction 2 | 0.048 | 51.6 |
| fraction 3 | 0.051 | 47.9 |
| fraction 4 | 0.048 | 46.3 |
| Filtrates, 15 nm | | |
| fraction 1 | 0.008 | 48.7 |
| Filtrates, 3 kDa | | |
| fraction 1 | 0.036 | 51.1 |
| fraction 2 | 0.037 | 42.8 |
| fraction 3 | 0.048 | 39.5 |
| fraction 4 | 0.048 | 39.9 |

Tab. 2 gives the concentrations of the unaltered ground water (about 50 Bq/dm³) as well as of the respective filtrate fractions. The values indicate that the filtrations through the 400 nm and 15 nm filters do not decrease the dissolved radium. No sorption effects on the filter materials were observed. A different result was found for the 3 kDa filter. The marked radium decrease with progressing filtration may be caused by filter clogging (for the problem of filter clogging see e.g., /3/) and would point to a slight sorption effects. However, if the data of the fractions are randomly scattered, the overall concentration appears somewhat lower when compared to the original state. Testing for significance, this hypothesis must be rejected if a low error probability is set (#5%). The analyses of the filters confirm for this ground water that practically no radium is bound to colloids that are larger than several nanometers in diameter. According to ICP-MS analysis, the present colloids are mainly ferric hydrous oxides.

For the drain solution (ii) and groundwater from Aquifer no. 3 (iii), the charge state of Ra was investigated by free liquid electrophoresis similarly to the work of Benes et al. /4/. The behaviour of the major natural radium isotopes ²²⁶Ra and ²²³Ra was traced with the shorter living ²²⁴Ra (3.66 d) because the detection method for the electrophoresis required a higher activity level. ²²⁴Ra was obtained from a generator /5/ fed with 5 MBq of ²²⁸Th. After the eluate was chemically processed to prepare the test solutions, amounts of 0.05-0.1 cm³ were injected into the filled electrophoresis tube. The radionuclide distribution was directly followed using a gamma-ray sensitive NaI(Tl) detector which scanned the tube /6/. However, ²²⁴Ra could not be measured due to its low emission probability of the 241 keV photon (4.10% /7/). Therefore, the gamma radiation of its decay product ²¹²Pb was measured at 239 keV (43.5% /4/). The activity distribu-

tion was recorded in time intervals of about 50 h.

For GwIII (pH 7.4) it was found that the majority of radium exists as cations. The electrophoretic mobility was $6.5 \times 10^{-4} \text{ cm}^2 \text{ s}^{-1} \text{ V}^{-1}$ corresponding to Ra^{2+} . Benes et al. [4] gave a value of $(6.02 \pm 0.11) \times 10^{-4} \text{ cm}^2 \text{ s}^{-1} \text{ V}^{-1}$ for 0.01 M chloride solutions for pH 2 to 7 and 25°C. The existence of neutral complexes could not be ruled out. In the drain solution (ii) in addition to the radium cations, anionic species (ca. $4 \times 10^{-4} \text{ cm}^2 \text{ s}^{-1} \text{ V}^{-1}$) were detected when the migration direction was reversed. There were less anions than cations. No radium remained at the starting point, i.e., neutral species were not found.

To compare the findings with available data, the radium speciation was calculated using the program package RAMESES VIII and the following thermodynamic equilibrium data [8, 9]:

| | | | | | |
|------------------|---|----------------------|---|---------------------------------|------------------|
| Ra^{2+} | + | SO_4^{2-} | W | $\text{RaSO}_4(\text{aq})$ | $\lg K_1 = 2.43$ |
| Ra^{2+} | + | 2SO_4^{2-} | W | $\text{Ra}(\text{SO}_4)_2^{2-}$ | $\lg K_2 = 2.89$ |
| H^+ | + | SO_4^{2-} | W | HSO_4^- | $\lg K_3 = 1.98$ |

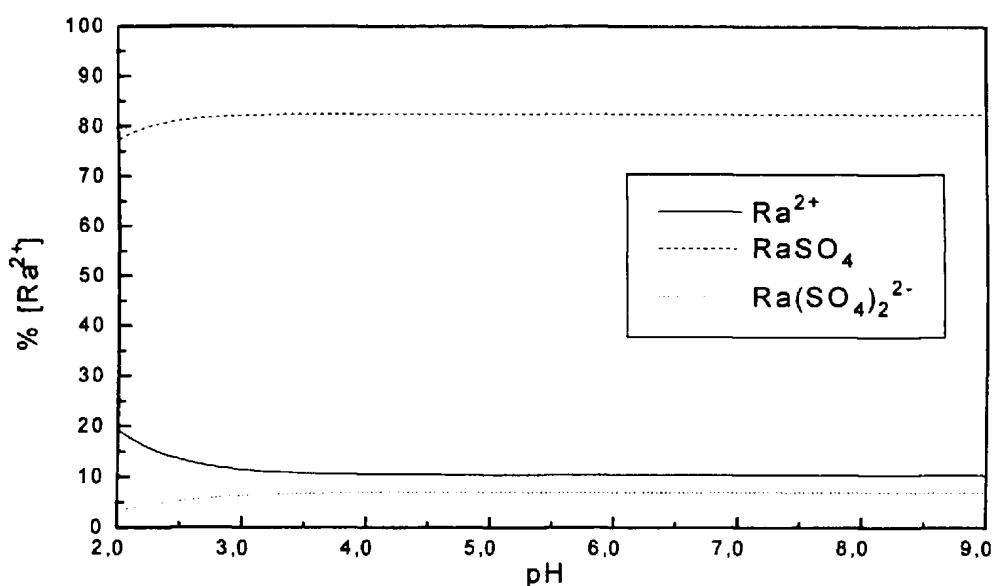


Fig. 1: Radium speciation diagram for the drain solution over a wide pH range. ($29.4 \text{ mmol SO}_4^{2-} / \text{dm}^3$, $0.9 \text{ Bq } ^{226}\text{Ra} / \text{dm}^3 \times 1.09 \times 10^{-13} \text{ mol Ra} / \text{dm}^3$)

Fig. 1 shows the speciation of radium in DFE from pH 2 to 9. At pH 2.6, the pH of the drain solution, the radium is predicted to exist to 82% as undissociated RaSO_4 , to 13% as Ra^{2+} and to 5% as $\text{Ra}(\text{SO}_4)_2^{2-}$. When carbonate was included in the calculation the result did not change. When the results of the speciation calculation are compared with the results from the migration experiments, the ionic species agreed with each other, whereas the neutral RaSO_4 could not be found in the experiments. This is surprising because electrophoresis is a well-established method in speciation chemistry. Further verification of these results are being planned.

Acknowledgements

The authors are indebted to Dr. F. Sebesta and Prof. P. Benes, Czech Technical University of Prague, for their support with the preparation of the generator. The practical assistance of Dr. D. Schumann and Dr. M. Andrassy, Technical University Dresden and of the personnel of the Wismut GmbH involved in the ultrafiltration experiments is gratefully acknowledged. Analyses were performed by H. Neubert (LSC), U. Schaefer (AAS), Dr. W. Wiesener (ICP-MS), D. Birnstein (IC), M. Bothe, VKTA (gamma spectrometry), B. Gleisberg, VKTA (emanation method).

References

- /1/ Von Gunten, H. R., Benes, P.; Speciation of Radionuclides in the Environment, *Radiochim. Acta* **69**, 1 (1995).
- /2/ Vilks, P., Cramer, J. J., Shewchuk, T. A., Larocque, J. P. A.; Colloid and particulate matter studies in the Cigar Lake natural-analog program, *Radiochim. Acta* **44/45**, 305 (1988).
- /3/ Karlsson, S., Peterson, A., Hakansson, K., Ledin, A., Fractionation of Trace Metals in Surface Water with Screen Filters, *Sci. Total. Environ.* **149**, 215 (1994).
- /4/ Benes, P., Obdrzalek, M., Use of Radiotracer Method for the Analysis of the State of Radium in Waste and Surface Waters, *Hydrochemia '80*, Bratislava 1980, Proc. p. 139.
- /5/ Sebesta, F., Sary, J., A Generator for Preparation of Carrier-Free ^{224}Ra , *ibid.* **21**, 151 (1974).
- /6/ Rosch, F., Dreyer, R., Khalkin, V. A., Prinzipien der Elektromigrationsmessungen. *Analytik von Komplexbildungsgleichgewichten*, ZfK-677, August 1989.
- /7/ Schötzig, U., Schrader, H., *Halbwertszeiten und Photonen-Emissionswahrscheinlichkeiten von häufig verwendeten Radionukliden*, 4. Auflage, PTB-Ra-16/4, Braunschweig, Juli 1993.
- /8/ Benes, P., Obdrzalek, M., Cejchanova, M., The Physicochemical Forms of Traces of Radium in Aqueous Solutions Containing Chlorides, Sulfates and Carbonates, *Radiochem. Radioanal. Letters* **50**, 227 (1982).
- /9/ Smith, R. M., Martell, A. E., *Critical Stability Constants*, vol. 4, Inorganic Complexes, New York: Plenum 1976.

DENSITY, SPECIFIC SURFACE AREA AND POROSITY OF ELBE VALLEY SEDIMENTS

G. Schuster*, L. Baraniak, M. Thieme, G. Bernhard, H. Nitsche, K. Nindel¹, J. Schreyer¹
 Forschungszentrum Rossendorf e.V., Institute of Radiochemistry; *WIP TU Dresden
¹ WISMUT GmbH, Chemnitz

Permeability and sorption are major parameters for the transport of radionuclides in the geological formations. They depend on the physico-chemical microstructure of the rock material. Therefore, the values of the density, the specific surface area and the porosity of the solid phase are necessary for the quantitative determination of the migration behaviour. Results of such investigations on sandstones and clays of the Elbsandsteingebirge are presented. They were used to investigate the sorption and extraction behaviour in Elbe valley sediments /1,2/.

1. Density of the rock materials

Depending on the definition of the volume v , three different density relations exist:

$$\begin{array}{llll}
 \text{Geometrical density} & k = m/v & v = V_{\text{solid}} & + V_{\text{closed pores}} & + V_{\text{open pores}} \\
 \text{Material density} & k = m/v & v = V_{\text{solid}} & + V_{\text{closed pores}} & \\
 \text{Theoretical density} & k = m/v & v = V_{\text{solid}} & &
 \end{array}$$

The geometrical density is commonly used for calculating metal and radionuclide migration in aqueous solutions. The geometrical and material density and the open porosity were determined with the penetration immersion method. It is based on the buoyancy in xylol /3/. From the compact rock material slices were cut that had of 15-mm diameter and 5-mm thickness. The accuracy of this method is $F = \pm 0.001 \text{ g/cm}^3$. The results of the density measurements are given in Tab. 1.

Tab.1: Results of the measurements of the geometrical- and material density

| sample | density [g/cm ³] | | specific surface area [m ² /g] | |
|----------------------------------|------------------------------|----------|---|----------------------------|
| | geometrical | material | particle diameter 0.063-0.63 μm | particle diameter 1-2.5 mm |
| cenomanian quader sandstone | 2.24 | 2.65 | < 1 | < 1 |
| cenom. quad. sandst., leached | 2.13 | 2.65 | < 1 | < 1 |
| turonian maser sandstone | 2.14 | 2.64 | 6.1 | - |
| tur. mas. sandst., with limonite | 2.11 | 2.65 | < 1 | 1.4 |
| turonian clay | 2.07 | 2.55 | - | - |
| porous lime marl | 2.01 | 2.65 | 8.9 | 8 |
| lime marl | 2.45 | 2.66 | 12.6 | 10.4 |

Leaching is a treatment with dilute sulfuric acid, porous lime marl equivalent was formed by longtime contact with acidic, oxygen rich water.

The geometrical density values for all sandstone samples including the clay-containing samples are within a range of 2.0 - 2.5 g/cm³. The material density of almost all samples is 2.65 g/cm³. This value is comparable with that of quartz which has a theoretical density of 2.65 g/cm³. This agreement between the material density and the theoretical density suggests, that the closed porosity is zero for all that samples. However, deviations from this value may not be due to closed porosity alone but they can also be a result of a different chemical composition. The samples consist of pure, highly dense quartz particles with a fine grain binder of quartz and clay between the particles.

2. Specific Surface Area

The measurements were performed according the method of Haul and Dümbgen /4/. After annealing the samples at 200°C, they were cooled to -195°C in a nitrogen atmosphere. The amount of nitrogen adsorbed is measured by the pressure decrease in the calibrated volume.

Calculation of the specific surface areas were made using an approximation method based on the BET theory. The particle diameter of the samples was about 3 mm. The accuracy of the results is within $\pm 10\%$. The results of this measurements are given in Tab. 1.

The small values of the specific surface area show, that the fine grained binder does not essentially increase the small surface area values of the large quartz particles forming the quader sandstone. Consequently it was not found a relation between the particle size and the surface area for this materials. They mainly consists of very smooth and tight quartz particles. The larger clay content of the turonian sandstones cause a higher specific surface area. The clay related lime marl rocks have a specific surface areas of 7 - 9 m²/g and show a decrease of the surface from the fine-grained material to the coarser one. Here a much larger adsorption capacity for radionuclides can be expected.

3. Open porosity and the pore size distribution

The open rock porosity which is defined by the integral porosity and the pore size distribution is the most important parameter for the transport of radionuclides through sandstone. For pore-sizes determination from 1.8 nm - 80 μm , mercury porosimetry is a suitable method. In this method, mercury is pressed into the pores with pressures up to 420 MPa. Using the following equation the pore volume for a special pore size can be calculated from the volume of the intruded Hg at the corresponding pressure:

$$r = \frac{2 F \cdot \cos \theta}{p}$$

F = surface tension p = pressure θ = wetting angle r = pore radius

This method is not very accurate for fine pore sizes range from 1.5 - 300 nm. Therefore, pore sizes for the lime marl samples were additionally determined using the gas adsorption desorption hysteresis method. The samples for the Hg porosimetry were compact pieces with a volume of approximately 1 cm³. The adsorption desorption method samples were particles from about 3 mm. The results are shown in Tab. 2.

Tab. 2: Open porosity and pore size values for 4 pore size regions taken from Hg porosity measurements

| sample | open porosity [vol %] | | | | G porosity |
|-------------------------------|------------------------|----------------------------|------------------------|-------------------|------------|
| | < 0.0018 μm | 0.0018 - 4.2 μm | 4.2 - 85 μm | >85 μm | |
| cenomanian sandstone s | 0 | 3.07 | 17.43 | 0.09 | 20.83 |
| turonian sandstone | 0 | 16.35 | 1.48 | 0 | 17.83 |
| cenomanian sandstone n | 0 | 1.06 | 14.22 | 0.11 | 15.39 |
| cenom. sandstone leached | 0 | 1 | 17.66 | 0.7 | 19.36 |
| turon. sandstone with limonit | 0 | 6.94 | 17.41 | 0 | 24.35 |
| lime marl | 0.32 | 5.73 | 0.32 | 0 | 6.37 |
| porous lime marl | 0 | 22.15 | 1.25 | 0.02 | 23.42 |
| turonian clay | 0 | 17.33 | 1.55 | 0 | 18.88 |

Tab. 2 shows that the porosity corresponds well with the density measurements. The sandstones with open porosities of 15 - 24% have a large permeability for water. The 6.37% open porosity found for lime marl explains why this material acts as a barrier layer in the geological formations. Geologically acid leaching and oxidation processes cause a high and fine porosity in porous lime marl.

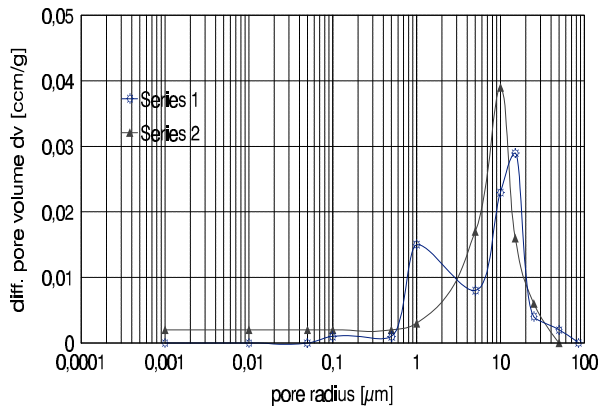


Fig. 1: Pore size distribution of cenomanian quader sandstone of different sampling locations. Series 1 = southfield, Series 2 = northfield

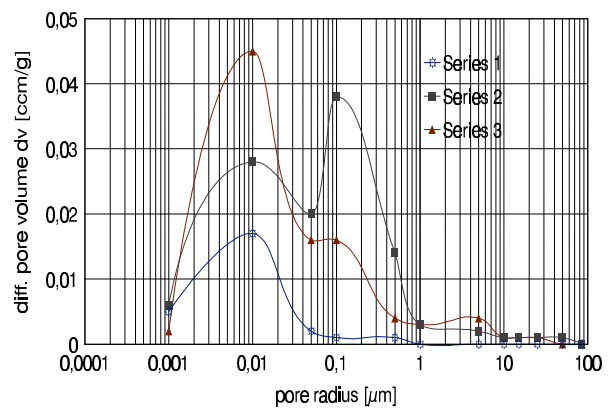


Fig. 2: Pore size distribution of materials with fine porosity. Series 1: Lime marl, Series 2: Porous lime marl, Series 3: Turonian clay

The pore size distribution is shown in Fig. 1 and Fig. 2. In Fig. 1 two sandstones are compared that were taken from different locations. Sample 2 has a unimodal porosity with a maximum pores diameter of 10 μm , whereas sample 1 has a bimodal porosity with maxima at 1 and 15 μm . Figure 2 shows pore size distributions for the lime marl materials with small pores. The lime marl (1) has a very small unimodal porosity of very fine pores. The porous lime marl (2) and the turonian clay (3) have a much higher bimodal porosity mainly in the fine-pore range which extends also into the larger-pore range. The main peak lies at 10 nm for the turonian clay at 10 nm and at 100 nm for the porous marl.

Acknowledgement

We gratefully acknowledge the collaboration for porosity measurements with Dr. I. Haase, TU Dresden and Dr. H.P. Martin, TU-BA Freiberg

References

- /1/ Baraniak L., Thieme M., Bernhard G., Nindel K., Schreyer J., Nitsche H.; Radium Sorption on Sandy and Clayey Sediments of the Upper Elbe River Valley . This report
- /2/ Thieme M., Baraniak L., Bernhard G. Nindel K., Schreyer J.; Sequential Extraction of Radioactivity containing Sedimentary Rocks of the Königstein Region. This report
- /3/ Dörr W., Assmann H., Meyer G., Steven J.; Bestimmung der Dichte, offenen Porosität, Porengrößenverteilung und spezifischer Oberfläche von UO_2 Pellets. Journal of Nuclear Materials **81**, 135 - 141 (1979)
- /4/ R. Haul, G. Dümbgen; Vereinfachte Methode zur Messung von Oberflächengrößen durch Gasadsorption. Chem. Ing. Techn. **32** (5), 349 - 354 (1960)

SEQUENTIAL EXTRACTION ON RADIOACTIVITY-CONTAINING SEDIMENTARY ROCKS OF THE KÖNIGSTEIN REGION, SAXONY

M. Thieme, L. Baraniak, G. Bernhard, K. Nindel¹, J. Schreyer¹, H. Nitsche
Forschungszentrum Rossendorf e.V., Institute of Radiochemistry
¹ WISMUT GmbH, Chemnitz

We performed chemical extraction experiments on several activity-containing rock types in order to obtain information on the binding of radium. This knowledge could help to assess the probability for radium to be transferred from the rock to the fluids in contact under natural conditions.

Sequential extraction consists of a multistep treatment of the rock using chemicals of increasing potential for dissolving certain mineral groups. The approach assumes that the chemical reactions proceed with a high selectivity and without re-distribution of the dissolved species. However, this is not always the case /1/.

In the present study, the following six-step treatment sequence was compiled on the base of the literature /2-8/. The target compounds are specified.

- 1) 1 M NH₄ac, pH = 7.0, 1 h
6 fractions of water-soluble salts and of species bound by ion exchange;
- 2) 1 M Naac + Hac, pH = 5.0, 5 h
6 fraction of bound carbonates;
- 3) 0.1 M NH₃OHCl - 0.01 M HNO₃, pH = 2, 12 h; following series I substituted by 0.2 M (NH₄)₂ox - 0.2 M H₂ox - 0.1 M Hasc, pH 6 3.0, ca. 96°C, 1 h
6 fractions of amorphous/crystalline iron and manganese oxides;
- 4) 30% H₂O₂, pH 6 2.0, 85°C, 2 h 6 fractions of organic components (or sulphides);
- 5) 0.25 M EDTA - 1.7 M NH₃, 85°C, 5 h 6 fraction of barium sulphate;
- 6) HNO₃ konz. or *aqua regia*, digestion using a micro wave apparatus
6 residual fraction (e.g. crystalline (alumo) silicates).

According to the recommendation /8/, a low sulphate concentration (0.0005 M) was adjusted in the steps 1) through 4) to diminish the unwanted dissolution of BaSO₄. Additionally, the rock samples were also directly digested for comparison. Moreover, data from X-ray fluorescence analysis were included.

The experiments were divided in the following manner:

- three series (I-III) consisting of the treatment of six activity-containing rock types after decompactation and milling:
 - claystone, lithology t₁t (no. 527),
 - sandstone, c₁s_{qu} (435), leached,
 - sandstone, c₁s_{qu} (439),
 - sandstone ("Wurmsandstein"), c₁c_{wu} (437),
 - sandstone ("Wechsellagerung"), c₁c_{wl} (4381, silt, and 4382, coarse).
- (The first letter of the lithologic symbols designates turonian or cenomanian origin.)
- one series (IV) on three selected activity-containing rock types (439, 437, 4382; samples in duplicate) starting with a leaching step (0.025 M H₂SO₄, leach time 9 weeks) derived from the procedure in the mine.
- one series (V) consisting of the treatment of four turonian rock types (fraction <1 mm) which were previously undergone sorption tests in solutions with ²²⁶Ra /13/:
 - sandstone containing limonite, t₁s_{li} (452),
 - lime marl ("Pläner"), t₁p (423),
 - porous lime marl ("Pläneräquivalent") t₁p_ä, (427),
 - claystone, t₁t (457).

The extraction was followed by centrifugation and filtration (0.45 μm). The separation of radium from the filtrates is regularly achieved by the precipitation of $(\text{Pb},\text{Ba},\text{Ra})\text{SO}_4$. This required specific adaptation measures to diminish masking effects owing to present complexants. Referring to /9,10/ the sulphate precipitate was dissolved in $\text{EDTA}+\text{NH}_3$, followed by precipitation of $(\text{Ba},\text{Ra})\text{SO}_4$, which was finally taken up by a gelling cocktail for liquid scintillation counting (LSC, Beckman 6000 LS). An α/β discrimination was omitted. The LS spectra reflected a very good separation of radium. The ingrowth of the decay products was accounted for. The radium determination in the extraction media was standardized using known amounts of ^{226}Ra along with each of the batches. Generally, a high reproducibility of the determination was achieved. Corresponding to the level of the blank results, a detection limit of about 0.01 kBq/kg was derived.

In addition to the extraction behaviour of radium, the release of Mg, Ca, Ba, Fe, Al and U was followed by atomic absorption spectrometry (AAS 4100, Perkin-Elmer) and ICP-MS (ELAN 5000, Perkin-Elmer).

The fractions obtained for the respective steps form patterns which in most cases revealed to be characteristic in terms of the element and the rock type.

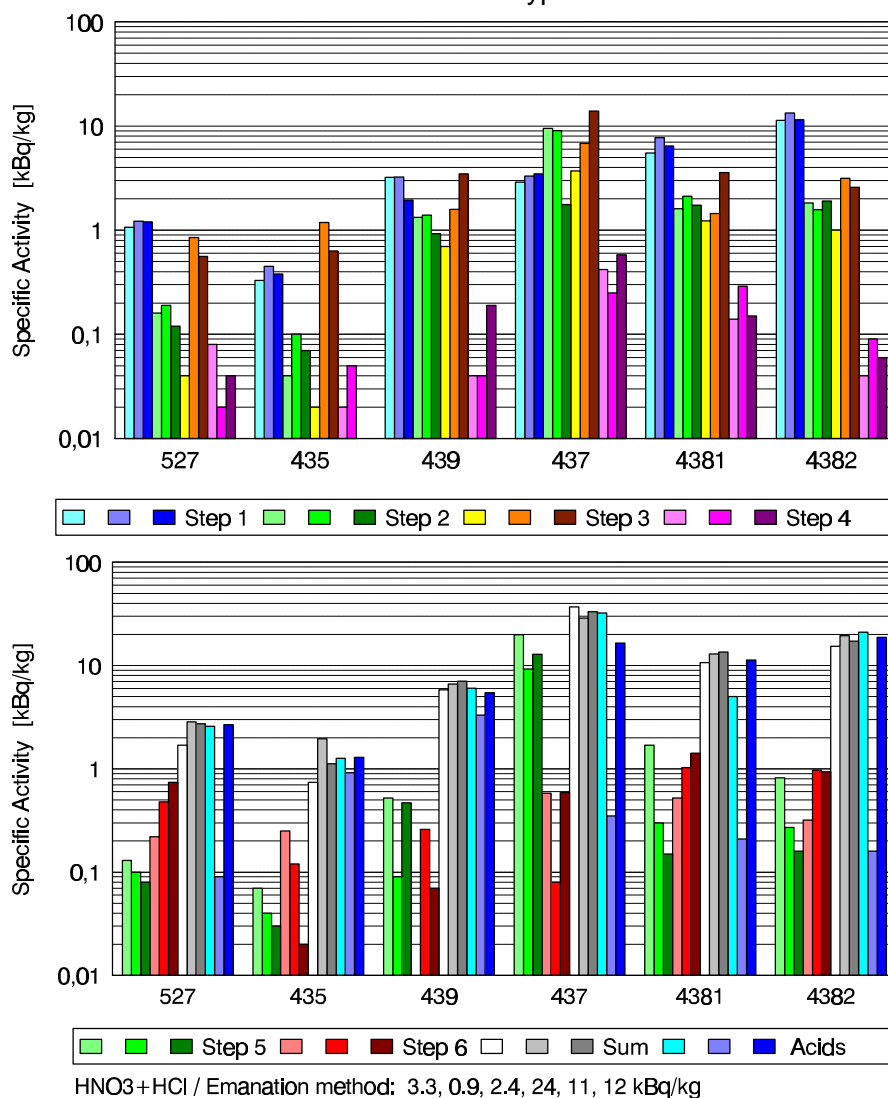


Fig. 1: Plot of the activity concentrations of radium released in sequential six-step extraction treatments on different activity-containing rock sorts; three parallel series (I-III) displayed side by side; *up*: fractions of the steps 1) to 4) (see text); *down*: fractions of the steps 5) and 6), sums of the individual fractions and release values of treatments using concentrated acids (HNO_3 , $\text{HNO}_3 + \text{HF}$ and $\text{HCl} + \text{HNO}_3$, respectively).

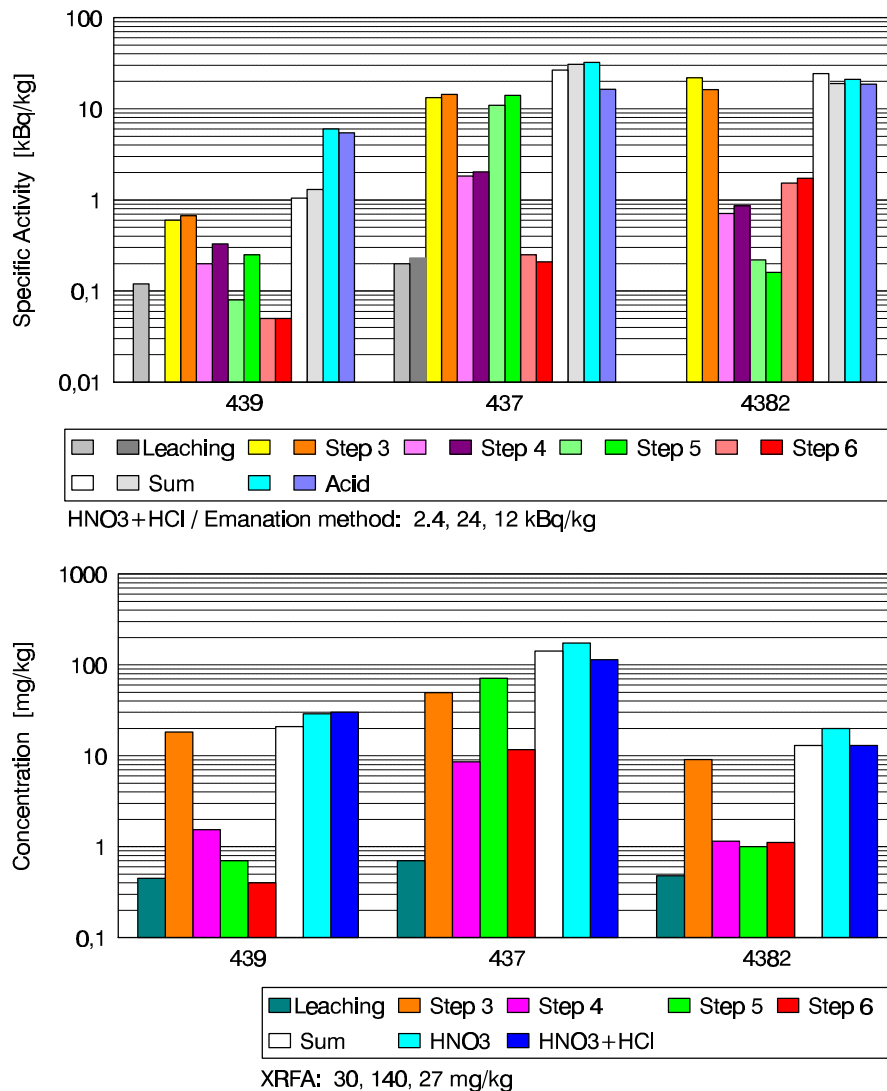


Fig. 2: Plot of concentrations released in sequential extraction treatments including H₂SO₄ leaching (series IV) on three different activity-containing rock sorts (in duplicate); fractions of the individual steps, their sums and the release values of treatments using concentrated acids (HNO₃ and HNO₃ + HCl, respectively); *up*: activity concentration patterns for ²²⁶Ra; results of the duplicate tests displayed side by side; *down*: concentration patterns for Ba; results averaged.

The results for the extraction of radium from the original ore-containing rocks are summarized as histograms in Figs. 1a and 1b. The activity fractions ratioed by the sample mass were displayed on a logarithmical scale. The following features are seen from the diagrams:

- The results of the individual series (I-III), which are displayed side by side, are in a principal agreement. Higher deviations are observed in connection with the exchange of the chemicals in step 3).
- The sums of the fractions agree with the values obtained for the direct acid treatment of the rocks (HNO₃, HNO₃+HF, HNO₃+HCl), with the exception of the mixture containing HF. According to these data, the following rank of the releasable amounts of radium is formed $c_1c_{wu}, 437 > c_1c_w, 4382 > c_1c_w, 4381 > c_1s_{qu}, 439 > t_1t, 527 > c_1s_{qu}, 435$.
- With the most types (527, 439, 4381 and 4382), the Ra release dominates in the first step, i.e. under application of comparatively soft extraction conditions (neutral medium, monovalent cation). This means, that a considerable fraction of Ra must be bound only loosely. The corresponding binding site is supposed to be a clay component. According to X-ray diffrac-

tion, kaolinite is present as the main matrix mineral. It is a bilayered silicate, which has (low) cation exchanging potentials /11/ and may fix also radium /12/. According to the extraction patterns, Ca is probably bound together with Ra.

Unlike the clear dominance of the step 1) for the radium release, uranium was extracted mainly by a stronger attack. However, this is not true in case of the rock samples which were characterized by the spontaneous release of sulphuric acid.

- With Wurmsandstein c_1c_{wi} (437), another situation seems to be present. Here, the Ra extraction pattern has a pronounced fraction in step 5), i.e. Ra is bound considerably stronger than in the cases mentioned above. Because the pattern is similar to that of barium, we conclude that Ra is fixed to $BaSO_4$.

The results of the series IV for c_1s_{qu} (439), c_1c_{wu} (437) and c_1c_{wi} (4382) are shown in Fig. 2.

- The Ra fractions of the leach step (Fig. 2a) were found to be very low (about the detection limit). This finding agrees with the experience in mining.
- The striking similarity between the patterns of Ra and Ba (Fig. 2b) leads to the conclusion that radium is bound to $BaSO_4$ in all these cases including c_1s_{qu} (435) (cf. series I-III). This seems to be in contradictory to the fact that the release maxima were measured in the step 3). This finding may be caused by the specific dissolution behaviour of small amounts of barium sulphate in presence of oxalate.
- The extraction behaviour of uranium was found to be quite different from that of radium. The application of sulphuric acid in the laboratory leaching treatment led to a strong release of U, which exceeded the effects of the following steps by 1-2 orders of magnitude.

Finally, the extraction results for the radium-loaded turonian rock types (series V) are discussed. The patterns may be divided into two groups. The first one with limonite containing sandstone t_1s_{Li} and lime marl t_1p was characterized by easily dissolved radium:

step 1) > step 2) > step 3).

By contrast, for porous lime marl t_1p_A , which was found to have the highest distribution ratios /13/, and claystone t_1t the following rank applied:

step 3) > step 4) > step 5) > step 6) > step 2) > step 1).

Obviously, these rock types caused a considerably stronger fixation of radium. The reasons for this difference will be connected with the mineralogical composition. However, unequivocal conclusions provide sorption studies on single minerals and autoradiographic examinations of compact rocks after having loaded.

Acknowledgements

The careful work of H. Neubert is acknowledged. The authors are also indebted to U. Schaefer and W. Wiesener for doing the numerous AAS and ICP-MS analyses.

References

- /1/ Shan Xiao-Quan, Chen Bin: Evaluation of Sequential Extraction for Speciation of Trace Metals in Model Soil Containing Natural Minerals and Humic Acid, *Anal. Chem.* **65**, 802 (1993).
- /2/ Tessier, A., Campbell, P. G. C., Bisson, M.: Sequential Extraction Procedure for the Speciation of Particulate Trace Metals, *Anal. Chem.* **51**, 844 (1979).
- /3/ Förstner, U.: Bindungsformen von Schwermetallen in Sedimenten und Schlämmen: Sorption/Mobilisierung, chemische Extraktion und Bioverfügbarkeit, *Fres. Z. Anal. Chem.* **316**, 604 (1983).
- /4/ Plater, A. J., Ivanovich, M., Dugdale, R. E.: Uranium Series Disequilibrium in River Sediments and Waters: The Significance of Anomalous Activity Ratios, *Appl. Geochem.* **7**, 101 (1992).
- /5/ Margane, J., Boenigk, W.: Reinigungsleistung thermischer Dekontaminationsverfahren für Schwermetalle, *Entsorgungspraxis* **1993**, 30.
- /6/ Fujiyoshi, R., Okamoto, T., Katayama, M.: Behavior of Radionuclides in the Environment. 2. Application of Sequential Extraction to Zn(II) Sorption Studies, *Appl. Rad. Isot.* **45**, 165 (1994).

- /7/ Růde, T. R., Puchelt, H.: Arsenbindungsformen in Böden, 72. Jahrestagung der DGM, Freiberg, 17.-25.09.94.
- /8/ Beneš, P., Sedláček, J., Šebesta, F., Šandrik, R., John, J.: Method of Selective Dissolution for Characterization of Particulate Forms of Radium and Barium in Natural and Waste Waters, *Water Res.* **15**, 1299 (1981).
- /9/ Stewart, B. D., McKlveen, J. W., Glinski, R. L.: Determination of Uranium and Radium Concentration in the Waters of the Grand Canyon by Alpha Spectrometry, *J. Radioanal. Nucl. Chem.* **123**, 121 (1988).
- /10/ Chalupnik S., Lebecka, J. M.: Determination of ^{226}Ra , ^{228}Ra and ^{224}Ra in Water and Aqueous Solutions by Liquid Scintillation Counting, *Proc. Liquid Scintillation Spectrometry 1992*, Radiocarbon 1992, 397.
- /11/ Jasmund, K., Lagaly, G. (Hrsg.), *Tonminerale und Tone*, Darmstadt: Steinkopff, 1993.
- /12/ Beneš, P., Borovec, Z., Strejc, P.: Interaction of Radium with Freshwater Sediments and their Mineral Components, II. Kaolinite and Montmorillonite, *J. Radioanal. Nucl. Chem.* **82**, 275 (1984)
- /13/ Baraniak, L., Thieme, M., Bernhard, G., Nindel, K., Schreyer, J.: Sorption Behaviour of Radium on Sandy and Clayey Sediments of the Upper Saxon Elbe River Valley, this report.

MODELLING OF RADIUM MIGRATION PROCESSES IN THE UPPER ELBEVALLEY SANDSTONE SEDIMENTS

H. Funke, L. Baraniak, M. Thieme, K. Nindel¹, J. Schreyer¹
 Forschungszentrum Rossendorf e.V., Institute of Radiochemistry
¹ WISMUT GmbH, Chemnitz

Transport modelling was performed of radium migration in characteristic sediments of the upper Saxon Elbe river valley using the radionuclide transport model of Hadermann /1/. The model uses the experimental determined distribution ratios R_d /2/ as chemical input.

The radioactive transport equation is given by:

$$\frac{\partial C}{\partial t} + a \frac{\partial C}{\partial x} - \frac{\partial}{\partial x} \left(D \frac{\partial C}{\partial x} \right) - \lambda C = 0$$

- x = coordinate of the linear migration path,
- λ = radionuclide decay constant,
- u = nuclide velocity
- v_D = water (Darcy-) velocity,
- R_d = distribution ratio,
- ρ = medium bulk density,
- ∇P = pressure gradient.
- C = radionuclide concentration,
- a = longitudinal dispersivity,
- R_f = retention factor,
- ϵ = medium effective porosity,
- k = permeability,

The velocities, chemical and material constants are connected by the usual relations $v_D = k \nabla P / \mu$, $u = v_D / R_f$, $R_f = 1 + D R_d / \epsilon$.

For constant material properties and the constant boundary conditions:

$$C(x = 0, t) = C_0 \exp(-\lambda t)$$

the solution of the transport equation simplifies to:

$$C(x, t) = \frac{C_0}{2} \left[\operatorname{erfc} \left(\frac{x + ut}{2 \sqrt{a D t}} \right) \exp \left(-\frac{x}{a} \right) + \operatorname{erfc} \left(\frac{x - ut}{2 \sqrt{a D t}} \right) \right] \exp(-\lambda t)$$

Normalized spacial radium concentration profiles C/C_0 were calculated for 2500, 5000, 7500, and 10000 years. The data include geomechanical values for k , ∇P , a and the measured values of the distribution ratio R_d of radium, ϵ and D in the various sediments /2/. Tab. 1 shows the data for three different sediments that are in contact with low mineralized groundwater of this area.

Tab.1: Datasets for the examples

| Geomaterial | Fig.-Nr. | R_d [mL/g] | k_f [m/s] | ∇P [mWs/m] | v_D [m/s] | ϵ [Vol %] | D [g/cm ³] | a [m] |
|-------------------|----------|-----------------|-------------------|-----------------------|----------------------|-----------------------|-----------------------------|------------|
| $c_1 S_{qu}^1$ | 1 | 64 | $1 \cdot 10^{-5}$ | $1 \cdot 10^{-7}$ | $5.5 \cdot 10^{-12}$ | 18.2 | 2.25 | 30 |
| $t_1 p_{equiv}^2$ | 2 | 2870 | $1 \cdot 10^{-7}$ | 10 | $4.2 \cdot 10^{-6}$ | 23.8 | 2.01 | 1 |
| $t_1 S_{li}^3$ | 3 | 53 | $4 \cdot 10^{-5}$ | $1 \cdot 10^{-2}$ | $1.8 \cdot 10^{-6}$ | 22.7 | 2.11 | 30 |

¹) cenomanian sandstone, ²) porous lime marl ("Pläneräquivalent")
³) limonite-rich turonian sandstone

The radium transport for the upper Elbevalley region will be exemplified using these three scenarios.

Fig. 1 shows that the radium concentration decreases to about 0.1 % of the initial concentration after a migration distance of only 0.5 meters. This is due to the low Darcy velocity in the cenomanian sandstone.

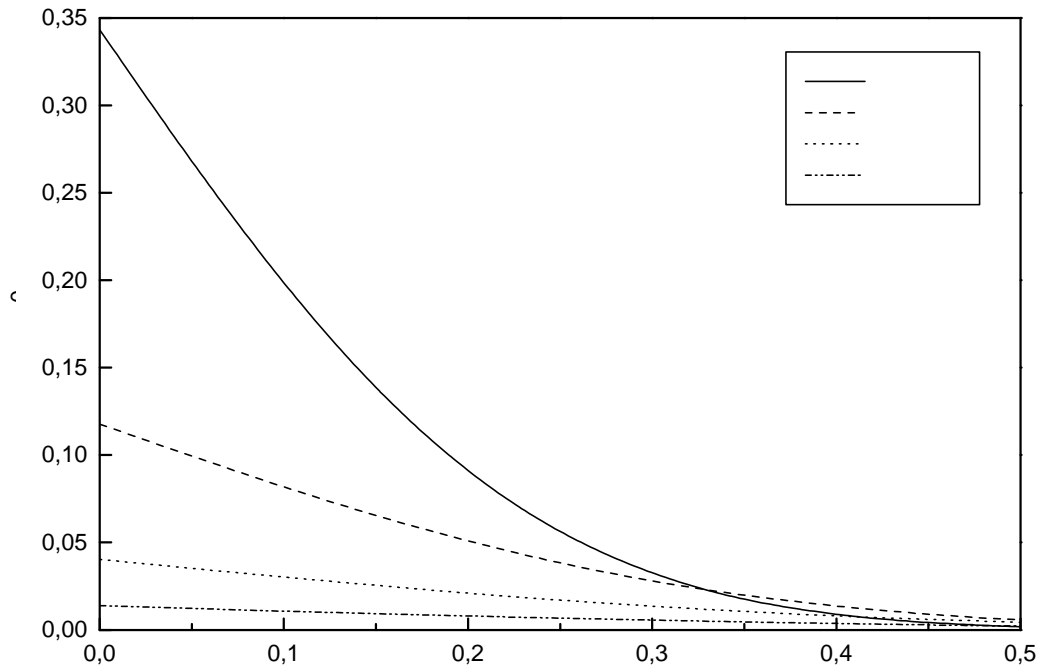


Fig. 1: Radium migration in cenomanian sandstone under groundwater conditions

The results for the porous lime marl environment are shown in Fig. 2. The high values of distribution ratio R_d and the velocity v_D compensate each other to reach a maximum migration distance of 60 m after 10000 years.

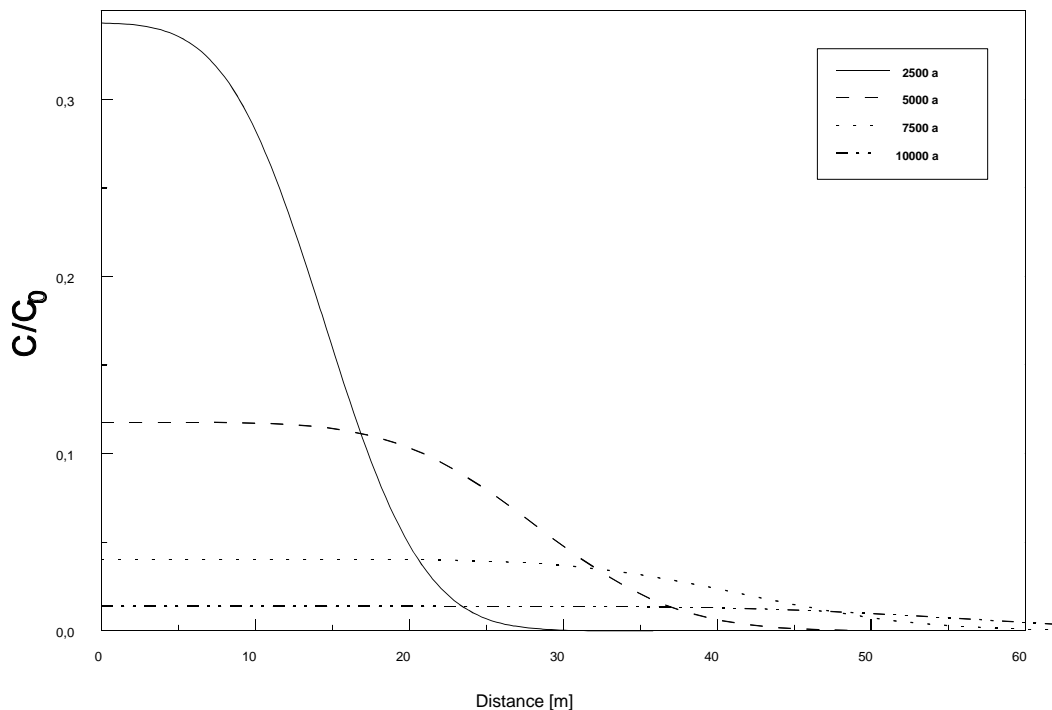


Fig. 2: Radium migration in porous lime marl ("Pläneräquivalent") under groundwater conditions

The decrease of a hypothetical contamination of the groundwater with 100 Bq/l during the transport through the limonite-rich turonian sandstone is shown in Fig. 3.

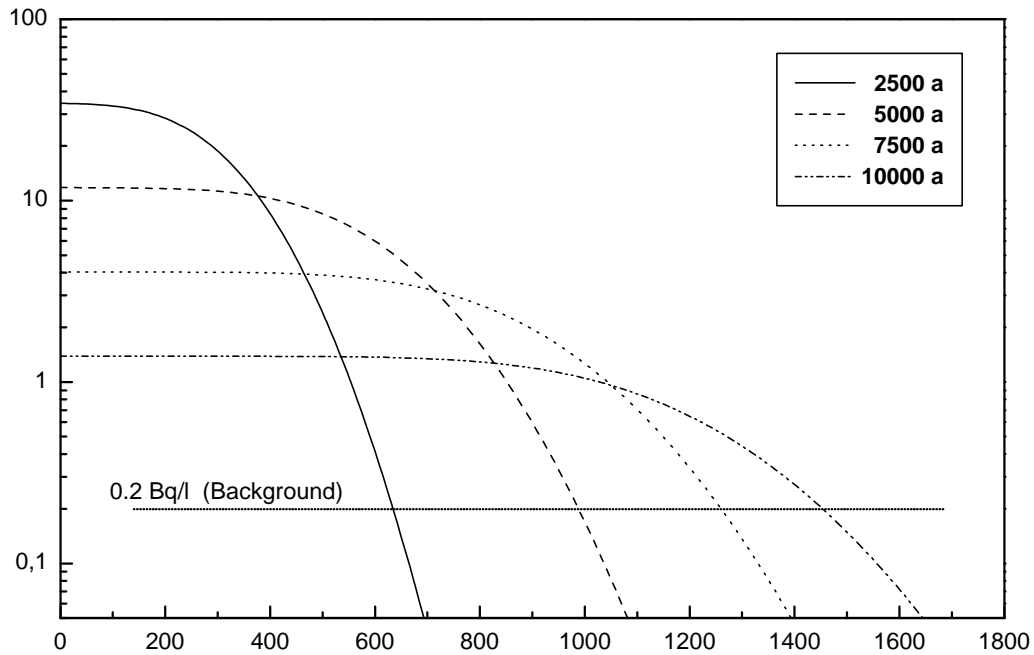


Fig. 3: Radium migration in limonite - rich turonian sandstone under groundwater conditions

The activity is plotted over the distance. The assumed activity will fall below the background activity of 0.2 Bq/L after 2500 years and 600 meters distance from the source. After 10000 years this level is reached at 1500 meters.

For all three examples radium migrates relatively short distances. The calculation assume only homogeneity of the porous sediments. The distribution ratios R_d for mine-water contaminated groundwater are substantially higher /2/ which results in an even lower migration distance.

References

- /1/ Hadermann, J., Radionuclide Transport through Heterogeneous Media, Nuclear Technology **47**, 312 (1980)
- /2/ Baraniak, L., Thieme, M., Bernhard, G., Nindel, K., Schreyer, J., Radium Sorption on Sandy and Clayey Sediments of the Upper Elbe River Valley, this Report

DIRECT ALPHA - SPECTROSCOPIC MEASUREMENT OF THIN-LAYER CONCRETE SOURCES

C. Nebelung , S. Hübener, G. Bernhard
Forschungszentrum Rossendorf e.V., Institute of Radiochemistry

Concrete coming from decommissioned or defunct nuclear installations must be measured for radioactivity to decide if it can be released to the uncontrolled environment.

For gamma- and beta-activity measurements, in-situ methods are available. The low range of alpha-particles (a few μm in solids, cm in gases) complicates the in-situ measurements of alpha-activity. It is therefore necessary to take specimens for the analysis of actinides.

The clearance levels are 0.5 Bq/g /1/ and 0.3 Bq/g /2/ for most artificial actinides. For every nuclide, according to the 10 μSv -concept, individual clearance levels are calculated according to the latest recommendations /3/. In addition to the total activity, the specific activity of each nuclide has to be measured.

The method developed for the direct alpha spectroscopic measurement of large area thin layer sources utilized a gridded ionisation chamber (GIC) and a semiconductor (large area passivated ion-implanted planar silicon, PIPS) detector. The thickness of the concrete sources was between 5 and 10 μm . The detection efficiency was determined experimentally using various concretes with defined amounts of actinide. It was possible to calculate the specific activity of sources with an unknown actinide content /4/.

Tab. 1 summarizes the performance data of GIC and PIPS for a 5 μm thick sample. The detection efficiency, the resolution and the background were determined experimentally.

Tab. 1: Comparison between GIC and PIPS for 5 μm concrete sources

| detector | GIC | PIPS |
|--|-------|-------|
| detector area [cm ²] | 314.2 | 50.3 |
| detection efficiency g | 0.345 | 0.196 |
| resolution [keV] | 850 | 900 |
| background $k_0 = R_0$ [h ⁻¹] | 94.2 | 2.6 |
| k_n^* with $t_0 = 20$ h and $t_b = 6$ h [Bq/g] | 0.030 | 0.054 |
| k_n^* with $t_0 = t_b = 20$ h [Bq/g] | 0.020 | 0.037 |
| R_n^* with $t_0 = 20$ h and $t_b = 6$ h [Bq/g] | 0.015 | 0.027 |
| R_n^* with $t_0 = t_b = 20$ h [Bq/g] | 0.010 | 0.019 |

k_n^* and R_n^* are calculated /5/; k_n^* = detection limit, R_n^* = recording limit
 t_0 = measuring time of the background, t_b = measuring time of the source

The detection limit of GIC is lower, in spite of the high background, due to the larger source area. The detection limit of the total specific activity /4/ measured for both GIC and PIPS is < 0.02 Bq/g. For PIPS, this limit is lower than expected.

The determination of a single nuclide by GIC is shown in Tab. 2. The samples were WAK concrete (from the reprocessing plant for nuclear fuels in Karlsruhe) to which Am-241 was added.

Tab. 2: Expected and measured specific activity of WAK concrete with added Am-241

| added Am-241 [Bq/g] | specific activity, expected [Bq/g] | specific activity, measured [Bq/g] |
|---------------------|------------------------------------|------------------------------------|
| 0 | - | 0.238 ± 0.014 |
| 0.04 | 0.278 | 0.282 ± 0.011 |
| 0.1 | 0.338 | 0.341 ± 0.012 |
| 9.64 | 9.88 | 9.85 ± 0.18 |

The measured total specific activity is comparable to the expected values. The expected values are the sum of the measured "inactive" concrete and the added Am-241.

The spectroscopic evidence of the added Am-241 is shown in Fig. 1. All alpha-spectra were background subtracted.

Fig. 1 shows the comparison between “inactive” WAK-concrete and WAK-concrete with various Am-241 contents.

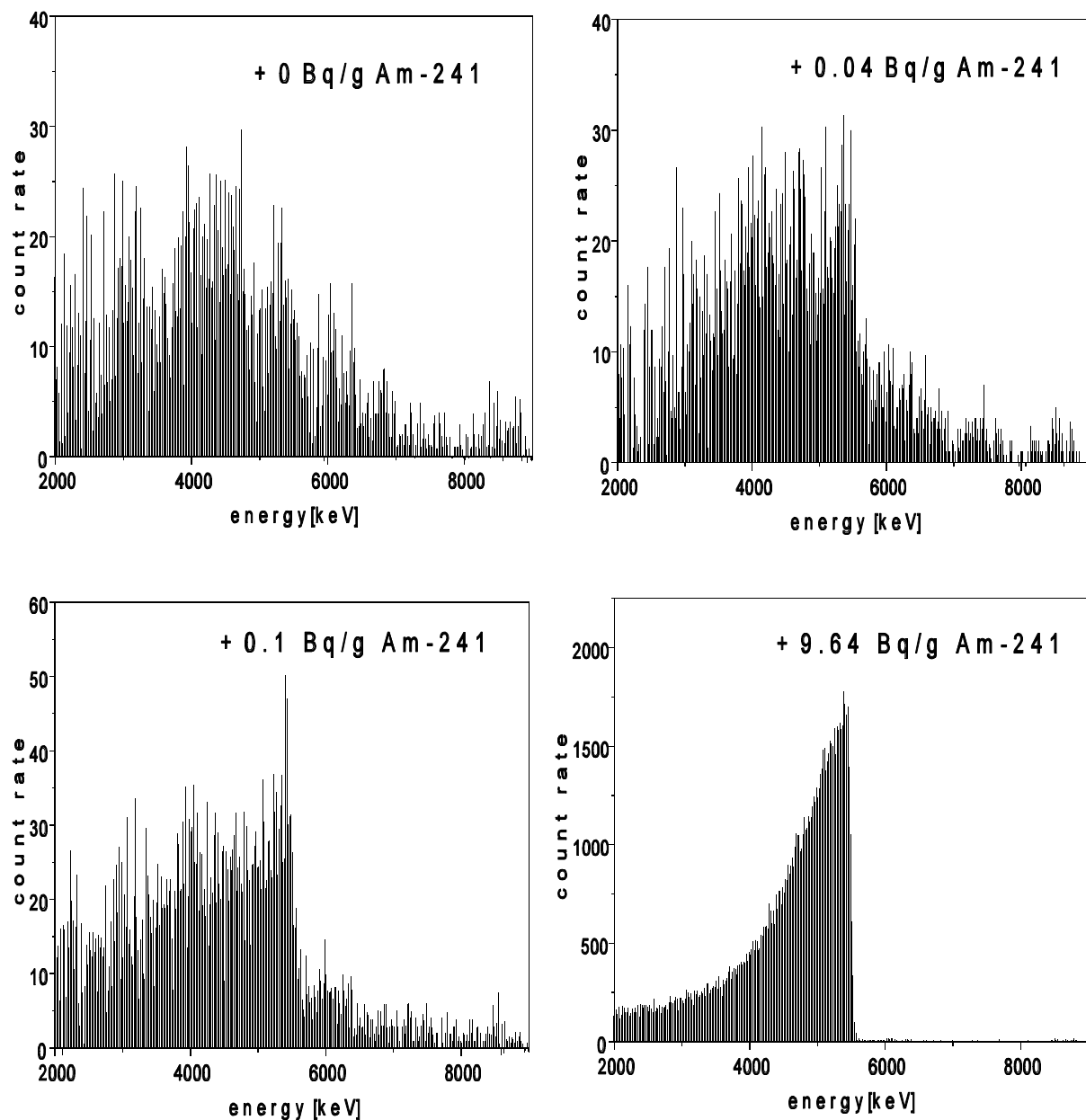


Fig. 1: Alpha-spectra of WAK-concrete, various contents of Am-241, 20 h measuring time, 5 μ m thickness, background spectrum subtracted

The alpha-spectra of concrete with added Am-241 show a typical deep high energy flank of Am-241 at the energy 5.5 MeV for Am-241, even in the 0.04 Bq/g sample. This high energy side of a peak is used to identify nuclides.

The measurement of an “inactive” concrete of the nuclear power plant Niederaichbach KKN with a total specific activity of 0.13 Bq/g /4/ shows that it is possible to detect natural Th and U and their daughter products with GIC; with the PIPS-detector only the Th-230 peak is visible (Fig. 2).

The direct measurement is not only a method for detecting the total alpha-activity but is also applicable for detecting single nuclides in large area samples, a few μ m thick. The thinner the

sample and the larger the area of both source and detector, the greater is the accuracy of the measurement.

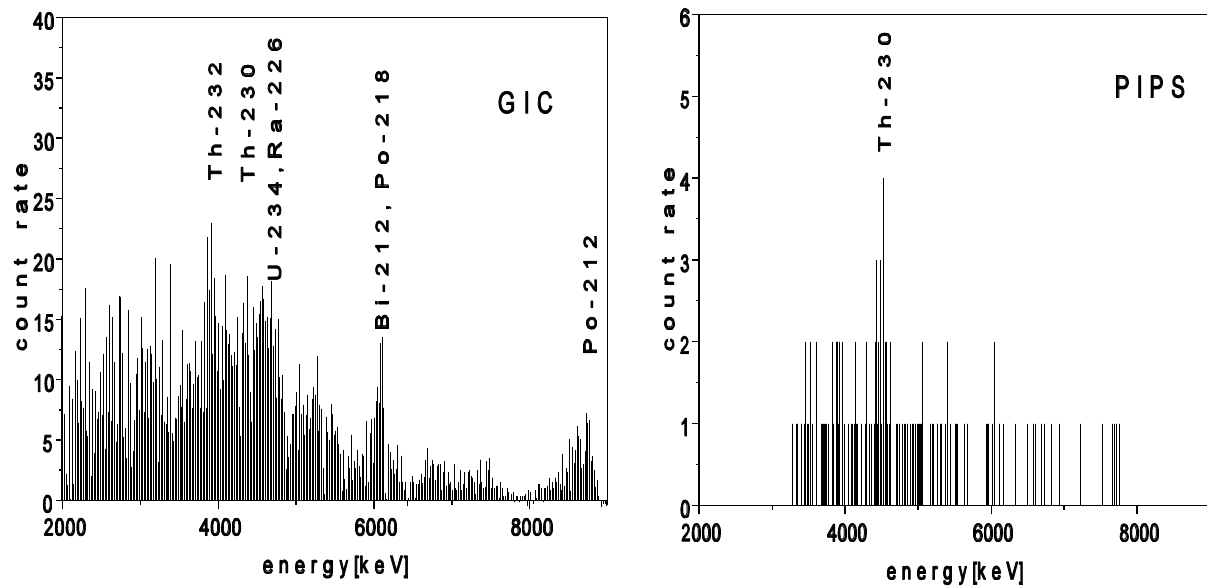


Fig.2: Alpha-spectra of "inactive" KKN concrete, various detectors
20 h measuring time, 5 μ m thickness, background spectrum subtracted

Acknowledgement

This study was supported by the Bundesminister für Forschung und Bildung of the Federal Republic of Germany under contract number 02 S 7442 2.

References

- /1/ *Strahlenschutzverordnung 1989*, 4. Auflage, Bundesanzeiger Verlags-GmbH., Köln (1993)
- /2/ Warnecke, E., *Recommended Clearance Levels for Radionuclides in Solid Materials*, IAEA, Division of Nuclear Fuel Cycle and Waste Management, 8783y Draft, Dec. 1993
- /3/ Poschner, J., Schaller, G., Richtwerte für die spezifische Aktivität von schwachkontaminierten Abfällen, die konventionell entsorgt werden können, BfS-ISH 169/95
- /4/ Nebelung, C., Hübener, S., Bernhard, G., Nitsche, H., Tagungsband "IV. Stilllegungskolloquium Hannover und 3. Statusbericht Stilllegung und Rückbau kerntechnischer Anlagen", Bad Dürkheim 8. -10.11.95, S.417-424
- /5/ DIN 25482 Teil 1, April 1989

Behaviour of Colloids and Aerosols

DEPENDENCE OF SCATTERED LIGHT INTENSITIES ON THE PARTICLE CONCENTRATION OF LOW-CONCENTRATED COLLOIDS

G. Hüttig, W. Richter¹, H. Zänker

Forschungszentrum Rossendorf e.V., Institute of Radiochemistry

¹Technische Universität Dresden, WIP

As we discussed earlier in /1,2/, environmental colloids present a special challenge for particle measuring techniques. Primarily low particle concentrations represent a problem for colloid measurement. We tested two particle measuring instruments for their suitability to characterize low-concentrated colloids /1,2/. The results were unsatisfactory and disappointing.

In 1995 we performed similar experiments with a photon correlation spectroscopy BI-90 from Brookhaven Instruments Corp. with the newly-developed Model BI-9000 AT Digital Correlator and a 2 W Argon ion laser from Lixel. The objective was a) to examine the photomultiplier count rate response, being a measure of scattered light intensity, as a function of colloid concentration and b) to determine the lower limit of detection.

A photon correlation spectroscopy has two lower limits of detection. The first limit is the concentration level where first deviation of the photomultiplier count rate from the background count rate occurs. The second is the concentration level above which particle size determinations are reliable. In this work, the detection limit concerning with the count rate increase is discussed. The question of reasonable particle sizing is the topic of the next article /3/

Water, even in its purest form, shows some light scattering due to the unavoidable presence of dust and due to minute solvent density fluctuations. Only if the scattered light intensity (count rate) from the particles under study is clearly larger than this background level, the particles will be detectable at all. We investigated the dependence of count rate on the particle concentration in suspensions of monodisperse, spherical polystyrene latex standard particles of varying particle size (Duke Scientific Corp.) in Milli-Q water (see below) within a broad range of particle concentrations. In order to find the optimum instrument adjustments, we also varied the laser power and the degree of attenuation (the latter is done by means of a set of absorption filters arranged in a filter wheel located at the beam entrance to the cuvette). The scattering angle of the BI-90 is 90°. The laser wavelength was 514.5 nm.

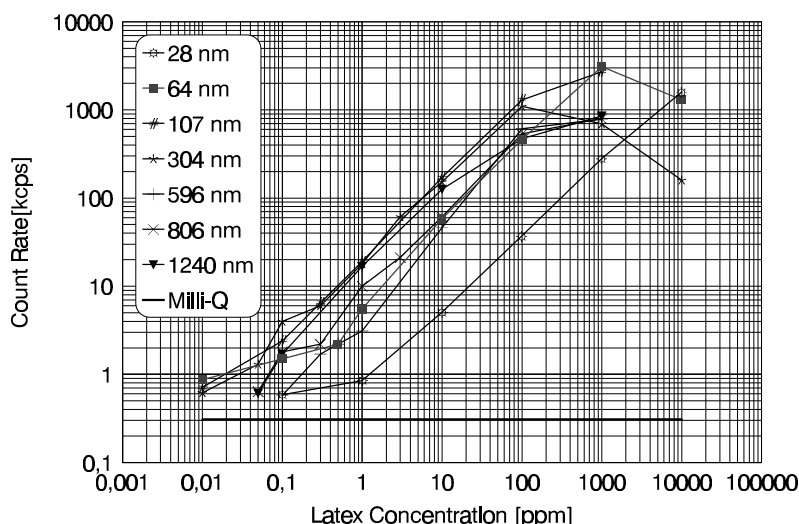


Fig. 1: Dependence of scattered light intensities on the latex concentration; laser power 400 mW, attenuator 3

In Fig. 1 and Fig. 2, the count rate vs. concentration relationships for seven polystyrene latex standards (particle sizes between 28 and 1240 nanometers) for attenuator 3 and laser powers of 400 mW and 1 W are given. The count rates of the Milli-Q water are shown as thick horizontal lines (the Milli-Q count rates vary by a factor of about 2). Milli-Q water (Millipore Corp.) has an extremely low particle concentration (it is, for instance, used in the microelectronics industry) and its count rate can serve as a reference for waters with low particle concentration. For a

laser power of 400 mW (Fig. 1) the linear range of the count rate vs. Latex concentration plot extends over 3 to 4 orders of magnitude. The lower limit of detection varies between 0.01 ppm (particle sizes of 64, 107 and 304 nm), 0.05 ppm (806 and 1240 nm), 0.1 ppm (596 nm) and 1 ppm (28 nm). Results for a laser power of 100 mW (not shown) were similar, but the lower limit of detection is not as good as for 400 mW power. Fig. 2 shows that an increase of the laser power to 1 W does not yield any improvement in detection. The higher laser power does increase the light intensity scattered by the latex standard particles, but it raises the scattered light intensity from the Milli-Q water, too. The latter overcompensates the former.

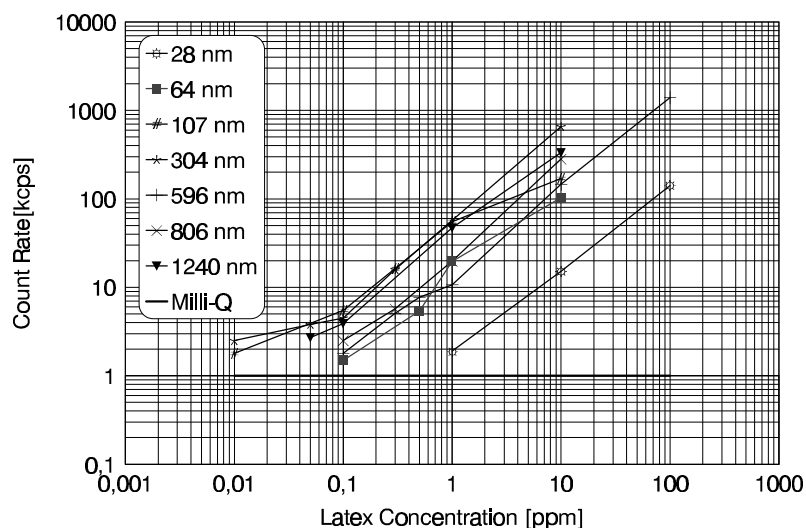


Fig. 2: Dependence of scattered light intensities on the latex concentration; laser power 1 W, attenuator 3

The curves shown in Fig. 1 and Fig. 2 can be used to estimate the particle concentration of unknown colloids. Such estimates have, however, limitations. The figures demonstrate that a given count rate can be assigned to a concentration range of approximately 2 orders of magnitude for the particle sizes studied. This range of uncertainty of assignment will be less if the particle size distribution of the unknown colloid is successfully determined by photon correlation spectroscopy. It is, however, broadened if particles with unknown refractive indices and non-spherical forms are investigated. Pronounced variations of count rate vs. concentration plots as a function of the particle material was shown by Ledin et al. who investigated artificial colloids of Fe_2O_3 , $\text{Al}(\text{OH})_3$, SiO_2 , kaolinite, illite and humic acid /4/. Nevertheless, photon correlation spectroscopy, unless intended as a means of particle sizing, can provide valuable information on the particle concentration. Chemical and gravimetric methods of determining particle concentrations are certainly often less ambiguous. They are, however, invasive and tend to alter the samples prior to measurement which can lead to artefacts and systematic errors.

References

- /1/ Zänker, H., Wruck, D., Martin, S. I., Testing a Model 4700 Photon Correlation Spectroscopy from Malvern Instruments for the Investigation of Environmental Colloids. Report FZR-94, Forschungszentrum Rossendorf e.V., Institute of Radiochemistry, Annual Report 1994, June 1995, p. 46
- /2/ Zänker, H., Testing a Microtrac Ultrafine Particle Analyzer UPA-150 from Leeds & Northrup for the Investigation of Environmental Colloids. Report FZR-94, Forschungszentrum Rossendorf e.V., Institute of Radiochemistry, Annual Report 1994, June 1995, p. 49
- /3/ Richter, W., Zänker, H., Hüttig, G., Testing of a Photon Correlation Spectroscopy with Low-Concentration Colloids. This report
- /4/ Ledin, A., Karlsson, S., Düker, A., Allard, B., Applicability of Photon Correlation Spectroscopy for Measurement of Concentration and Size Distribution of Colloids in Natural Waters., *Anal. Chim. Acta* **281**, 421(1993)

TESTING OF A PHOTON CORRELATION SPECTROSCOPE WITH LOW-CONCENTRATION COLLOIDS

W. Richter¹, H. Zänker, G. Hüttig

Forschungszentrum Rossendorf e.V., Institute of Radiochemistry

¹ Technische Universität Dresden, WIP

As was shown in the preceding article /1/, a photon correlation spectroscopy (PCS, BI-90, Brookhaven Instruments Corp.) is suited to provide an estimate on the particle concentration in a colloidal suspension. The main use of a PCS, however, is measuring of particle sizes and particle size distributions for heterodisperse colloidal suspensions. Here we discuss the lower limit of detection for particle sizing.

We used suspensions of polystyrene latex standard particles from Duke Scientific Corp. with particle sizes of 28, 64, 107, 304, 596, 806 and 1240 nm which were diluted with Milli-Q water (cf. /1/). The scanning electron micrograph in Fig. 1 exemplifies for the 806 nm standard that these latex particles are monodisperse and that they agree well with the nominal particle size value. The figure also demonstrates that there is no tendency of agglomeration. Because of their shape as ideal spheres, these particles are ideally suited for testing the photon correlation spectroscopy.

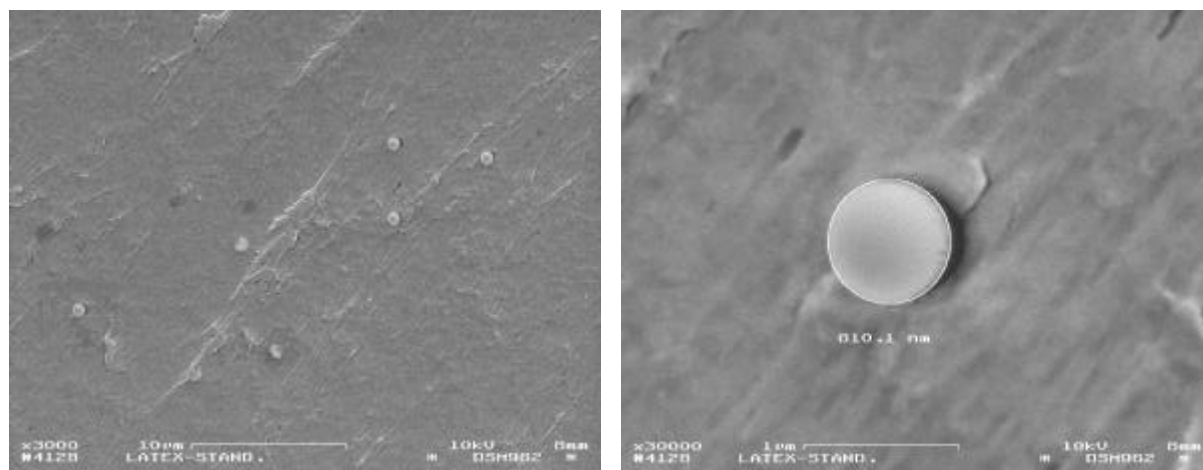


Fig. 1: Scanning electron micrograph of 806 nm polystyrene latex particles from a suspension of 1 ppm. Magnification: left 1 : 3000, right 1: 30000

Tab. 1: Measured particle size of polystyrene latex standards as a function of concentration (laser power 400 mW, attenuator 3)

| Concentration | Measured Particle Size [nm] | | | | | | |
|---------------|-----------------------------|--------------|---------------|---------------|---------------|---------------|----------------|
| | 28 nm Stand. | 64 nm Stand. | 107 nm Stand. | 304 nm Stand. | 596 nm Stand. | 806 nm Stand. | 1240 nm Stand. |
| 1 % | 28.3* | 19.1 | n.m. | 1.7 | n.m. | n.m. | n.m. |
| 0.1 % | 31.3* | 64.5±1 | 65.6* | 43.4* | 104.6* | 83.9±10 | 166.9±25 |
| 100 ppm | 30.6* | 68.3±5 | 109.1±10 | 334.6±100 | 415±60 | 711±80 | 730±120 |
| 10 ppm | 28.4±4 | 69.6±5 | 109.0±10 | 303.9 ±30 | 546.3±60 | 612±80 | 1312* |
| 5 ppm | 35.3±2 | n.m. | n.m. | n.m. | n.m. | n.m. | n.m. |
| 3 ppm | m.n.s. | n.m. | n.m. | n.m. | n.m. | 654±80 | 908±120 |
| 1 ppm | m.n.s. | 58.7±8 | 106.9±10 | 296.4±30 | 517.9* | 770±90 | m.n.s. |
| 0.3 ppm | m.n.s. | 85.5* | 114.9±10 | 309.9±30 | m.n.s. | m.n.s. | m.n.s. |
| 0.1 ppm | m.n.s. | m.n.s. | 95.7±15 | m.n.s. | m.n.s. | m.n.s. | m.n.s. |

n.m. = not measured m.n.s. = measurement not successful

* These are average values because the device erroneously indicated multimodal size distributions

Because the measurements are very sensitive to dust in the solution and to dirt on the cuvette walls, it is essential to use clean cuvettes (we used quartz cuvettes) and low-particles water (Milli-Q water) and to work in a clean atmosphere (we used a laminary flow bench).

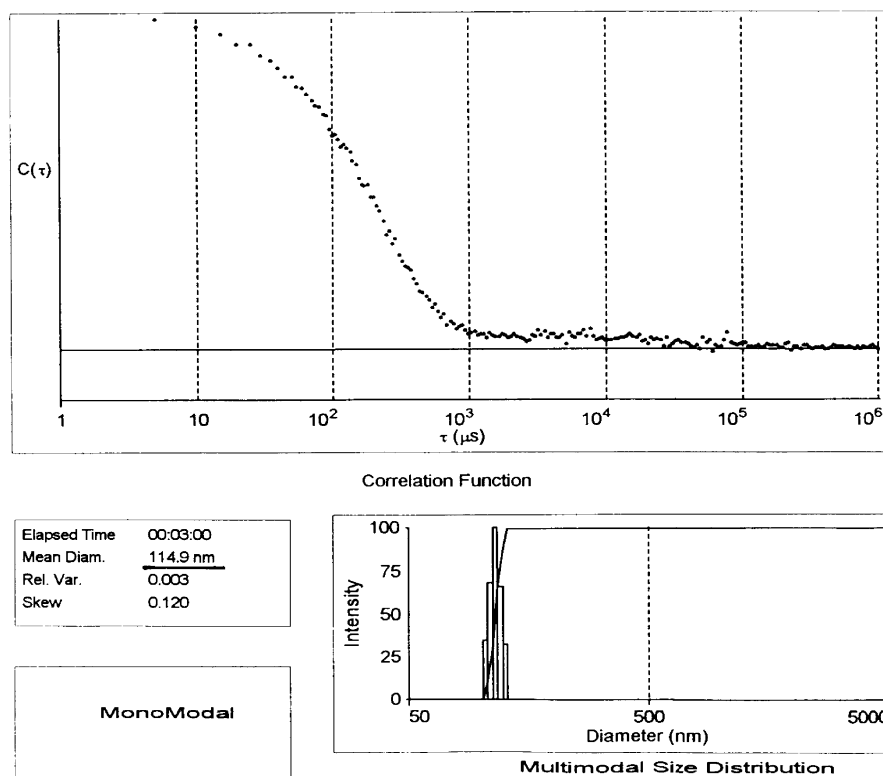


Fig.2: Computer print-out of a particle size measurement with the BI-90

The measurements of the latex standards were done with varying laser powers. For very dilute samples, a measuring time of 10 to 20 seconds was selected and the measurements were repeated ten times. This minimizes the artifacts. Fig. 2 shows an example of the autocorrelation function $C(J)$ (see /2/) of the 107-nm standard at a concentration of 0.3 ppm. The method of Non-Negatively constrained Least Squares (NNLS) /2/ was used to derive particle size distributions from $C(J)$. The resulting distribution of our example is depicted in the lower part of Fig. 2. It is monomodal as one could expect from the sample. The peak is relatively narrow and the calculated mean particle diameter is 114.9 nm, which is quite good compared to the nominal 107-nm standard.

Tab. 1 shows the measured particle sizes (positions of peak maxima) of the diluted polystyrene latex standards at a laser power of 400 mW. According to the producer of the device, the error for particle size determination is # 5%. As is to be seen from Tab. 1, this claim is met for particle sizes of up to 300 nm as long as the concentrations are not too low. Count rate sensitivity (cf. /1/) and particle sizing accuracy are excellent in the region from 60 to 300 nm. The minimum concentration at which the particle size can still be determined with an error of # 10% is 0.1 to 0.3 ppm (particle size errors of # 10% are still acceptable for our purposes). For colloidal suspensions of very low particle sizes, as exemplified here by the 28 nm standard, the lower limit of successful particle sizing lies at a concentration of 5 ppm. The error of particle sizing is greater with particle sizes of 600 to 1240 nm. The lower limit of successful particle sizing rises to 1 to 3 ppm for such particles. For some cases, i. e. for larger particles, an increase in the laser power to 1 or 2 W leads to an improvement of the sensitivity and accuracy of the BI-90 (not shown here). Fig. 3 provides a survey of the upper and lower limits of detection for particle sizing.

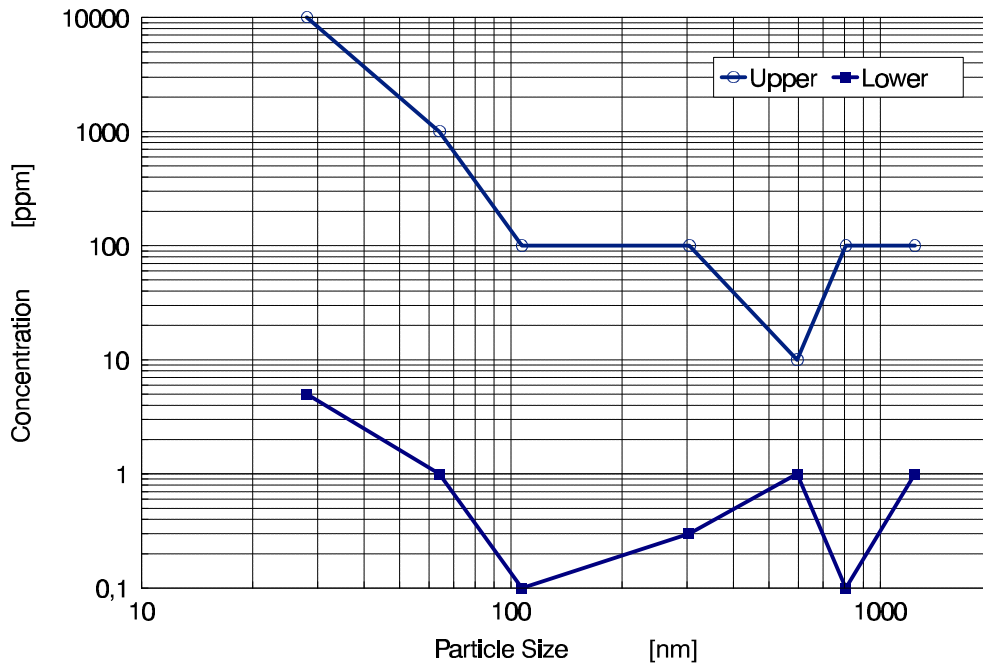


Fig. 3: Upper and lower limits of particle sizing with the BI-90. Measured with polystyrene latex standards of Duke Scientific Corp.

In summary, we found through measurements on standard polystyrene latex particles that the lower limit for particle sizing lies at a concentration between 0.1 and 5 ppm, depending on the particle size. Below this lower limit, the device can still indicate the presence or absence of particles by the count rate. The particle size, however, is calculated to be 0 or unreasonably high (several μm) in this concentration region. High laser powers and many repeated measurements with short measuring times are recommended for dilute colloids. This applies for instance to groundwaters and mining waters. Compared to the UPA-150 from Leeds & Northrup that we tested earlier /3/, the BI-90 has about 30-fold lower detection limit.

References

- /1/ Hüttig, G., Richter, W. Zänker, H.: Dependence of Scattered Light Intensities on the Particle Concentration of Low-Concentrated Colloids. This Report
- /2/ Grabowski, E.F. and Morrison, I.D.: Particle Size Distributions from Analysis of Quasi-Elastic Light-Scattering Data. In: Dahneke, B.E. (Ed.), *Measurement of Suspended Particles by Quasi-Elastic Light Scattering*. Wiley-Interscience, New York etc., 1983, p. 199
- /3/ Zänker, H.: Testing a Microtrac Ultrafine Particle Analyzer UPA-150 from Leeds & Northrup for the Investigation of Environmental Colloids. Report FZR-94, Forschungszentrum Rosendorf e.V., Institute of Radiochemistry, Annual Report 1994, June 1995, p. 49

FIRST RESULTS OF SEQUENTIAL FILTRATION OF GROUNDWATER FROM AN AQUIFER IN THE UPPER ELBE VALLEY SANDSTONE

H. Zänker, G. Hüttig, E. Christalle*, W. Richter¹

Forschungszentrum Rossendorf e.V., Institute of Radiochemistry; * Zentralabteilung Analytik

¹ Technische Universität Dresden, WIP

A groundwater sample from an aquifer in the sandstone of the upper Elbe valley was analyzed for its particle content. We used sequential filtration and characterized the particles in the individual filtrates by light scattering and scanning electron microscopy (SEM) in combination with energy dispersive X-ray spectroscopy (EDX). These experiments serve as tests of our experimental techniques that precede more detailed studies of particle behavior in groundwaters. The groundwater was sequentially filtered six days after sampling. Each filtrate was filtered through a filter having the next smaller pore size. The filters had pore sizes of 5000, 1000, 400, 100, 50, 15 nm (Nuclepore filters) and 30 000 Daltons (Amicon filter; corresponding to a geometric pore size of about 4 nm). Fig. 1 shows the photomultiplier count rate of a BI-90 photon correlation spectroscopy that was measured in the filtrates from each step of the sequential filtration.

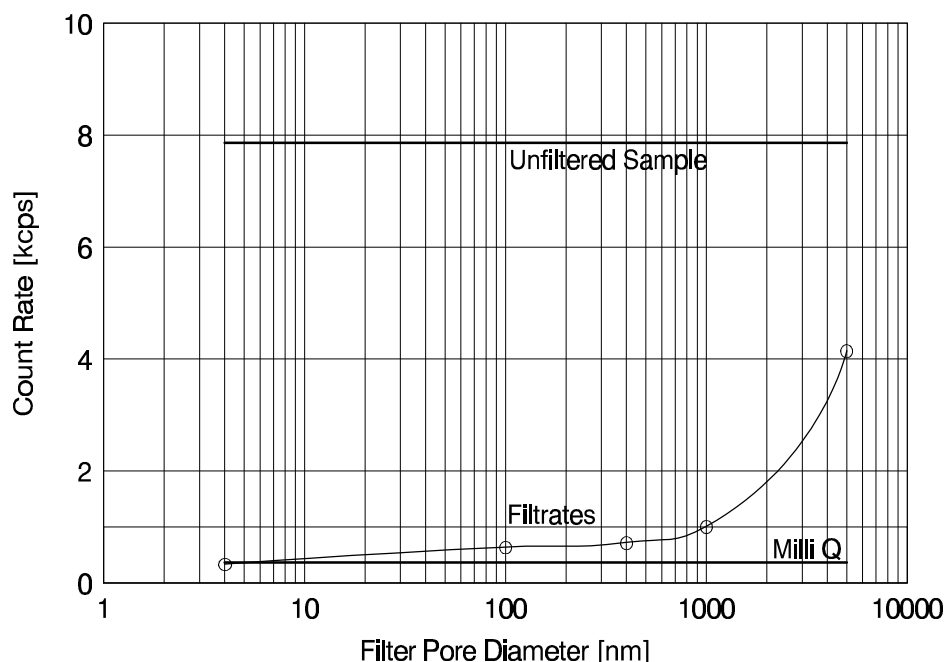


Fig. 1: Decrease of BI-90 photomultiplier count rate by sequential filtration of the groundwater sample (Laser power 900 mW, scattering angle 90°, attenuator 3)

The count rate decreases with decreasing filter pore size; from a count rate of the untreated groundwater to a rate that is comparable to extremely particle-free Milli-Q water. Considering the measuring conditions of the spectroscopy (laser power, degree of attenuation), a rough estimate of the samples' particle concentration can be derived from the count rates. As indicated in Fig. 2 in /1/, the unfiltered groundwater should have a particle concentration of about 0.1 to 10 ppm, assuming that the sizes and refractive indices are not too different for the natural particles and the polystyrene latex particles that were used as the reference (for using scattered light intensities as indicators of particle concentrations and its limitations see /2,3,4/).

In addition to the measurements of scattered light from the liquid samples the filter cakes were examined by SEM and EDX. Fig. 2 shows an example of a particle found on the first filter. The particle is significantly larger than the 5000-nm filter's pore size. Surprisingly, we even found particles that were larger than 5000 nm on the next smaller filter with 1000-nm pore size. We found particles that were larger than the pore size of the corresponding prefilter on all the filters

of the sequential filtration procedure. Fig. 3 and Fig. 4 show examples of particles lying on the 400 nm and 15 nm filters. The corresponding prefiltration steps were through the 1000 nm and 50 nm filters. Fig. 2 through Fig. 4 also show that the 'too large' particles appear to consist of much smaller particles. This means that colloidal matter must have passed the next filters in form of small colloids which then agglomerated in the filtrate or on the filter.

Fig. 5 shows the EDX analysis of the particle that is depicted in Fig. 3. This particle consists of a high fraction of iron minerals, a high fraction of clay minerals and possibly silica (K, Mg, Al, Si), some barite (Ba, S) and presumably some organic matter.

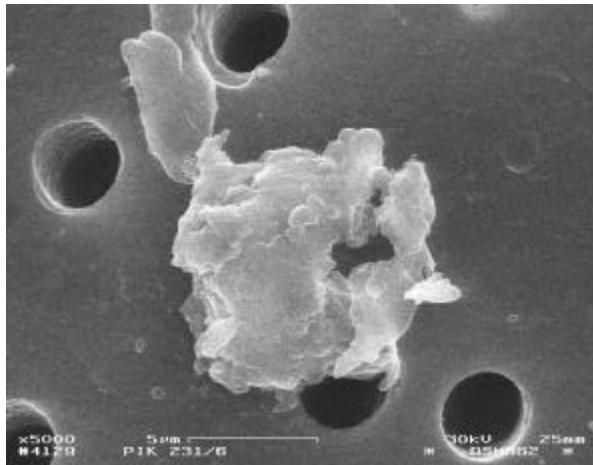


Fig. 2: A 9700-nm particle on a 5000-nm Nuclepore filter; no prefiltration of the groundwater

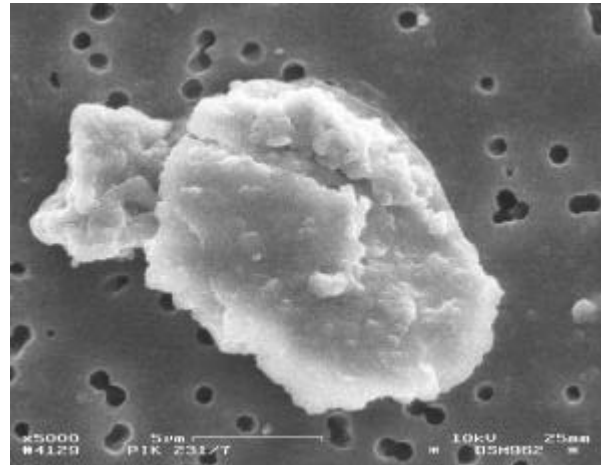


Fig. 3: A 13000-nm particle on a 1000-nm Nuclepore filter; prefiltration through a 5000-nm filter

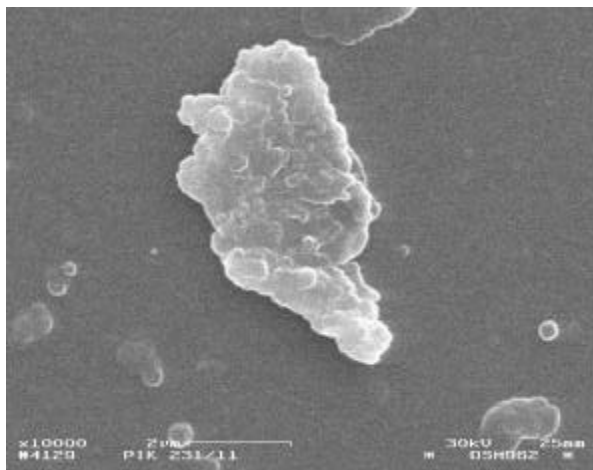


Fig. 4: A 5600-nm particle on a 15-nm Nuclepore filter; prefiltration through a 50-nm filter

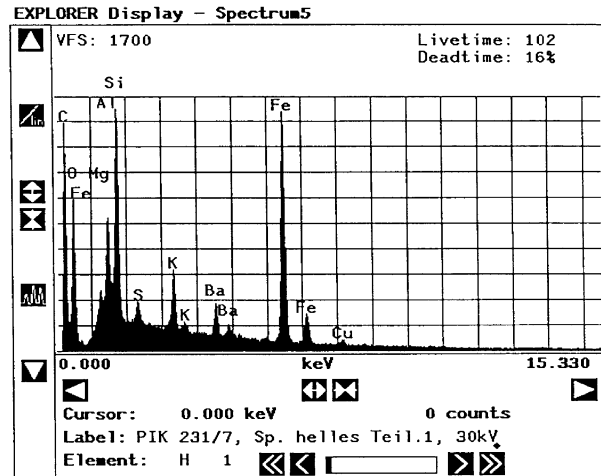


Fig. 5: EDX spectrum of the particle shown in Fig. 3

There is no doubt that filtration, although it is frequently used in colloid science, is not a highly reliable technique for colloid characterization. Filtration is adversely affected by filter clogging /5/, 'self-coagulation' due to concentration polarization /4, 6, 7/, adsorption of small particles onto large ones and onto the filter material /7/, electrostatic interactions between particles and filter /8/, conformation changes of the particles during filtration, broad filter pore size distributions and sometimes even membrane fabrication faults. Screen filters, such as Nuclepore filters, have the great advantage of possessing fairly defined and uniform pore sizes and exhibit only little particle adsorption. However, they suffer more than other filter types from clogging

problems. Karlsson et al. demonstrated that 400-nm and 200-nm pore size Nuclepore filters have an effective pore size of only 50 nm after the filtration of 2 to 3 mL/cm² of water from a Swedish lake /5/. This problem alone explains why particle size distributions derived solely from filtration data must often be viewed as semi-quantitative /8/.

One explanation for the presence of particles on the filters that are 'too large' compared with the filter pore size of the corresponding prefiltration step may be 'self-coagulation'. This phenomenon results from the increased concentration of colloids in the diffusion layer at the membrane surface due to slow back-diffusion of larger retained particles into the solution (concentration polarization). As a result, colloid concentrations at the membrane surface may be orders of magnitude larger than in the bulk solution, leading to an almost instantaneous coagulation /6/. Filtration and SEM observations alone can be misleading in such cases.

Meanwhile, our available methods for colloid characterization has become significantly broader. We are now able to carry out particle sizing directly on the aqueous solutions with our photon correlation spectroscope, ICP-MS on solutions and on filters (after digesting the filter cakes), gravimetry on filters and scanning as well as transmission electron microscopy on filters. Soon, particle-induced X-ray emission spectrometry (PIXE) for the filters will be available. However, environmental colloids tend to exhibit broad and multimodal particle size distributions. Therefore we are currently optimizing our filtration procedures. In the future, filtrations and all characterization experiments will be done as quickly as possible after sampling. Significant particle coagulation takes place in environmental samples within hours or days /7/. Concentration polarization and 'self-coagulation' during the filtration process can be minimized by using very slow flow rates of filtration and low concentration factors, i.e. avoiding filtering to dryness /3, 6, 7/. The number of filtration steps should be reduced. Filtration should be accompanied (perhaps even replaced) by centrifugation as a technique of fractionation. Although centrifugation has its drawbacks too, it could be less prone to artefacts.

References

- /1/ Hüttig, G., Richter, W., Zänker, H.: Dependence of Scattered Light Intensities on the Particle Concentration of Low-Concentrated Colloids. This report
- /2/ Ledin, A., Karlsson, S., Düker, A., Allard, B.: Application of Photon Correlation Spectroscopy for Measurement of Concentration and Size Distribution of Colloids in Natural Waters. *Anal. Chim. Acta* **281**, 421 (1993)
- /3/ Perret, D., Newman, M.E., Nègre, J.-C., Chen, Y., Buffle, J.: Submicron Particles in the Rhine River. I. Physico-chemical Characterization. *Wat. Res.* **28**, 91 (1994)
- /4/ Gschwend, P.M., Reynolds, M.D.: Monodisperse Ferrous Phosphate Colloids in an Anoxic Groundwater Plume. *J. Contaminant Hydrol.* **1**, 309 (1987)
- /5/ Karlsson, S., Peterson, A., Hakansson, K., Ledin, A.: Fractionation of Trace Metals in Surface Water with Screen Filters. *Sci. Total. Environ.* **149**, 215 (1994)
- /6/ Buffle, J. and Leppard, G.G.: Characterization of Aquatic Colloids and Macromolecules. 2. Key Role of Physical Structures on Analytical Results. *Environ. Sci. Technol.* **29**, 2176 (1995)
- /7/ Stumm, W.: *Chemistry of the Solid-Water Interface*. John Wiley & Sons, New York etc. 1992, p. 282
- /8/ Mc Carthy, J.F. and Degueldre, C.: Sampling and Characterization of Colloids and Particles in Groundwater for Studying their Role in Contaminant Transport. In: J. Buffle and H.P. van Leeuwen (Eds.), *Environmental Particles*, Vol. 2, Lewis Publishers, Boca Raton etc., 1993 p. 247

PRODUCTION OF NH_4Cl AND $(\text{NH}_4)_2\text{SO}_4$ AEROSOLS AND INTERACTION WITH IODINE

M. Kalberer¹, B. Eichler¹, R. Dressler¹, U. Baltensperger¹, H.W. Gäggeler^{1,2}, S. Hübener
Forschungszentrum Rossendorf e.V., Institute of Radiochemistry

¹ Paul Scherrer Institut, Laboratory of Radio- and Environmental Chemistry

² Universität Bern, Institute of Inorganic Chemistry

Halogens are of great interest in atmospheric chemistry. Natural and anthropogenic halogen compounds play a key role in the ozone depletion processes in the stratosphere. Whereas the relevant gas phase reactions are well known, the heterogeneous interactions of gas phase molecules with solid or liquid surfaces are still not well understood. In an earlier study /1/ iodine and bromine adsorption on graphite and silver aerosols was investigated.

The present work focussed on the adsorption of iodine on NH_4Cl and $(\text{NH}_4)_2\text{SO}_4$ aerosols which belong to the main components of the atmospheric aerosol. To obtain an aerosol with a constant particle concentration and size distribution, the corresponding salts were pressed into pills of 10 mm diameter and 3 mm height. 2 - 3 pills were heated in a glass tube in a tubular oven at a temperature of 200°C and 240°C for NH_4Cl and $(\text{NH}_4)_2\text{SO}_4$, respectively. Under these conditions aerosol distributions and concentrations could be kept constant for several hours. A mean diameter of about 200 nm and 100 nm was obtained for NH_4Cl and $(\text{NH}_4)_2\text{SO}_4$, respectively, and a particle concentration of 10^6 particles/cm³ for both aerosols.

The aerosols were introduced into the gas-jet system at the U-120 cyclotron of the FZR. Iodine was produced in the target chamber as a fission product of an uranium target which was irradiated with neutrons. The neutrons were produced by the nuclear reaction $^9\text{Be}(d,n)^{10}\text{B}$.

Iodine adsorbed to aerosol particles and in gaseous form, was transported through a polyethylene capillary from the target chamber to the laboratory. The iodine activity was measured on a glass fiber filter positioned on a Ge-detector using the 1313-keV line of ^{136}I . To determine the fraction of the iodine adsorbed to the aerosol particles, a silver coated quartz tube was installed in the line before the aerosol reached the detector. The gaseous iodine adsorbed quantitatively on the wall of the tube, whereas the particulate fraction passed through the tube to reach the detector. Seventy percent of the measured iodine activity was adsorbed on NH_4Cl aerosol particles, and 87 % on the $(\text{NH}_4)_2\text{SO}_4$ aerosol particles.

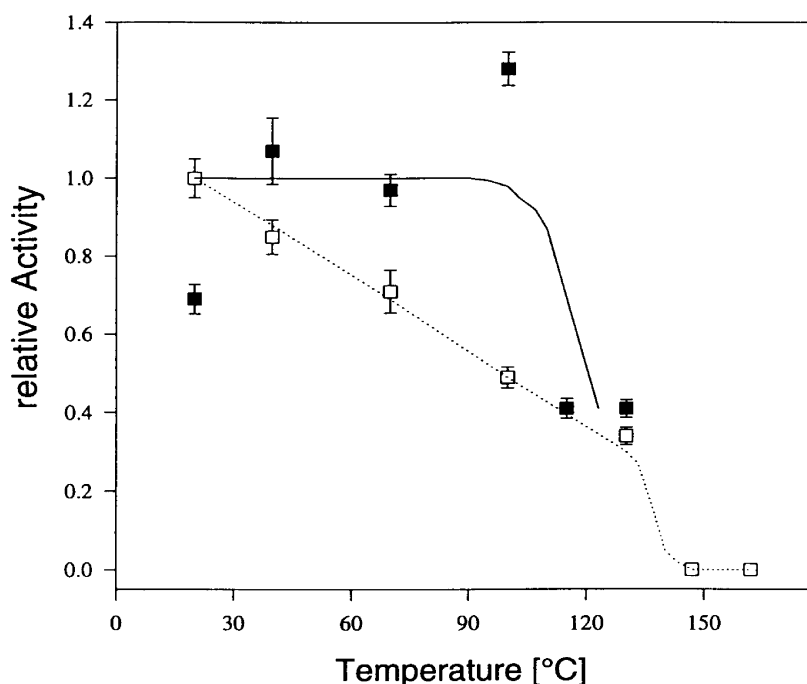


Fig. 1: Deposition of iodine (^{136}I) from NH_4Cl (~) and $(\text{NH}_4)_2\text{SO}_4$ (€) aerosols

To determine the desorption of iodine from the aerosol particles, the silver-coated quartz tube was heated in a modified gaschromatographic oven. The desorption time in the oven was 10 s.

Fig. 1 shows the desorption curves for NH_4Cl and $(\text{NH}_4)_2\text{SO}_4$. In order to correct for the variability of the experimental parameters such as the beam intensity, all values were normalized to the ^{94}Sr activity which absorbs strongly to the aerosol particles. For the NH_4Cl experiments, this normalized activity was set to one for room temperature. For the $(\text{NH}_4)_2\text{SO}_4$ experiments, the average of the datapoints between room temperature and 100°C was normalized to one.

The adsorbed iodine activity decreased continuously with increasing temperature in the experiments with the NH_4Cl -aerosol. Above about 140°C , the iodine was quantitatively desorbed. The iodine desorption from $(\text{NH}_4)_2\text{SO}_4$ aerosol particles showed a different behaviour: desorption was observed only above 100°C . The apparent increase of the relative activity between 20°C and 100°C , is most likely due to undetermined experimental errors. Therefore, we assumed a constant value over this range.

References

- /1/ Ammann, M., Baltensperger, U., Boichert, U.K., Eichler, B., Gäggeler, H.W., Jost, D.T., Türler, A., Weber, A.P.: Interaction of Single HI, HBr, and NO_2 Molecules with Aerosol Particles. *J. Aerosol Sci.* **26**, 61 (1995)

GENERATION AND CHARACTERIZATION OF SODIUM CHLORIDE AEROSOLS

D. Rettig, P. Merker
 Forschungszentrum Rossendorf e.V., Institute of Radiochemistry

We are planning to experimentally investigate the adsorption of toxic substances on particle surfaces. These require the use and characterization of well-defined sub-micrometer aerosols. In this paper we describe the use of a well-known method for aerosol generation. Sodium chloride aerosols are produced by nebulizing salt solutions in a Collision atomizer and subsequently evaporating the water of the small droplets with a diffusion dryer. The unimodal polydisperse aerosols that were generated were characterized by measuring the particle size distribution with a scanning mobility particle sizer (SMPS). The particle size spectra in dependence of the nebulized salt solution concentration offers the possibility to study the coagulation as well as inertial settling processes in the different compartments of the experimental arrangement.

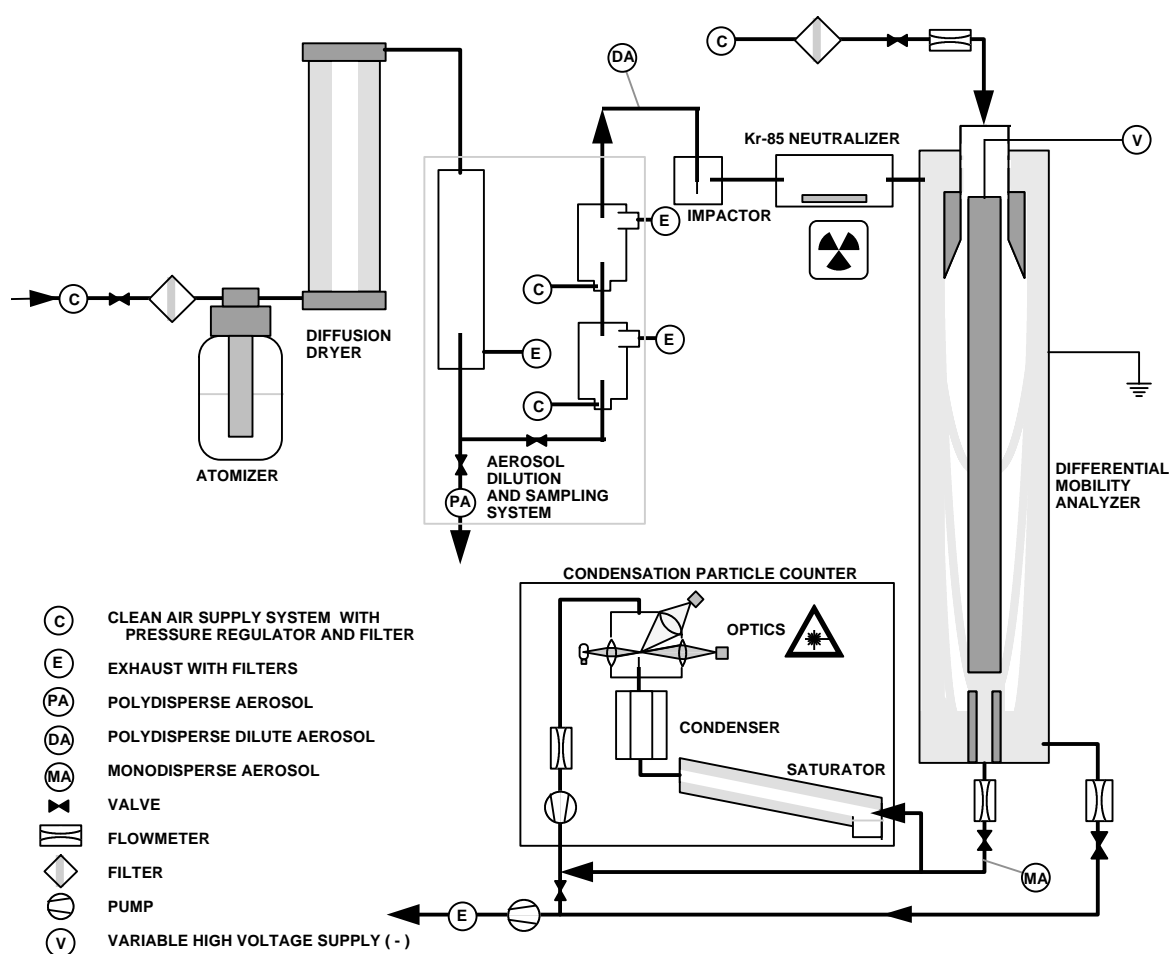


Fig. 1: Experimental set-up showing the atomizer and the dryer (TOPAS GmbH, Dresden), the aerosol diluter (PALAS GmbH, Karlsruhe) and the SMPS (Model 3934, TSI Inc., St. Paul, MN, USA)

The experimental set-up is shown in Fig. 1. The SMPS consists of a Kr-85 neutralizer, a differential mobility analyzer (DMA), a condensation particle counter (CPC), and a personal computer with software to control the instruments and to perform data reduction. In the DMA, different fractions of positively charged particles with a certain electrical mobility reach the slit below the inner rod and thereafter the CPC. Fractionization results from deflection of the

charged particles from the direction of the laminar gas flow in the electric field between the central rod and the tubular wall of the DMA. Because a defined, stable electrical charge distribution is established for the particles in the Kr-85 neutralizer, the concentration of charged particles counted in the CPC, at a given electrical field strength in the DMA can be related to the particle concentration of a particle class having a defined range of mobility equivalent diameters.

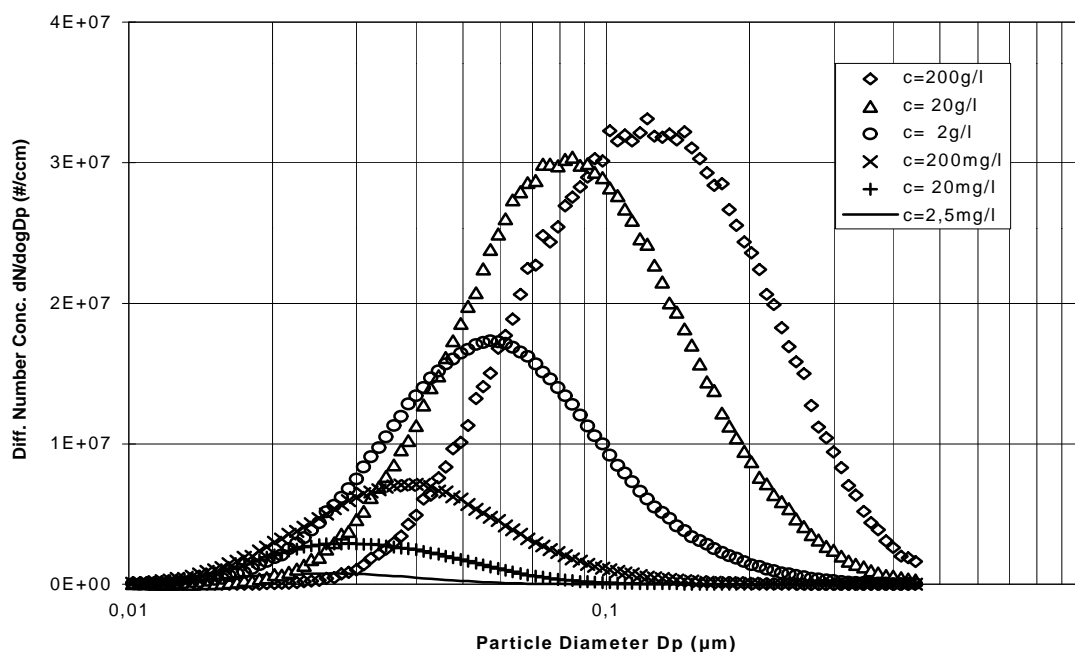


Fig. 2: Dependence of the particle size distribution on the sodium chloride concentration c of the solution in the atomizer (air flow to the atomizer = 270 l/h)

ROTH and GEBHART /1/ found that the droplet size distribution of a primary solution fog generated in Collison atomizers is independent of the concentration of the nebulized sodium chloride solution. From the particle distributions shown in Fig. 2, the total volume or mass concentration of sodium chloride in the aerosols can be calculated, assuming cubical or spherical particle shapes. Cubes were identified for aerosol particles larger than $0.04 \mu\text{m}$ in electron micrographs. The total volume concentrations of the sodium chloride aerosols exhibit a linear relationship to the concentration of the sprayed solutions up to about 1g/L . This indicates that there are no significant losses of sodium chloride aerosol. According to /1/ the particle number concentration produced from the atomizer is constant and, if conserved in the drying process, particles generated from a 2.5 mg/L solution should reach median diameters as low as $0.003 \mu\text{m}$. As can be seen in Fig. 2, the median particle diameter did not fall below $0.02 \mu\text{m}$. This means that an intensive coagulation process occurred during the drying and shrinking of the droplets. As a result, relatively stable aerosols can be sampled after passing the surge tube. In summary, sodium chloride aerosols can be reproducibly produced with a Collison atomizer and a diffusion dryer. The particles have a well-defined log-normal size distribution (geometric standard deviation between 1.5 and 1.7), a median diameter between 0.02 and $0.120 \mu\text{m}$ and a concentration of up to 2×10^7 particles/ cm^3 . Thus they are applicable for future radionuclide aerosol transport experiments.

References

/1/ Roth,C., Gebhart, J.; J. Aerosol Sci. **25**, 313 (1994)

Organic Matter and their Interaction with Radionuclides

SYNTHETIC HUMIC ACIDS: SYNTHESIS AND CHARACTERIZATION IN COMPARISON TO NATURAL MATERIALS

S. Pompe, M. Meyer, M. Bubner, A. Brachmann, R. Nicolai¹, K.H. Heise, H. Nitsche
 Forschungszentrum Rossendorf e.V., Institute of Radiochemistry,
¹ Institute of Bioinorganic and Radiopharmaceutical Chemistry

The goal of our studies is the synthesis of functional models for humic acids (HA's). They have a chemical behavior similar to natural HA's but a considerably simpler overall structure and a defined functionality that can be varied through changing the preparation conditions. Using these model substances and HA's isolated from natural sources, we want to investigate the complexation behavior of HA's with uranyl and other heavy metal ions.

The condensation and dehydration products of reducing sugars and α -amino acids, melanoidins or browning products, have properties like humic substances and are described in the literature as similar to humic substances and are sometimes used as models for these substances /1/.

The synthesis of the HA model substances is based on the preparation of "standard melanoidin" by Enders and Theis /1/. We synthesize HA's from different sugars and α -amino acids. In the present work we synthesized an artificial HA using phenylalanine, glycine and xylose and characterized it /2/. We compared commercially available purified natural HA from Fluka with our synthetic product. Both HA's were characterized by their elemental composition, structure (infrared spectroscopy), functional properties and fluorescence behavior (time-resolved laser-induced fluorescence spectroscopy). The functional groups, carboxylic, phenolic OH and ester groups were determined radiometrically by methylation with [¹⁴C]-diazomethane. The carboxylic groups were also determined by calcium acetate exchange.

Tab. 1: Elemental composition of synthetic and natural HA

| Element [%] | Synthetic HA | Natural HA (Fluka) | Literature /3/ |
|----------------|--------------|--------------------|----------------|
| C | 65.04 ± 0.15 | 57.40 ± 0.15 | 50 - 60 |
| H | 5.37 ± 0.05 | 3.87 ± 0.01 | 4 - 6 |
| N | 5.17 ± 0.01 | 0.95 ± 0.01 | 2 - 6 |
| S | - | 2.15 ± 0.04 | 0 - 2 |
| O ^a | 24.42 ± 0.21 | 35.63 ± 0.12 | 30 - 35 |

^a The oxygen content was calculated from the difference to 100%.

Tab. 1 shows the results of the elemental analysis for synthetic and natural HA's. Our synthetic product has an elemental composition comparable to literature values for natural HA's from different origins /3/. It has a slightly higher amount of carbon and nitrogen than the natural HA from Fluka. The elemental composition of a synthetic HA can be influenced by varying the precursor sugar and amino acids as well as their proportions.

Tab. 2: Functional groups of natural and synthetic HA's (^a rel. std. dev. ± 30%)

| Functional group | Radiometr. determin. ^a [meq/g] | | Calciumacetate exchange [meq/g] | | Lit. /4/ Natural |
|---------------------|---|---------|---------------------------------|-----------|---------------------|
| | Synthetic | Natural | Synthetic | Natural | |
| -COOH + phenol. -OH | 3.8 | 8.5 | - | - | 5.6 - 8.9 |
| -COOH | 1.1 | 4.2 | 1.2 ± 0.1 | 3.8 ± 0.1 | 1.5 - 5.7 |
| phenol. -OH | 2.7 | 4.3 | - | - | 2.1 - 5.7 |
| -COOR | 2.3 | 2.4 | - | - | - |

Tab. 2 exhibits the HA functional groups. The synthetic HA has less functional groups than the natural HA from Fluka. Particularly the amount of carboxylic groups, which are the most important functional groups for the complexation of metal ions, are less than in Fluka HA. However, HA's exist with less functional groups and less carboxylic groups /4/. In order to simulate the functionality of the most abundant HA's, the amount of carboxylic groups can be increased by synthesizing HA's from highly dilute solution, lowering the temperature during the preparation or using glutamic acid as precursor.

Functionality was also studied by capillary electrophoresis.

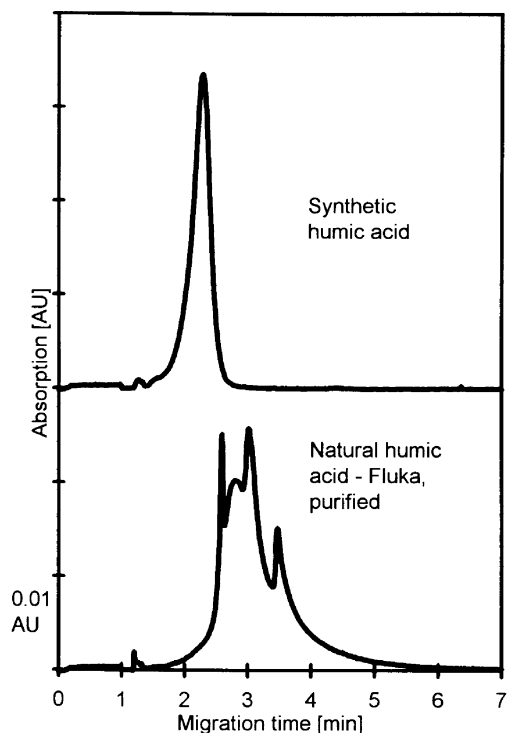


Fig. 1: Electropherograms of synthetic and Fluka HA. Separation conditions: buffer KH_2PO_4 (3 mM) - $\text{Na}_2\text{B}_4\text{O}_7$ (6 mM), pH 8.9; fused silica capillary 75 μm i.d. x 40 cm; separation voltage 30 kV; temperature 30°C; sample volume 70 nl; detection 214 nm

Fig. 1 depicts the electropherograms. Similar to other natural HA's /5/, the purified Fluka HA shows superimposed peaks which we cannot assign to any specific substances at the moment. The synthetic product exhibits only one peak in the electropherogram. This reflects the greater homogeneity (smaller charge/size-ratio distribution) of this substance when compared to the natural HA. The shorter migration time of the synthetic HA under the separation conditions can be explained by a higher molecular size and less dissociated functional groups which are the charge carriers of the HA. The relatively lower content of functional groups when compared to Fluka HA was experimentally determined. The higher molecular size was established by size exclusion chromatography /6/.

The infrared spectra of the HA's investigated are shown in Fig. 2. The spectrum of the synthetic HA closely resembles the spectrum of Fluka HA.

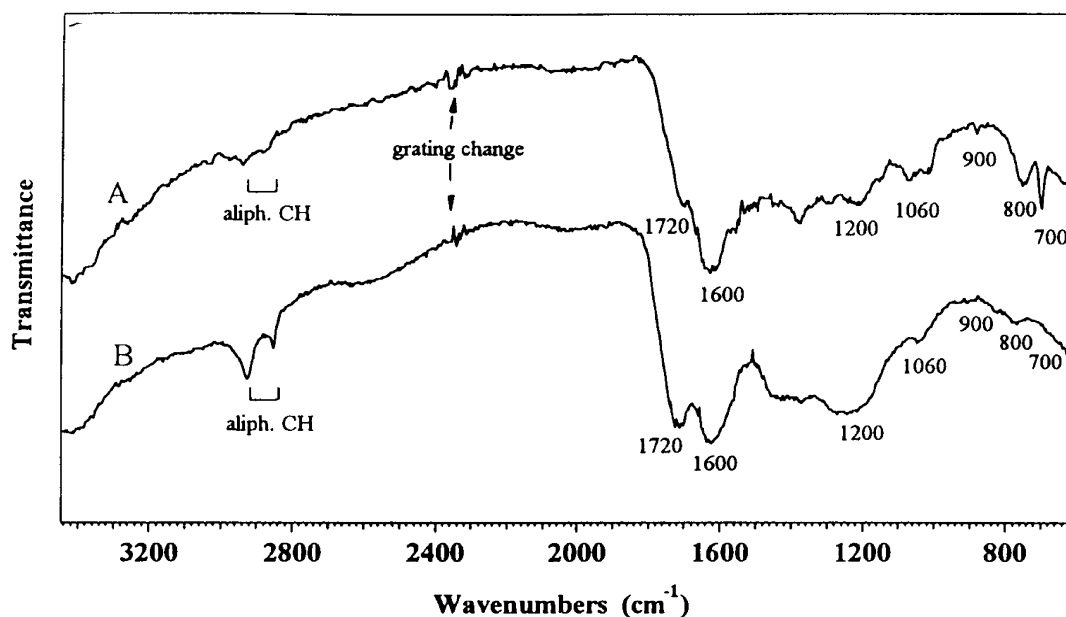


Fig. 2: IR Spectra of synthetic (A) and Fluka HA (B)

Major bands characteristic for HA's occur at about 2900 cm⁻¹ and 2800 cm⁻¹ (aliphatic C-H, CH₂, CH₃), 1720 cm⁻¹ (C=O of COOH and ketonic C=O), 1600 cm⁻¹ (aromatic C=C and H bonded C=O), 1200 cm⁻¹ (C-O stretching and OH deformation of COOH), 1060 cm⁻¹ (C-O), 900 cm⁻¹ and 800 cm⁻¹ (olefinic C-H). Both HA's differ in aromatic and aliphatic carbon content as it is indicated by the bands at 700 cm⁻¹ for aromatic carbon and at 2840 and 2900 cm⁻¹ for aliphatic carbon. The synthetic product has more aromatic carbon due to the use of phenylalanine as precursor substance. The structural deviations of the synthetic HA from Fluka HA can be considerably influenced through variation of the precursor substances. However, it is not necessary to design a structural model for investigations of the complexation behavior of HA's; more important is the functionality. Both HA's also show similarities in their fluorescence behavior. The wavelength regions of the fluorescence bands lie close to one another and the shape of both bands are similar. Both substances exhibit a very short monoexponential fluorescence lifetime decay: (5 ± 0.01)ns for the natural and (7 ± 0.03)ns for the synthetic product. This study presents first results in developing a functional model for HA's. Our product exhibits humic-acid-like characteristics. Further investigations are underway to improve this HA model. Of primary interest is an increase in the number of functional groups, particularly the number of carboxylic groups.

Acknowledgement

We thank R. Ruske for purification of the humic acid from Fluka and for the methylation of the humic acids with [¹⁴C]diazomethane and H. Görner for the determination of the elemental compositions.

References

- /1/ Enders, C., Theis, K.: Die Melanoidine und ihre Beziehung zu den Huminstoffen. Brennstoff Chemie **19**, 360 (1938).
- /2/ Pompe, S., Bubner, M., Denecke, M. A., Reich, T., Brachmann, A., Geipel, G., Nicolai, R., Heise, K.H., Nitsche, H.: A Comparison of Natural Humic Acids with Synthetic Humic Acid Model Substances: Characterization and Interaction with Uranium (VI), accepted by Radiochimica Acta.
- /3/ Stevenson, F. J.: *Humus Chemistry, genesis, composition, reactions*, John Wiley and Sons, Inc., New York 1982.
- /4/ Grauer, R.: *Zur Koordinationschemie der Huminstoffe*, Paul Scherrer Institut, Switzerland, Bericht Nr. 24 (1989), p. 7.
- /5/ Pompe, S., Heise, K.H., Nitsche, H.: Capillary electrophoresis for a "finger-print" characterization of fulvic and humic acids, J. of Chromatography A, in press.
- /6/ Schmidt, M.: this report.

CHARACTERIZATION OF CARBOXYLIC GROUPS IN SYNTHETIC HUMIC SUBSTANCES BY PYROLYSIS GAS CHROMATOGRAPHY

R.Jander, S. Pompe, M. Bubner, K.H. Heise
Forschungszentrum Rossendorf e.V., Institute of Radiochemistry

Pyrolysis gas chromatography (Py-GC) can be used to characterize polymers. The aim of our investigations was to determine characteristic features of synthetic humic acids (HA's) that we use as models for complexation experiments with metal ions [1]. We wanted to determine if the carboxylic groups in a HA from a mixture of aliphatic and aromatic amino acids as precursors differ from each other. Ring bond carboxylic groups will exhibit a much different chemical behavior than aliphatic bond carboxylic groups.

We methylated the HA to distinguish between the different carboxylic groups. We have investigated: 1) a synthetic HA from glycine, phenylalanine and xylose (a), 2) a permethylated HA (b), and 3) a partially methylated HA (c). The permethylation of HA (a) to obtain HA (b) was carried out with diazomethane. HA (b) was partial saponified to obtain HA (c).

The Py-GC experiments were carried out with a gas chromatograph (HP 5890, HEWLETT-PACKARD, Palo Alto, PA, USA), that was online coupled with the pyrolysis equipment (PYROPROBE Mod. 2000, CDS Analytical Inc., Oxford, PE, USA) and a mass selective detector (HP 5971a). The column used (PERMABOND OV1-DF-0.25; Macherey & Nagel, Düren, Germany) had a length of 50 meters and a inner diameter of 0.32 millimeters. Samples of about 250 micrograms were weighed out in a quartz tube. The pyrolysis temperature was 700°C for 15 seconds with a heating rate of 10°C per millisecond from room temperature to the final temperature.

The gas chromatograph was started at 45°C and held for 4 minutes. Then the temperature was increased to 200°C with a rate of 4°C/min where it was hold for one minute. Heating was continued from 200°C to 280°C with a rate of 25°C/min. The end temperature of 280°C was held for 25 minutes. The significant mass peaks were evaluated with the HP software ChemStation^(R) (HPG 1034 MS) and the HP mass library (NBS 75K).

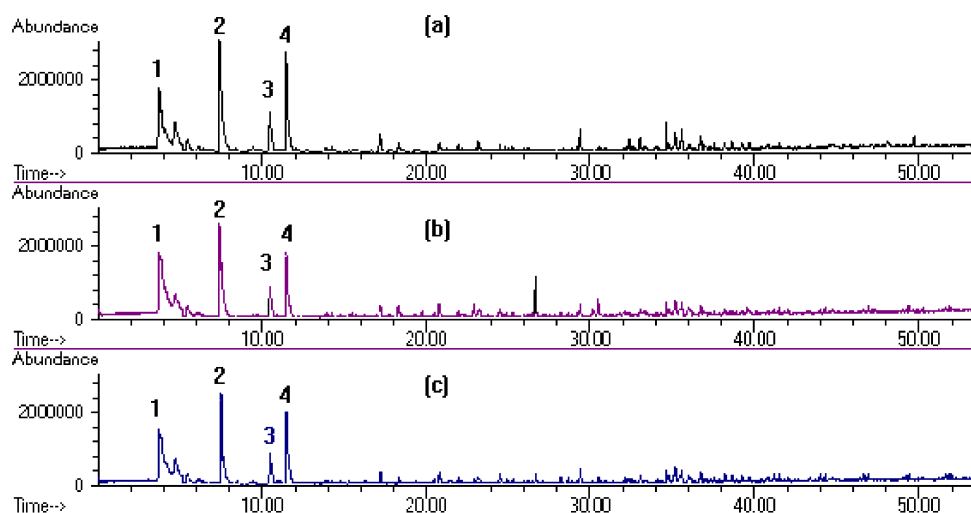


Fig. 1: Pyrolysis gas chromatogram of three different humic acids
a) synthetic b) permethylated c) permethylated and partially saponified

Fig. 1 shows the Py-GC chromatograms of the three HA's (a), (b), and (c). The chromatograms have similar complex structures. The peaks in the range from 2 to 12 minutes have no relevance. Peak (1) is representative for carbon dioxide, formed by decarboxylation reactions. The other peaks were identified as toluene (2), ethyl benzene (3), and styrene (4). These components are formed by thermal decomposition of aromatic structures in the HA's. Significant differences for the interpretation of chromatograms are the small peaks near the background noise. Therefore, the regions of interest (ROI) were expanded. Fig. 2 shows one ROI with retention times between 19 and 24 minutes. Methyl esters were identified. They are due to the

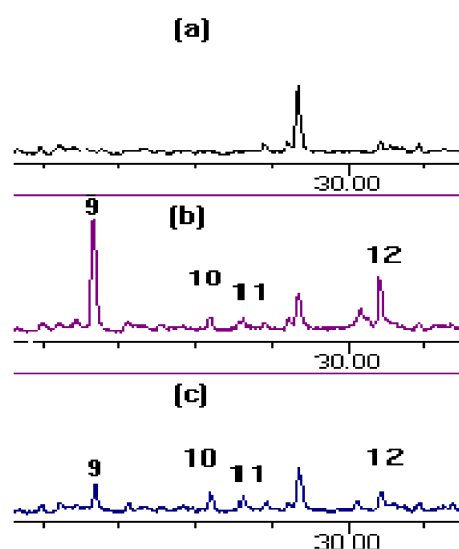
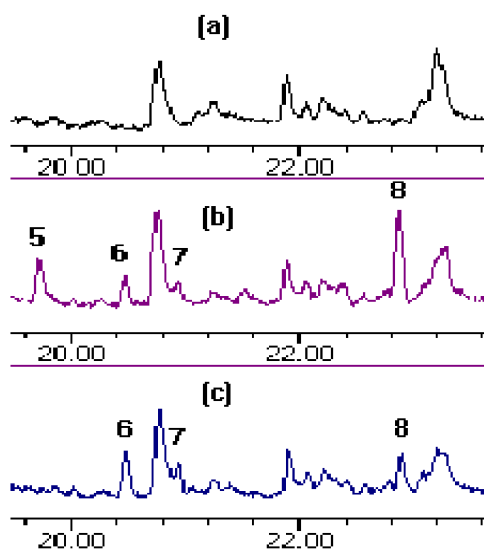


Fig. 2: Expanded region of interest (19 to 24 min) Fig. 3: Expanded region of interest (28 to 31 min)

methylation of the humic acids carboxylic groups with diazomethane. The peak at about 19.7 minutes (5) in HA (b) does not exist in the HA's (a) and (c). It is identified as benzoic acid methyl ester. Its absence in HA (c) may be interpreted with the saponification of this simple ester structure in the HA. The peaks on 22.8 minutes (8) in HA (b) and HA (c) are representative for phenylacetic acid methylester. Remarkable is the existence of this component in HA (c). It may be caused by incomplete saponification of these ester structure. Other esters are found in HA (b) and HA (c). Fig. 3 shows that in the ROI near 28.7 minutes a peak that is identified as phenylpropionic acid methyl ester (9), and the peak near the ROI of 30.2 minutes that is from 2-propenoic-3-phenyl methylester (12). The existence of such "longer chain esters" would be a consequence of the insertion of methylene groups in the "side chain" configuration of the phenyl structures by reaction with diazomethane. Similar types of insertion reactions have been described earlier /2/. Existence of this components also in HA (c) can be interpreted as incomplete saponification of this ester structure. The aromatic character of all esters comes from the phenylalanine as precursor for the HA synthesis. Esters of aliphatic carboxylic acids were not found in the HA's.

In contrast to the original HA (a), both HA's (b) and (c) show peaks at about 20.5 minutes and 20.9 minutes (Fig. 2). These additional peaks were interpreted as undecene (6) and undecane (7). In the ROI, shown in Fig. 3, are visible tridecene (10) at about 28.6 minutes and tridecane (11) at 29.4 minutes. In the other ROI's we also found alkanes and alkenes with chain lengths up to C₂₁. The long chain hydrocarbons may be due to the methylation with diazomethane, because these peaks do not exist in the chromatogram of original HA (a).

The results of the pyrolysis gas chromatography have shown that carboxylic groups in aromatic structures that are similar to their precursor substance phenylalanine. Otherwise should be formed also aliphatic acids or esters. No aliphatic acids or esters of aliphatic acids were found. However, we found those in natural HA's and in HA's that we synthesized without aromatic amino acid precursors /3/. The experiments indicate also that methylene groups are introduced in the HA by the reaction with diazomethane. This may influence the HA's complexation behavior. We are currently clarifying this question and continue characterizing other synthetic humic acids.

References

- /1/ S. Pompe, M. Bubner, M.A. Denecke, T. Reich, A. Brachmann, G. Geipel, R. Nicolai, K.H. Heise, H. Nitsche: Uranyl-Complexation of Humic Acids: A Comparison of Natural Materials with Model Substances; *Radiochim. Acta* 1996, accepted
- /2/ B. Eistert, M. Regitz, G. Heck, H. Schwall: C-H-Insertionen aliphatischer Diazoverbindungen in: Houben-Weyl (ed. by E. Müller), *Methoden der Organischen Chemie*, Vol.X/4, p. 639 f.; Thieme Verlag, Stuttgart 1968
- /3/ R. Jander, S. Pompe, M. Bubner, K.H. Heise; unpublished results

THERMOANALYSIS OF METHYLATION REACTIONS OF SYNTHETIC HUMIC ACIDS

G. Schuster*, S. Pompe, M. Bubner, K.H. Heise
Forschungszentrum Rossendorf e.V., Institute of Radiochemistry, * WIP TU Dresden

Thermoanalytical investigations were performed on a synthetic humic acid, prepared from phenylalanin and xylose, its methylated products and a complex formed following treatment with uranyl ions. The results provide a) qualitative fingerprints for the identification of the synthetic humic acids and its methylated derivatives, b) quantitative estimates of the amount of the bound methyl groups and c) a method for the determination of the bound uranium in uranyl compounds of the humic acid.

Experimental

Using a TG/DTA thermoanalyzer (STA 92, Setaram), the samples were heated under oxygen at 5°C/min up to 700°C. Mass losses, DTA effects and reaction enthalpies were measured of this oxidative decomposition depending on temperature. For analytical measurements the samples were thermoanalytically oxidized by annealing them at a heating rate of 25°C/min under oxygen in a carbon, hydrogen, water analyzer (RC 412, Leco), in which the CO₂ and water formed were quantitatively determined by infrared measurements. Experimental details are reported in /1/.

Samples

The preparation of the samples is described in /2/. The sample description and their identification are as follows:

- M1 = unchanged synthetic humic acid
- M7 = synthetic humic acid, phenolic OH groups methylated
- R6 = synthetic HA, phenolic and carboxylic OH groups partially methylated
- M5 = synthetic HA, permethylated
- M1U = uranyl compound of the humic acid M1

Results of the DTA measurements:

The most sensitive signals of the oxidative destruction of the synthetic humic acids are the DTA diagrams, which are depicted in Fig. 1.

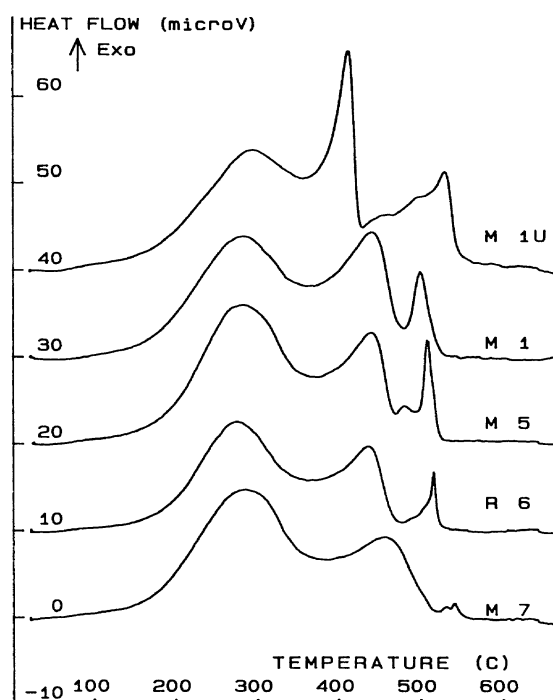


Fig. 1: DTA diagrams for the oxidative decomposition of synthetic humic acids: M5 permethylated, M7 phenolic OH groups methylated, R6 partial methylated, M1 synthetic humic acid, M1U Uranyl compound of the synthetic humic acid M1. The scale is valid for all samples. HF start for all is zero.

For all samples, the methylated compounds show an increase of the first peak in comparison to the second at nearly unchanged temperature. The temperature of the third small peak increases with the extent of methylation and the peak shape changes. The DTA diagrams give characteristic, qualitative fingerprints for this humic acids and its methylated derivatives. The upper curve of Fig. 1 shows the DTA diagram of the a uranyl compound M1U of the humic acid M1, prepared by reacting a suspension of solid humic acid M1 with uranyl nitrate solutions /2/. Here the temperature of

the main DTA peak is shifted to lower values. This is reported to be characteristic for humates of multivalent metal cations in /3/. Additionally the second peak is sharper and more intense and the third extends over a larger temperature region compared to the humic acid. These differences in the DTA curve can be used for the qualitative identification of the uranyl compounds.

Analytical measurements and evaluations:

The amount of C and H were determined for the entire oxidative decomposition as well as for single temperature regions from the amount of CO₂ and H₂O formed in this oxidation reaction. A typical diagram of such a measurement is shown in Fig. 2 for the synthetic humic acid M1 and its permethylated derivate M5.

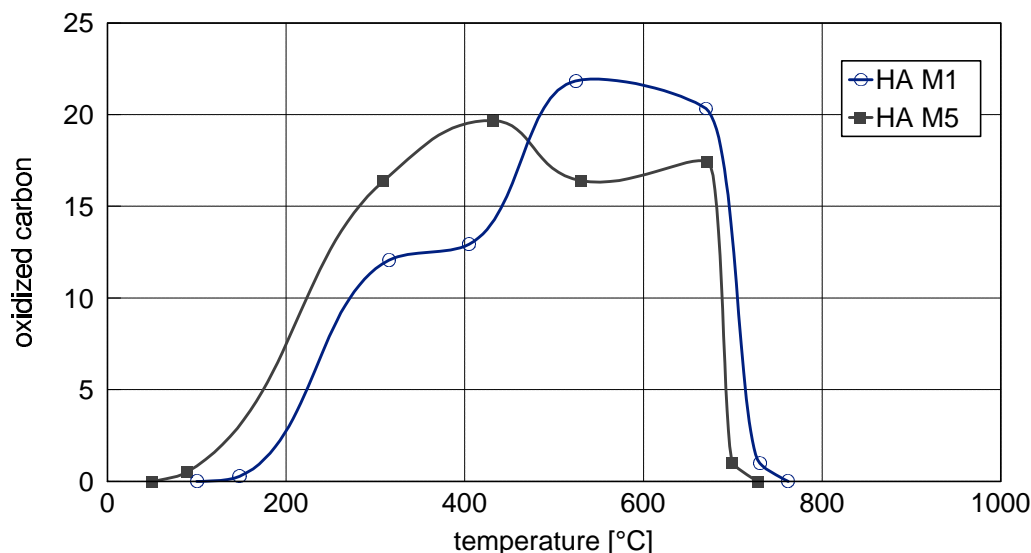


Fig. 2: Oxidation of carbon in humic acids depending on the temperature. M1 = synthetic humic acid, M5 = permethylated synthetic humic acid

From these measurements, the C, H, moisture and for pure carbon - hydrogen compounds the O content can be calculated. The oxidation residue can also be measured by this method but it is easier to obtain it from thermogravimetric measurements. The oxidation residue and the amount of H₂O as moisture are important corrections for the elemental analysis. They are given in the Tab. 1 for the synthetic humic acids investigated.

Tab. 1: Values for the moisture content and the oxidation residue for the synthetic humic acid M1, its methylated derivatives and the uranyl humate M1U

| sample | moisture content [w%] | oxidation residue [w%] |
|--------|-----------------------|------------------------|
| M 1 | 4.07 | 0.44 |
| M 7 | 2.05 | 1.67 |
| R 6 | 0.55 | 1.14 |
| M 5 | 2.01 | 1.07 |
| M 1U | 4.78 | 7.14 |

From these results one can conclude that dry humic acids can be prepared without annealing to more than 100°C and furthermore that the control of the moisture content plays an important role. The oxidation residue may consist of sodium chloride from the preparation and cleanup procedures. The H : C and O : C ratios were calculated for the different temperature regions from C and H values and the mass loss. The nitrogen content taken from the elemental analysis /2/ was subtracted for the calculation of oxygen. The results are given in Tab. 2.

Tab. 2: H : C and O : C ratios and the number of CH₃ groups calculated from the increase of the H and C content caused by methylizing of synthetic humic acids

Complete reaction

| sample | temp. range [°C] | H:C molar ratio | O:C molar ratio | equiv. CH ₃ groups [mequ/g] |
|--------|------------------|-----------------|-----------------|--|
| M1 | 20 - 975 | 0.88 | 0.21 | - |
| M7 | 20 - 975 | 1.14 | 0.11 | 15.9 |
| R6 | 20 - 975 | 1.07 | 0.11 | 11.6 |
| M5 | 20 - 975 | 1.19 | 0.07 | 18.6 |

Temperature range of the first thermoanalytical peak (Fig. 1)

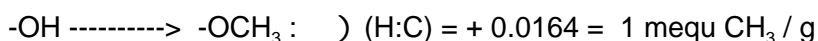
| sample | temp. range [°C] | H:C molar ratio | O:C molar ratio | equiv. CH ₃ groups [mequ/g] |
|--------|------------------|-----------------|-----------------|--|
| M1 | 20 - 405 | 1.6 | 0.39 | - |
| M7 | 20 - 440 | 1.48 | 0.04 | - 9.6 |
| R6 | 20 - 420 | 1.60 | 0.1 | 0 |
| M5 | 20 - 432 | 1.62 | 0.17 | 0.16 |

Residual reaction from the end of the first peak up to 975 °C

| sample | temp. range [°C] | H:C molar ratio | O:C molar ratio | equiv. CH ₃ groups [mequ/g] |
|--------|------------------|-----------------|-----------------|--|
| M1 | 405 - 975 | 0.46 | 0.02 | - |
| M7 | 440 - 975 | 0.74 | 0.12 | 25.5 |
| R6 | 420 - 975 | 0.59 | 0 | 11.6 |
| M5 | 432 - 975 | 0.88 | 0 | 18.7 |

Discussion of the H : C

The aim of the methylation reaction is to replace exchangeable H atoms in the carboxylic and phenolic OH groups by CH₃. This causes a 2 to 1 increase in the H:C and a decrease of the molar ratio of O : C per mol CH₃. Therefore methylation formally is a hydrating respectively reduction of the humic acid (Tab. 2). The destruction of the oxygen rich groups takes place in a low temperature range of up to 430 °C. Moreover, methylation increases the amount of thermostable hydrogen rich groups. That is surprising and cannot be explained by the oxidation of high reactive methoxylic groups /4/. For example, for the exchange of 1 mol H atoms with 1 mol methyl groups in 100 g humic acid M1, the following is valid:



If indeed only CH₃ groups would be introduced, then a measured H : C increase of 0.0164 causes blocking by CH₃ groups of one mequ carboxylic acid and phenolic OH groups per gram humic acid. In this manner the number of CH₃ groups introduced into the humic acid were calculated and are listed in Tab. 2. An incorporation of 11.6 to 18.6 mequ/g for the different methylation reactions were calculated with this assumption. These values are too high in comparison with acidimetric titrations results or with methylation with C14 diazomethan, where only 3.8 mequ methyl groups/g was found for the protonexchange capacity PEC in sample M1. The large difference between these values and the fact of the high thermostability of the hydrogen rich groups indicate, that in addition to the methylation of this small number of OH groups, further reactions take place, which increase the H : C ratio. This could be the breaking of double bonds and the fragmentation of the macromolecule which would explain the fact that after methylation an increase of aliphatic hydrocarbons were found by pyrolysis gas chromatography /6/. Further investigations are necessary to obtain a clear picture of these reactions.

Calculations on the basis of the oxidation residue

The corrected oxidation residue from the uranyl compound of the synthetic humic acid M1U amounts to 7.14 %. The oxidation was thermoanalytically controlled to obtain U₃O₈ by annealing

under oxygen up to 800°C. Bound uranium was 0.25 mmol per gram humic uranyl compound, calculated on the basis of the molar O : U ratio of U_3O_8 and the oxidation residue. That corresponds to the saturation of 0.5 mequ PEC per gram humic uranyl compound by uranium. The defined oxidation of the uranium to U_3O_8 in the oxidation residue is a favourable method for the determination of uranium bonded to uranyl humates. With the sensitivity and the accuracy of 1 µg of the used thermal balance depending on the sample mass, the error of the method can be minimized to 0.005 %,

References

- /1/ Schuster, G., Bubner, M., Heise, K.H. : Thermoanalytical Investigations on the Chemical Constitution and the Oxidative Decomposition of the Natural Humic Compounds. Forschungszentrum Rossendorf, Institute of Radiochemistry, Annual report FZR - 94, 63 (1994)
- /2/ Pompe, S., Bubner, M., Denecke, M., Reich, M., Brachmann, A., Geipel, G., Nicolai, R., Heise, K.H., Nitsche, H.: Comparison of Natural Humic Acids with Synthetic Humic Acid Model Substances: Characterization and Interaction with Uranium VI. Accepted for Publication in Radiochimica Acta
- /3/ Khairy, A.H., Ziechmann, W. : Influence of the Concentration of Humic Acids on their Fragmentation in Alkaline Solutions. Z. Pflanzenernährung und Bodenkunde **145**, 600 (1965)
- /4/ Schnitzer, M., Hoffmann, J. : Thermogravimetry of Soil Humic Compounds. Geochimica and Cosmochimica Acta **29**, 859 (1965)
- /5/ Schuster, G., Braun, G., Henkel, K. : Fehlerbetrachtung zur gravimetrischen O/U Bestimmung. Report ZfK 489 (1981)
- /6/ Jander, R., Bubner, M., Pompe, S., Heise, K.H. : Characterization of Carboxylic Groups in Synthetic Humic Substances by Pyrolysis Gas Chromatography. This report

COMPLEXATION OF U(VI) WITH MODEL SUBSTANCES SIMULATING HUMIC ACID FUNCTIONALITY

A. Brachmann, G. Geipel, V. Brendler, G. Bernhard, H. Nitsche
Forschungszentrum Rossendorf e.V., Institute of Radiochemistry

For simulating the functionality of humic acids, simple organic substances like salicylic, phthalic or malonic acids are used as model compounds. Spectra of each component can be identified using time-resolved-laser-fluorescence spectroscopy and complex spectra can be deconvoluted. These studies can be used to elucidate uranium-humic acid complexation.

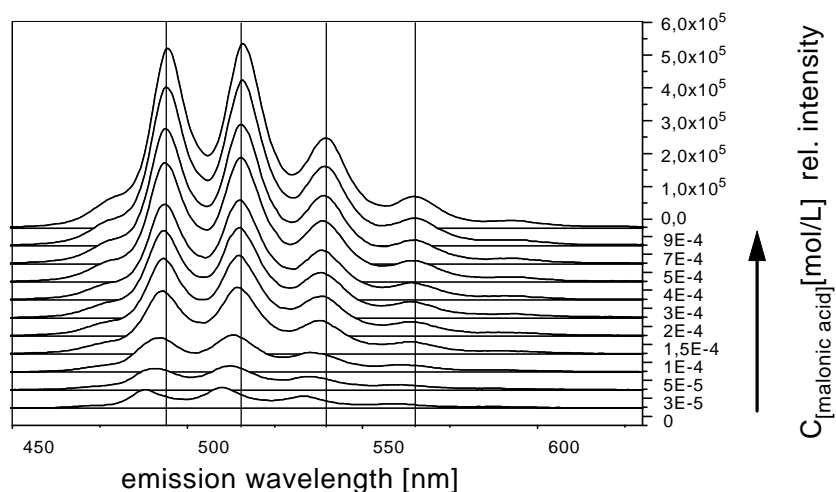
Despite of the complex structure of humic acid molecules, functionality toward the complexation with metal ions at a pH below 7, attributed to the interaction with the carboxylic groups [1,2]. In order to obtain information on the spectral changes of the uranyl fluorescence due to the complexation with the carboxylic groups we measured the fluorescence of the uranyl ion and its complexes with simple mono- and dicarboxylic acids (salicylic, phthalic and malonic acids).

Salicylic and phthalic acid have a strong fluorescence in the UV/VIS region but the fluorescence lifetimes are short in comparison with the fluorescence of the uranyl ion. This allows discrimination between the fluorescence of the organic molecule and the uranyl ion. No fluorescence of malonic acid could be observed. The spectral changes of the uranyl ion fluorescence complexed by carboxylic groups depends of the structure of the organic molecule. Uranyl salicylic and phthalic acid do not show any shift in position and change of halfwidth compared to the uranyl fluorescence bands. Only fluorescence depletion and no quenching was observed for these complexes. However, uranyl complexed by malonic acid shows both spectral shift and strong fluorescence enhancement. Also the fluorescence lifetime increased. It is obvious that changes of the intramolecular energy transfer and the influence of the ligand field play an important role for the observed fluorescence behavior. We present the system uranyl - malonic acid in more details. A set of uranyl fluorescence spectra were recorded (Fig. 1).

Fig. 1: Measured uranyl malonate spectra as a function of malonate concentration

The overall uranyl concentration was held constant ($7.5 \cdot 10^{-6}$ mol/L) and the concentration of malonic acid was from 0 to $9 \cdot 10^{-4}$ mol/L. All measurements were done at pH 4, $22 \pm 1^\circ\text{C}$ and a constant ionic strength of 0.1 M (NaClO_4). Time-resolved fluorescence spectra allow to assess the

number of fluorescent species involved (Fig. 2). Four species contributing to the fluorescence could be resolved over the entire concentration range. But no spectra with mono exponential decay were found, indicating that each spectrum represents a mixture of at least two species. Tab. 1 summarizes the calculated fluorescence decay parameters (decay constant J) and error values ($3F$) for the observed species.



| species | $J \pm 3F$ [ns] |
|----------------------------|-----------------|
| UO_2^{2+} | 1155 ± 190 |
| $\text{UO}_2(\text{OH})^+$ | 3394 ± 1344 |
| UO_2HMA^+ | 1450 ± 118 |
| UO_2MA | 6058 ± 1275 |

Tab. 1: Fluorescence decay constants of species involved in the uranyl - malonate system, uncertainties are $3F$

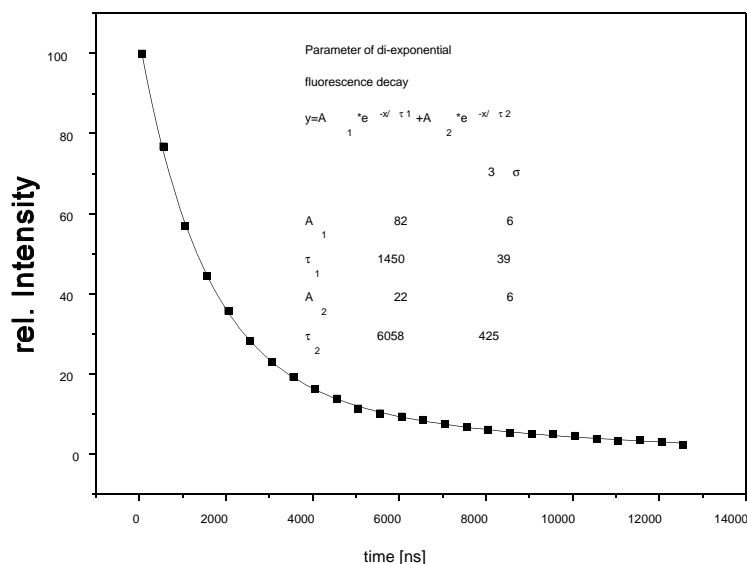
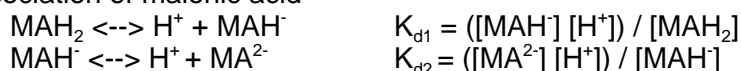


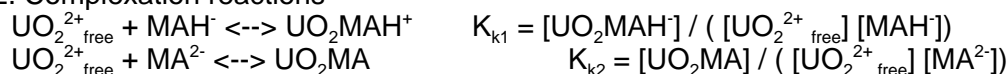
Fig. 2: Fluorescence decay of mixed uranyl malonate spectra

The parameter fit of the multi exponential fluorescence decay allows the separation of spectra. However, results are only correct when the fluorescence yields are comparable. At high malonate concentrations, no significant fluorescence for uncomplexed uranyl or uranyl hydroxid could be found. These spectra were used for generation of the unknown uranyl malonate spectra using the lifetime fit procedure followed by a gaussian fit (Fig. 3). The spectra of free uranyl and uranyl hydroxide were known from earlier measurements. By using conventional peak deconvolution (method of least squares), all measured spectra could be resolved into the individual spectral contributions of the involved species. The results of peak deconvolution were used to calculate the uranyl malonate speciation based on the following model /4/:

1. Dissociation of malonic acid



2. Complexation reactions



3. Balance

$$\begin{aligned} \text{Ma}_{\text{total}} &= \text{MAH}_2 + \text{MAH}_2 + \text{MAH}^- + \text{MA}^{2-} + \text{UO}_2\text{MAH}^+ + \text{UO}_2\text{MA} \\ \text{UO}_2^{2+} \text{ total} &= \text{UO}_2^{2+} \text{ free} + \text{UO}_2\text{MAH}^+ + \text{UO}_2\text{MA} \end{aligned}$$

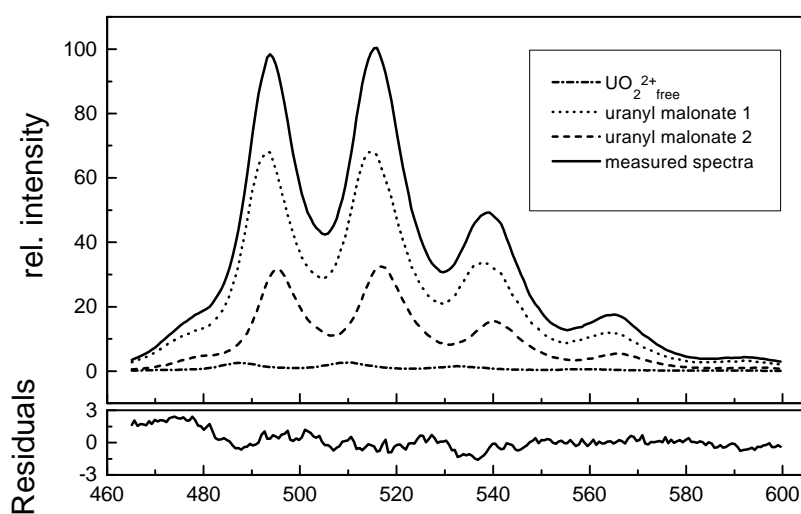


Fig. 3: Result of the peak deconvolution the lifetime fitting procedure

The spectrum of the first hydrolytic uranyl species (UO_2OH^+) was included in the peak deconvolution because of its strong fluorescence yield. According to the NEA database /3/ only a minor amount (<5%) of UO_2OH^+ is present at our experimental condition. For that reason it is not included in the proposed model. A least-square algorithm was used to fit the results of peak deconvolution to the proposed model. The above mentioned model was found to fit the measured data. The analysis of the data led to the conclusion that a single positively charged 1 : 1 complex and at higher ligand concentration a neutral 1 : 1 complex is formed. The formation of the neutral uranyl malonate species involves the complete dissociated malonic acid

results of peak deconvolution to the proposed model. The above mentioned model was found to fit the measured data. The analysis of the data led to the conclusion that a single positively charged 1 : 1 complex and at higher ligand concentration a neutral 1 : 1 complex is formed. The formation of the neutral uranyl malonate species involves the complete dissociated malonic acid

and a small amount of the single dissociated part as well, releasing one proton. Fig. 4 shows the speciation calculated for the investigated concentration range.

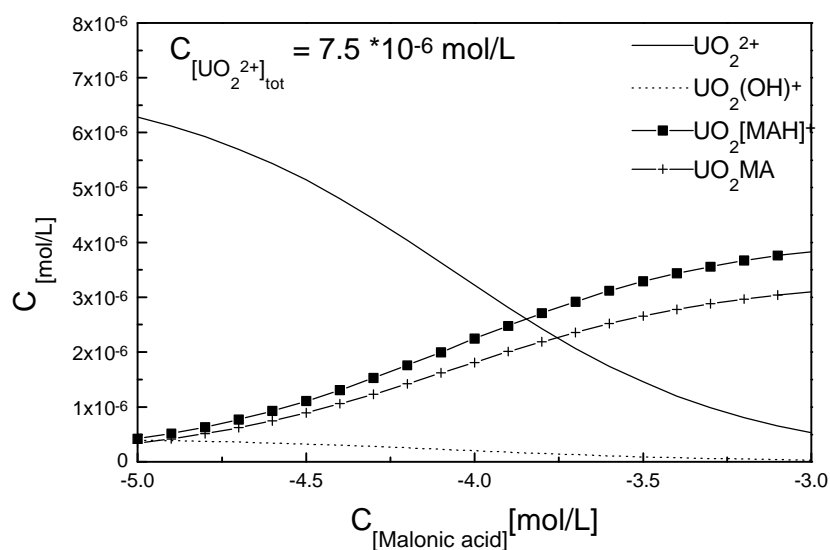


Fig. 4: Speciation diagram for the uranyl malonate system

Two further models were tested. The first involving only the 1 : 1 complex and the second involving the 1 : 1 and 1 : 2 ($UO_2(MA)_2$) complexes. No significant values for the complex-ation constants could be found over the whole investigated concentration range. The comparison with published data for uranyl humic acid complexation led to the conclusion that the un-

charged uranyl malonate species is more representative for uranyl humic acid complexes than the positive charged 1 : 1 uranyl malonate complex. The calculated conditional complexation constants based on the above mentioned model are summarized in Tab. 2.

| | |
|---------------|-------------------|
| $\log K_{k1}$ | $3.9 \pm 0.9(3F)$ |
| $\log K_{k2}$ | $5.5 \pm 0.6(3F)$ |

Tab. 2: Complexation constants for the Uranyl-malonate system

References

- /1/ Czerwinski, K.R.; Buckau, G.; Scherbaum, F.; Kim, J.I.: Complexation of the Uranyl Ion with Aquatic Humic Acid; *Radiochimica Acta* **65**, 111-119, 1994
- /2/ Moulin, V.; Tits, J.: Complexation Behaviour of Humic Substances towards Actinides and Lanthanides Studied by Time-Resolved Laser-Induced Spectrofluorometry; *Radiochimica Acta* **58/59**, 121-128, 1992
- /3/ Grenthe, I.; Fuger, J.; Konings, R.J.M.; Lemire, R.J.; Muller, A.B.; Nguyen-Trung Cregu, Ch.; Wanner, H.; *Chemical Thermodynamics of Uranium*, NEA OECD, 1992
- /4/ Paramonova, W.I.; Mosevich, A.N.; MaTsy-Guan; Using of ion exchange for investigation of the bounding condition in solution (in Russian); *Radiokhimiya* **11**, 682-694 (1964)

INVESTIGATIONS ON THE HYDROTHERMAL DEGRADATION OF WOOD IN FLOODED MINES

K. Jelen¹, R. Schiene¹, K. Fischer¹, L. Baraniak, H. Nitsche

Forschungszentrum Rossendorf e.V., Institute of Radiochemistry

¹ Technische Universität Dresden, Institute of Plant and Wood Chemistry, Tharandt

Vast amount of wood were used to shore up the shafts of several underground uranium mines that are located in Saxony and Thuringia, Germany. In the process of flooding these mines, the wood is exposed (in depths of up to 1900 meters) to pressures up to 200 bar and temperatures up to 70 °C. Under the given conditions, the mine wood can degrade to phenolic and saccharic compounds /1/. Organic substances which are being produced by this process can influence the chemical properties and subsequently the migration behaviour of radionuclides and heavy metals. Therefore, we are investigating the composition and the amount of carbohydrates and phenolic compounds, that are formed by the degradation of wood.

Three different wood samples were investigated. They were obtained from the remediation company WISMUT GmbH and had different age and structure. The samples were degraded by contacting them with water in an autoclave to simulate the temperature and pressure conditions of the flooded mine. A volume ratio of wood-to-water of between 1 to 9 and 1 to 15 was used because this value was estimated for the conditions of the mine located in the town of Schlema. All wood samples were analysed by Pyrolysis-Gaschromatography-Mass Spectroscopy (Pyrolysis-GC/MS) /2/ before and after the degradation treatment. The mass peaks were identified by comparing them to literature data /3, 4/ and to the mass spectra library that is part of the instrument's data analysis routine. The samples, the degradation conditions and the analysis results are summarized in Tab. 1 and Tab. 2.

| sample | degradation conditions | amount of lignin (%) | |
|-------------------|---|----------------------|-------------------|
| | | before degradation | after degradation |
| 1 (W/L-NB-P1.1) | T=100 °C ambient pressure 5 hours | 80.9 | 77.2 |
| 2 (W/L-NB-P2.1) | | 80.9 | 69.0 |
| 3 (W/L-NB-P3.1) | | 53.6 | 49.7 |
| 1' (W/N-p,T-P1.1) | 70 °C, 90 bar, 5 h | 54.2 | 49.8 |

Tab. 1: Sample identification, degradation conditions and lignin content for wood degradation experiments

| sample | amount of wood substance in the hydrothermal extract (%) | phenolic pyrolysis products (%) | amount of C1, C2, Guaiacol (%) | |
|-------------------|--|---------------------------------|--------------------------------|----------------------|
| | | | untreated wood | hydrothermal extract |
| 1 (W/L-NB-P1.1) | 6.8 | 50.1 | 61.1 | 78.1 |
| 1' (W/N-p,T-P1.1) | 3.5 | 61.2 | | 81.9 |
| 2 (W/L-NB-P2.1) | 9.9 | 41.1 | 64.9 | 79.9 |
| 3 (W/L-NB-P3.1) | 14.1 | 23.1 | 63.0 | 70.1 |

Tab. 2: Phenolic pyrolysis products in the hydrothermal extract and such with reduced and without side chain related to their total amount

The results in column three of Tab. 1 show that the hydrothermal treatment decreases the amount of wood lignin. Increased pressure accelerates this process. Pyrolysis-GC/MS analysis of the dried hydrothermal extract, shown in column three of Tab. 2, revealed that substantial amounts of phenolic compounds are being generated by the wood degradation. Again, increased pressure intensifies this process. Three different phenolic pyrolysis products were identified in untreated and hydrothermally treated wood samples. They had a) a complete side chain (propane unit, C3), b) a reduced side chain (C2, C1) and c) no side chain (Guaiacol). The sums of reduced side chain phenols and of phenols with no side chain found in untreated

wood and in the dried hydrothermal extracts are shown in column 4 of Tab. 2. The main phenolic compounds were 4-Vinylguaiacol in the untreated wood and Guaiacol in the hydrothermal extracts. The mass spectrum of the untreated wood and the hydrothermal extract of sample 2 (W/L-NB-P 2.1) is shown in Fig. 1.

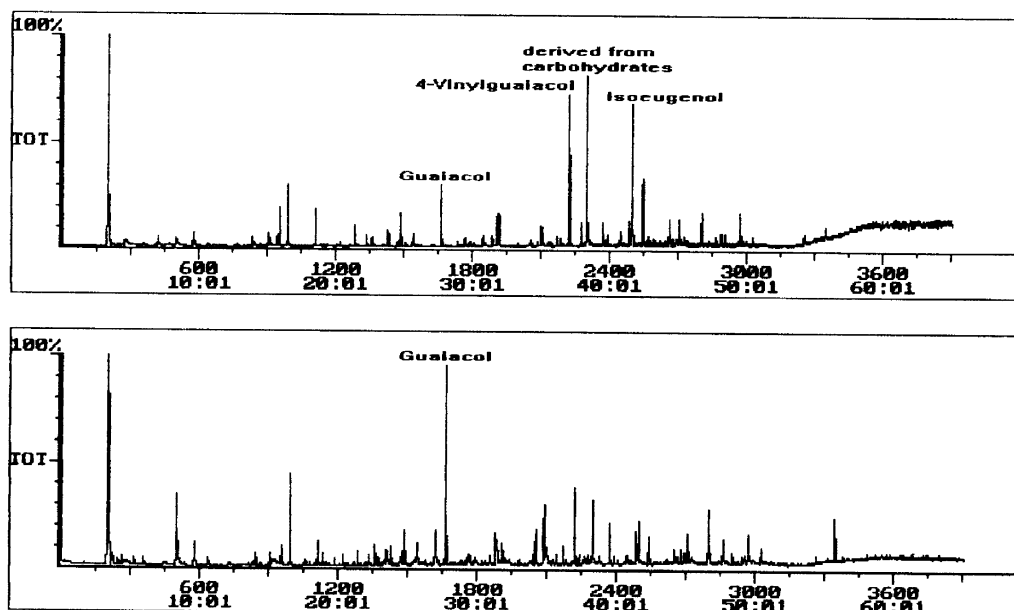


Fig. 1: Pyrograms of a wood sample and of its hydrothermal extract (W/L-NB-P2.1)

The results indicate that the lignin changes with hydrothermal treatment of the wood. The increased amount of phenolic pyrolysis products with a complete side chain (C3) can be caused by increased condensation of the original phenolic substance. Different fragmentation patterns obtained from pyrolysis of the hydrothermal extracts can be attributed to the increased concentration of compounds with no (Guaiacol) or a reduced side chain (C2, C1). This may be the result of the modified dissolved lignin. There are two possible reasons. Either the degree of condensation of this lignin decreases or phenols without and with reduced side chains form during the hydrothermal treatment.

This investigation has shown that hydrothermal wood degradation lowers the lignin content of the wood and increases the concentration of phenolic compounds.

Acknowledgement

This work was supported by the Sächsisches Ministerium für Wissenschaft und Kunst under contract no. 4-7541.83-FZR/402.

References

- /1/ Bobleter, O., Concin, R.: Degradation of Poplar Lignin by Hydrothermal Treatment, *Cellulose Chem. Technol.* **13**, 583 (1979).
- /2/ Zier, N.: Strukturelle Merkmale eines Organosolv-Lignins bei Variation der Aufschlußparameter, Dissertation, TU Dresden, 1996
- /3/ Faix, O., Meier, D., Fortmann, I.: Thermal Degradation Products of Wood: Gas Chromatographic Separation and Mass Spectrometric Characterization of Monomeric Lignin Derived Products, *Holz als Roh- und Werkstoff* **48**, 281 (1990).
- /4/ Faix, O., Meier, D., Fortmann, I.: Thermal Degradation Products of Wood. A Collection of Electron-Impact (EI) Mass Spectra of Monomeric Lignin Derived Products. *Holz als Roh- und Werkstoff* **48**, 351 (1990)

SIZE EXCLUSION CHROMATOGRAPHY (SEC) OF LIGNIN AND HUMIC ACIDS

M. Schmidt, L. Baraniak, G. Bernhard, H. Nitsche
Forschungszentrum Rossendorf e.V., Institute of Radiochemistry

As one method for characterizing natural organic matter, including humic acids and lignin SEC was employed for determining the molecular weight distribution.

By this method molecules are separated according to their size. The stationary phase consists of silica-gel particles with a size of 5 μm and a pore diameter of 25 nm (Progel-TSK, column G 3000 SWXL). Small molecules penetrate into the pores while larger ones are excluded from the pore volume and eluted without detectable retention. Thus larger molecules elute first and smaller ones last. Phosphate buffer (2.5 mmol L⁻¹, pH 7.0) was used as an eluent to testing the column according to Frimmel /1/.

The column was calibrated using protein standards with molecular weights ranging from 669,000 to 255 u. As molecules are fractionated by their size (i.e. hydrodynamic radius) and not by weight, the results obtained differ according to the calibration. A spherical molecule, e.g. a protein, may have the same molecular weight as a linear molecule like e.g., polyethyleneglycol, but has a smaller hydrodynamic radius. This leads to different results for molecular weights depending on calibration. The value obtained by this method is often referred to as "apparent molecular weight, amw".

Lignin: Different lignin samples, organosolv and N-modified lignins /2,3/, were dissolved in a few drops 0.1 M NaOH, mixed with the phosphate buffer, filtered (0.45 μm) and then analyzed (Fig. 1). All samples contain up to 45 percent molecules with an amw larger than 450,000 u (upper exclusion volume of the column). Furthermore, they all show characteristic peaks corresponding to 58,000 ($\pm 4,000$), 30,000 ($\pm 2,000$) and 12,500 ($\pm 1,500$) u. Aqueous extracts of wood samples from an underground mine contain mostly smaller molecules (<165,000 u).

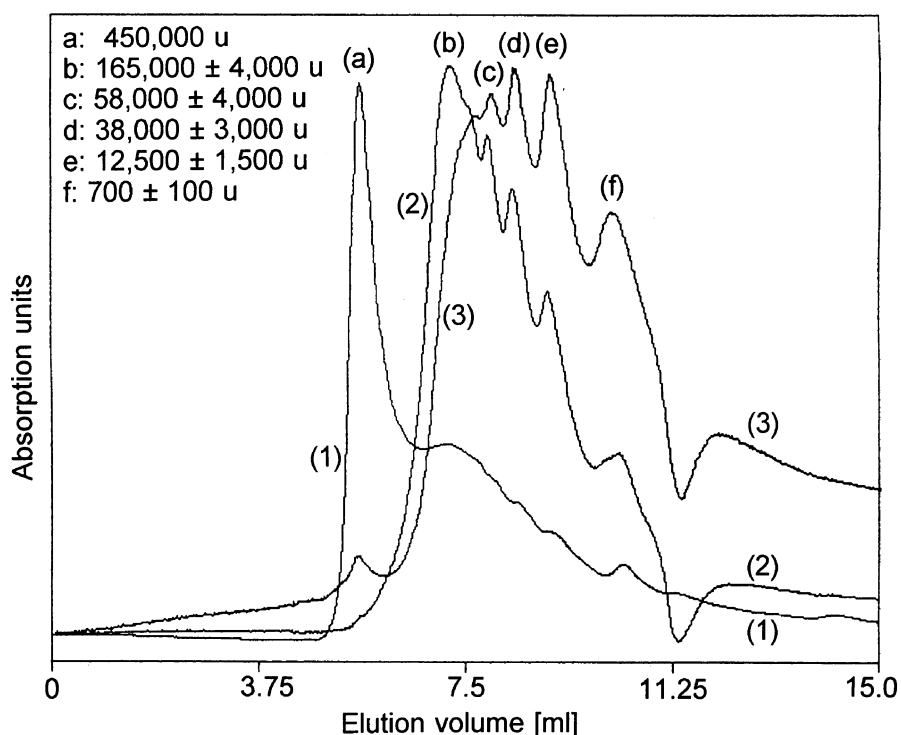


Fig. 1: Size exclusion chromatogram of different lignin samples. (1) organosolv-lignin, highest peak referring to > 450,000 u; (2), (3): aqueous extracts of wood samples from an underground mine. (2.5 mmol L⁻¹ phosphate buffer, pH 7.0, 25°C, 32 bar, $\delta = 254$ nm; column Progel-TSK G 3000 SWXL).

Humic Acid: Solutions of artificial and purified humic acid (Fluka) /4/ were ultracentrifuged using

Centricon filters with decreasing pore size (100, 30, 10, and 3 kD). The filtrate was analyzed by SEC. In contrast to the lignin samples, both humic acids exhibit a continuous distribution of molecular weights with only one maximum. It is shifted towards lower molecular weights with decreasing pore size. For unfiltered purified humic acid the maximum of the distribution corresponds to $225,000 \pm 8,000$ u whereas unfiltered artificial humic acid contains molecules with a weight of $410,000 \pm 10,000$ (70 %) u and $> 450,000$ u (30%). This means that artificial humic acid consists of molecules which are about twice the weight of purified humic acid.

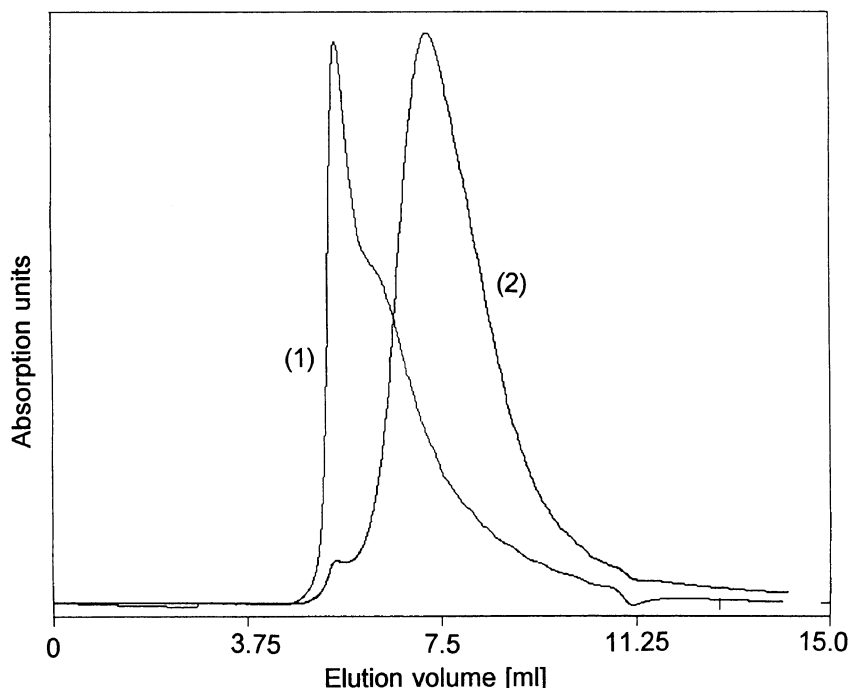


Fig. 2: Size exclusion chromatogram of artificial (1) and purified humic acid (2). (2.5 mmol L⁻¹ phosphate buffer, pH 7.0, 25°C, 32 bar, $\lambda = 254$ nm; column Progel-TSK G 3000 SWXL).

Acknowledgements

We thank R. Schiene and K. Jelen, Technische Universität Dresden, Institute of Plant and Wood Chemistry, Tharandt, for supplying the lignin samples.

This study was supported by the Sächsisches Ministerium für Wissenschaft und Kunst under contract no. 4-7541.83-FZR/402.

References

- /1/ Frimmel, F. H.: Der Einsatz physikalischer Trennmethode und ableitbare Aussagen. In: *Refraktäre organische Säuren in Gewässern* (F. H. Frimmel, G. Abbt-Braun; eds.) Chap. 3, Deutsche Forschungsgemeinschaft, Mitteilung XII der Senatskommission für Wasserforschung; Verlag Chemie, Weinheim 1993.
- /2/ Zier, N.: Strukturelle Merkmale eines Organosolv-Lignins bei Variation der Aufschlußparameter. Ph.D. Thesis, Technische Universität Dresden, 1996.
- /3/ Schiene, R., Maletzky, F., Fischer, K., Krusche, K., Zier, N., Götze, T.: Chemical Modification of Organosolv Lignins. Second European Workshop on Lignocelluloses and Pulp. Proceedings, 237. Grenoble 1992.
- /4/ Pompe, S., Bubner, M., Denecke, M. A., Reich, T., Brachmann, A., Geipel, G., Heise, K.H., Nitsche, H.: A comparison of Natural Humic Acids with Synthetic Humic Acid Model Substances: Characterization and Interaction with Uranium (VI). *Radiochim. Acta*, in press.

COMPLEXATION OF U(VI) WITH LIGNIN DEGRADATION PRODUCTS: DETERMINATION OF COMPLEX STABILITY BY ION-EXCHANGE AND TIME-RESOLVED LASER FLUORESCENCE SPECTROSCOPY

M. Schmidt, L. Baraniak, G. Geipel, G. Bernhard, H. Nitsche
Forschungszentrum Rossendorf e.V., Institute of Radiochemistry

Schubert's method [1] was used to determine the conditional stability constant of a spruce lignin (Organosolv-lignin, methanolic extract at pH 13, [2]) with U(VI) at pH 6. The lignin serves as a model substance for mine-water-dissolved organic matter of uranium mines of the Erzgebirge, Saxony.

The method is based on the distribution of a metal cation between an ion exchange resin and a ligand according to their stability constants (K).

$$K = \frac{[U(VI) \& Lignin]}{[U(VI)][Lignin]}$$

[U(VI) - Lignin] = concentration of complex [mol L⁻¹]; [U(VI)] = concentration of free metal [mol L⁻¹]; [Lignin] = content of free ligand [g L⁻¹]

The distribution ratio, D, of the metal ion between resin and solution in the presence of a ligand is given by

$$D = \frac{M_r}{M_f + M_c} \times \frac{V_s}{m_r}$$

M_r = moles metal bound to the resin, M_f = moles free metal, M_c = moles complexed metal,
V_s = Volume of the solution [mL], m_r = mass of the resin [g]

In absence of a ligand, the distribution ratio D₀ is constant for low concentrations of uranium. Assuming a mononuclear complex, a plot of log (D₀ / D - 1) vs. log (A_i) yields log K as the intercept and the number of ligands per complex molecule as the slope [3] (Fig. 1). If the initial concentration of ligand (A_i) is much larger than the concentration of the complex, the ligand concentration is constant and equal to (A_i). All experiments were carried out at 25 ± 1°C and an ionic strength of 0.01 M NaClO₄ using the cation exchange resin Dowex 50 WX 8 in the sodium form and ²³⁴U as a tracer.

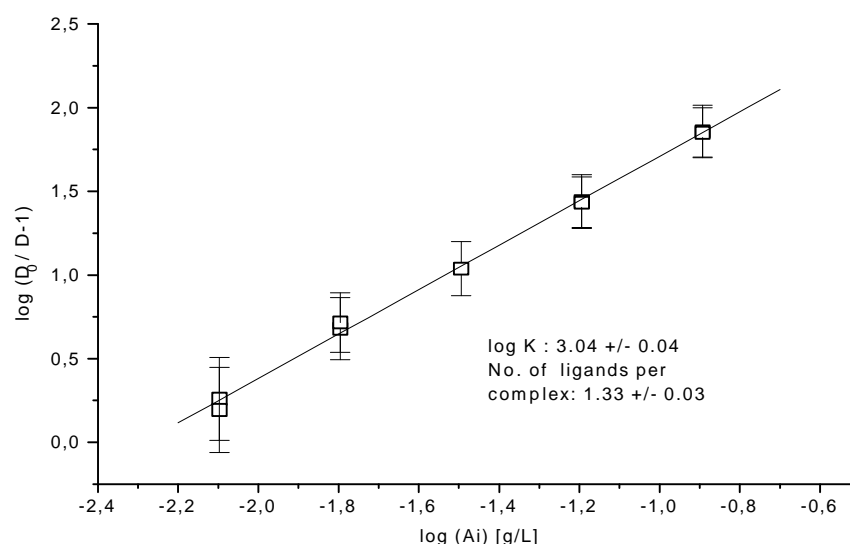


Fig. 1: Uranium complexation with lignin at pH 6 in 0.01 M NaClO₄, 25°C

From the plot, the complex stability constant is found to be 3.04 ± 0.04, and the number of ligands per uranium atom is 1.33 ± 0.03, which means that formation of 1:1 and higher com-

plexes occurs. Log K is based on the weight of the lignin ($K [L g^{-1}]$).

The complex stability was also determined by laser induced fluorescence. The excitation wavelength was set at 355 nm and the fluorescence wavelength was measured in the spectral range of 415 to 600 nm (Fig.2). The experiments were carried out with a lignin concentration of $0.1 g L^{-1}$ and U(VI)-concentrations varying from 5 to $40 \mu mol L^{-1}$.

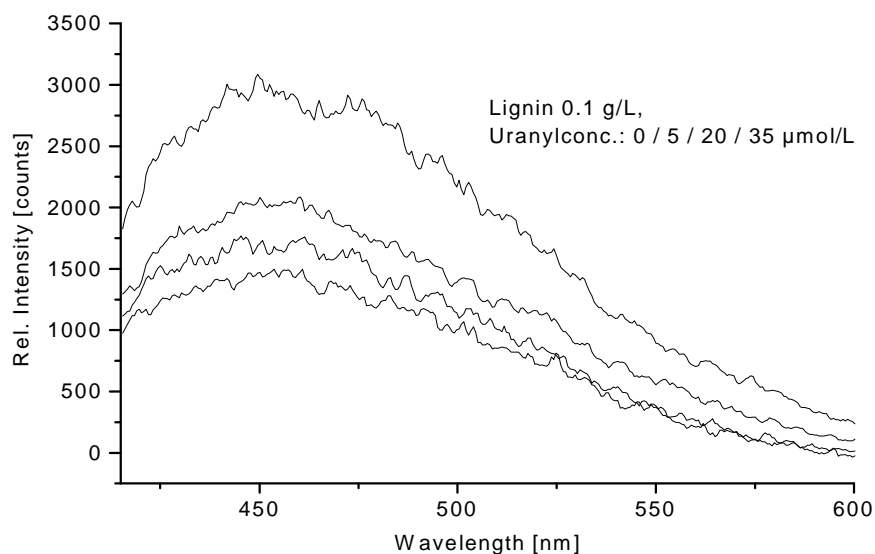


Fig. 2: Emission spectra of lignin measured by TRLFS at a delay time of 50 ns after excitation (355 nm) in 0.1 M $NaClO_4$, at pH 6.0 with $0.1 g L^{-1}$ lignin and (from top to bottom) increasing concentrations of U(VI) ($0, 5, 20, \text{ and } 35 \mu mol L^{-1}$).

At delay times from 50 to 100 ns after application of the laser pulse, the fluorescence signal of uncomplexed lignin was detected. It decreases with increasing uranium and therefore increasing complex concentration. The lifetime of lignin was found to be 14 ± 2 ns. From the decay of the fluorescence intensity the amount of uncomplexed ligand was determined. Using a value of 1.3 for the number of ligands per complex molecule that was determined by ion-exchange, the complex stability constant was found to be 3.2 ± 0.3 . This is in good agreement with the results found by the ion exchange method and earlier experiments with mine-water dissolved organic substances /4/.

Acknowledgements

This work was supported by the Sächsisches Ministerium für Wissenschaft und Kunst under contract no. 4-7541.83-FZR/402.

We thank R. Schiene and K. Jelen from the Technische Universität Dresden, Institute of Plant and Wood Chemistry, Tharandt, for supplying the lignin.

References

- /1/ Schubert, J.: The Use of Ion Exchangers for the Determination of Physical-Chemical Properties of Substances, particularly Radiotracers, in Solution. I. Theoretical. *J. Phys. Colloid Chem.* **52**, 340 (1948).
- /2/ Zier, N.: Strukturelle Merkmale eines Organosolv-Lignins bei Variation der Aufschlußparameter. Ph.D. Thesis, Technische Universität Dresden, 1996.
- /3/ Ardakani, M.S., Stevenson, F.J.: A Modified Ion-Exchange Technique for the Determination of Stability Constants of Metal-Soil Organic Matter Complexes. *Soil Sci. Soc. Amer. Proc.* **36**, 884 (1972).
- /4/ Baraniak, L., Geipel, G., Bernhard, G., Nitsche, H.: Laser-Induced Photo Acoustic Spectroscopy of the Interaction of U(VI) with Mine-Water Dissolved Organic Substances. In: *FZR, Institute of Radiochemistry, Annual Report* (H. Nitsche, ed.). 1994.

INVESTIGATION OF MICROBIAL DEGRADATION OF [¹⁴C]PCB NO.77 IN SOIL

M. Bubner, K. H. Heise, M. Matucha¹, V. Sasek²

Forschungszentrum Rossendorf e.V., Institute of Radiochemistry

¹Academy of Sciences of the Czech Republic, Prague, Institute of Experimental Botany

²Academy of Sciences of the Czech Republic, Prague, Institute of Microbiology

Macromolecular humic material is particularly able to adsorb Polychlorinated Biphenyls (PCB) and thus influences the fate of PCB in soil. PCB bound in humic material may change the chemical properties of humic acids, especially their complexing behavior against heavy metals. Our research focusses on the PCB degradation in soils and the binding of the degradation products to the soil and to humic acids.

Model experiments are carried out using [¹⁴C]PCB No. 77 /1/ on loess chernozem from Beuna/Merseburg and well defined cultures of the white rot fungi: *Phanerochaete chrysosporium*, *Coriolopsis polyzona*, *Trametes versicolor*, *Pleurotus ostreatus*, and *Hirneola nigricans*. The PCB degradation was investigated either with the pure [¹⁴C]PCB congener in water solution /2/ and with soil-bound [¹⁴C]PCB congener /3/. We can quantitatively access the transformation process by measuring the portion of radioactivity in the individual components of the system and in the isolated transformation products. The separation of unchanged PCB from the products of biotransformation in the experiments with the "pure PCB congener" was achieved by extraction with ethylacetate and water /2/. Radioactivity in the separated components was established by direct LSC-measurement in the extracts, or in case of the mycelium, after sample oxidation. The distribution of radioactivity in the soil was determined after separation of the soil components and subsequent sample oxidation. Separation of the soil fragments was carried out by two different extraction methods that are commonly applied for humic acid isolation /3/: the alkaline extraction, according to Tab. 1, and the extraction with a range of organic solvents, according to Tab. 2. The [¹⁴C]PCBs were analyzed with capillary GC-MS and capillary GC-ECD /4/, radio-HPLC and TLC in connection with autoradiographic detection.

Tab. 1: Extraction and fractionation of soil for humic acid isolation (1. method)

| Procedure / Solvent | Extract |
|---------------------------|------------------------------|
| 2 % HCl, H ₂ O | metals |
| hexane | monomers, PCBs |
| 2 M NaOH | humic acids |
| residue | inorganics, insoluble humins |

Humic acid isolation from alkaline extract and purification:

precipitation with 2M HCl
centrifugation and washing with water
solution in 2M NaOH
precipitation
centrifugation and washing with water
dialysis
lyophilization

The results from our degradation experiments with "pure [¹⁴C]PCB" (4 weeks), and with soil-bound [¹⁴C]PCB (3 weeks), are as follows:

1. In degradation experiments with "pure [¹⁴C]PCB", the main portion of radioactivity is accumulated in the mycelium (50 to 75%, maximum in *Coriolopsis polyzona*). The total mineralization with only *Phanerochaete chrysosporium* slightly exceeded 1% and the unchanged PCB was smaller than 20 %. The final distribution pattern of radiolabel differed in the individual fungal species and was also influenced by the concentration of PCB.
2. In degradation experiments with soil-bound [¹⁴C]PCB, more than 90 % of the radioactivity was extracted by organic solvents (hexane, ether, benzene, acetone and ethanol). The radioactive components of all these extracts were identified by TLC as unchanged parent substance.

The dimethylformamide extract with the humic acids contained 1 to 3 % and the insoluble residue 2 to 8 % of the radioactivity. The recovery of the radioactivity was 95 to 101 %. The bound residue could not be identified. The radioactivity in the dimethylformamide extract was identified by TLC after reextraction with heptane. The extractable radioactivity was shown to be larger than 90% the parent substance [¹⁴C]PCB. Less than 0,1% of the radioactivity remained in the dimethylformamide residue. This means, no more than 0,1 % of the parent compound was bound chemically into the humic acid matrix during this short-time degradation experiment.

Tab. 2: Soxhlet extraction and fractionation of soil (2. method)

| Solvent | Extract |
|-------------------|--------------------------------|
| ether | monomers, lipophilic compounds |
| benzene | monomers, fats, resins, waxes |
| acetone | monomers |
| ethanol | alkaloids, tannins |
| dioxane | humic acid precursors, lignin |
| dimethylformamide | humic acids |
| pyridine | humic acids |
| ----- | |
| residue | inorganics, insoluble humins |

The radioactivity of bound residue resulting from humic acid extraction with alkali was much higher (20 to 25 %) than the radioactivity in the residue of dimethylformamide extract. From this we can conclude that the soil matrix, in particular the humic substances, bind the lipophilic PCB very strongly and that subsequent degradation processes are hindered and may take very long time. Physically soil-bound PCBs can be liberated or displaced from the humic matrix by dimethylformamide. The "bound residue" of PCB seems to contain the parent substances and their transformation products. They will be released or destroyed often only during the degradation processes of the humic matrix.

"Long term" degradation processes with soil- and humic acid-bound [¹⁴C]PCB of much higher specific radioactivity are part of an ongoing study.

Acknowledgment

These studies were supported by the Bundesminister für Forschung und Technologie of the Federal Republic Germany and the Federal Government for Strategic Planning of the Czech Republic under Scientific & Technological Cooperation between Germany and Czech Republic.

References

- /1/ M. Bubner, M. Meyer, K. Fuksova, M. Matucha, K. H. Heise, H. Nitsche; Synthesis of ¹³C- and ¹⁴C-Labelled PCB Congeners, 8th International Bioindicators Symposium, 22 - 28 May 1995, Ceske Budejovice, Czech. Rep., submitted to Journal of Ecological Chemistry
- /2/ B. R. M. Vyas, V. Sasek, M. Matucha, M. Bubner; Degradation of 3,3',4,4'-Tetrachlorobiphenyl by Selected White Rot Fungi; Chemosphere **28**, 1127 - 34 (1994)
- /3/ M. Bubner, M. Matucha, V. Sasek, K. H. Heise, H. Nitsche, J. Veleminsky, J. Spizek; Investigation of Microbial Degradation of PCB Congeners Using Isotopically Modified Tracers; 8th International Bioindicators Symposium, 22 - 28 May 1995, Ceske Budejovice, Czech Rep., submitted to Journal of Ecological Chemistry
- /4/ A. Pacakova - Kubatova; Analysis of Toxic PCB in Delor 106 and 103 by Capillary GC - MS and GC - ECD; Diploma - Thesis, Charles University, Prague (1994)
- /5/ M. Bubner, M. Meyer, R. Jander, K. H. Heise, M. Matucha, A. Pacakova-Kubatova; Optimization of the Conditions of the [¹⁴C]Chlorination for [¹⁴C]Polychlorinated Biphenyls (PCB) Synthesis and Gas Chromatographic Analysis; Report FZR, Institute of Radiochemistry, Annual Report 1994, 68 - 70 (1995)

TiO₂-PHOTOCATALYZED OXIDATION OF ORGANIC COMPOUNDS

E. Förster, K.H. Heise, K. Wolf, H. Nitsche
 Forschungszentrum Rossendorf e.V., Institute of Radiochemistry

Introduction

We have a large stock pile of highly radioactive carbon-14 labeled organic compounds with different chemical properties. It is necessary to convert this hazardous material that is partly decomposed by autoradiolysis, into a stable chemical form. Generally, barium carbonate C-14 is a widely accepted stable chemical form for safe disposal of carbon-14. This requires, however, complete oxidation of carbon-14 labeled organic compounds to carbon dioxide. The absorption with sodium hydroxide and the subsequent precipitation with an aqueous solution of barium chloride is a well-known method.

We have investigated the oxidation of different non-labeled organic model compounds by photocatalytic oxidation and by oxidation with modified sulfuric-chromic acid. Here we report the photocatalytic oxidation and in the following article the sulfuric-chromic acid oxidation.

Near-UV illuminated TiO₂-suspensions provide a powerful wet oxidation method of general applicability. This process has already been described in many papers (e.g./1/). The illumination of TiO₂ (anatase) in water with light of wavelength < 400 nm generates excess electrons in the conduction band (e_{CB}⁻) and positive "holes" (h_{VB}⁺) in the valence band of TiO₂ crystal (eq.1).



At the surface of semiconductor particles the "holes" react with the adsorbed H₂O or OH⁻ to form OH[•] radicals (eq. (2)). Excess electrons in the conduction band react with oxygen to form an oxygen ion radical (eq. 3). This reaction inhibits the recombination of "holes" and excess electrons and thus the reverse reaction of eq. (1). Molecular oxygen must be present in all oxidative degradation processes.

Experimental

All chemicals were analytical grade. The titanium dioxide photo catalyst was Degussa P 25 grade (70% anatase). Oxygen with a purity of 99.995% was used. Fig. 1 shows a schematic of the UV conversion set up.

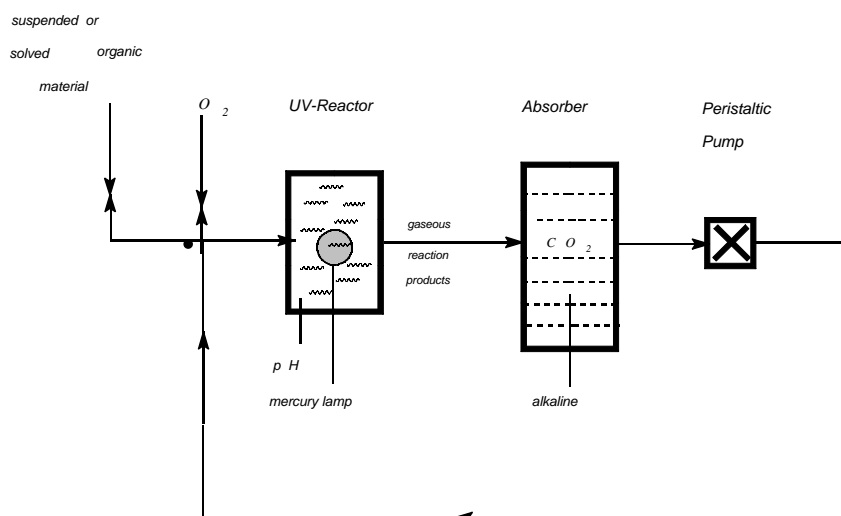


Fig. 1: Schematic of apparatus for photocatalyzed oxidation

The volatile or gaseous reaction products are continuously circulated in an oxygen stream (about 17 mL/min.) through the photoreactor by means of simple build-in peristaltic pump (ISMATEC Mini S 6). This allows very high conversion rates. A 125 watt medium-pressure mercury lamp was immersed into the reaction vessel (borosilicate glass). The organic compound and 0.5 mL of 30% hydrogen peroxide or 0.20 g Oxone® (potassium peroxy mono-sulfate) were added to a ultrasonicated suspension of 0.4 grams of titanium dioxide in 200 mL water. The addition of hydrogen peroxide or Oxone® may enhance the rate of photo degradation. Then, the pH was adjusted to 3.0 and it was transferred in the photoreactor. During the irradiation, usually 24 hours, the aqueous phase was stirred continuously and oxygen was circulated in the loop through the photo reactor and the gas washing bottles. The carbon dioxide evolved in this process was transported by a gas stream and absorbed in a 0.5 N NaOH solution.

Oxygen and incompletely oxidated gaseous products, e.g. carbon monoxide, remain in the reactor to recirculate for further oxidation. The CO₂ evolution and the measurements of Total Organic Carbon (TOC) provide the mass balance of the overall degradation process. Carbon dioxide was absorbed on sodium hydroxide and determined by titration, according to a modified method of WINKLER /2/. The TOC in the residue was measured for a few samples by the combustion method using a TOCOR 2 TOC-Analyzer. The results of some selected substances are given in Tab. 1.

| Substance Name | Contents [mg] | Additivs | Recovery % CO ₂ | TOC [mg C/L] | pH | |
|---|------------------|--------------------------------------|-------------------------------|-----------------|----------|-----|
| | | | | | starting | end |
| Benzoic acid | 194 | 0.5 mL H ₂ O ₂ | 89,2 | | 3,0 | 3,1 |
| 4-Hydroxybenzoic acid | 238 | without | 95,3 | | 3,1 | 5,2 |
| 4-Hydroxybenzoic acid | 238 | 0.5 mL H ₂ O ₂ | 96,6 | | 3,5 | 7,5 |
| 4-Hydroxybenzoic acid | 238 | 0.2 g Oxone | 101,3 | | 2,9 | 2,5 |
| o-Toluic acid | 204 | 0.5 mL H ₂ O ₂ | 96,6 | | 2,9 | 2,2 |
| Biphthalate, potass. salt | 306 | 0.5 mL H ₂ O ₂ | 78,7 | | 3,2 | 8,1 |
| Biphthalate, potass. salt | 306 | 0.2 g Oxone | 92,1 | | 3,0 | 4,9 |
| Acetic acid, sodium salt (3 H ₂ O) | 817 | 0.5 mL H ₂ O ₂ | 94,5 | | 3,8 | 8,7 |
| Nonanoic acid | 211 | 0.5 mL H ₂ O ₂ | 95,3 | | 3,1 | 2,9 |
| Succinic acid | 354 | 0.5 mL H ₂ O ₂ | 98,3 | | 3,0 | 6,8 |
| Succinic acid | 354 | 0.2 g Oxone | 100,2 | | 2,9 | 2,6 |
| Chloroacetic acid | 566 | 0.5 mL H ₂ O ₂ | 85,6 | | 3,0 | 2,0 |
| Glycine | 450 | 0.5 mL H ₂ O ₂ | 92,7 | | 3,1 | 3,5 |
| Thiourea | 913 | 0.5 mL H ₂ O ₂ | 4,5 | | 3,0 | 1,6 |
| Acetone | 232 | 0.5 mL H ₂ O ₂ | 83,8 | | 3,6 | 4,4 |
| Formamide | 450 | 0.5 mL H ₂ O ₂ | 70,4 | 65 | 3,0 | 7,9 |
| Acetophenone | 180 | 0.5 mL H ₂ O ₂ | 95,4 | | 3,2 | 3,5 |
| 1,2,4-Trichlorobenzene | 363 | 0.5 mL H ₂ O ₂ | 80,6 | 29 | 3,8 | 4,4 |
| 2-Nitrophenol | 338 | 0.2 g Oxone | 89,1 | | 3,0 | 2,6 |
| Aniline hydrochloride | 259 | 0.5 mL H ₂ O ₂ | 90,3 | | 3,3 | 2,3 |

Tab. 1: Conditions and results of photocatalytical degradation for some organics

The kinetics of the degradation process of aromatic systems can be demonstrated by UV-absorption spectra (UV-Vis spectrophotometer: Model 8452 A, Hewlett Packard). Fig. 2 shows the UV-absorption spectra of 4-hydroxybenzoic acid, a typical compound of the stockpile, as a function of irradiation time. Curve A shows the undegraded compound. After about ten minutes of irradiation the aromatic compound convert to yellow-brown chinons (curves B to E). The conversion to chinons is completed after about 80 minutes. After 400 minutes of irradiation the spectrum (curve H) shows only a small signal between 200 and 230 nm which may indicate the formation of aliphatic compounds.

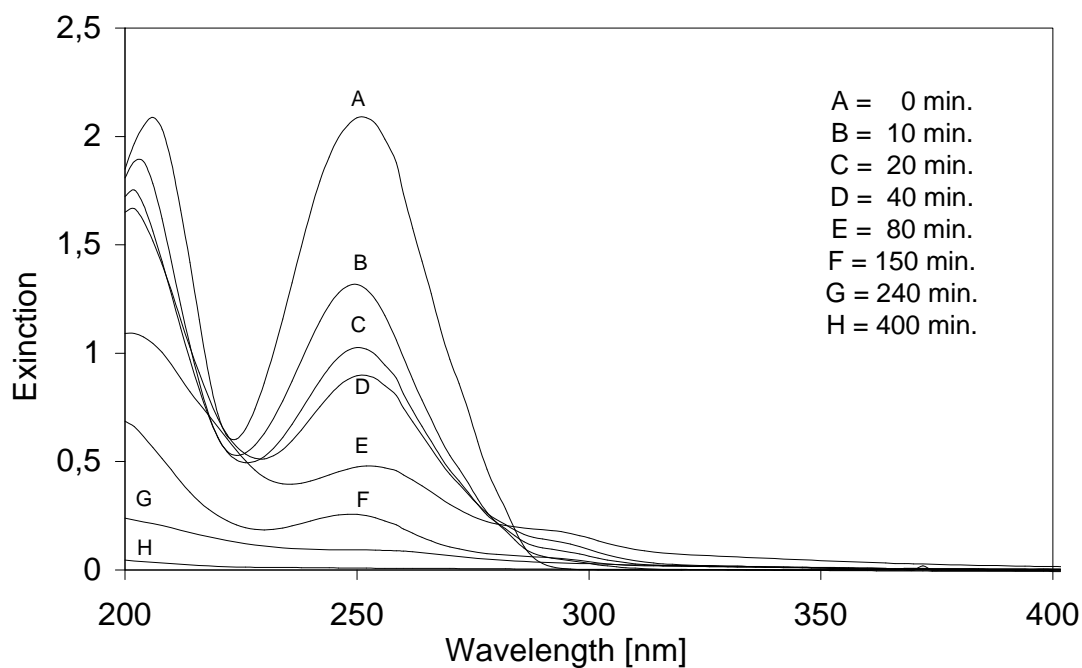


Fig. 2: Kinetics of photocatalytic degradation of 4-hydroxybenzoic acid (dilution 1:50)

We have developed a unique method for the safe conversion of highly concentrated carbon-14 labeled organic compounds into stable carbon dioxide C-14.

Acknowledgements

This study was supported by Sächsisches Ministerium für Wissenschaft und Kunst under contract No. 4-7581.312/20.

References

- /1/ M.R. Hoffmann, S.T. Martin, W. Choi, D.W. Bahnemann, Chem. Rev. **95**, 69 - 96 (1995)
- /2/ G. Jander, K.F. Jahr, *Maßanalyse*, 15th ed., de Gruyter, Berlin, New York 1989, p. 144

MINERALIZATION OF ORGANIC COMPOUNDS WITH SILVER CONTAINING SULFURIC-CHROMIC ACID

E. Förster, K.H. Heise, K. Wolf, H. Nitsche
Forschungszentrum Rossendorf e.V., Institute of Radiochemistry

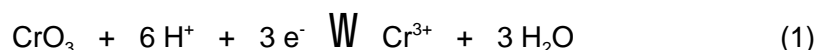
Introduction

Organic compounds, with few exceptions, are readily oxidized in hot anhydrous mixtures of fuming sulfuric, phosphoric, chromic, and iodic acids. Such combinations are commonly known as the VAN SLYKE-FOLCH /1/ or the ALLISON /2/ oxidizing mixture. Using these reagents, however, has the following disadvantages:

1. Quaternary ammonium salts, acetic acid, compounds that yield acetic acid on wet combustion, and polymers are oxidized with great difficulty.
2. The oxidizing reagents, cannot be reclaimed. They are hazardous wastes and have to be disposed off.

For example, chromic acid reacts with acetic acid to form acetyl chromate. Acetyl chromate was found to be relatively stable against oxidation /3/. Silver catalyses the oxidation of such compounds. A 65% sulfuric-chromic acid which contains silver sulfate was used for analytical determination of COD (Chemical Oxygen Demand) by titration or photometric measurement according to DIN 38409/41.

We have employed a modified method of this process for wet combustion of our organic model compounds. The reaction involved is as follows:



The amount of CrO_3 is calculated for the oxidation of 4 millimole carbon, using its lowest oxidation number - 4 (e.g. methane) to CO_2 (oxidation number + 4). To assure that the reaction is completed, an excess of 50% CrO_3 was used. The concentration of the oxidant in the mixture is limited by its solubility.

Experimental

A 250-ml three-necked flask was equipped with a magnetic glass stirrer, a dropping funnel with pressure equalizing tube, a thermometer and a reflux condenser. An amount of organic compound equaling an equivalent of 4 millimoles of carbon was treated for 4 hours at 140 - 150°C with a solution of 52 mL of water, 0.50 g of silver sulfate, 48 mL of concentrated sulfuric acid (95%), and 1.6 g of chromium trioxide or a regenerated spent solution (see below).

Evolved CO_2 and other volatile products in the carrier stream are passed successively through the reflux condenser, a safety bottle, and two gas traps. Carbon dioxide was absorbed by 0.2 M sodium hydroxide and was then determined by titration according to WINKLER /4/. The nitrogen gas stream (about 17 mL/min.) was circulated with a peristaltic pump (ISMATEC Mini-S 6). The apparatus was cleaned with pure nitrogen (99.998%) prior to its use. Tab. 1 shows the results of this oxidation process.

Electrolytic regeneration of spent oxidation solution

To minimize the acid waste, we have investigated anodic oxidation of the Cr(III) in the spent oxidation solution which contain 63 to 80% of sulfuric acid. The anodic regeneration of Cr(III) is well known and used at the technical scale for solutions with a concentration of up to 30% sulfuric acid /5/.

The studies were carried out in a H-cell with platinum electrodes separated by a glass frit with a G4 porosity. The catholyte compartment was charged with 65% H_2SO_4 and the anolyte compartment was usually charged with about 100 mL of spent oxidation solution, consisting of 16 millimoles chromium(III/VI), 65% sulfuric acid (after repeated regeneration cycles 80%), and 0.5 g silver sulfate. Experiments were performed with an anodic current density of 166 mA/cm²

(area 6 cm²) at a temperature of 55 to 60°C, which is caused by ohmic heating in the cell. The progress of oxidation was controlled by measuring the solution's extinction with a spectral colorimeter (Spekol 11) at 590 nm (pathlength 2 mm). Pure solutions of chromic acid do not absorb at this wavelength. Complete oxidation of the spent oxidation solution required approximately 8 hours and was indicated by a decrease of the extinction below 0.080.

| Substance | Carbon | Recovery | Regen. | Substance | Carbon | Recovery | Regen. |
|-------------------|--------|-------------------|----------|-----------------------|--------|-------------------|----------|
| | mM | % CO ₂ | Solution | | mM | % CO ₂ | Solution |
| Cyclohexane | 4 | 20,6 | n | Formamide | 4 | 86,4 | y |
| Dodecane | 4 | 15,7 | y | Thiourea | 4 | 99,4 | n |
| Vaseline | ~4 | 94,5 | y | Phthalic acid | 3,57 | 97,7 | y |
| Paraffin wax | ~4 | 89,5 | y | 4-Hydroxybenzoic acid | 4 | 98,2 | n |
| Benzene | 4 | 38,0 | y | 2-Toluic acid | 4 | 100,0 | y |
| Xylenes (isomers) | 4 | 89,5 | y | Ethylacetate | 4 | 93,7 | y |
| Ethylbenzene | 4 | 75,0 | y | Tripalmitin | 4 | 95,0 | y |
| Acetic acid | 2,4 | 98,9 | y | Tributyl phosphate | 4 | >100 | n |
| Lauric acid | 4 | 93,1 | y | Ethyl alcohol | 4 | 92,3 | y |
| Palmitic acid | 4 | 95,7 | n | 1-Propanol | 4 | >100 | n |
| Stearic acid | 4 | 96,5 | y | 2-Propanol | 4 | 86,5 | y |
| Succinic acid | 4 | 95,0 | n | 2-Methyl-1-propanol | 4 | 58,8 | y |
| Glycine | 4 | 101,0 | n | n-Dodecanol | 2 | 55,8 | y |
| Bromacetic acid | 4 | 100,1 | n | 2-Nitrophenol | 4 | 93,0 | y |
| 2-Cyanacetamide | 4 | 94,3 | y | Triethylamine | 4 | 95,3 | y |
| Dicyandiamide | 4 | 90,5 | y | Glycerol | 4 | 86,5 | n |

Tab. 1: Results of the oxidation process for different organic substances (n = new solution, y = regenerated spent oxidation solution)

A loss of oxidation power was not observed, even after repeated regenerations. The density of the anolyte increases during the regeneration. To compensate for this increase, the initial density of the oxidation solution was decreased to 1.55 to 1.61 g/cm³ by dilution.

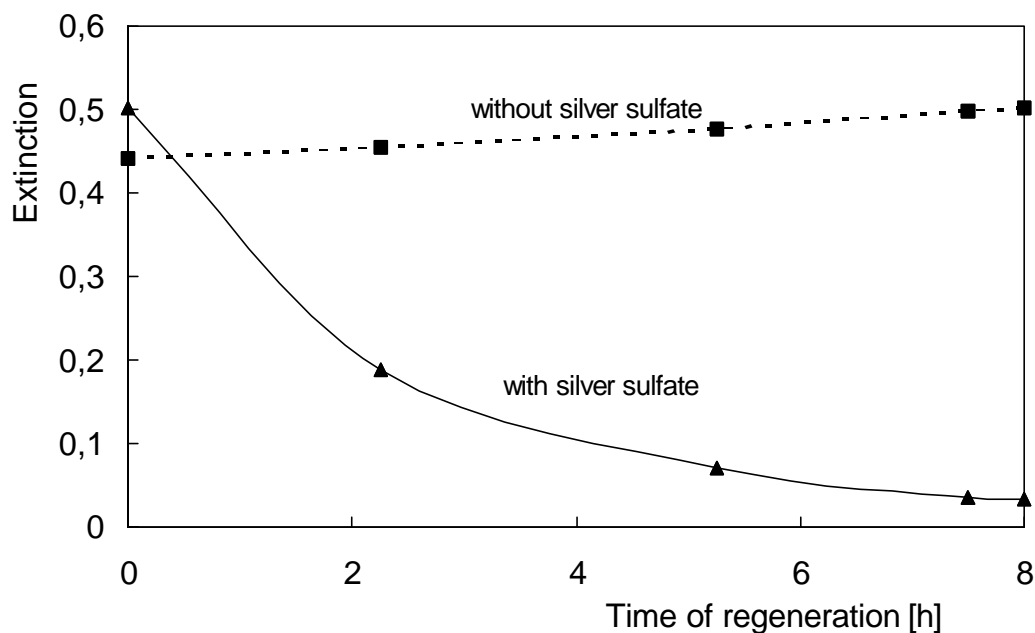


Fig. 1: Time dependence of the anodic regeneration process of a spent oxidation solution containing Cr(III)

Fig. 1 shows the time dependence of the regeneration process with and without silver. Catalytic amounts of silver or other heavy metal salts are necessary for the anodic oxidation of Cr(III) /6/. This method was successfully applied to a variety of different organic classes of substances that are shown in Tab. 1.

Acknowledgements

This study was supported by Sächsisches Ministerium für Wissenschaft und Kunst under contract No. 4-7581.312/20.

References

- /1/ T.S. Aguilar, N.J. Benevenga, A.E. Harper, *Bol. Soc. Quim. Peru* **49**, 27 (1983)
- /2/ L.E. Allison, *Soil Sci. Soc. Am. Proc.* **24**, 36 (1960)
- /3/ F.V. Raaen, G.A. Ropp, H.P. Raaen, *Carbon-14*, Series in Advanced Chemistry, Mc-Graw-Hill, New York 1968, p. 245 - 247
- /4/ G. Jander, K.F. Jahr, *Maßanalyse*, 15th ed., de Gruyter; Berlin, New York 1989, p. 144
- /5/ *Gmelins Handbuch d. anorganischen Chemie*, Chrom Teil A, Lieferung 2, Verlag Chemie, Weinheim 1963, p. 679 - 680
- /6/ H. Herbst, K. Petz, J. Stenzel, *Dechema-Monographien* Vol. 125, Verlag Chemie, Weinheim 1992, p. 243 - 257

Application of X-Ray Absorption Spectroscopy

A PREPARATION METHOD OF SOLID SAMPLES FOR EXAFS MEASUREMENTS

R. Nicolai¹, K.H. Heise, T. Reich

Forschungszentrum Rossendorf e.V., Institute of Radiochemistry,

¹Institute of Bioinorganic and Radiopharmaceutical Chemistry

For correct EXAFS measurements, it is important that the sample has a high degree of homogeneity. For solid samples this can often be a technical problem. It is quite common to put solid and powdered substances between thin sheets of polyethylene. However, the layer thickness of the sample may vary considerably over the cross section of the photon beam. Especially when the amount of available substance is very small as in the case of radioactive samples. Therefore, for EXAFS measurements of solid radioactive compounds, we have developed a preparation method where the sample is embedded in a solid matrix material and pressed into a pellet. This technique yields homogeneous samples and can be applied to the preparation of radioactive samples in a glove box.

The matrix material used for EXAFS measurements has to possess the following properties: a) chemically inert with respect to the sample, b) mechanically suited to form stable pellets by applying pressure, c) low absorption of the photon beam. We have found that Teflon^(R) satisfies these conditions. In addition, the hydrophobic character of Teflon is favorable for handling and storage of samples.

Usually, Teflon is available only as a granulate with a particle size of ca. one millimeter. To obtain homogeneous pellets it is necessary to reduce the Teflon particle size by grinding. However, at room temperature, Teflon is soft and not brittle enough for grinding. We found that good results can be obtained by cooling the Teflon granulate in liquid nitrogen prior to grinding. Grinding of Teflon together with the sample, e.g., crushed minerals, rocks, etc., yields a homogeneous mixture of powdered material with a typical particle size of <1 μ m which can be pressed into pellets. It is remarkable that the Teflon matrix has a high capacity to embed solid samples. The homogeneity of the pellets was checked by Scanning Electron Microscopy (SEM) and Energy Dispersive X-ray Analysis (EDX).

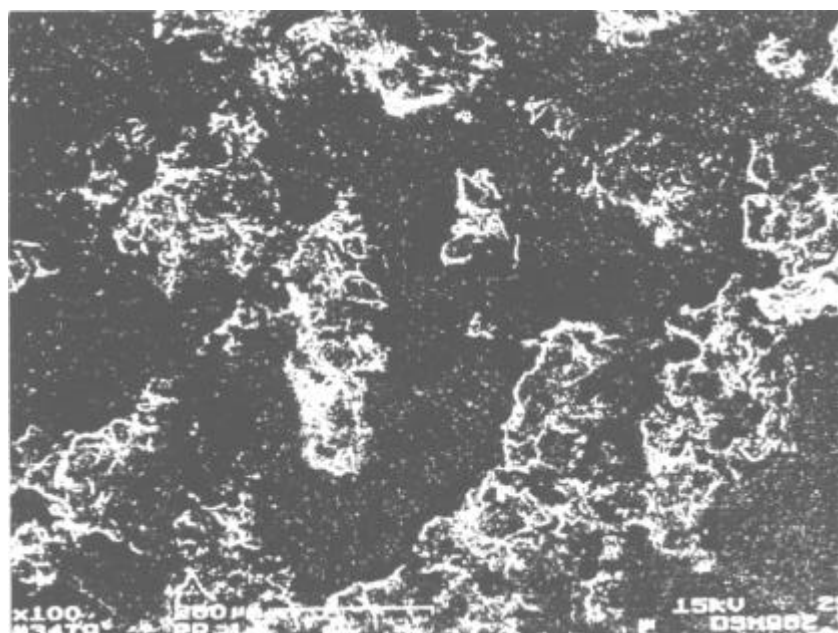


Fig. 1: SEM-micrographs of two uranyl silicate - teflon pellets, teflon is grinded by room temperature

As an example, Fig. 1 shows an image of a pellet which was formed after grinding Teflon granulate and uranyl silicate dihydrate at room temperature. When the same mixture was

ground at low temperature, the resulting pellet had a much better homogeneity, as shown Fig. 2. In the both examples, the mass ratio of Teflon to uranyl silicate was 12.5 to 1.

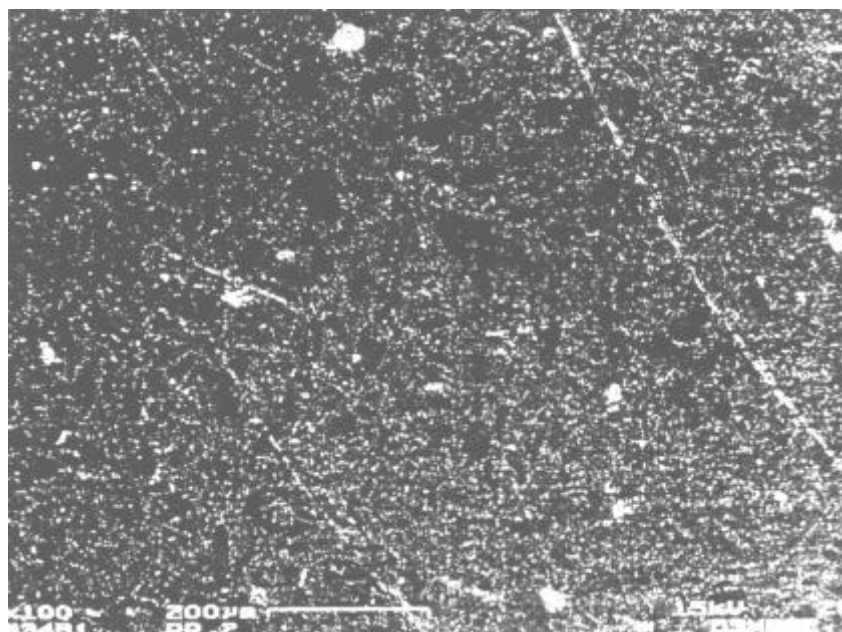


Fig. 2: SEM-micrographs of two uranyl silicate - teflon pellets, teflon is grinded by deep-freeze

The EXAFS measurements of different solid substances have demonstrated the high quality of the prepared pellets /1/ which have a 13 mm diameter and a thickness of approximately 2 to 3 mm. The ratio of Teflon matrix to sample can be varied over a wide range, e.g., 5 - 500 mg substance can be pressed with 200 - 400 mg Teflon powder. For future EXAFS measurements of highly radioactive samples, the geometry and dimensions of the pellets will be optimized further to reduce the amount of sample used and do match the cross section of the incoming photon beam.

To prepare the pellet, a stainless steel capsule (PERKIN-ELMER) was filled with Teflon granulate and the sample and tightly closed. Before the capsule was inserted into a conventional vibrating mill (PERKIN-ELMER), the capsule was cooled for 1 to 2 min. in a liquid nitrogen bath. Then the mixture was ground for 90 sec. After the capsule was allowed to warm up to room temperature, the powdered mixture was filled in the die and was placed in the hydraulic press (PERKIN-ELMER) which was operated for three minutes at a pressure of 10.5 tones/cm².

Acknowledgment

We thank R. Müller and E. Christalle from the Zentralabteilung "Analytik" in the Forschungszentrum Rossendorf for SEM micrographs and EDX analysis and also for helpful interpretations of results.

References

- /1/ S. Pompe, M.A. Denecke, H. Moll, M. Bubner, H. Funke, T. Reich, K.H. Heise, G. Bernhard, H. Nitsche; Investigation Of The Interaction Of Humic Acids With Uranyl Ions By Extended X-ray Absorption Fine Structure Spectroscopy, this paper

INVESTIGATION OF THE INTERACTION OF HUMIC ACIDS WITH URANYL IONS BY EXTENDED X-RAY ABSORPTION FINE STRUCTURE SPECTROSCOPY

S. Pompe, M. A. Denecke, H. Moll, M. Bubner, H. Funke, T. Reich, K.H. Heise, G. Bernhard, H. Nitsche
Forschungszentrum Rossendorf e.V., Institute of Radiochemistry

In continuation of our investigations on humic substances and their role in the migration and retardation of heavy metals in the environment /1-2/, we are studying the interaction of uranyl ions with natural humic acid (HA) from Fluka and with well-characterized synthetic HA /2/. In this study we present U L_{III} -edge EXAFS results on uranyl humates prepared under different conditions. Spectra were recorded at room temperature in transmission mode at the Hamburg Synchrotron Laboratory at the beamline RÖMOII.

Sample SYN1 was synthesized by shaking a suspension of synthetic HA and uranyl solution at pH<1. The other samples were prepared from solutions of HA's and uranyl at pH 4-5. The samples were measured in solid form, dispersed in Teflon, or as wet paste (SYN2, Fluka2). Our goal was to compare the uranyl humates of natural and synthetic HA's (Fluka1, SYN3), uranyl humates with relatively high and low loadings (SYN1-SYN3) as well as dry and wet samples (Fluka1, Fluka2).

Fig. 1 depicts U L_{III} -edge EXAFS spectra and their corresponding Fourier transforms (FT's) of samples Fluka1 and SYN3 having relatively low uranyl loadings of 11% and 17% PEC¹, respectively. The first two U-O shells were Fourier filtered and fitted to the EXAFS equation. The fit results are listed in Tab. 1. The U-O_{ax} distances in the uranyl unit are the same to within the experimental error ($\pm 0.02D$) for both samples. Furthermore, both the number of equatorial next-nearest neighbors and their bond distances are similar. The near order surrounding of uranium in our synthetic product is comparable to that found in the natural uranyl humate.

The U-O distances in uranyl humates with relatively high and low loadings (SYN1-SYN3) are the same in all samples and show no apparent function of loading. To investigate the influence of water on the coordination of uranium in uranyl humates, we compared the dry sample Fluka1 to the wet paste Fluka2. Both samples have comparable uranyl loadings. The fit results from these samples show no remarkable influence of water; the U-O_{ax} and U-O_{eq} distances are the same.

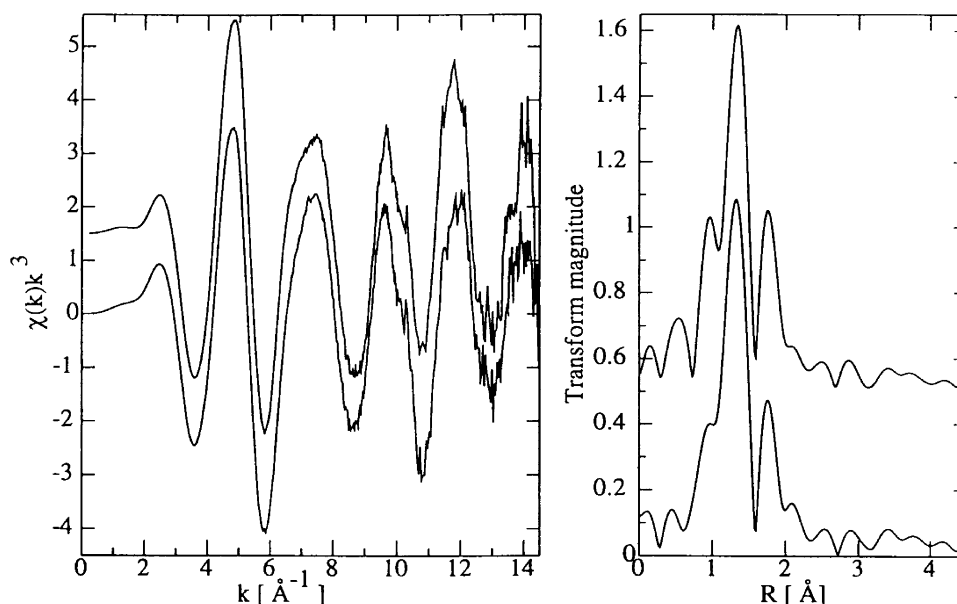


Fig. 1: k^3 -weighted U L_{III} -edge EXAFS spectra (at left) and their corresponding Fourier transforms (at right, k -range 2.8-14.3 \AA^{-1} , rectangular window) for uranyl humates prepared from natural HA Fluka (Fluka1, top) and from synthetic HA (SYN3, bottom).

¹ PEC = Proton exchange capacity of carboxylic groups

Tab. 1: EXAFS structural parameters for the first two uranium coordination shells in uranyl humates.) E_0 was held constant at -13 eV.

| Sample | State | Loading [%PEC] | U-O _{ax} | | | U-O _{eq} | | |
|--------|-------|----------------|-------------------|-------|----------------------------------|-------------------|-------|----------------------------------|
| | | | N* | R [D] | F ² [D ²] | N | R [D] | F ² [D ²] |
| SYN1 | dry | 119 | 2 | 1.78 | 0.002 | 5.2 | 2.38 | 0.014 |
| SYN2 | paste | 96 | 2 | 1.78 | 0.002 | 5.0 | 2.38 | 0.012 |
| SYN3 | dry | 17 | 2 | 1.78 | 0.002 | 5.0 | 2.38 | 0.012 |
| Fluka1 | dry | 11 | 2 | 1.78 | 0.002 | 4.8 | 2.37 | 0.010 |
| Fluka2 | paste | 10 | 2 | 1.77 | 0.002 | 4.3 | 2.37 | 0.008 |

* Held constant during the fit.

The EXAFS spectra and fit results of all samples investigated are similar. These spectra apparently reflect a structure averaged over a large number of HA functional groups binding uranium. Systematic EXAFS experiments on a series of uranyl humates prepared from HA's, which are chemically modified to block certain functional groups, are planned. From these studies, we hope to obtain information concerning the complexation on specific HA binding sites.

References

- /1/ Reich, T., Pompe, S., Moll, H., Brendler, V., Heise, K.H., Baraniak, L., Bernhard, G., Nitsche, H.: A study of the complexation of Uranyl Ions with Humic Acids, HASYLAB Annual Report 1994, p. 609.
- /2/ Denecke, M. A., Pompe, S., Moll, H., Heise, K.H., Reich, T., Bernhard, G., Nitsche, H., EXAFS Studies on Anhydrous Complexes of Uranyl and ortho-Substituted Benzoic Acids, Forschungszentrum Rossendorf Annual Report 1995.
- /3/ Pompe, S., Bubner, M., Denecke, M. A., Reich, T., Brachmann, A., Geipel, G., Nicolai, R., Heise, K.H., Nitsche, H.: A Comparison of Natural Humic Acids with Synthetic Humic Acid Model Substances: Characterization and Interaction with Uranium(VI), accepted by Radiochimica Acta, 1995.

EXAFS STUDIES ON ANHYDROUS COMPLEXES OF URANYL AND ORTHO-SUBSTITUTED BENZOIC ACIDS

M.A. Denecke, S. Pompe, H. Moll, K.H. Heise, T. Reich, G. Bernhard, H. Nitsche
Forschungszentrum Rossendorf e.V., Institute of Radiochemistry

As part of our studies on humic acid complexes /1/, we have synthesized various uranyl - carboxylic acid complexes. These compounds should serve as models for understanding the complexation of the uranyl unit onto important functional groups of humic acids. Here we present results of U L_{III} -edge EXAFS measurements of anhydrous complexes of uranyl and ortho-substituted benzoic acids: uranyl salicylate, uranyl phthalate, and uranyl methoxybenzoate. The anhydrous compounds were chosen so that U-O distances from crystal water can be excluded in the analysis of the EXAFS spectra.

The EXAFS oscillations for the compounds studied and their respective Fourier transforms (FT's) are shown in Fig. 1. The spectra are all dominated by oscillations from the uranyl unit (U-O_{ax}), seen as the first peak in the FT's at approximately 1.3 Å. The next FT peak in the uranyl salicylate spectrum or two peaks in the spectra of the other two compounds represent oxygen atoms in the plane equatorial to the uranyl unit (U-O_{eq}), stemming from the coordinating organic acids.

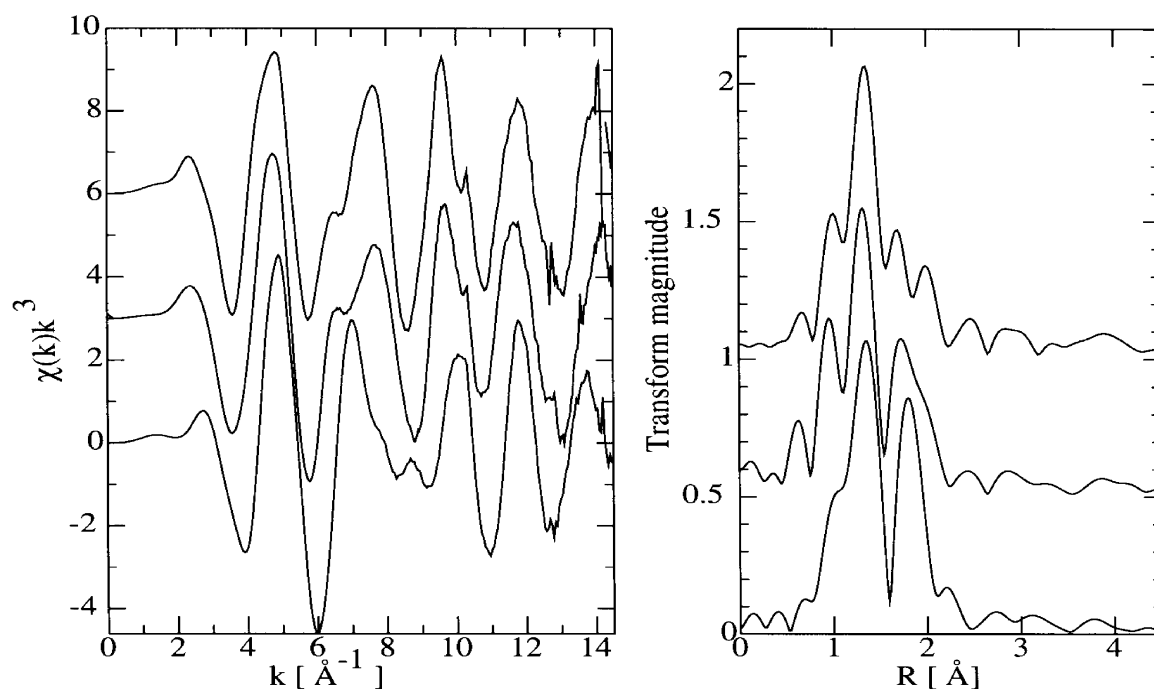


Fig. 1: k^3 -weighted U L_{III} -edge EXAFS spectra and their corresponding Fourier transforms (k-range 2.8-14.3 \AA^{-1} , rectangular window) for anhydrous uranyl complexes.

From top to bottom: uranyl methoxybenzoate, uranyl phthalate and uranyl salicylate.

Inspection of the k^3 -weighted spectra shows that uranyl salicylate is quite different than the other two compounds. The form of the EXAFS oscillations for uranyl phthalate and uranyl methoxybenzoate, compounds having only $-\text{COO}^-$ groups for coordinating the uranyl group, are similar to one another. The presence of the phenolic $-\text{OH}$ group seems to be the decisive factor in the structure of the complex formed; substitution of the phenolic $-\text{OH}$ group with either a $-\text{COOH}$ group or a $-\text{OMe}$ group leads to similar changes in the uranium coordination.

The U-O_{ax} and U-O_{eq} FT peaks were Fourier filtered and fitted to the EXAFS equation using theoretical phase shifts and scattering amplitudes calculated with FEFF6 /2/. The number of oxygen atoms in the first shell was held constant at two, E_0 was -13 to -14 eV. The fit parameters obtained are listed in Tab. 1.

Tab. 1: Fit parameters to Fourier filtered U L_{III} -edge data for the compounds indicated.

| Compound (uranyl:acid ¹) | U-O _{ax} | | U-O _{eq} | | |
|--------------------------------------|-------------------|----------------------------------|-------------------|-------|----------------------------------|
| | R [Å] | F ² [Å ²] | N | R [Å] | F ² [Å ²] |
| uranyl salicylate (1:2) | 1.78 | 0.003 | 3.6 | 2.32 | 0.003 |
| uranyl phthalate (1:2-3) | 1.77 | 0.002 | 5.0 | 2.39 | 0.008 |
| uranyl methoxybenzoate (1:2) | 1.78 | 0.002 | 4.3 | 2.44 | 0.010 |

¹Determined from the samples' carbon content.

The U-O_{ax} bond lengths are the same to within the experimental error for all three compounds. The U-O_{eq} distances increase in the series uranyl salicylate < uranyl phthalate < uranyl methoxybenzoate. The four short equatorial bonds in uranyl salicylate are interpreted as resulting from the coordination of both the -OH and -COOH groups onto the uranyl unit, under formation of a 6-membered chelate ring (see Fig. 2, left). Similar short U-O_{eq} bond lengths for another uranyl salicylate chelate are reported in /3/.

Replacing the phenolic -OH group by -COOH or -OMe groups leads to a change in the type of complex formed. Both uranyl phthalate and uranyl methoxybenzoate exhibit IR-bands characteristic for bidentate coordination of the carboxylate oxygen atoms to the uranyl unit. Bidentate coordinated carboxylate groups have relatively long bond lengths /4/. The increased bond length in these compounds compared to the salicylate reflects this. Furthermore, the phthalate compound also exhibits a strong C=O Band at 1706 cm⁻¹ indicating the presence of "end-on" coordinated -COO-groups in uranyl phthalate. Combining the information from IR, the uranyl:acid ratios and the EXAFS fits, the coordination of uranium depicted in Fig. 2 are postulated for uranyl phthalate and uranyl methoxybenzoate.

Of the three compounds studied, the U-O bond lengths obtained for uranyl phthalate are the most similar to the axial distance of 1.78 Å and U-O_{eq} distance of 2.38 Å observed in uranyl humates /5/. This similarity may lie in the fact that both uranyl humates and the uranyl phthalate exhibit a uranium coordination of different bonding types.

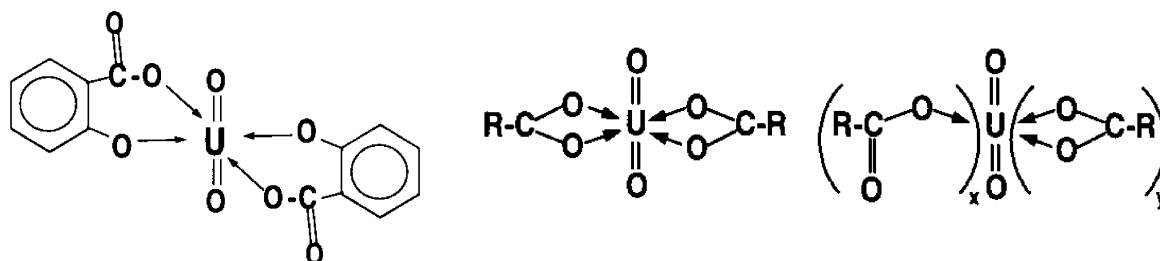


Fig. 2: Proposed structure for anhydrous uranyl salicylate (left) and the uranium coordination in uranyl methoxybenzoate (middle) and uranyl phthalate (right; $x + 2y = 5$; $y \dots 0$)

References

- /1/ Reich, T., Pompe, S., Moll, H., Brendler, V., Heise, K.-H., Baraniak, L., Bernhard, G., Nitsche, H.: *HASYLAB Annual Report 1994*, p. 609.
- /2/ Mustre de Leon, J., Rehr, J. J., Zabinsky, S. I., Albers, R. C.: *Phys. Rev. B* **44**, 4146 (1991).
- /3/ Nassimbeni, L. R., Rodgers, A. L., Haigh, J. M.: *Inorgan. Chim. Acta* **20**, 149-153 (1976).
- /4/ Carrell, C. J., Carrell, H. L., Erlebacher, J., Glusker, J. P. : *J. Am. Chem. Soc.* **110**, 8651-6 (1988).
- /5/ Pompe, S., Denecke, M. A., Moll, H., Bubner, M., Funke, H., Reich, T., Heise, K.H., Nitsche, H.: *HASYLAB Annual Report 1995*.

EXAFS DETERMINATIONS OF URANIUM STRUCTURES: THE URANYL ION COMPLEXED WITH TARTARIC, CITRIC, AND MALIC ACIDS

P. G. Allen¹, D. K. Shuh¹, J. J. Bucher¹, N. M. Edelstein¹, T. Reich, M. A. Denecke, H. Nitsche
Forschungszentrum Rossendorf e.V., Institute of Radiochemistry
¹Lawrence Berkeley National Laboratory, Chemical Sciences Division, USA

The uranium L_{III}-edge extended X-ray absorption fine structure (EXAFS) was measured for 1:1 mixtures of the uranyl ion with tartaric, malic, and citric acids /1/. The room temperature EXAFS of these mixtures at pH = 3 show the characteristic short uranium-oxygen interactions of the uranyl ion, UO₂²⁺, at 1.80 Å along with five oxygen near neighbors around the uranyl equatorial plane at 2.40 Å. In addition, the EXAFS of each solution reveal a U-U interaction at 3.92 Å (see Fig. 1), indicating the presence of a uranyl dimer structure. Based on models proposed from earlier potentiometric titration experiments, it is concluded that the dimer is the ligand bridged species, (UO₂)₂(L)₂, in which bridging occurs through the "-hydroxyl groups of the polycarboxylate ligands (see Fig. 2).

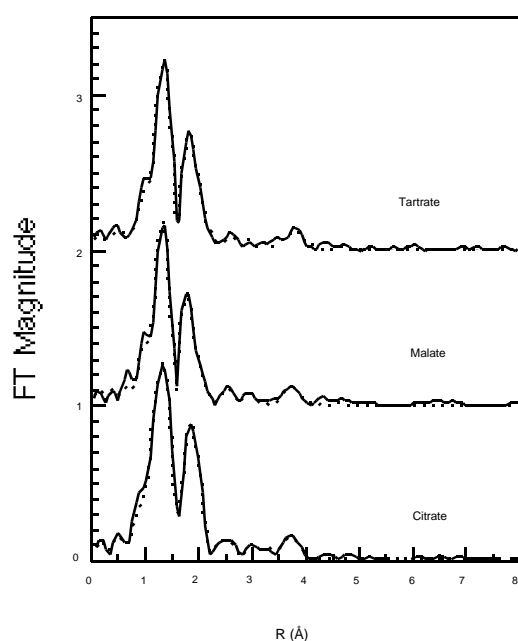


Fig. 1: Fourier transforms of U L_{III} EXAFS for 1:1 mixtures of uranyl with tartrate, malate, and citrate ligands at low pH. The solid line is the experimental data, and the dashed line corresponds to the best theoretical fit of the data. The U-U peak at 3.75 Å (uncorrected for phase shift) is evidence for the dimeric structure.

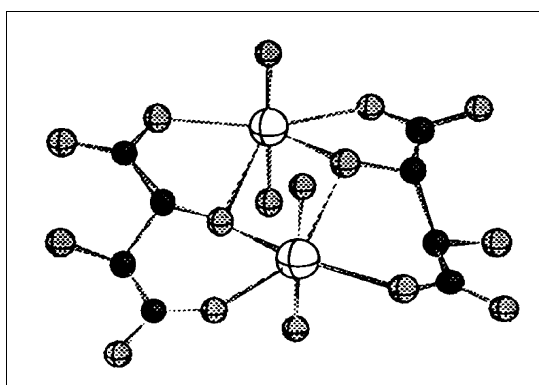


Fig. 2: The structural model for the uranyl tartrate dimer, (UO₂)₂(L)₂ where L=tartrate. The uranyl groups are bridged by "-hydroxyl groups.

References

/1/ Allen, P.G., Shuh, D.K., Bucher, J.J., Edelstein, N.M., Reich, T., Denecke, M.A., Nitsche, H.: EXAFS Determinations of Uranium Structures: The Uranyl Ion Complexed with Tartaric, Citric, and Malic Acids. *Inorg. Chem.*; accepted for publication.

DETERMINATION OF THE ARSENIC OXIDATION STATE IN ENVIRONMENTALLY RELEVANT WATERS BY XANES SPECTROSCOPY

M.A. Denecke, H. Moll, S. Pompe, D. Rettig, H. Friedrich, G. Bernhard, T. Reich, H. Nitsche
Forschungszentrum Rossendorf e.V., Institute of Radiochemistry

The problem of arsenic in water from decommissioned uranium mines and uranium ore processing plants is one regional to Saxony. Arsenic is found in association with uranium in the Erzgebirge. The amount of arsenic in uranium mine waters and leach water from mine tailing piles is on the order of 1-10 mg As/L. The arsenic content is greater in collecting basins of uranium ore processing plants, approximately 100 mg As/L. Knowledge of the oxidation state of arsenic in such waters, combined with the arsenic concentration and the water's ionic strength, allows one to estimate the mine water's redox potential. Using the redox potential can help to predict the speciation of other heavy metals present in the water and thereby assess the risk for their migration. We have, therefore, determined the oxidation state of arsenic in samples of mine water originating from a decommissioned mine based on their As K-edge energies of absorption. Using X-ray absorption near-edge structure (XANES) spectroscopy has the advantage that one may determine arsenic oxidation states in samples containing other components which could interfere in "classical" electrochemical measurements. The As K-edge absorption maxima for elemental arsenic, As_2O_3 , and As_2O_5 reported in an early X-ray absorption study /1/ are separated from one another by more than 4 eV. This shift is large enough to identify these oxidation states in a given sample by XANES.

We measured As K-edge XANES spectra for samples containing arsenic in the +3 and +5 oxidation states. Transmission, room temperature spectra of an analytical grade As_2O_3 sample (Aldrich Chemical Company, Inc.), a freshly prepared sample of $\text{H}_3\text{AsO}_4 \times \frac{1}{2}\text{H}_2\text{O}$ /2/ and solutions of AsO_3^{3-} (18 g As/L; 0.24 M) and AsO_4^{3-} (220 g As/L; 2.9 M) were recorded at HASYLAB on the RÖMOII beamline using a Si-311 double-crystal monochromator. The solid samples were measured dispersed in Teflon and pressed as tablets. The spectra are depicted in Fig. 1. The energy scale of all spectra was calibrated relative to the inflection point (defined as 11870 eV) in a As_2O_3 reference spectrum either measured simultaneously or, in the case of the AsO_4^{3-} solution, measured prior to and following recording the sample spectrum.

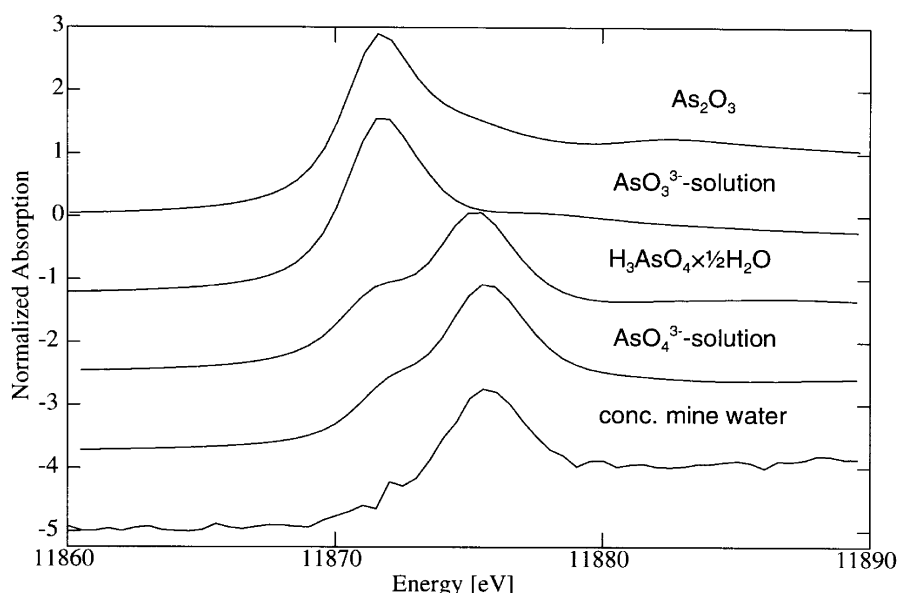


Fig. 1: As K-edge XANES spectra of samples having arsenic in oxidation states +3 and +5 and the spectrum of a concentrated uranium mine water sample containing $4 \cdot 10^{-3}$ mol As/L. The spectra are shifted along the y-axis for clarity.

The position of the main absorption peak, E_{max} , was determined both as the energy of the absorption maximum in each spectrum and as the corresponding zero value of the first deriva-

tive spectra. The energies obtained from both methods were to within 0.2 eV of one another. The averaged results from both methods are listed in Tab. 1. As one would expect, E_{max} increases with increasing arsenic valence; between arsenic(III) and arsenic(V) samples, a shift of ~4 eV was observed.

Tab. 1: Energies of As K-edge absorption maxima for arsenic(III), arsenic(V), and uranium mine water samples.

| Sample | E_{max}^1 [eV] | Arsenic Valence |
|---|------------------|-----------------|
| As_2O_3 | 11871.7 | 3+ |
| AsO_3^{3-} - solution; pH=13 | 11871.8 | 3+ |
| $H_3AsO_4 \cdot \frac{1}{2}H_2O$ | 11875.3 | 5+ |
| AsO_4^{3-} - solution; pH=10 | 11875.6 | 5+ |
| Uranium mine water; 4×10^{-3} mol As/L (transmission) | 11875.6 | 5+ |
| Uranium mine water; 4×10^{-4} mol As/L (fluorescence) | 11875.6 | 5+ |

¹ ± 0.5 eV

A water sample from a decommissioned uranium mine in Königstein, Saxony, was collected and its arsenic concentration determined to be 0.03 g As/L (4×10^{-4} M). Due to the relatively low arsenic concentration, a fluorescence XANES spectrum of this sample was measured using the fluorescent X-ray ion chamber described by Lytle, et al. /3/. A sample of the same mine water was concentrated to approximately 1/10 its original volume and its transmission spectrum recorded (see Fig. 1). We wanted to ascertain if concentrating the sample had any effect on the XANES spectrum. E_{max} in both the transmission and the fluorescence spectra was determined to be ~11875 eV (Tab. 1) so that concentrating the sample has no effect on the position of the absorption maximum. Furthermore, this energy is the same as that found for the two arsenic(V) samples. We therefore conclude that the arsenic in the mine water is in the +5 oxidation state. The success of the valence determination in the mine water sample render further studies on other environmentally relevant samples feasible. Studies of arsenic containing water samples from collecting basins of uranium ore processing plants are planned. In addition, the determination of the arsenic valence in biological material as part of an investigation of the environmental arsenic cycle will also be pursued.

However, prior to these investigations, further study of the As K-edge XANES features in single valent compounds is needed. The structure on the rising edge at ~11871 eV in the arsenic(V) spectra has the same energy as E_{max} in the arsenic(III) spectra. This strongly suggests that our arsenic(V) samples contain traces of As_2O_3 reagent used in their preparation. In the future, the EXAFS of the reference compounds will also be measured and compared to X-ray diffraction data to ensure the integrity of the samples. Furthermore, the effect that the bonding partner to arsenic, e.g. dissolved, complex-forming organics present in mine and ore processing plant waters, has on the XANES will also be studied.

References

- /1/ Agarwal, B. K., Verma, L. P.: Chemical effects in x-ray K absorption spectra of arsenic. *J. Phys. C* **1**, 208-9 (1967).
- /2/ Jander, G. and Blasius, E.: *Lehrbuch der analytischen und präparativen anorganischen Chemie*, S. Hirzel Verlag, Leipzig, 1966.
- /3/ Lytle, F. W., Gregor, R. B., Sandstrom, D. R., Marques, E. C., Wong, J., Spiro, C. L., Huffman, G. P., Huggins, F. E.: *Nucl. Instr. Meth.* **226**, 542-8 (1984).

EXAFS STUDY OF URANIUM (VI) SORBED ONTO SILICA

T. Reich, H. Moll, M.A. Denecke, G. Geipel, G. Bernhard, H. Nitsche, P.G. Allen¹, J.J. Bucher¹, N. Kaltsoyannis¹, N.M. Edelstein¹, D.K. Shuh¹

Forschungszentrum Rossendorf e.V., Institute of Radiochemistry

¹Lawrence Berkeley National Laboratory, Chemical Sciences Division, Berkeley, USA

Extended X-ray absorption fine structure (EXAFS) analysis was applied to the study of uranyl species at precipitated silicic acid and silica gel [1]. For the sorption experiments, fresh silicic acid was precipitated from a sodium metasilicate solution by adding concentrated HCl. Samples 1 and 2 were prepared from precipitated silicic acid by shaking 1 g of sorbent with 20 mL of 0.01 M and 0.05 M $\text{UO}_2(\text{ClO}_4)_2$ solutions for 50 hours, respectively. At the beginning, the pH of the mixture was adjusted to a value of 4. In the same way, sample 3 was prepared by sorption of uranyl ions from a 0.05 M uranyl perchlorate solution onto silica gel (Merck). Analytical results characterizing samples 1 - 3 are given in Tab. 1.

Tab. 1: Surface area, pH at the end of the sorption, and amount of U(VI) sorbed onto silicic acid and silica gel.

| Sample | Sorbent | Spec. Surface Area [m ² /g] | UO_2^{2+} [mol/L] | pH | U loading mg U/g |
|----------|--------------|--|----------------------------|------|------------------|
| <u>1</u> | silicic acid | 80 | 0.01 | 3.93 | 4.86 |
| <u>2</u> | silicic acid | 80 | 0.05 | 4.00 | 5.86 |
| <u>3</u> | silica gel | 471 | 0.05 | 3.65 | 42.9 |

The experimental EXAFS spectra of samples 1 - 3 are shown in Fig. 1. No differences were observed between the two sorbents, silicic acid and silica gel, which were amorphous to X-ray powder diffraction. A change in the speciation of the uranyl perchlorate solution at pH 4 by increasing the molarity from 0.01 to 0.05 did not appear to change the surface uranyl species of samples 1 and 2. The observed structure of the surface species is interpreted as an inner-sphere, mononuclear, bidentate complex. This is based on the observed splitting of equatorial oxygen shell, their coordination numbers, and a lack of U-U scattering contributions to the EXAFS (see Tab. 2 and Fig. 1).

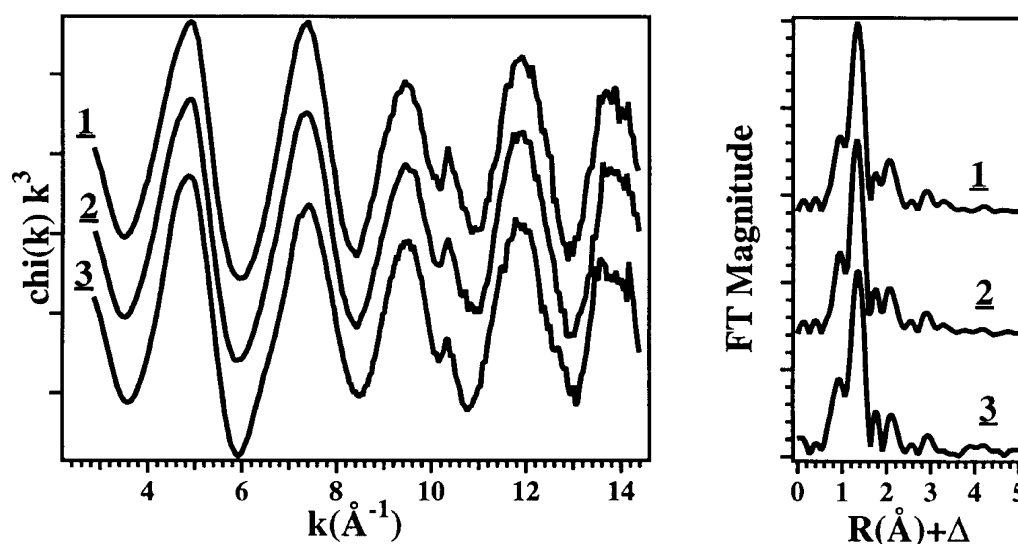


Fig. 1: Left panel: Experimental U L_{III} edge EXAFS spectra of uranyl sorbed from a 0.01 M uranyl solution onto silicic acid (1), uranyl sorbed from a 0.05 M uranyl solution onto silicic acid (2), and uranyl sorbed from a 0.05 M uranyl solution onto silica gel (3). Right panel: Fourier-transformed EXAFS of samples 1 - 3.

Tab. 2: Structural parameters of uranyl sorbed on silicic acid and silica gel obtained by EXAFS analysis of the Fourier-filtered spectra in the 0.5 - 2.7 Å range.

| Sample | U-O(ax) | | | U-O(eq 1) | | | U-O(eq 2) | | |
|----------|---------|------|----------------------------------|-----------|------|----------------------------------|-----------|------|----------------------------------|
| | N | R(Å) | F ² (Å ²) | N | R(Å) | F ² (Å ²) | N | R(Å) | F ² (Å ²) |
| <u>1</u> | 2 | 1.78 | 0.002 | 2.6(4) | 2.27 | 0.007 | 1.8(3) | 2.50 | 0.003 |
| <u>2</u> | 2 | 1.78 | 0.002 | 2.1(4) | 2.27 | 0.006 | 2.2(5) | 2.48 | 0.006 |
| <u>3</u> | 2 | 1.78 | 0.002 | 4(1) | 2.29 | 0.014 | 1.6(7) | 2.50 | 0.004 |

Sorption studies to clarify which of the equatorial oxygen shell is involved in the bonding with the silicate's silanol groups are planned. Another future task will study the structure of surface species as a function of a wider pH range and lower uranyl concentrations. These future investigations may clarify the fundamental differences between the present EXAFS study of uranyl sorbed onto silica gel and the results of Ref. /2/.

References

- /1/ Reich, T., Moll, H., Denecke, M. A., Geipel, G., Bernhard, G., Nitsche, H., Allen, P. G., Bucher, J. J., Kaltsoyannis, N., Edelstein, N. M., Shuh, D. K.: Characterization of Hydrated Uranyl Silicate by EXAFS, *Radiochim. Acta*, accepted for publication.
- /2/ Dent, A. J., Ramsay, J. D. F., Swanton, S. W.: An EXAFS study of uranyl ion in solution and sorbed onto silica and montmorillonite clay colloids. *J. Colloid Interface Sci.* **150**, 45 (1992).

STRUCTURAL INVESTIGATIONS OF TECHNETIUM AND RHENIUM COMPLEXES BY EXAFS.

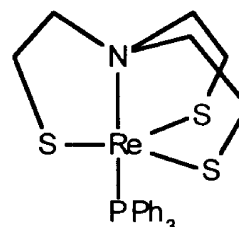
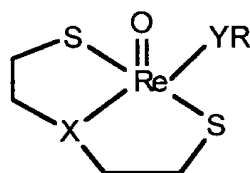
1. STUDIES ON "n+1" MIXED-LIGAND RHENIUM COMPLEXES

T. Reich, G. Bernhard, H. Nitsche, H. Spies¹, B. Johannsen¹
Forschungszentrum Rossendorf e.V., Institute of Radiochemistry
¹Institute of Bioinorganic and Radiopharmaceutical Chemistry

Introduction

X-ray Absorption Spectroscopy (XAS) is a well established technique for the determination of element-specific information on oxidation states of an absorbing atom and on structural parameters of its nearest-neighbor environment /1/. XAS has become a valuable tool for studies of metal-based drugs and environmentally-relevant systems /2/. This technique also extends the capability of studying radioactive technetium in small solid and liquid samples. This is crucial for the understanding of ^{99m}Tc radiopharmaceuticals as well as of the behavior of the nuclear fission's by-product ⁹⁹Tc in the geosphere as a function of its oxidation state /3,4/. As a result of the extremely small amount of technetium present in ^{99m}Tc radiopharmaceuticals (10⁻⁶-10⁻⁸ M), XAS studies employ the long-lived isotope ⁹⁹Tc (K edge at 21.044 keV) or rhenium (L_{III} edge at 10.535 keV) as surrogates.

As part of their joint research on radiotracers in biosystems, the Institute of Radiochemistry and the Institute of Bioinorganic and Radiopharmaceutical Chemistry at the Research Center Rossendorf studied novel rhenium complexes by Extended X-ray Absorption Fine Structure (EXAFS) spectroscopy. The aim of this study was the evaluation of the EXAFS method for the determination of structural parameters of the nearest-neighbor environment of Re(V) and Re(III) in "n+1" mixed-ligand complexes. To this end we report on a comparison of coordination numbers and inter-atomic distances obtained by EXAFS analysis with those known from recent single-crystal X-ray diffraction (XRD) studies for the following complexes (1, /5/; 2, /6/; 3, /7/; 4, /8/):



- | | | |
|----------|---|----------|
| <u>1</u> | X = S, YR = SEt | <u>4</u> |
| <u>2</u> | X = O, YR = S-C ₆ H ₄ -OMe(p) | |
| <u>3</u> | X = O, YR = Se-C ₆ H ₅ | |

Fig. 1: Rhenium compounds used for EXAFS measurements.

Experimental

Samples were prepared for measurements by mixing the rhenium complex with BN powder and pressing it into pellets. Rhenium L_{III} edge XAS spectra of samples 1-3 were measured at room temperature in transmission mode at the Stanford Synchrotron Radiation Laboratory (SSRL) on beamline 2-3 using a Si(220) double-crystal monochromator. Sample 4 was measured at the Hamburger Synchrotronstrahlungslabor (HASYLAB) on beamline RÖMO II equipped with a Si(311) double-crystal monochromator. For the EXAFS analysis we used the software package EXAFSPAK /9/. For energy calibration purposes, the first inflection point of the absorption edge was defined as 10535 eV. Theoretical scattering amplitudes and phases were calculated with the program FEFF6 /10/. The program Atoms version 2.42g, which is part of FEFF6, was used to calculate inter-atomic distances in the complexes 1-4 from the atomic coordinates measured by XRD.

Results and Discussion

The EXAFS spectra and their corresponding Fourier transforms (FT's) of 1-4 are shown in Fig. 2. The fit results of the EXAFS spectra are given in Tab. 1. During the fit, the coordination numbers N of all shells were kept constant. As a result of the limited data range of the EXAFS spectra, differences in the distance from the central rhenium atom to sulfur or carbon atoms of less than 0.15 Å cannot be resolved. These atoms were fitted as single coordination shells, e.g., Re-S and Re-C. To compare the EXAFS results with those from XRD, we averaged the Re-S and Re-C inter-atomic distances measured by XRD over the corresponding coordination shells (see Tab. 1).

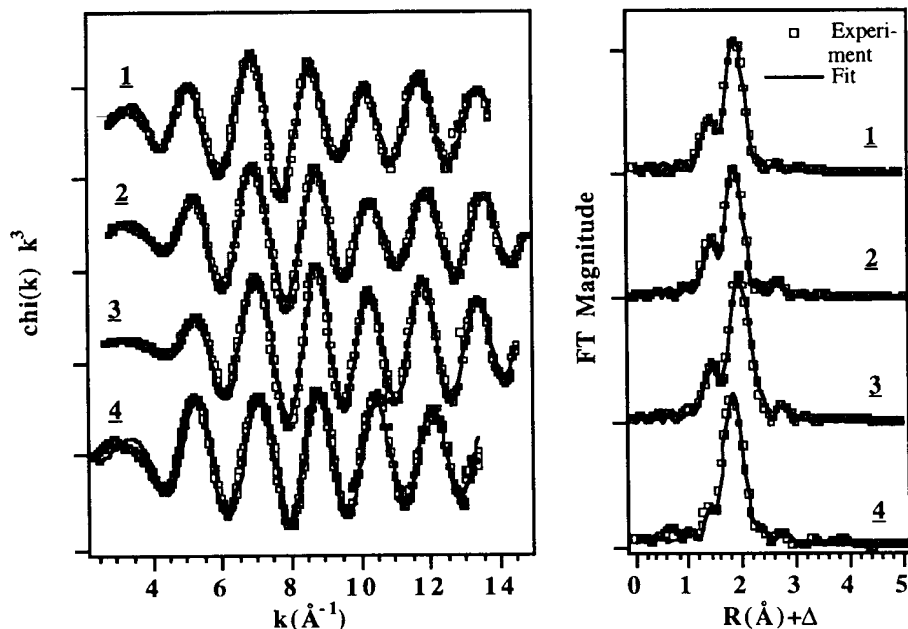


Fig. 2: Left panel: Experimental Re L_{III} edge EXAFS of complexes 1-4. Right panel: Fourier-transformed EXAFS of samples 1-4.

The coordination sphere of complexes 1-3 consists of a monodentate ligand YR and 3-thiapentane-1,5-dithiol or 3-oxapentane-1,5-dithiol ($HS-CH_2CH_2-X-CH_2CH_2-SH$, $X = O, S$) as chelate ligands with three donor atoms /6,7,11/. These "3+1"-oxorhenium(V) complexes possess a distorted tetragonal pyramidal coordination around the rhenium atom as shown for compound 3 in Fig. 3.

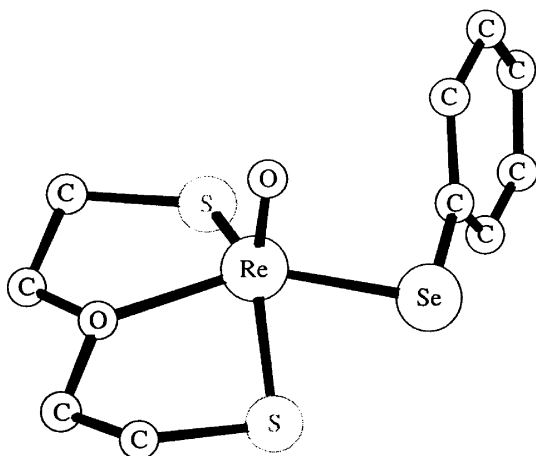


Fig. 3: A drawing illustrating the solid-state conformation of (3-oxapentane-1,5-dithiolato)(benzeneselenolato)-oxorhenium(V) (3).

The EXAFS spectrum of complex 1 is dominated by the scattering of electrons origination from the absorbing rhenium atom off the four neighboring sulfur atoms. These give rise to the main peak in the FT centered around 2.0 Å (see Fig. 2). The shoulder at lower R is a result of the shorter Re=O bond. Note that a small feature above the noise level can be observed in the FT centered at 2.7 Å. This small peak can be explained as follows: the four carbon atoms of the tridentate dithiol ligand are located in the range of 3.26 - 3.40 Å from the rhenium. The distance to the nearest carbon atom of the monodentate S \bar{E} t ligand is with 3.39 Å within the same range. Thus, five carbon atoms with an average distance of 3.35 Å

can be considered as a Re-C coordination shell giving rise to the small feature observed in the FT. The inter-atomic distances obtained by EXAFS are in good agreement with the XRD results. For the Re=O bond, the EXAFS gives a 0.03 Å longer distance than XRD, which is slightly more than the typical experimental uncertainty of the EXAFS analysis of ± 0.02 Å. A fit of the EXAFS with coordination numbers allowed to vary gives 0.9 and 4.0 for the Re=O and Re-S coordination shells, respectively. In the best fit for Re-C coordination shell, N equals 2.4 ± 0.7 . The similar situation has been observed for all fits with variable coordination numbers of the other complexes studied. Thus, reliable coordination numbers can be obtained by EXAFS for the first Re=O coordination shell and shells of neighboring atoms with higher atomic number like S or Se. For the light atoms at a longer distance such as Re-C, the error in N can be up to 50%.

For complex 2, the inter-atomic distances are in agreement with the XRD results. It should be noted that the Re-O shell at 2.08 Å contributes less than 5% to the total EXAFS and partially overlaps with the dominating Re-S shell at 2.29 Å. Therefore it might be difficult to observe the presence of a single Re-O bond for this type of rhenium or technetium complexes by EXAFS if the presence of such a bond is not known *a priori*. The Re-C inter-atomic distance in complex 2 is 0.18 Å shorter than in 1. This significant decrease is due to the shorter Re-O bond length in the tridentate dithiol ligand in 2 as compared to the corresponding Re-S bond in 1. Although it might not be possible to obtain structural parameters for the Re-X (X=O,S) shell by EXAFS for the reasons mentioned before, a reduction of the Re-C distance will be indicative for a decrease of the Re-X bond.

Tab. 1: Structural parameters of compounds 1-4. Comparison of EXAFS with XRD analysis.

| Sample | Re=O | | | Re-O | | | | Re-S | | | | |
|----------|-------|----------------------------------|------|-------|----------------------------------|-------|------|-------------------|----------------------------------|-------|------|-------------------|
| | EXAFS | | | EXAFS | | | | EXAFS | | | | |
| | N | F ² (Å ²) | R(Å) | N | F ² (Å ²) | R(Å) | R(Å) | N | F ² (Å ²) | R(Å) | R(Å) | |
| <u>1</u> | 1 | 0.002 | 1.69 | 1.66 | | | | | 4 | 0.003 | 2.31 | 2.31 [*] |
| <u>2</u> | 1 | 0.002 | 1.69 | 1.68 | 1 | 0.004 | 2.08 | 2.11 | 3 | 0.002 | 2.29 | 2.29 [*] |
| <u>3</u> | 1 | 0.002 | 1.68 | 1.65 | 1 | 0.001 | 2.07 | 2.10 | 2 | 0.002 | 2.29 | 2.28 [*] |
| <u>4</u> | | | | | 1 [#] | | | 2.18 [#] | 4 | 0.002 | 2.27 | 2.25 [*] |

| Sample | Re-Se | | | | Re-C | | | |
|----------|-------|----------------------------------|------|------|-------|----------------------------------|------|-------------------|
| | EXAFS | | | XRD | EXAFS | | | XRD |
| | N | F ² (Å ²) | R(Å) | R(Å) | N | F ² (Å ²) | R(Å) | R(Å) |
| <u>1</u> | | | | | 5 | 0.011 | 3.34 | 3.35 [*] |
| <u>2</u> | | | | | 4 | 0.006 | 3.16 | 3.15 [*] |
| <u>3</u> | 1 | 0.002 | 2.42 | 2.41 | 4 | 0.006 | 3.16 | 3.15 [*] |
| <u>4</u> | | | | | 6 | 0.014 | 3.20 | 3.12 [*] |

*) Averaged value of N inter-atomic distances.

#) Parameters for the Re-N bond.

The coordination of rhenium in complex 3 is similar to that of 2 except that the sulfur atom of the monodentate ligand is replaced by selenium. Electron scattering off the selenium atom contributes approximately 40% to the EXAFS and is also the reason for a larger EXAFS amplitude of 3 in the k range of 3 - 10 Å⁻¹ as compared to the spectrum of 2 (see Fig. 2). It is known that high Z elements, e.g., selenium, are easier to detect by EXAFS than low Z elements, e.g., carbon and oxygen /1/. As in the case of complex 2, electron scattering off the oxygen atom of the tridentate dithiol ligand contributes less than 5% to the EXAFS amplitude. Therefore, the Re-O shell could be included in the fit only because its presence was known *a priori*. The inter-atomic distances obtained of all four coordination shells are in agreement with the XRD results.

Complex 4 is a trigonal-bipyramidal mixed-ligand Re(III) complex /8/. Three sulfur atoms coordinate the rhenium atom in the equatorial plane. The nitrogen and phosphorus atoms are in *trans* position to each other. EXAFS analysis can not distinguish between neighboring elements like phosphorus and sulfur. Therefore, the phosphorus atom was treated in the fit

as an additional sulfur atom in the Re-S coordination shell. The inter-atomic distance of the Re-S shell obtained is in agreement with XRD results. We like to emphasize that we do not report on parameters of the Re-N bond. An attempt to include a Re-N coordination shell gave a bond distance in agreement with the XRD result. But this might be an accidental coincidence. We believe that this shell should not be included in a fit because the separation in distance from the dominating Re-S shell is 0.10 Å, which is less than the expected resolution given by our data range in k-space.

In summary, the possibilities and limitations of the EXAFS analysis have been studied for several "n+1" mixed ligand rhenium complexes. The inter-atomic distances obtained by EXAFS are in excellent agreement with the XRD results. The coordination numbers for the Re=O, Re-S, and Re-Se shells deviate less than 12% from the expected values. It was possible to measure the distance between rhenium and carbon atoms which do not form bonds with the central atom. Although, the coordination number for the Re-C shell has a large uncertainty of approximately 50%, the inter-atomic distance is accurate within ± 0.02 Å. The reason for the somewhat larger deviation between EXAFS and XRD results for the Re-C bond length in **4** is not clear and will be investigated further. Observed changes of the Re-C distance can be used to estimate the Re-X (X=O,S) bond length of tridentate dithiol ligands. This is especially valuable because the direct measurement of the Re-X bond length by EXAFS may be difficult. In conclusion, analysis of the Re L_{III} or Tc K edge EXAFS is a valuable tool for the accurate determination of structural parameters of "n+1" mixed ligand rhenium or technetium complexes. This is especially important for amorphous solid or liquid complexes where XRD can not be applied.

Acknowledgment

We thank R. Nicolai for her help during the sample preparation. We are grateful to P.G. Allen, M.A. Denecke, and D.K. Shuh for their help during the experiments. The majority of the EXAFS experiments were performed at SSRL, which is operated by the U.S. Department of Energy, Office of Basic Energy Sciences, Division of Chemical Sciences. We thank also HASYLAB for its support during the EXAFS experiment.

References

- /1/ Koningsberger, D. C., Prins, R.: *X-ray absorption. Principles, application, techniques of EXAFS, SEXAFS and XANES*, 1st ed., John Wiley and Sons, Inc., New York 1988.
- /2/ Elder, R. C., Eidsness, M. K.: *Chem. Rev.* **87**, 1027 (1987).
- /3/ Almahamid, I., Bryan, J. C., Bucher, J. J., Burrell, A. K., Edelstein, N. M., Hudson, E. A., Kaltsoyannis, N., Lukens, W. W., Shuh, D. K., Nitsche, H., Reich, T.: *Inorg. Chem.* **34**, 193 (1995).
- /4/ Martin, J. L., Yuan, J., Lunte, C. E., Elder, R. C., Heineman, W. R., Deutsch E.: *Inorg. Chem.* **28**, 2899 (1989).
- /5/ Leibnitz, P.: private communication (1994).
- /6/ Spies, H., Fietz, T., Pietzsch, H.-J., Johannsen, B., Leibnitz, P., Reck, G., Klostermann K.: *J. Chem. Soc. Dalton Trans.* 2277 (1995).
- /7/ Fietz, T., Spies, H., Leibnitz, P., Scheller D.: *J. Coord. Chem.*, accepted for publication (1995).
- /8/ Spies, H., Glaser, M, Pietzsch, H.-J., Hahn, F.E., Kintzel, O., Lügger T.: *Angew. Chem.* **106**, 1416 (1994).
- /9/ George, G. N., Pickering, I. J.: EXAFSPAK, A suite of computer programs for analysis of X-ray absorption spectra. Stanford Synchrotron Radiation Laboratory, Stanford, CA, USA (1995).
- /10/ Mustre de Leon, J., Rehr, J. J., Zabinsky, S. I., Albers, R. C.: *Phys. Rev. B* **44**, 4146 (1991).
- /11/ T. Fietz, T.: Rhenium-Komplexe mit 3+1-Koordination, Thesis (1995).

Chemistry of Heaviest Elements

MONTE CARLO SIMULATION OF REACTION GAS CHROMATOGRAPHY OF GROUP 6 ELEMENTS

A. Vahle, S. Hübener, R. Dressler¹, B. Eichler¹, A. Türler¹

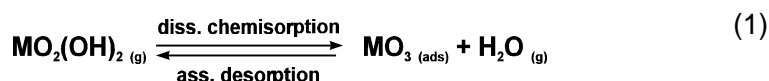
Forschungszentrum Rossendorf e.V., Institute of Radiochemistry

¹ Paul Scherrer Institut, Laboratory of Radio- and Environmental Chemistry

Gas chromatographic techniques have proven to be well suited to study kinetics and thermodynamics of desorption-adsorption processes at trace levels. For this reason isothermal on-line gas chromatography is a favored technique for studying the chemical properties of the heaviest elements available only in quantities of single, short-lived atoms. However, the data of chromatography experiments cannot provide direct evidence of the species involved and hence the basic processes determining the chromatographic transport. Indirect evidence is possible, if predicted data, based on thermodynamic arguments and model calculations, corresponds with experimental results.

Model calculations by the Monte Carlo method have been applied to simulate the transport of volatile species through a gas chromatographic column for the case of simple reversible adsorption as the basic process /1,2/. Experimental data like the elution yield of isothermal gas chromatography and thermochromatograms were reproduced very well.

The chromatographic transport of group 6 elements in the O₂-H₂O_(g)/SiO_{2(s)}-system is governed by the surface reactions dissociative chemisorption and associative desorption as basic processes (M = Cr, Mo, W):



For this kind of chromatography, we use the term reaction gas chromatography in order to distinguish it from "normal" gas chromatography characterized by the transport of species with the same chemical state in the adsorbed and gaseous state /3/.

In Monte Carlo simulations of chromatography, the different kinds of basic processes have to be considered; the adsorption residence time, J_a, must be defined. In the case of simple reversible adsorption J_a is defined by the Frenkel equation, and the period of oscillations of the adsorbed species perpendicular to the surface, J₀, has to be varied /1,2/. In the special case of reaction gas chromatography of group 6 elements in the O₂-H₂O_(g)/SiO_{2(s)}-system, J_a is determined mainly by the kinetics of the rate controlling associative desorption reaction and the collision probability of water molecules with the adsorbate. We define J_a by a Frenkel-type equation and operate with a pseudo-period of oscillations, J₀^{*}, evaluated approximately from Eq. (2):¹

$$J_0^* = \sqrt{\frac{2 B M}{R T}} \cdot \frac{c_{\text{ads}}^* (\text{MO}_3)}{c_{\text{gas}} (\text{H}_2\text{O})} \cdot e^{\frac{) S_{\text{diss. ads}}}{R}} \quad (2)$$

The term was obtained assuming that the volatile species MO₂(OH)₂ is immediately desorbed, t_r · t_{ads}, p = 1 atm and

$$\frac{4}{d} \cdot \frac{c_{\text{ads}}^* (\text{MO}_3)}{c_{\text{gas}} (\text{H}_2\text{O})} \cdot e^{\frac{) H_{\text{diss. ads}}}{RT}} \cdot e^{\frac{) S_{\text{diss. ads}}}{R}} \gg 1.$$

Values of J₀^{*} can vary immensely. However, they are greater than those of J₀ (10⁻¹² - 10⁻¹⁴ s).

¹ t_r = retention time, M = mol mass of the transported species in the gaseous phase, R = gas constant, T = Temperature, c_{ads}^{*} (MO₃) = standard concentration of MO₃ in the adsorbed state = 2,679·10¹⁹ cm⁻², c_{gas} (H₂O) = concentration of H₂O in the gaseous phase,) S_{diss. ads}^{*} = standard entropy of dissociative adsorption,) H_{diss. ads}^{*} = standard enthalpy of dissociative adsorption, t_{ads} = total adsorption residence time

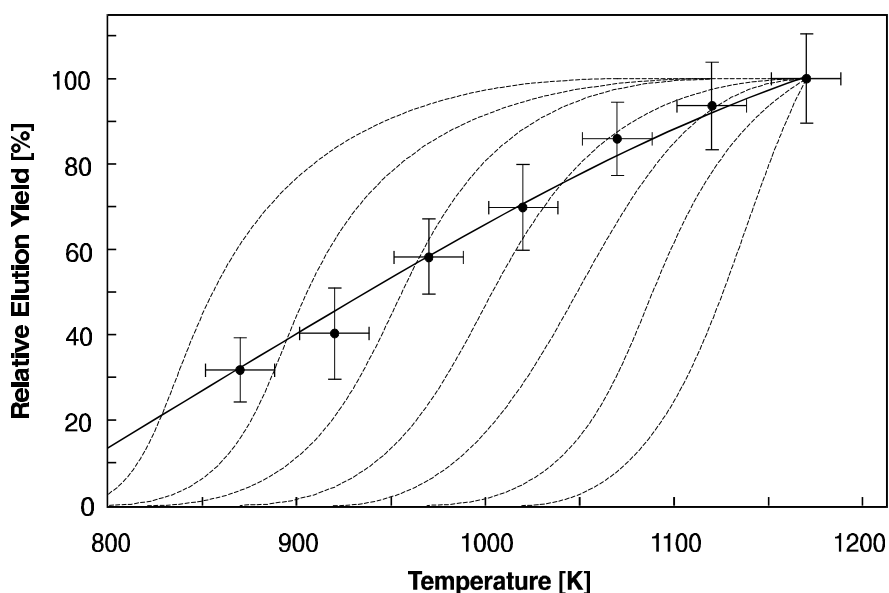


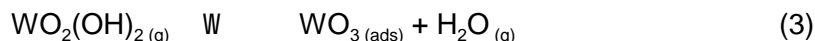
Fig. 1: Relative elution yield of ^{169}W as a function of the column temperature in isothermal on-line gas chromatography:

Experimental data and calculated yield curves. $p(\text{H}_2\text{O}) = 780 \text{ Pa}$, $v_0(\text{He}) = 1 \text{ l min}^{-1}$, $v_0(\text{O}_2) = 0.5 \text{ l min}^{-1}$

Solid line: Calculated by the Monte Carlo method assuming transport via reaction (3) with $\Delta S_{\text{diss.ads}}^{\text{E}} = -41 \text{ J mol}^{-1} \text{ K}^{-1}$ and $\Delta H_{\text{diss.ads}}^{\text{E}} = -41 \text{ kJ mol}^{-1}$.

Dashed lines: Calculated by the Monte Carlo method assuming reversible adsorption with $\Delta H_{\text{diss.ads}}^{\text{E}} = -180 \text{ kJ mol}^{-1}$ to -240 kJ mol^{-1} in steps of 10 kJ mol^{-1} .

In Fig. 1 experimental elution yields of ^{169}W are compared with results of Monte Carlo simulations. The dashed lines were obtained for different values of $\Delta H_{\text{ads}}^{\text{E}}$, assuming simple reversible adsorption as the basic process. None of these curves can reproduce the experimental data. The solid line was calculated assuming that tungsten is transported via reaction (3):



The shape of this calculated-yield curve reproduces the experimental data very well. $\Delta H_{\text{diss.ads}}^{\text{E}}$ was determined to be -41 kJ mol^{-1} and corresponds with the value of $-25 \pm 31 \text{ kJ mol}^{-1}$ expected for reaction (3) from thermodynamic considerations.

The elution yield here is less dependent on column temperature than in the case of simple reversible adsorption. For this reason a significant increase of the elution yield can be only obtained with an extreme temperature increase.

An increase in the partial pressure of water in the carrier gas results in an increase of the elution yield, too. The retention time will be diminished due to the rising number of effective collisions.

Acknowledgements

These studies were supported by the BMBF of the FRG under contracts 06 DR 101 D and 06 DR 666 I(4)/1.

References

- /1/ Zvara, I.: Simulation of Thermo-chromatographic Processes by the Monte Carlo Method. *Radiochim. Acta* **38**, 95 (1985)
- /2/ Türler, A., Gregorich, K. E., Hoffman, D. C., Lee, D. M., Gäggeler, H.W.: A Simulation of Isothermal Gas Chromatography Using the Monte Carlo Method. PSI Condensed Matter Research and Material Sciences Progress Report 1991, Villigen, Annex III, Annual Report, p. 68 (1992)
- /3/ Suzuki, M., Smith, J. M.: Transport and Kinetic Parameters by Gas Chromatographic Techniques. *Adv. Chromatogr.* **13**, 241 (1975)

THERMOCHROMATOGRAPHY OF HEAVY ACTINIDES ON METAL SURFACES AT HIGH TEMPERATURES

St. Taut, S. Hübener, B. Eichler¹, H.W. Gäggeler^{1,2}, M. Schädel³, E. Jäger³, W. Bröchle³

Forschungszentrum Rossendorf e.V., Institute of Radiochemistry

¹ Paul Scherrer Institut Villigen, Laboratory for Radio- and Environmental Chemistry

² Universität Bern, Institute of Inorganic Chemistry

³ Gesellschaft für Schwerionenforschung Darmstadt mbH

To obtain information about the electronic state of actinides the characterization of their metallic properties is a useful method, because the most notable differences in electronic behavior are found in their metallic state. Because actinides beyond Es are available only in trace amounts, only very few experimental physicochemical data exist for these elements.

It was experimentally proven that the macroscopic sublimation enthalpies of many elements correlate to their adsorption enthalpies which can be derived from thermochromatographic deposition temperatures. This opens the opportunity to search with this method for quantitative data even for the highest actinides, which are available only in amounts for atom-at-a-time chemistry.

The experimental setup in this work provides high temperatures, which were unreachable until now. Thus, in preparation for future experiments with elements beyond Fm, a series of thermochromatographic data from earlier experiments /1/ could be completed.

Fig. 1 shows the used thermochromatographic apparatus. The gradient oven is a commercial model HTM LORA 36. The maximum temperature, theoretically available in the hottest zone of the oven, is 2100 K. For our experiments we used 1550 K in the starting position. The metallic columns were made from foils and had an inner diameter of 4 mm. They were inserted in a Ta support tube inside the oven. To prevent oxidation of this tube it was flushed with He from outside. He was also used as carrier gas with a velocity of 30 cm/s. The gases were purified from water with molecular sieve and from oxygen with a Ti getter at 1200 K. The whole setup was preconditioned for half an hour at working temperature before the experiment.

The actinides under study we obtained from the heavy actinide fractions of Sg chemistry experiments, carried out at the UNILAC accelerator of the GSI Darmstadt using the $^{248}\text{Cm} + ^{22}\text{Ne}$ reaction /2/.

After purification, the actinides were evaporated from a nitric acid solution in a Ta boat. A small piece of La was added in order to reduce the actinides to their metallic state. The boat was inserted in the apparatus through a sluice. Then the sluice was flushed with carrier gas, and the boat was rapidly brought in starting position. After 30 minutes, the experiment was ended by switching off the heating. Since the temperature fell by about 100 K within a few seconds the chromatographic process stopped immediately.

The nuclide distribution along the thermochromatographic column was determined off-line by alpha counting of 1 cm column sections with charged particle detectors.

Fig. 1: Scheme of Experimental Setup

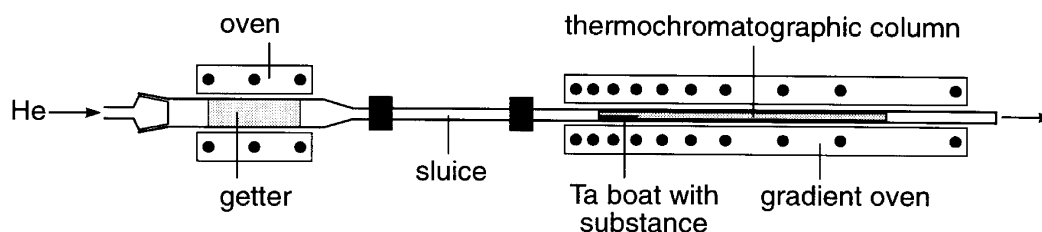


Fig. 2 shows as a typical chromatogram the activity distribution of ^{248}Cf , ^{253}Es and ^{255}Fm on a V column. To derive the adsorption heat from the deposition temperature the program TECRAD /3/ was used.

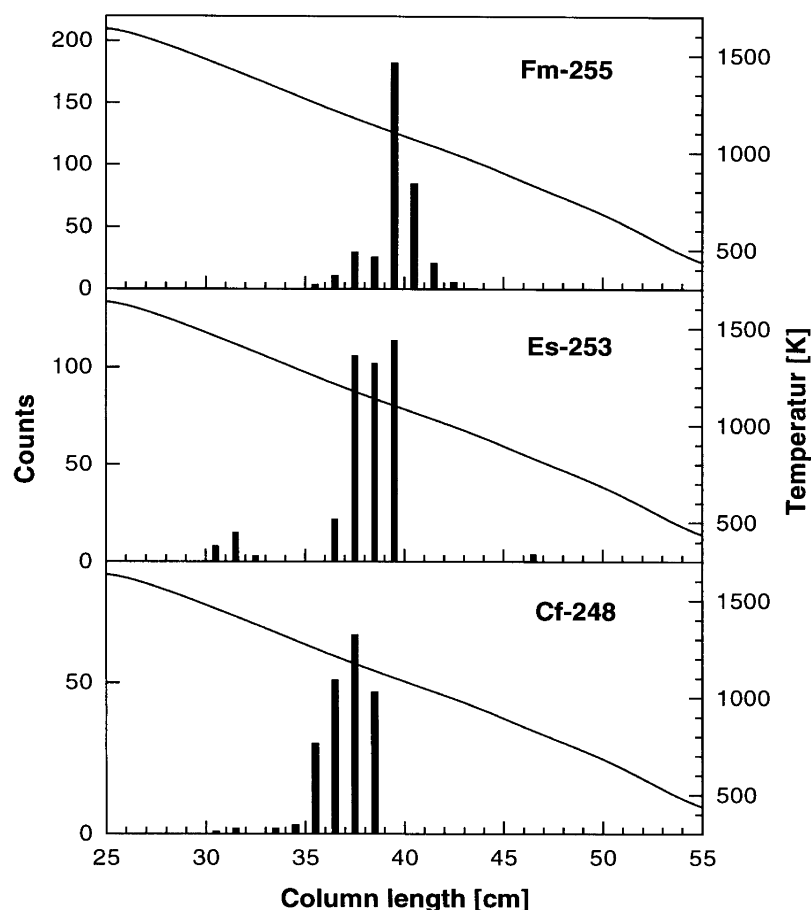


Fig. 2: Thermochromatogram of ^{248}Cf , ^{253}Es and ^{255}Fm on a V column

Using the semi-empirical MIEDEMA method it is possible to theoretically calculate adsorption heats /4/. Tab. 1 summarizes the experimental deposition temperatures, adsorption heats and the calculated adsorption heats /4/ in comparison to sublimation heats from /5,6,7/.

Tab. 1: Deposition Temperatures, Sublimation and Adsorption Enthalpies of Actinides;
* double Peak

| Actinide | Subl. Enth. [kJ/mol] | Column | Deposition Temp. [K] | Adsorption Enthalpy [kJ/mol] | | |
|-----------|----------------------|--------|----------------------|------------------------------|----------|---------------------|
| | | | | This Work | Lit. /2/ | Calc. for M(II) /6/ |
| Cf | 206 /5/ | Nb | 1360 | -343 | | -397 |
| | | Ta | 1378 | -348 | | -361 |
| | | V | 1180 | -299 | | -340 |
| | | Mo | 1274 | -322 | | -339 |
| Es | 133 /6/ | Nb | 1180 | -299 | -290 | -228 |
| | | Ta | 1337, 1162* | -338, -294* | | -294 |
| | | V | 1142 | -289 | | -274 |
| | | Mo | 1274 | -322 | | -274 |
| Fm | 143 /7/ | Nb | 1142 | -289 | -270 | -224 |
| | | Ta | 1162 | -294 | -280 | -280 |
| | | V | 1103 | -280 | | -263 |
| | | Mo | 1142 | -289 | -290 | -262 |

As expected the deposition temperatures of Cf, Es and Fm differ in most cases from each other reflecting the tendency from metallic tri- to divalency in the second part of the actinide series. Thus, both chemical separation and characterization is possible.

Cf on Nb and Ta shows its position between the trivalent and divalent actinides. Surprising is its rather low adsorption enthalpy on V compared to Nb and Ta.

In contrary to the results, obtained by direct measurement of vapor pressures in /6, 7/ we can clearly see differences in the metallic properties of Es and Fm, especially on Mo.

Acknowledgements

The authors wish to express appreciation to K. E. Gregorich and N. Trautmann for providing the ²⁴⁸Cm targets.

This work was supported by both BMBF, contract 06DR666I(4)/1 and DFG, contract Hu642/1-1.

References

- /1/ Hübener, S., Eichler, B., Schädel, M., Brüche, W., Gregorich, K. E., Hoffman, D. C., J. All. Comp. **213/214**, 429 (1994),
- /2/ Schädel, M. et. al, GSI Scientific Report 1995, in preparation
- /3/ Funke, H., Hübener, S., Roß, A., Eichler, B., Annual Report Institut of Radiochemistry, Report No. FZR-43, (1993), 53
- /4/ Eichler, B., in preparation
- /5/ Ward, J. W., Kleinschmidt, R. G. Haire, J. Phys. (Paris), Colloq., **40** , 33 (1979)
- /6/ Kleinschmidt, P. D., Ward, J. W., Matlack, G. M., J. Chem. Phys. **81** , 473 (1984)
- /7/ Haire, R. G., Gibson, J. K., J. Chem. Phys. **91** , 7085 (1989)

STUDIES OF MOLYBDENUM OXICHLORIDES AS HOMOLOGUES OF ELEMENT 106 OXICHLORIDES

A. Türler¹, B. Eichler¹, D.T. Jost¹, R. Dressler¹, D. Piguet¹, H.W. Gäggeler^{1,2}, S. Hübener, M. Boettger, M. Grantz

Forschungszentrum Rossendorf e.V., Institute of Radiochemistry

¹ Paul Scherrer Institut, Laboratory of Radio- and Environmental Chemistry

² Universität Bern, Institute of Inorganic Chemistry

In preparation for an experiment to study the chemical properties of element 106, seaborgium (Sg), using the On-line Gas Chromatography Apparatus OLGA III, experimental conditions were optimized with short-lived carrier-free activities of the lighter homologue element Mo.

Vapor pressures of macroscopic amounts give a good relative measure of the volatility of compounds. In Fig. 1 the vapor pressure curves of the monoatomic gas over the respective solids for Mo- and W-chlorides and oxichlorides are shown /1,2/. For Mo the compound MoO_2Cl_2 has the highest volatility, whereas the pure chloride MoCl_5 is not stable at higher temperatures and decomposes. In contrast to WCl_6 , the compound MoCl_6 is not stable.

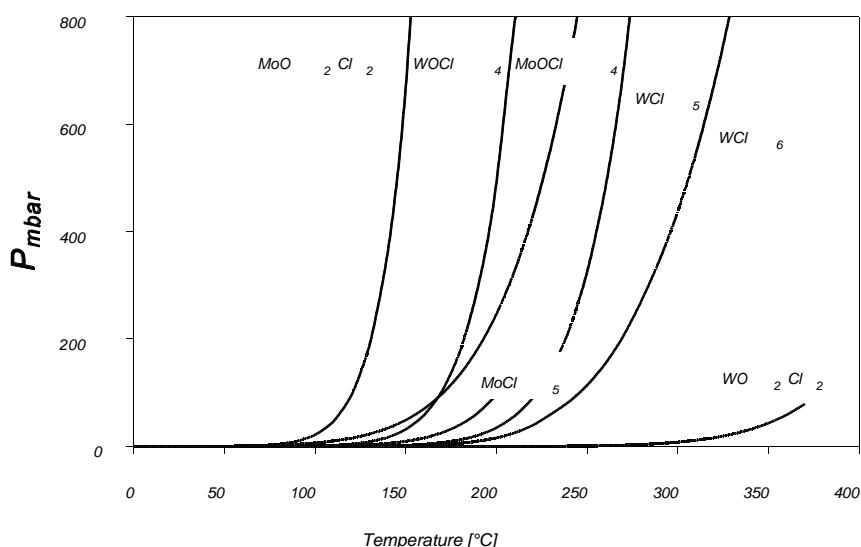


Fig. 1: Vapor pressure curves of group 6 chlorides and oxichlorides.

Short-lived Mo-isotopes were produced from a ^{235}U fission target at the U-120 cyclotron at the Forschungszentrum Rossendorf. At the U-120 cyclotron neutrons can be produced in the reaction $^9\text{Be}(d,n)^{10}\text{B}$. A He/C aerosol gas-jet was used to rapidly transport the reaction products to the chromatography apparatus. Two different chlorinating systems were tested. Namely, 300 ml/min O_2 which was saturated with SOCl_2 vapors at room temperature and 100 ml/min O_2 with traces of HCl (0.5-15 ml/min). The PSI tape system was used to subsequently step the separated activities in front of a HPGe detector where the characteristic γ -rays of Mo isotopes were registered. In this manner long-lived activities were suppressed. The nuclides 58.8-s ^{104}Mo and 35.6-s ^{105}Mo were identified after chemical separation. With the mixture O_2/SOCl_2 as reactive gases, the yield curve shown in Fig. 2 was measured. The volatility of the Mo compound indicated the formation of MoO_2Cl_2 for which an adsorption enthalpy ($\Delta H_a^{0(T)}$) of -90 kJ/mol was measured. This value was in agreement with an earlier measurement /3/. The absolute chemical yield could not be determined, due to the fact that the pressure in the target chamber could not be maintained, when the unseparated activities were collected directly on the tape system. Pressure differences in the target chamber greatly affected the range of fission products in He and thus the transport efficiency.

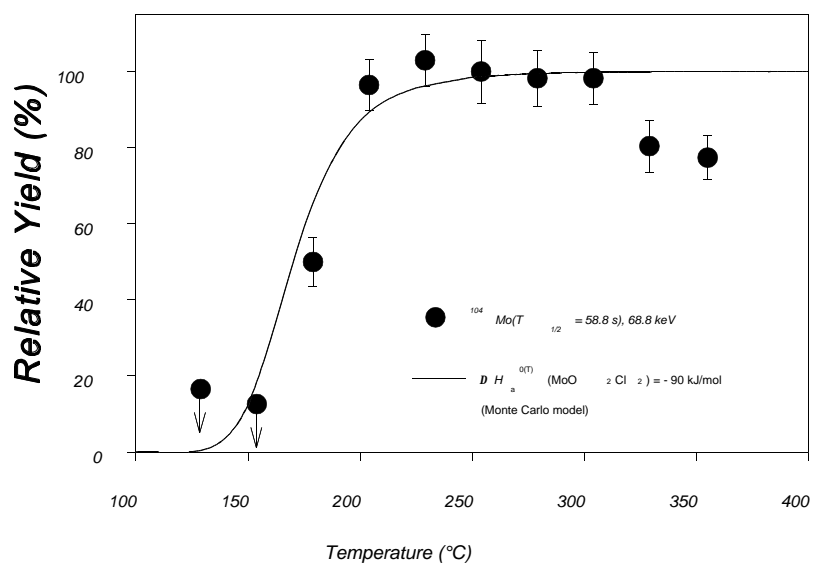


Fig. 2: Yield curve measured for Mo-oxichloride with $O_2/SOCl_2$ as reactive agents.

With O_2/HCl as reactive gases, about 3 times higher yields were observed at 350°C isothermal temperature. When measuring the yield curve, the yield slowly decreased, but even at 100°C ^{104}Mo and ^{105}Mo were still clearly identified. Obviously a different Mo compound was formed. We attributed this behavior to a chemical transport reaction, which previously had been described in the literature /4/. It appeared as if in the reaction with HCl a volatile intermediate species of the form $MoO_2Cl_2 \cdot H_2O$ was formed.

Apparently, the chemical yield in the $O_2/SOCl_2$ system was rather low (~20%). The low yield was attributed to the formation of SO_3 droplets in the recluster chamber which significantly interfered with the recluster process and also the deposition of the activity on the tape. This problem could only be solved in subsequent studies by using Cl_2 saturated with $SOCl_2$ and traces of O_2 as reactive gases.

References

- /1/ Knacke, O., Kubaschewski, O., Hesselmann, K.: *Thermochemical Properties of Inorganic Substances*, Springer-Verlag, 2nd Ed., Berlin 1991
- /2/ Jefimov, A.I.: *Svoistva Neorganiceskikh Soedinenii, Spravochnik*, Izd. Khimija, Leningrad 1983
- /3/ Türler, A., Yakushev, A.B., Eichler, B., Gäggeler, H.W., Jost, D.T., Scherer, U.W.: On-Line Gas Phase Isothermal Chromatography of Molybdenum and Tungsten Oxichlorides as Homologues of Element 106 with OLGA III. PSI Annex IIIA Annual Report 1993, 98 (1994)
- /4/ Chernikov, S.S., Tarakanov, B.M.: Investigation of the Chemical Transport of Molybdenum (VI) Oxide by Hydrogen Chloride by the Methods of Infrared and Ultraviolet Spectroscopy. *Russ. J. Inorg. Chem.* **18**, 22 (1973)

MODEL EXPERIMENTS FOR THE SEPARATION OF ELEMENT 106 SORPTION BEHAVIOUR OF SHORT-LIVED Mo ISOTOPES ON CATION AND ANION EXCHANGERS

D. Schumann¹, M. Andrassy¹, H. Nitsche¹, S. Hübener, M. Grantz, St. Taut, R. Brückner*, H. Guratzsch*

Forschungszentrum Rossendorf e.V., Institute of Radiochemistry

* Department of New Accelerators

¹ TU Dresden, Institute of Analytical Chemistry

Chemical studies of element 106 require an effective separation from the actinides and element 104 that are produced either directly in nuclear reactions or as a decay product. One of the methods used for fast separation of heavy elements in aqueous solution is ion exchange on cation and anion resins with various acids or complexing agents as eluents. For the development of chemical systems applicable in fast on-line experiments with transactinides, usually the lighter homologs and pseudo-homologs are used in model experiments. Very often chemical systems are chosen in which all elements of the same subgroup show a common chemical behaviour to separate them from the other reaction products. In /1/ we reported on a chemical system which allows to separate subgroup IV elements and lanthanides from W and Mo by use of cation exchange from diluted HCl/HF containing aqueous solutions. This chemical system was successfully applied in on-line experiments with short-lived W, Hf and Lu isotopes /2/. In separation experiments of W from Hf with the ARCA apparatus best results were obtained when HNO₃ was used instead of HCl. Irreversible adsorption on the titanium slider could be nearly suppressed with solutions of 0.1 M HNO₃/1x10⁻³ M HF /3/.

Mo is expected to behave somewhat different from W because higher distribution coefficients on the cation exchanger DOWEX 50x8 from HCl/HF solution were observed /1/. Therefore, we studied the sorption behaviour of short-lived Mo isotopes produced in the reaction ²³⁵U (n,f) at the U-120 cyclotron in Rossendorf. Neutrons were obtained by the reaction ⁹Be (d,n)¹⁰B. For the transport of the activity from the target chamber to the chemical setup the He/MoO₃ gas-jet system described in /4/ was used. For the chemical separation, columns (3x30 mm) were filled with DOWEX 50x8 and DOWEX 1x8 (200-400 mesh, 80 mg). The (-activity of each column was measured with a HPGe detector.

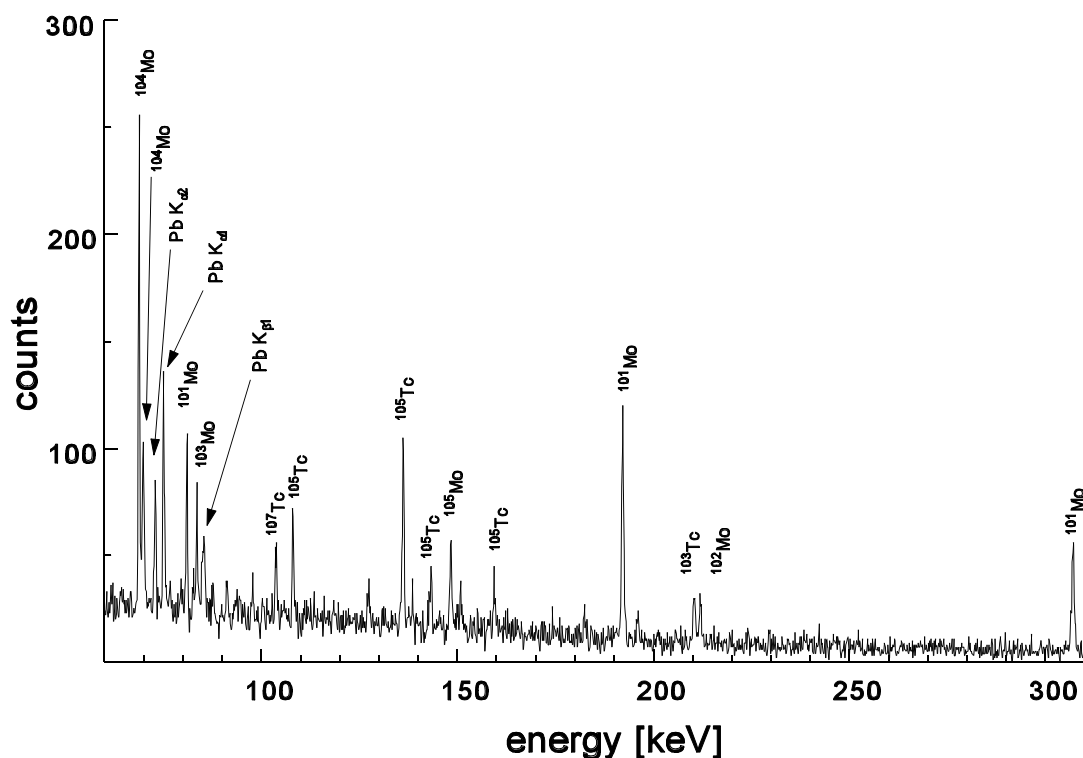


Fig. 1: (-spectrum of the DOWEX 1x8 column, solution 0.05 M HCl/10⁻³ M HF

Fig. 1 shows the γ -spectrum of the DOWEX 1x8 column using 0.05 M HCl/ 10^{-3} M HF for the separation. It can be seen that only Mo and its decay product Tc pass the cation exchange column, all other fission products, especially La, Ba, Nb and Zr are adsorbed on DOWEX 50x8. Tab. 1 shows the sorption of Mo on DOWEX 50x8 obtained with various HCl/HF and HNO₃/HF solutions using a gas flow of 2 l/min, a flow rate of the aqueous phase of 2 ml/min and a measuring time of 20 minutes of each column. The γ -ray of ¹⁰⁴Mo (68.8 keV) was used for calculating the distribution of Mo.

| HF | HCl | % adsorption on DOWEX 50x8 | HNO ₃ | % adsorption on DOWEX 50x8 |
|---------------------|--------|----------------------------|------------------|----------------------------|
| 10^{-3} M | 0.05 M | 25.9 | 0.05 M | 43.3 |
| 10^{-3} M | 0.1 M | 33.4 | 0.1 M | 56.8 |
| $5 \cdot 10^{-4}$ M | 0.1 M | 50.0 | 0.1 M | 63.3 |
| 10^{-4} M | 0.1 M | 66.8 | 0.1 M | 62.0 |

Tab. 1: Adsorption of Mo on DOWEX 50x8 in dependence on the HCl, HF and HNO₃ concentration

For nearly all cases the separation with HCl shows better results than with HNO₃. HF concentrations that are below 10^{-3} M cannot be used. The results for 0.05 M HCl/ 10^{-3} M HF and 0.1 M HCl/ 10^{-3} M HF are in good agreement with the values found in batch experiments /1/. This system appears not be suitable to separate element 106 from 104 because the possible 106-homolog Mo is partially retained on the cation exchange column. However, this cation exchange system may be useable to determine the chemical properties of 106. Because W is retained much less than Mo, one could conclude from the sorption behaviour if 106 behaves more like W or Mo.

Acknowledgement

The authors are very grateful to the FZR-cyclotron staff for their services. This work was supported by BMBF, contract 06DD477D.

References

- /1/ D. Schumann, S. Fischer, R. Dressler, St. Taut, H. Nitsche, N. Trautmann, M. Schädel, W. Bröchle, B. Schausten, A.F. Novgorodov, R. Misiak., B. Eichler, H. Gäggeler, D. Jost, A. Türlér, H. Bruchertseifer, Radiochim. Acta, 1995, in print
- /2/ D. Schumann, R. Dressler, S. Fischer, St. Taut, R. Binder, Z. Szegłowski, B. Kubica, L. I. Guseva, G. S. Tikhomirova, O. Constantinescu, V. P. Domanov, M. Constantinescu, Dinh Thi Lien, Yu. Ts. Oganessian, V. B. Brudanin, H. Bruchertseifer, Radiochim. Acta **69**, 35 (1995)
- /3/ R. Günther, W. Paulus, A. Posledni, J. V. Kratz, M. Schädel, W. Bröchle, E. Jäger, E. Schimpf, B. Schausten, D. Schumann, R. Binder, GSI -Scientific Report 1994, p. 302
- /4/ S. Hübener, H. Heyne, G. Hüttig, A. Ross, R. Brückner, H. Guratzsch, S. Fischer, R. Binder, FZR-43 Annual Report 1993, p. 55

CALCULATION OF RATE CONSTANTS OF THE BASIC REACTIONS OF REACTION GAS CHROMATOGRAPHY - SOLVING THE DIFFERENTIAL EQUATION SYSTEM

M. Grantz, S. Hübener

Forschungszentrum Rossendorf e.V., Institute of Radiochemistry

The study of the chemical behavior of the group 6 elements Mo and W in trace amounts is a first step to characterize element 106. The chromatographic transport of group 6 element trioxides in the system O_2 - $H_2O_{(g)}/SiO_{2(s)}$ is governed by the surface reactions dissociative chemisorption and associative desorption, typical for reaction gas chromatography [1]. The retention time observed in isothermal on-line gas chromatographic experiments with short-lived Mo- and W-isotopes is too long for studying ^{265}Sg and ^{266}Sg with half lives between 10 and 30 s. In order to find out the rate controlling step of the chromatographic process of group 6 element trioxides in the O_2 - $H_2O_{(g)}/SiO_{2(s)}$ - system and hence to establish experimental conditions favourable for a fast transport and high elutions yields, the kinetics of basic reactions of the chromatographic process must studied in detail.

The basic assumption in this approach is the postulation of adsorbed hydroxide as the central reaction component. This requires splitting the associative desorption into the formation of the adsorbed group 6 element hydroxide out of adsorbed trioxide and water vapour followed by the simple desorption of the hydroxide. The dissociative adsorption is separated into a simple adsorption of the gaseous hydroxide and the formation of solid trioxide under loss of water. The rate constants of these reactions can be described by Arrhenius equations and at least one of them is rate determining in fast gas chromatographic transport.

Other rate constants are given by the nuclear decay and the convective flow. In this model, the surface diffusion is neglected and the gaseous hydroxide is the only species which is transported in the gas phase over macroscopic distances.

Under conditions of pseudo first order reactions, this system of differential equations has analytical solutions. The pseudo first order conditions are reached when the partial pressure of water is so high relative to the adsorbed trioxides that the reaction does not change the partial pressure of water in the gas phase. This boundary condition is reached under normal experimental conditions for studying trace amounts of group 6 element trioxides. The other boundary condition of the system is the constancy of mass of the group 6 elements distributed between the different species.

As the adsorbed hydroxide is the central component, its concentration profile has to be calculated at first. Therefore it is necessary to convert the first order differential equation into a second order differential equation to obtain only one species with an unknown time dependency. The analytical solution of this equation gives the time dependent concentration profile of the adsorbed hydroxide $MO_2(OH)_2$ with M representing one of the group 6 elements:

$$[MO_2(OH)_2]_{ad(t)} = \alpha_1 e^{-at} e^{(t)} + \alpha_2 e^{-at} e^{-(t)} + c [k^2 - 2ak + b]^{-1} e^{-kt}$$

α_1 and α_2 are functions of the boundary conditions, $($ is equal to $[a^2 - b]^{1/2}$, the coefficients a,b,c, are functions of the rate constants of the basic reactions (they are the coefficients of the first order, the zeroth order and the inhomogeneity terms, respectively), and $k = \ln(2)/t_{1/2}$ the rate constant of radioactive decay.

The concentration profiles of the adsorbed trioxide and the gaseous hydroxide are given by inhomogeneous linear differential equations dependent on only one species, because the concentration profile of the adsorbed hydroxide has been analytical solved as mentioned above. The rate constant of convective flow can be calculated from macroscopic parameters. This gives the chance to prove the assumed reaction system experimentally and to calculate the rate constants of the basic reactions from experimental data such as deposition temperature, the curve of concentration profile along the tube from thermochromatography, retention time and elution profile from isothermic gas chromatography, and the dependence of experimental data from the half life of the studied isotopes.

Acknowledgements

The support of these studies by the BMBF of the Federal Republic of Germany under contract 06 DR 666 I (4)/1 is gratefully acknowledged.

References

- /1/ Vahle A., Hübener S., Dressler R., Eichler B., Türler A.: Monte Carlo Simulations of Reaction Gas Chromatography of Group 6 Elements. This report

FIRST ON-LINE GAS CHEMISTRY OF ELEMENT 106 (SEABORGIUM)

S. Hübener for a collaboration between

LBNL Berkeley - Universität Bern - GSI Darmstadt - FLNR Dubna - TU Dresden - Chalmers University of Technology Göteborg - GH Kassel - ITS and LLNL Livermore - Universität Mainz - University Oslo - Forschungszentrum Rossendorf e.V. - JAERI Tokai and PSI Villigen

For the first time the chemical properties of element 106 (Sg = seaborgium) were successfully studied by a large international collaboration at the GSI UNILAC accelerator in Darmstadt. One of three experimental approaches using the PSI On-line Gas Chemistry Apparatus (OLGA) aimed to study:

- (i) the formation
- (ii) the volatility of element 106 oxichlorides
- (iii) the characteristic decay properties of ^{265}Sg and ^{266}Sg .

Conditions for an isolation of Sg were optimized by studying the chromatographic behavior of homologous Mo- and W-oxichlorides with $\text{SOCl}_2/\text{Cl}_2$ and $\text{O}_2/\text{SOCl}_2/\text{Cl}_2$ as chlorinating agents. Short-lived Mo-isotopes were produced from a ^{235}U fission target at the U-120 cyclotron at the Forschungszentrum Rossendorf, whereas short-lived W-isotopes (^{165}W - ^{169}W) were produced in the ^{20}Ne on ^{152}Gd reaction at the PSI PHILIPS cyclotron. At both facilities a He/C-jet was used to rapidly transport the reaction products to the chromatography apparatus. The volatility of the Mo compound indicated the formation of MoO_2Cl_2 for which an adsorption enthalpy ($\Delta H_a^{\text{O(T)}}$) of -90 kJ/mol was measured, while W formed the less volatile compound WO_2Cl_2 ($\Delta H_a^{\text{O(T)}} = -100$ kJ/mol). It was demonstrated that for isothermal temperatures above 275°C retention times are less than 10 s, and that the separation from group 4 (Hf) and group 5 (Ta) elements is good.

In a first experiment at the GSI UNILAC accelerator a ^{248}Cm target ($\approx 950 \mu\text{g}/\text{cm}^2$) was bombarded with 121 MeV ^{22}Ne ions. The OLGA was operated at isothermal temperatures between 300°C and 400°C. As reactive agents 100 ml/min Cl_2 saturated with SOCl_2 and 2 ml/min O_2 were added. Spontaneous fission decays and α -decays were registered with the GSI Rotating Wheel Multidetector Analyzer ROMA. In the ROMA system, the separated activities were deposited on thin polypropylene foils ($30\text{-}40 \mu\text{g}/\text{cm}^2$) at the periphery of a 64 position wheel. Every 10 s, the wheel was stepped to move the collected activity between 7 pairs of PIPS detectors. Due to geometric limitations the detector pairs were two wheel positions apart and the wheel was moved two positions at the time. All events were registered in an event-by-event mode. Due to a long-lived contamination from ^{212}Po in the 8.8 MeV region, where α -decays of ^{265}Sg are expected, the significance of the observed event chains had to be improved. Therefore, a mother-daughter recoil mode for ROMA was implemented. In this mode every second position on the wheel remains empty. Whenever an α -particle with the decay energy of ^{265}Sg or ^{266}Sg (between 8.5 and 9.0 MeV) was detected in a bottom detector, it was assumed that the daughter nucleus, ^{261}Rf or ^{262}Rf recoiled out of the KCl deposit on the polypropylene foil into the top detector. Such an event initiated the daughter search mode by causing a single step. In this mode the sources were removed from the detector pairs and empty positions were moved in-between. The system waited for 2 min for the decay of the daughter nuclides, before the parent mode was resumed.

In Tab. 1 all event chains attributed to the decay of ^{265}Sg or ^{266}Sg are summarized.

Tab. 1: $^{265,266}\text{Sg}$ events observed after chemical separation with OLGA III

| E_1 [MeV] | dt_1 [s] | E_2 [MeV] | dt_2 [s] | E_3 [MeV] | dt_3 [s] | Mode | Decay assignment | Column temper. [°C] |
|----------------|---------------|----------------|---------------|----------------|---------------|------|---|------------------------|
| 8.86 | 2.8 | 8.38 | 31.0 | 8.05 | 14.8 | | $^{265}\text{Sg} \xrightarrow{\alpha} ^{261}\text{Rf} \xrightarrow{\alpha} ^{257}\text{No}$ | 400 |
| 8.84 | 27.3 | 8.13 | 53.3 | - | - | MD | $^{265}\text{Sg} \xrightarrow{\alpha} ^{261}\text{Rf}$ or ^{257}No | 300 |
| 8.85 | 0.6 | 8.30 | 48.4 | - | - | MD | $^{265}\text{Sg} \xrightarrow{\alpha} ^{261}\text{Rf}$ or ^{257}No | 300 |
| 8.56 | 48.9 | SF | 2.8 | - | - | MD | $^{266}\text{Sg} \xrightarrow{\alpha} ^{262}\text{Rf}$ | 400 |

E_1 , E_2 , and E_3 are the energies of the first, second, and third α -event, respectively; dt_1 is the time between the end of collection and the first α -event, dt_2 is the time between the first and second α -event, and dt_3 is the time between the second and third α -event.

Two correlations observed in the daughter mode allowed the clear identification of ^{265}Sg . In addition, one very significant triple correlation was observed in the parent mode. Furthermore, a clear signature for the decay chain $^{266}\text{Sg} \rightarrow ^{262}\text{Rf}$ was registered with the 8.56 MeV α -decay followed 2.8 s later by a spontaneous fission.

Half lives and cross sections evaluated from the observed α -decays (68 % confidence interval [c.i.]) are summarized in Tab. 2.

Tab. 2: Half lives and cross sections of seaborgium nuclides

| Nuclide | Half life $t_{1/2}$ [s] | Cross section F [pb] |
|-------------------|-------------------------|------------------------|
| ^{265}Sg | 7.1 +8.6 / -2.5 | 270 +360 / -170 |
| ^{266}Sg | 34 +163 / -15 | 50 +115 / -41 |

The chemical results show that seaborgium forms an oxichloride, volatile at 300 - 400 °C, when Cl_2 , saturated with SOCl_2 , and small amounts of Q are present. Thermodynamic calculations indicate that SgO_2Cl_2 is formed in analogy to the known WO_2Cl_2 .

Acknowledgements

The work of the group at Forschungszentrum Rossendorf was supported by the BMBF of the FRG under contract 06 DR 666 I (4)/1.

II. PUBLICATIONS, PATENTS, LECTURES AND POSTERS

PUBLICATIONS

Allen, P.G., J.J. Bucher, D.L. Clark, N.M. Edelstein, S.A. Ekberg, J.W. Gohdes, E.A. Hudson, N. Kaltsoyannis, W.W. Lukens, M.P. Neu, P.D. Palmer, T. Reich, D.K. Shuh, C.D. Tait, B.D. Zwick; Multinuclear NMR, Raman, EXAFS, and X-ray Diffraction Studies of Uranyl Carbonate Complexes in Near-neutral Aqueous Solution. X-ray Structure of $[\text{C}(\text{NH}_2)_3]_6[(\text{UO}_2)_3(\text{CO}_3)_6] \cdot 6.5\text{H}_2\text{O}$
Inorg. Chem. **34**, 4797 (1995)

Allen, P.G., I. Almahamid, R. A. Andersen, G. Bernhard, J.C. Bryan, J.J. Bucher, A.K. Burrell, D.L. Clark, N.M. Edelstein, S.A. Ekberg, J.W. Gohdes, E.A. Hudson, N. Kaltsoyannis, W.W. Lukens, W. Matz, H. Moll, M.P. Neu, H. Nitsche, P.D. Palmer, T. Reich, K. Roberts, D.K. Shuh, C.D. Tait, B.D. Zwick; Studies of Actinides by X-ray Absorption Spectroscopy
Stanford Synchrotron Radiation Laboratory, Annual Report 1994

Al Mahamid, I., J.C. Bryan, J.J. Bucher, A.K. Burrell, N.M. Edelstein, E.A. Hudson, N. Kaltsoyannis, W.W. Lukens, D.K. Shuh, H. Nitsche, T. Reich; Electronic and Structural Investigations of Technetium Compounds by X-ray Absorption Spectroscopy
Inorg. Chem. **34**, 193 (1995)

Al Mahamid, I., Becraft, K., Nitsche, H.; Complexation of plutonium(V) with nitrilotriacetic acid; Radiochim. Acta. **68**, 63 (1995)

Baraniak, L., L. Thieme, M. Schuster, G. Funke, A. Otto; Stofftransportvorgänge des Radiums in gelaugten und ungelagerten Sedimenten im Bereich der Lagerstätte Königstein
FZR, Interner Bericht, Nov. 1995

Brendler, V., G. Geipel, G. Bernhard, H. Nitsche; Possible Impacts of Phosphate Influx on the Uranium Speciation and Migration in Seepage Waters;
Proc. Intern. Conf. Workshop "Uranium Mining and Hydrogeology", Freiberg, Germany, Oct. 1995; Verlag Sven v. Loga, Köln 1995, p.61

Buchanan, B.B., J.J. Bucher, D.E. Carlson, N.M. Edelstein, E.A. Hudson, N. Kaltsoyannis, T. Leighton, W. Lukens, D.K. Shuh, H. Nitsche, T. Reich, K. Roberts, P. Torretto, J. Woicik, W.-S. Yang, A. Yee, B.C. Yee; A XANES and EXAFS Investigation of the Speciation of Selenite following Bacterial Metabolization
Inorg. Chem. **34**, 1617 (1995)

Denecke, M.A., H. Moll, S. Pompe, D. Rettig, H. Friedrich, G. Bernhard, T. Reich, H. Nitsche; Determination of the Arsenic Oxidation State in Environmentally Relevant Waters by XANES Spectroscopy
HASYLAB Annual Report 1995, p. 593

Denecke, M.A., S. Pompe, H. Moll, K.H. Heise, T. Reich, H. Nitsche; EXAFS Studies on Anhydrous Complexes of Uranyl and Ortho-Substituted Benzoic Acids
HASYLAB Annual Report 1995, p. 629

Hudson, E.A., L.J. Terminello, B.E. Viani, T. Reich, J.J. Bucher, D.K. Shuh, N.M. Edelstein; X-ray Absorption Studies of Uranium Sorption on Mineral Substrates; Application of Synchrotron Radiation Techniques to Materials Science;
Materials Research Society Symposium Proceedings, Vol. 375, Pittsburgh 1995, p.235

Hüttig, G.; Verfahren zur Oberflächencharakterisierung von Gesteinen und Mineralien
FZR, Inst. f. Radiochemie, 31.01.1995 (interner Bericht)

Martin, H.P., E. Müller, Y. Knoll, R. Strienitz, G. Schuster; Silicon Carbide Derived from Silica Sol and Sugar

J. of Mat. Science Letters **14**, 620 (1995)

Moll, H., W. Matz, G. Schuster, E. Brendler, G. Bernhard H. Nitsche; Synthesis and Characterization of Uranyl-Orthosilicate $(\text{UO})_2\text{SiO}_4 \cdot 2\text{H}_2\text{O}$
J. of Nucl. Materials **227**, 40-49 (1995)

Nebelung, C., S. Hübener, G. Bernhard; Bestimmung von Actiniden in Bauschutt; Tagungsband der 27. Jahrestagung Fachverband für Strahlenschutz e.V.; Entsorgung: Wiederverwertung-Beseitigung; Wolfenbüttel, Germany, 25.-29.09.1995; Band II, S. 549-552

Nitsche, H., Synchrotron X-ray Absorption Spectroscopy: a New Tool for Actinide and Lanthanide Speciation in Solids and Solution;
J. Alloys and Compounds **223**, 274 (1995)

Pompe, S., M.A. Denecke, H. Moll, M. Bubner, H. Funke, T. Reich, K.H. Heise, H. Nitsche; Investigation of the Interaction of Humic Acids with Uranyl Ions by Extended X-Ray Absorption Fine Structure Spectroscopy (EXAFS)
HASYLAB Annual Report 1995, p. 595

Teterin, Yu.A., V.I. Nefedov, K.E. Ivanov, A.S. Baev, G. Geipel, T. Reich, H. Nitsche; Photoelectron Study of the Interaction of $\text{UO}_2(\text{ClO}_4)_2$ with Calcite
Dokl. Akademii Nauk **344**, 206 (1995) (in Russian)

Reich, T., S. Pompe, H. Moll, V. Brendler, K.-H. Heise, L. Baraniak, G. Bernhard, H. Nitsche; A Study of the Complexation of Uranyl Ions with Humic Acids by EXAFS
HASYLAB Annual Report 1994, p.609

Rettig, D., H. Funke, G. Hüttig, P. Merker, C. Nebelung, H. Zänker; Fission Product Vapour Reactions in the Primary Circuit
EUR 16503, Luxembourg 1995

Shuh, D. K., Kaltsoyannis, N., Bucher, J. J., Edelstein, N. M., Clark, S. B., Nitsche, H., Reich, T., Hudson, E. A., Al Mahamid, I., Torretto, P., Lukens, W., Roberts., K., Yee, B. C., Carlson, D. E., Yee, A., Buchanan, B. B., Leighon, T., Yang W.-S., Bryan, J. C.; Environmental Applications of XANES: Speciation of Tc in Cement after Chemical Treatment and Se after Bacterial Uptake;
Mater. Res. Soc. Symp. Proc. **344**, 323 (1995)

Vahle, A., S. Hübener, B. Eichler; Thermochromatographic Studies of Oxide and Hydroxide Species of Molybdenum - Model Experiments with Respect to the Physico-chemical Characterization of Element 106
Radiochimica Acta **69**, 233 (1995)

PATENTS

Näfe, H., D. Rettig; Referenzelektrode für galvanische Zellen mit einem kationenleitenden Festelektrolyten
Offenlegungsschrift DE 4412540 A1 (07.09.1995)

LECTURES

H. Nitsche

Das Institut für Radiochemie des Forschungszentrums Rossendorf: Ein wissenschaftliches Profil. Philipps-Universität Marburg, Fachbereich Kernchemie
Marburg, Germany, February 1995

G. Bernhard, G. Geipel, H. Nitsche

Die Bestimmung der Speziation der Uranylionen in umweltrelevanten Haldensicker- und Grubenwässern des Uranerzbergbaus
Chemiedozententagung 1995
Jena, Germany, 12.-15.03.1995

S. Hübener

On-line Gaschromatographie der Hydroxide der Elemente der 6. Gruppe
3. Workshop "Chemie der schwersten Elemente"
Mainz, Germany, 15.-17.03.1995

S. Taut

Schnelle Ionenaustauschversuche mit trägerfreiem Zr, Nb und Mo in schwach HCl/HF-sauren Lösungen
3. Workshop "Chemie der schwersten Elemente"
Mainz, Germany, 15.-17.03.1995

A. Vahle

Chromatographie mit W-Isotopen im O_2 - $H_2O_{(g)}/SiO_{2(s)}$ -System
3. Workshop "Chemie der schwersten Elemente"
Mainz, Germany, 15.-17.03.1995

H. Nitsche, S. Pompe, M. Bubner, K.H. Heise, G. Geipel, A. Brachmann, L. Baraniak, M. Schmidt, G. Bernhard, M.A. Denecke, T. Reich

Characterization and Derivation Methods of Humic Materials and Related Effects on Radionuclide Complexation
209th American Chemical Society National Meeting, Division of Nuclear Chemistry & Technol.
Anaheim, CA, USA, 02.-06.04.1995

H. Nitsche

Symposium on Environmental f-Element Chemistry
209th American Chemical Society National Meeting, Division of Nuclear Chemistry & Technol.
Anaheim, CA, USA, 02.-06.04.1995

E.A. Hudson, L.J. Terminello, B.E. Viani, J.J. Bucher, D.K. Shuh, N.M. Edelstein, T. Reich

Uranium and Thorium Sorption on Minerals Studied by X-ray Absorption Spectroscopy
209th American Chemical Society National Meeting, Division of Nuclear Chemistry & Technol.
Anaheim, CA, USA, 02.-06.04.1995

G. Bernhard

Radioökologische Forschungen vor dem Hintergrund der Hinterlassenschaften des Uranerzbergbaus
Hochschule für Technik und Wirtschaft
Dresden, Germany, 13.04.1995

S. Hübener, C. Nebelung, G. Bernhard

Freimessung von Bauschutt - Low-level Messung von Alpha-Strahlern
Seminar am Institut für Strahlenschutzphysik, Technische Universität Dresden,
Dresden, Germany, 27.04.1995

C. Nebelung, S. Hübener, G. Bernhard, Ch. Lierse
Analytische Verfahren zur Beurteilung kontaminierter Betonflächen
Workshop "Freimessung"
Karlsruhe, Germany, 09.05.1995

M. Bubner, M. Matucha, V. Sasek, K.H. Heise, H. Nitsche, J. Veleminski, J. Spizek
Investigation of PCB Congeners Using Isotopically Modified Tracers
8th Intern. Bioindicators Symposium
Ceske Budejovice, Czech, 22.-28.05.1995

C. Nebelung, S. Hübener, G. Bernhard
Kurzbericht zum Stand der Entwicklungsarbeiten des BMBF-Projektes 02 S 7442
Arbeitskreis "Freimessung von Anlagenteilen und Bauschutt aus dem Abbau kerntechnischer
Anlagen des Brennstoffkreislaufes"
Karlsruhe, Germany, 30.05.1995

T. Reich
EXAFS Untersuchungen von Uranylkomplexen in Lösungen
Universität Leipzig, Inst. f. Physikalische und Theoretische Chemie
Leipzig, Germany, 26.06.1995

H. Nitsche
Environmental Radiochemistry Using Hard X-ray Synchrotron Radiation: Research and Beam
Line Layout.
Université de Paris-Sud, Institut de Physique Nucléaire
Orsay, France, June 1995

H. Nitsche
Radiochemistry Research at the Forschungszentrum Rossendorf.
University of Helsinki
Helsinki, Finland, June 1995

H. Nitsche
Research Related to Environmental Remediation and Nuclear Waste Disposal.
VTT Technical Research Centre of Finland
Espoo, Finland, June 1995

H. Nitsche
Actinide Solubility and Speciation Studies for Nuclear Waste Performance Risk Assessment.
Teollisuuden Voima Oy (TVO), Nuclear Waste Management
Helsinki, Finland, June 1995

L.R. Morss, M.A.J. Schmidt, K.L. Nash, P.G. Allen, J.J. Bucher, N.M. Edelstein, M.A. Denecke,
H. Nitsche, T. Reich
Spectroscopic Studies of Lanthanide Coordination in Crystalline and Amorphous Phosphates
210th American Chemical Society National Meeting, Division of Nuclear Chemistry & Technol.
Chicago, IL, USA, 20.-24.08.1995

T. Reich, M.A. Denecke, S. Pompe, H. Nitsche, D.K. Shuh, P.G. Allen, J.J. Bucher, N.M.
Edelstein
Characterization of the Complexation of Uranyl Ions with Humic Acid by X-ray Absorption
Spectroscopy
210th American Chemical Society National Meeting, Division of Nuclear Chemistry & Technol.
Chicago, IL, USA, 20.-24.08.1995

E.A. Hudson, L.J. Terminello, B.E. Viani, J.J. Bucher, D.K. Shuh, N.M. Edelstein, M.A. Denecke, T. Reich
EXAFS Studies of Uranium Sorption on Layer-Silicate Minerals
210th American Chemical Society National Meeting, Division of Nuclear Chemistry & Technol.
Chicago, IL, USA, 20.-24.08.1995

G. Bernhard, H. Friedrich, W. Boessert
Strategy for the Decommissioning of the Radiochemical Plants
5th Intern. Conf. on Radioactive Waste Management and Environmental Remediation
Berlin, Germany, 03.-08.09.1995

G. Bernhard, G. Geipel, V. Brendler, H. Nitsche
Speciation of Uranium in Natural Aquatic Systems of a Uranium Mining Area
5th International Conference on the Chemistry and Migration Behaviour of Actinides and Fission Products in the Geosphere "Migration '95"
Saint-Malo, France, 10.-15.09.1995

H. Nitsche
Geochemical Models and Modelling
5th International Conference on Chemistry and Migration Behavior of Actinides and Fission Products in the Geosphere "Migration '95"
Saint-Malo, France, 10.-15.09.1995

H. Nitsche, I. Al Mahamid, K. Becraft, R. Gatti
Complexation Behavior of Plutonium in the Presence of Organic Materials Relevant to the Radioactive Waste at U.S. Department of Energy Sites.
5th International Conference on Chemistry and Migration Behavior of Actinides and Fission Products in the Geosphere "Migration '95"
Saint-Malo, France, 10.-15.09.1995

T. Reich, H. Moll, M.A. Denecke, G. Geipel, G. Bernhard, H. Nitsche, P.G. Allen, J.J. Bucher, N. Kaltsoyannis, N.M. Edelstein, D.K. Shuh
Characterization of Hydrous Uranyl Silicate by EXAFS Analysis
5th International Conference on the Chemistry and Migration Behaviour of Actinides and Fission Products in the Geosphere "Migration '95"
Saint-Malo, France, 10.-15.09.1995

G. Geipel, V. Brendler, G. Bernhard, H. Nitsche
Speciation of Uranium in Seepage Water of Tailing Piles from Uranium Mining
Internationale Konferenz und Workshop: Uran-Bergbau und Hydrogeologie
Freiberg, Germany, 04.-07.10.1995

H. Nitsche
Reactive Transport Modelling
Speciation of Uranium in Seepage Water of Tailing Piles from Uranium Mining
Internationale Konferenz und Workshop: Uran-Bergbau und Hydrogeologie
Freiberg, Germany, 04.-07.10.1995

M. Thieme, G. Geipel, G. Bernhard, H. Nitsche
Laboratory Simulation for the Sorption of U, Th and Pb on Rock Materials from Uranium Mining
Internationale Konferenz und Workshop: Uran-Bergbau und Hydrogeologie
Freiberg, Germany, 04.-07.10.1995

P.G. Allen, D.K. Shuh, J.J. Bucher, N.M. Edelstein, C.E.-A. Palmer, T. Reich, M.A. Denecke, H. Nitsche
XAFS Studies in Environmental Radiochemistry
22nd SSRL Annual User's Meeting

Stanford, CA, USA, 12.-13.10.1995

C. Nebelung, S. Hübener, G. Bernhard, H. Nitsche
Direktmessung von Actiniden in Beton durch α -Spektrometrie von Dünnschichtmeßpräparaten
IV. Stilllegungskolloquium Hannover
3. Statusbericht Stilllegung und Rückbau kerntechnischer Anlagen, S.417-424
Bad Dürkheim, Germany, 08.-10.11.1995

G. Geipel, G. Bernhard, A. Brachmann, V. Brendler, H. Nitsche
Determination of Uranium Species in Natural Aquatic Systems
Lawrence Livermore National Laboratory
Livermore, CA, USA, 14.11.1995

A. Brachmann, G. Geipel, G. Bernhard, H. Nitsche
Complexation of U(VI) with Model Substances for Simulating Humic Acid Functionality
Lawrence Livermore National Laboratory
Livermore, CA, USA, 14.11.1995

T. Reich
Photoelektronenholographie - eine neues Verfahren zur Strukturanalyse von Festkörperober-
flächen im Dreidimensionalen
Graduiertenkolleg des Inst. f. Physikalische und Theoretische Chemie der Universität Leipzig
Leipzig, Germany, 20.11.1995

G. Geipel, M. Thieme, G. Bernhard, V. Brendler, A. Brachmann, H. Nitsche
Uranium Mining in Saxony and Thuringia: A Short Overview and Results of Some Studies
Savannah River Ecological Laboratory
Aiken, SC, USA, 21.11.1995

A. Kubatova, M. Matucha, M. Bubner, K.H. Heise
Application of Isotopically Labelled Internal Standards in GC-MS Analysis of PCB's
Mini-Symposium on Microbial Degradations
Prague, Czech Republic, 27.11.-01.12.1995

P.G. Allen, D.K. Shuh, J.J. Bucher, N.M. Edelstein, T. Reich, M.A. Denecke, H. Nitsche
Applications of X-ray Absorption Spectroscopy to Problems in Environmental Radiochemistry
PACIFICHEM '95
Honolulu, HI, USA, 17.-22.12.1995

POSTERS

S. Pompe, K.H. Heise, H. Nitsche
Capillary Electrophoresis for a "Finger-Print" Characterization of Fulvic and Humic Acids
7th Intern. Symposium on High Performance Capillary Electrophoresis
Würzburg, Germany, 29.01.-02.02.1995

G. Geipel, A. Brachmann, V. Brendler, G. Bernhard and H. Nitsche
Bestimmung der Speziation des Uraniums mittels zeitaufgelöster Laserinduzierter
Fluoreszenzspektroskopie
Anakon'95
Schliersee, Germany, 24.-26.04.1995

M. Bubner, M. Meyer, K. Fuksova, M. Matucha, K.H. Heise, H. Nitsche
Synthesis of ^{13}C - and ^{14}C -Labelled PCB Congeners
8th Intern. Bioindicators Symposium
Ceske Budejovice, Czech Republic, 22.-28.05.1995

H. Uhlirva, M. Matucha, M. Kretschmar, M Bubner
Uptake and Distribution of [¹⁴C]trichloroacetic Acid in Norwegian Spruce Shoot
8th Intern. Bioindicators Symposium
Ceske Budejovice, Czech Republic, 22.-28.05.1995

E. Förster, K.H. Heise, M. Bubner, H. Nitsche
A Conditioning Method for the Safe Disposal of Highly Radioactive Unstable Carbon-14 Labelled
Organic Compounds
5th Intern. Conf. on Radioactive Waste Management and Environmental Remediation
Berlin, Germany, 03.-08.09.1995

A. Brachmann, G. Geipel, G. Bernhard, S. Pompe, M. Bubner, H. Nitsche
Zeitaufgelöste laserinduzierte Fluoreszenzspektroskopie an Huminsäuren und Untersuchung der
Komplexbildung mit umweltrelevanten Schwermetallen
25. GDCh-Hauptversammlung
Münster, Germany, 10.-16.09.1995

H. Moll, W. Matz, G. Schuster, E. Brendler, G. Bernhard, H. Nitsche
Synthese und Charakterisierung von Uranylorthosilicat, (UO₂)₂SiO₄·2H₂O
25. GDCh-Hauptversammlung
Münster, Germany, 10.-16.09.1995

G. Geipel, G. Bernhard, V. Brendler and H. Nitsche
Sorption of Uranium-(VI) on Rock Material of a Mine Tailing Pile: Solution Speciation by Fluores-
cence Spectroscopy
Fifth International Conference on the Chemistry and Migration Behaviour of Actinides and
Fission Products in the Geosphere
Saint Malo, France, 10.-15.09.1995

V. Brendler, G. Geipel, G. Bernhard and H. Nitsche
Complexation in the System UO₂²⁺/PO₄³⁻/OH⁻(aq.): Investigations Over Wide Ranges in pH and
Concentration
Fifth International Conference on the Chemistry and Migration Behaviour of Actinides and
Fission Products in the Geosphere
Saint Malo, France, 10.-15.09.1995

S. Pompe, M. Bubner, A. Brachmann, G. Geipel, R. Jander, L. Baraniak, T. Reich, M. Denecke,
K.H. Heise, H. Nitsche
Uranyl-Complexation of Humic Acids: A Comparison of Natural Materials with Model Substances
Fifth International Conference on the Chemistry and Migration Behaviour of Actinides and
Fission Products in the Geosphere
Saint Malo, France, 10.-15.09.1995

H. Moll, G. Geipel, G. Bernhard and H. Nitsche
Solubility and Speciation of (UO₂)₂SiO₄ · 2H₂O in Aqueous Systems
Fifth International Conference on the Chemistry and Migration Behaviour of Actinides and
Fission Products in the Geosphere
Saint Malo, France, 10.-15.09.1995

M. Thieme, G. Geipel, G. Bernhard and H. Nitsche
Laboratory Simulation for the Sorption of U, Th and Pb on Rock Materials from Uranium Mining
Fifth International Conference on the Chemistry and Migration Behaviour of Actinides and
Fission Products in the Geosphere
Saint Malo, France, 10.-15.09.1995

E.A. Hudson, P.G. Allen, L.J. Terminello, M.A. Denecke, T. Reich, J.J. Rehr, J.J. Bucher
XANES of the Uranyl Ion: Comparison of Experiment and Theory

22nd SSRL Annual User's Meeting
Stanford, CA, USA, 12.-13.10.1995

III. SEMINARS

TALKS OF VISITORS

Prof. Dr. Yury A. Teterin
Russian Academy of Science, Kurtshatov Institute, Moscow (Russia)
X-Ray Photoelectron Spectroscopy of the Lanthanoid Compounds
12.01.1995

Prof. Dr. Vadim I. Nefedov
Russian Academy of Science, Kurnakov Institute, Moscow (Russia)
Die Grundlagen von ESCA und die Identifizierung des chemischen Zustands
12.01.1995

Prof. Dr. Yury A. Teterin
Russian Academy of Science, Kurtshatov Institute, Moscow (Russia)
X-Ray Photoelectron Spectroscopy of the Actinide Compounds
16.01.1995

Prof. Dr. Vadim I. Nefedov
Russian Academy of Science, Kurnakov Institute, Moscow (Russia)
Die quantitative ESCA-Analyse
16.01.1995

Dr. Zenko Yoshida
Japan Atomic Energy Research Institute (JAERI), Tokyo (Japan)
07.03.1995

Prof. Dr. Claude Degueldre
Paul-Scherrer-Institut, Villigen (Szwitzerland)
Charakterisierung von Grundwasserkolloiden bezüglich nuklidspezifischer Migrationseigenschaften
30.05.1995

Dr. Ken Czerwinski
Technische Universität München
Understanding the Loading Capacity of Humic Acids: Examples with GOHY-573 Humic Acid
04.07.1995

Prof. Dr. Franz Baumgärtner
Technische Universität München
Die Kinetik der Tritium-Inkorporation in C₃- und C₄-Pflanzen
11.07.1995

Dr. Franz Scherbaum
Technische Universität München
Nutzung des laserinduzierten break-down-Effekts zur Analyse aquatischer Kolloidsysteme
26.07.1995

Prof. Dr. Andreas Schmidt-Ott
Gerhard-Mercator-Universität Duisburg
Erfassung von Partikeleigenschaften in Gassuspension
29.08.1995

Dr. Marc Lamoureux
Pacific Northwest Laboratory, Richland WA. (USA)
Chemical Speciation of Environmental Solids Using X-Ray Absorption Spectroscopy
30.08.1995

Dr. Cindy E. A. Palmer
Lawrence Livermore National Laboratory, Livermore CA.(USA)
To Migrate or not to Migrate - Investigations of Solubility, Speciation and Migration of Actinides
07.09.1995

Dr. Mikko Nyrki
Teollisuuden Voima OY (TVO), Helsinki (Finland)
An Overview about the Finnish Concept for the Disposal of Spent Fuel
17.10.1995

Dr. Ulla Vuorinen
Technical Research Centre, VTT , Helsinki (Finland)
An Overview about the Technical Research Centre of Finland - Activities of the Nuclear Waste Group in the Field of Solubilities of Elements
17.10.1995

Dr. Kaija Ollila
Technical Research Centre, VTT, Helsinki (Finland)
Studies on Uranium Speciation
17.10.1995

Dr. Mathias Kohler
US Geological Survey, Mento Parc C.A.(USA)
Adsorption and Transport of U(VI) in Batch and Column Experiments
23.10.1995

Dr. Mathias Kohler
US Geological Survey, Menlo Parc CA.(USA)
Uranium, Neptunium, and EDTA Adsorption an Goethite and Hematite
25.10.1995

Dr. Günter Meinrath
Forschungszentrum Karlsruhe
Spektroskopische Untersuchungen am sechswertigen Uran in wäßriger Lösung
26.10.1995

Prof. Dr. Vadim I. Nefedov
Russian Academy of Science, Kurnakov Institute, Moscow (Russia)
ESCA-Untersuchungen der Uranylwechselwirkungen mit Calcit- und Diabasoberflächen:
Bestimmung von Reaktionsprodukten und Bindungsabständen
02.11.1995

DC. Wolfgang Schindler
Kurt-Schwabe-Institut für Meß-und Sensortechnik, Meinsberg
Meßsonden für pH-Präzisionsmessungen in Tiefenwässern
16.11.1995

Prof. Dr. Igor L. Khodakovsky
Russian Academy of Science, Vernadsky Institute, Moscow (Russia)
International Projects on the Radiation Safety of the Biosphere
19.12.1995

Dr. Irina V. Tschernyshova
Russian Academy of Science, Vernadsky Institute, Moscow (Russia)
New Results of the Thermodynamic Investigations in the Vernadsky Institute
19.12.1995

WORKSHOP "Speciation"

Forschungszentrum Rossendorf, Institute of Radiochemistry and
Czech Technical University (CTU), Department of Nuclear Chemistry, Prague (Czech Republic)
Rossendorf, 23.-24.10.1995

Prof. Dr. Petr Benes (Prague)

Use of Radiotracer Methods for Speciation and Migration of Radionuclides and Trace Elements
in Natural Water

Dr. Karel Stamberger (Prague)

Discussion of the Interaction and Dispersion Processes and the Experimental Methodology

Dr. Lubomir Vopalka (Prague)

1-D-Model of Contaminants Migration Taking into Account the Complex Description in the
Interaction

Dr. Vinzenz Brendler (Rossendorf)

Speciation in the System $\text{UO}_2^{2+}/\text{PO}_4^{3-}/\text{H}_2\text{O}$

Dr. Harald Zänker, Dr. Wolfgang Richter, Gisela Hüttig (Rossendorf)

The Application of Filtration, Centrifugation, and Photon Correlation Spectroscopy to Detect
Colloidal Particles in Natural Water

Dr. Lutz Baraniak, Dr. Harald Funke (Rossendorf)

Sorption and Migration Behavior of Radium on Sediments of the Saxon Elbe River Valley

Dr. Karl Heinz Heise (Rossendorf)

Why Synthetic Humic Acids ?

IV. PERSONNEL

Director

Prof. Dr. H. Nitsche

Administrative Staff

H. Pospischil

K. Wünsche

Scientific Staff

Dr. T. Arnold*
Dr. L. Baraniak
Dr. G. Bernhard
Dr. V. Brendler⁺
Dr. M. Böttger*
Dr. M. Bubner
Dr. M. Denecke⁺

Dr. H.-J. Engelmann
Dr. E. Förster*
Dr. H. Funke
Dr. G. Geipel
Dr. K.H. Heise
Dr. S. Hübener
Dr. P. Merker

DC C. Nebelung
Dr. T. Reich
Dr. D. Rettig
Dr. S. Taut*
Dr. M. Thieme*
Dr. H. Zänker

Technical Staff

B. Eisold
J. Falkenberg
DI(FH) H. Friedrich
DI(FH) Ch. Fröhlich
G. Grambole
G. Heinz

H. Heyne
B. Hiller
DI(FH) G. Hüttig
DI(FH) R. Jander
P. Kluge
DI(FH) M. Meyer

Ch. Müller
H. Neubert
DC(FH) A. Otto*
A. Rumpel
R. Ruske
DI(FH) K. Wolf*

Graduate Students

DMin. A. Brachmann
DP M. Grantz
DC B. Mack

DC H. Moll
DC S. Pompe

DC M. Schmidt
DC A. Vahle

⁺ post doc

* term contract

V. ACKNOWLEDGEMENTS

Acknowledgements for financial and material support

The Institute is part of the Forschungszentrum Rossendorf e.V., which is financed in equal parts by the Federal Republic of Germany and the Free State of Saxony.

Four projects are supported by the Bundesministerium für Bildung, Wissenschaft, Forschung und Technologie (BMBF):

- Chemistry of heaviest elements
BMBF 06 DR 101
- Development of methods for the determination of alpha active nuclides in concrete
BMBF 02 S 7422
- Chemistry of element 106
BMBF 06 DR 666 I (4)/1
- Influence of humic acids on migration behavior of radioactive and non-radioactive heavy elements under natural conditions
BMBF 02 E 88150

One project was supported by Commission of the European Communities:

- An assessment of the status of activities for decommissioning of old uranium ore extract and treatment installations, and site remediation in Europe
Contract No. FI2D-CT93-0083
In collaboration with:
Institute for Nuclear Safety Research, FZR
Compagnie Générale des Matières Nucléaires (COGEMA), France
Empress Nacional del Uranio, S.A. (ENUSA), Spain

In addition, the Free State of Saxony provided support for the following projects:

- Chemical conversion of ^{14}C -labeled products to [^{14}C]Barium carbonate for long time disposal
SMWK AZ 4-7581.312/20
- Behavior of the natural daughter nuclides of radon-222 in surface relics of uranium milling and mining
SMWK 4.7541.83-FZR/303
- Mine-water induced wood decomposition and influence of the degradation products on radionuclide speciation, sorption and migration
SMWK 4.7541.83-FZR/402
- Influence of natural water-borne organic substances on the valency of radionuclides and toxic heavy metals
SMWK 4.7541.88-FZR/512
- The visit of Prof. V.I. Nefedov and K.E. Ivanov during 19.10.-04.11.1995 and 27.11.-20.12.1995, respectively, as participating guest of the Institute of Radiochemistry was financed in part by the SMWK project "Entwicklungshilfe" (2/901/181).

One project was supported by Deutsche Forschungsgemeinschaft:

- Properties of heavy actinides. DFG Hu 642/1-1

Three projects were supported by the following sponsors:

- Migration of ^{226}Ra in sediments of the Königstein uranium mine. was supported in part by a contract with the WISMUT GmbH.
- INTAS: Gas-phase chemistry studies of elements 104 and 106. In collaboration with:
University of Berne, Switzerland,
Joint Institute of Nuclear Research, Russia
INTAS 94-424.
- Development of experimental arrangements and methods for on-line high temperature gas chromatography of the heaviest elements. In cooperation with GSI. GSI DRNIK.